SEDIMENT DYNAMICS IN THE MACROTIDAL AVON RIVER ESTUARY, NOVA SCOTIA

SEDIMENT DYNAMICS IN THE MACROTIDAL AVON RIVER ESTUARY, NOVA SCOTIA

By

Joseph J. Lambiase, A.B., M.Sc.

A Thesis
Submitted to the School of Graduate Studies
in Partial Fulfilment of the Requirements
for the Degree
Doctor of Philosophy

McMaster University

April, 1977

DOCTOR OF PHILOSOPHY (1977)
(Geology)

McMASTER UNIVERSITY
Hamilton, Ontario.

TITLE: Sediment Dynamics in the Macrotidal Avon River Estuary, Nova Scotia

AUTHOR: Joseph John Lambiase, A.B. (Brown University)
M.Sc. (University of Rhode Island)

SUPERVISOR: Professor Gerard V. Middleton

NUMBER OF PAGES: xxvii, 415

ABSTRACT

The Avon River estuary is in central Nova Scotia and is part of the northeastern arm of the Bay of Fundy. Three major rivers discharge into the estuary which is approximately 16 km long and up to 2 km wide. There are three sand bodies at the estuary mouth and another three within the estuary.

The Avon River estuary is macrotidal; tidal range is 15.6 m at lunar perigee. Tidal currents represent the only hydraulic process that significantly affects sediment transport and distribution. Maximum bottom current velocities increase from 0.6 m/s at the estuary mouth to 1.7 m/s at the head of the system. Every location in the estuary is either flood current or ebb current dominant.

Mean grain size forms a different pattern on the surface of each sand body, but the overall trend is that grain size decreases sharply from the mouth of the estuary to the estuary head; thus, there is an inverse relationship between mean grain size and maximum current velocity. Cumulative curve analysis indicates that sediment samples are composed of three log-normal grain populations. A large, coarse population that is present at the estuary mouth is absent at the estuary head.

Grain size distribution is a function of maximum flow conditions; Shields' criterion indicates that the maximum grain size present in each location can be transported by the local hydraulic regime. Each grain population can be related to a sediment transport mechanism; the coarse population is transported by traction, the intermediate by intermittent suspension, and the fine by suspension. The transition from traction to intermittent suspension occurs when shear velocity approximately equals settling velocity; the intermittent suspension - suspension transition reflects the condition that shear velocity is approximately equal to 5 times settling velocity. Hydraulic sorting, produced by different transport rates for each transport mechanism and by local physiography, limits penetration of coarse sediment into the Avon River, and causes a deficiency of coarse sediment at the estuary head. This, in turn, produces the observed inverse relationship between mean grain size and current velocity.

There are three major classes of bedforms in the system including ripples, megaripples, and sand waves; transverse bars exist in one small area. Surface bed configuration reflects maximum flow conditions; each type of bedform occupies a different stability field on plots of water depth versus current speed and current speed versus mean grain size. Flow regime increases from the estuary mouth to the head, and internal structures reflect surface bedforms.

Sediment transport paths define net flood and net ebb sediment transport zones; transport zone position is a function of hydraulics and local physiography. Sand bodies lie at the junction of two or more transport zones. The three sand bodies at the estuary mouth form an ebb tidal delta. At the estuary head, one sand body is part of an ebb tidal delta, another is a tidal point bar, and the third is a flood tidal delta. Glacial till deposited in the estuary and tidal current transport of offshore sediment probably are the most important sediment sources; shoreline erosion also contributes a substantial amount of sediment. Sediment transport rates, aerial photographs, and surveying, echo sounding, and chart data indicate that the Avon River estuary has been stable since at least 1865 and that the system is in approximate dynamic equilibrium.

ACKNOWLEDGEMENTS

This study was supervised by Dr. G. V. Middleton; it benefited immensely from his guidance, suggestions and criticisms. Drs. R.G. Walker, W. James and M.J. Risk also made helpful suggestions. My colleagues, Bob Dalrymple and John Knight, supplied data, lent computer programs, discussed results, and made numerous comments and suggestions, all of which facilitated completion of the study.

Financial assistance was provided by the Department of Energy, Mines and Resources, and by Imperial Oil Company, Limited. Bedford Institute of Oceanography gave logistic support including boats and other equipment; individuals associated with Bedford Institute who were especially helpful include Dr. Dale Buckley, Dr. Carl Amos, and Mr. Ted Corbett.

Many individuals provided a variety of technical assistance. Neal Schoen and Bob Mepham provided excellent field assistance. Brent Smith conscientiously tended the stage recorder, and Maureen Dickson sieved many of the sediment samples. Joyce Allen typed the manuscript and Verena Tunnicliffe aided with drafting; Jack Whorwood provided

photographic assistance, and Mr. Keith Stevens served as an able pilot.

TABLE OF CONTENTS

Page

ABSTRACT iii

ACKNOWLEDGEMENTS vi

LIST OF FIGURES xvii

LIST OF PLATES xxiii

LIST OF TABLES xxiv

LIST OF SYMBOLS xxvi

CHAPTER 1: INTRODUCTION 1

PURPOSE 1

SCOPE 2

Significance of the Study 3

Previous Work 4

Summary 7

CHAPTER 2: THE STUDY AREA 8

Location and Setting 8

LOCATION 8

BEDROCK GEOLOGY 11

SURFICIAL GEOLOGY 13

LATE-PLEISTOCENE AND HOLOCENE HISTORY 15

TABLE OF CONTENTS (continued) Page

Chapter 2 continued

Climate 17

Bathymetry 18

Summary 25

CHAPTER 3: HYDRAULICS 27

Tides 27

Fresh Water Input 35

Waves and Storms 41

WAVES 41

STORMS 41

Tidal Currents 45

Hydraulic Parameters 57

Summary 66

CHAPTER 4: DISTRIBUTION AND MORPHOLOGY OF THE MAJOR INTERTIDAL SAND BODIES 68

Distribution 68

Morphology 73

NEWPORT BAR 74

MITCHENER BAR 74

HANTSPORT BAR 77

MIDDLE GROUND 79

TABLE OF CONTENTS (continued) Page

Chapter 4 continued

BOOT ISLAND BAR 79

WESTERN BAR 82

Sand Body Stability 84

Summary 92

CHAPTER 5: BEDFORMS, OTHER SURFACE FEATURES, AND INTERNAL STRUCTURES 93

Bedforms 93

RIPPLES 95

MEGARIPPLES 100

SAND WAVES 109

TRANSVERSE BARS 113

Other Surface Features 113

Internal Structures 120

Summary 129

CHAPTER 6: GRAIN SIZE DISTRIBUTION 131

Textural Analysis 131

GENERAL TRENDS 132

BOOT ISLAND BAR 135

WESTERN BAR 139

MIDDLE GROUND 141

TABLE OF CONTENTS (continued) Page

Chapter 6 continued

HANTSPORT BAR 142

MITCHENER BAR 146

NEWPORT BAR 148

Textural parameters and Bedforms 149

Cumulative Curve Analysis 151

CUMULATIVE CURVE DISSECTION 156

Boot Island Bar 158

Western Bar 159

Middle Ground 159

Hantsport Bar 161

Mitchener Bar 161

Newport Bar 162

Synthesis 162

Summary 163

CHAPTER 7: SEDIMENT TRANSPORT 165

Sediment Transport Paths 165

Sediment Transport Rates 174

BEDFORM MIGRATION 174

TRANSPORT EQUATIONS 180

SEDIMENT TRANSPORT RATES NEAR EACH SAND BODY AND IN THE MAJOR CHANNELS 185

TABLE OF CONTENTS continued Page

Chapter 7 continued

Newport Bar 188

Mitchener Bar 189

Hantsport Bar 189

Middle Ground 190

Boot Island Bar 191

Western Bar 192

Major Channels 193

NET SEDIMENT TRANSPORT IN THE ESTUARY 194

Summary 196

CHAPTER 8: INTERPRETATION OF GRAIN SIZE DISTRIBUTIONS 197

Initiation of Motion 197

Cumulative Curve Shape 201

RELATION OF TRANSPORT MECHANISMS TO CUMULATIVE CURVES 201

HYDRAULIC SORTING 211

Textural Parameters 220

GENERAL TRENDS 220

TRENDS IN MEAN GRAIN SIZE ON A SAND BODY SURFACE 221

TABLE OF CONTENTS continued Page

Chapter 8 continued

Middle Ground 221
Hantsport Bar 222
Boot Island Bar 223
Summary 224
CHAPTER 9: BEDFORM STABILITY 226
Bedform Classifications 226
Stability Limits of Each Bedform Type 238
RIPPLES 238
MEGARIPPLES 242
SAND WAVES 243
TRANSVERSE BARS 243
TRANSITIONS BETWEEN BED CONFIGURATIONS 244
Overall Trends and Bedform Sequences 248
Summary 252
CHAPTER 10: CONTROL OF SAND BODY SHAPE AND POSITION BY SEDIMENT TRANSPORT PATHS 254
Individual Sand Bodies 258
BOOT ISLAND BAR 258
WESTERN BAR 260

TABLE OF CONTENTS continued

Page

Chapter 10 continued

MIDDLE GROUND 261

HANTSPORT BAR 264

MITCHENER BAR 267

NEWPORT BAR 267

CENTRAL SAND RIDGE 270

Stability of the System 271

Sediment Source 277

POSSIBLE SOURCES 277

River Input 277

Remnant Glacial Till 277

Shoreline Erosion 278

Tidal Current Transport of Sediment from Minas Basin 278

RELATIVE IMPORTANCE OF CONTRIBUTING SOURCES 279

Summary 284

CHAPTER 11: CONCLUSIONS 286

Hydraulic Environment 286

Grain Size Distribution 287

Bedforms and Internal Structures 288

TABLE OF CONTENTS continued

	Page
Chapter 11 continued	
Sand Body Position, Sediment Source, and System Stability	289
SAND BODY POSITION	289
SEDIMENT SOURCE	290
SYSTEM STABILITY	290
REFERENCES	292
APPENDIX A: ECHO SOUNDING AND SURVEYING METHODS	315
Echo Sounding	315
Surveying	317
APPENDIX B: MEASUREMENT OF CURRENT VELOCITY, WATER TEMPERATURE, AND SALINITY, ESTIMATION OF FRESH WATER INPUT	320
Measurement of Current Velocity, Water Temperature, and Salinity	320
Estimation of Fresh Water Input	321
APPENDIX C: INTERNAL STRUCTURE MEASUREMENT	367
APPENDIX D: SEDIMENT SAMPLE ANALYSIS	388
Mechanical Analysis	388
Calculation of Textural Parameters	388

TABLE OF CONTENTS continued

Page

APPENDIX E: CALCULATION OF SEDIMENT TRANSPORT RATES 401

Bedform Migration 401

Transport Formulae 402

Application 402

Limitations 403

APPENDIX F: PETROGRAPHY 415

LIST OF FIGURES

Figure		Page
2-1	Location Map of the Bay of Fundy and Minas Basin	9
2-2	Location of the Study Area	10
2-3	Bedrock Geology	12
2-4	Surficial Geology	14
2-5	Intertidal Facies	16
2-6	Wind Direction Frequencies	20
2-7	Bathymetry	21
2-8	Bottom Profiles Across the Estuary	23
3-1	Tidal Ranges During Field Work	29
3-2	Current Station Locations	31
3-3	Neap and Spring Tidal Curves	32
3-4	Vertical Salinity Profiles	39
3-5	Relation of Tidal Current Speed to the Tidal Curves	46
3-6	Tidal Ellipse at the Estuary Mouth	48
3-7	Water Surface Level as a Function of Cross-sectional Area, Water Volume, and Current Speed	51
3-8	Hypsometric Curve	52
3-9	Maximum Mean Current Speeds, Maximum Near-Bottom Current Speeds, and Net Discharge Directions	54
3-10	Current Cells	56

3-11 Relation of Shear Stress, Shear Velocity, and Stream Power to Current Speed 62
3-12 Current Speed, Froude Number, Roughness Height, and the Darcy-Weisbach Friction Factor Through a Tidal Cycle 65
4-1 Location of Sand Bodies 69
4-2 Comparison of the Avon River Estuary to Meso- and Macrotidal Estuary Models 71
4-3 Contour Map and Cross-section of Newport Bar 75
4-4 Contour Map and Cross-section of Mitchener Bar 76
4-5 Contour Map and Cross-section of Hantsport Bar 78
4-6 Contour Map and Cross-section of Middle Ground 80
4-7 Contour Map and Cross-section of Boot Island Bar 81
4-8 Contour Map and Cross-section of Western Bar 83
4-9 1865 British Admiralty Map 89
5-1 Sinuous Ripples 96
5-2 Linguoid Ripples 97
5-3 Bedform Distribution at the Estuary Head 98
5-4 Bedform Distribution at the Estuary Mouth 99
5-5 Megaripples 101
5-6 Comparison of the Two Megaripple Types 103
5-7 Falling Water Marks on a Megaripple 105

5-8	Scour in a Megaripple Trough	106
5-9	Spur in a Megaripple Trough	107
5-10	Liquefaction Surface on a Megaripple	108
5-11	Length Versus Height for Megaripples and Sand Waves	110
5-12	Aerial View of Sand Waves	111
5-13	Ground View of a Sand Wave	112
5-14	Transverse Bars	114
5-15	Wave Ripples and Planed-off Surface	116
5-16	Ice-rafted Boulder with a Current Crescent	117
5-17	Mud Pebbles	118
5-18	Mud Drapes on Ripples	119
5-19	Internal Structures of Ripples	121
5-20	Internal Structures of Megaripples	123
5-21	Flaser Bedding	125
5-22	Parallel Lamination	126
5-23	Internal Structures of a Megarippled Sand Wave	128
6-1	Estuary Mouth Sediment Sample Locations	136
6-2	Mean Grain Sizes at the Estuary Mouth	137
6-3	Sediment Sorting at the Estuary Mouth	138
6-4	Skewness at the Estuary Mouth	140
6-5	Estuary Head Sediment Sample Locations	143
6-6	Mean Grain Sizes at the Estuary Head	144

6-7 Sediment Sorting at the Estuary Head 145

6-8 Skewness at the Estuary Head 147

6-9 Mean Size Versus Sorting of 3 Bedform Types 150

6-10 Typical Group 1, 2, and 3 Cumulative Curves 153

7-1 Ebb and Flood Channels 166

7-2 Stages in Bedform Reversal 168

7-3 Flood and Ebb dominant Megaripples 170

7-4 Internal Structures of Flood and Ebb Megaripples 171

7-5 Net Sediment Transport Directions 173

7-6 Sediment Transport Rates at the Estuary Mouth 176

7-7 Sediment Transport Rates at the Estuary Head 177

7-8 Comparison of Measured and Predicted Sediment Transport Rates 183

7-9 Predicted Sediment Transport Rates Through a Tidal Cycle 186

8-1 Predicted Competence Versus Coarsest Observed Grain Size 200

8-2 Settling Velocity at the C - A Boundary Versus Maximum Shear Velocity 204

8-3 Predicted Coarsest Suspended Grain Size Versus Grain Size at the C - A Boundary 207

8-4 Settling Velocity at the A - B Boundary Versus Maximum Shear Velocity 210

8-5 Hydraulic Sorting as a Function of Differential Transport Rates 216

9-1 Relation of Observed Bedform to Water Depth and Current Speed Through a Tidal Cycle 230

9-2 Observed Bedform as a Function of A) Maximum Current Velocity and Water Depth and B) Current Speed and Mean Grain Size 231

9-3 Observed Bedform as a Function of Maximum Shear Velocity and Mean Grain Size 233

9-4 Bedforms as a Function of Stream Power and Median Grain Size 234

9-5 Froude Number Versus Water Depth/Median Grain Size as a Criterion for Bedform Stability Fields 237

9-6 Mean Speed Versus Water Depth Through a Tidal Cycle for 3 Stations 246

9-7 Comparison of Bedform Sequences for A) the Avon River and B) Boothroyd (1969) 251

10-1 Relation of Bottom and Surface Current Directions to Sand Bodies 256

10-2 Surface and Bottom Current Directions Near Hantsport Bar 257

10-3 Formation Process of Middle Ground 263

10-4 Formation of Hantsport Bar 266

10-5 Mitchener Bar and Scroll Bars 268

10-6 Comparison of Newport Bar to Flood Tidal Deltas 269

10-7 Contour Map and Soundings of Sand Bodies at the Estuary Head 272

10-8 Contour Map and Soundings of Sand Bodies at the Estuary Mouth 273

10-9 Comparison of Cross-sections Across the Estuary from 3 Surveys 275

10-10 Areas of Lag, Rapid Shoreline Erosion, and Predicted and Measured Residual Currents in Windsor Bay 283

A-1 Echo Sounding Traverse Locations 316

LIST OF PLATES

Plate		Page
4-1	1963 aerial photograph of the estuary mouth	85
4-2	1974 aerial photograph of the estuary mouth	86
4-3	1963 aerial photograph of the estuary head	87
4-4	1974 aerial photograph of the estuary head	88

LIST OF TABLES

Table Page

2-1 Mean Monthly Precipitation, Wind Speed, and Temperature 19

3-1 Fresh Water Input 37

3-2 Effects of Hypsometry at 3 Cross-sections 49

3-3 Turbulence through a Tidal Cycle 59

3-4 Maximum Mean Velocity, Shear Velocity, Shear Stress, and Stream Power 63

4-1 Thickness and Elevation of Sand Bodies in 1865 and 1975 91

5-1 Comparison of Bedform Terminology 94

5-2 Summary of Megaripple Measurements 102

5-3 Summary of Internal Structures 122

6-1 Comparison of Textural Parameters from 1974 and 1975 133

6-2 Average Grain Size Distribution for Each Sand Body and the Whole System 155

6-3 Results of Cumulative Curve Dissection 157

7-1 Sediment Transport Rates for 2 Stations with 1 large Transport Rate 187

7-2 Net Transport Rates for 4 Cross-sections 195

8-1 Initiation of Movement 199

LIST OF TABLES continued

Page

8-2 Initiation of Intermittent Suspension 205

8-3 Criterion for Transition to Suspension 209

8-4 Relative Transport Rates of Grain Size Fractions 212

8-5 Flood Sediment Transport Rates for Station Horton South 215

9-1 Criteria for Bedform Stability 241

10-1 Average Bottom Current Deflections on Each Sand Body 259

10-2 Petrography 280

B-1 Current Measurements 324

B-2 Temperature and Salinity Measurements 346

B-3 Hydraulic Parameters 361

C-1 Bedform Measurements 374

C-2 Internal Structure Measurements 379

D-1 Grain Size Distributions 390

E-1 Sediment Transport Rates Computed with Engelund and Hansen's Transport Formula 406

LIST OF SYMBOLS

Symbol	Meaning
C	wave celerity
d, h	total water depth
D_f	fall diameter
D_{50}	median grain size
D_{35}	grain size of 35th percentile from coarse end
f	Darcy-Weisbach friction factor
F	wave fetch
Fr	Froude number
g	force of gravity
H	wave height
k	roughness height
L	lower stadia mark
m_o	slope of a line
P	wave period
Q	water discharge
Q_s	sediment discharge
Re	Reynolds number
s, σ	standard deviation

LIST OF SYMBOLS continued

Symbol	Meaning
T	turbulence
U	current velocity
$\bar{U}$	mean current velocity
U_{100}	current velocity 1 m from the bottom
U_p	upper stadia mark
U_*	shear velocity
$\sqrt{\bar{v}'}$	root mean square of vertical turbulence fluctuations
w	settling velocity
$\bar{x}$	mean
y	partial water depth
Z_o	depth of zero velocity
γ	specific weight of water
γ_s	specific weight of sediment
$\varkappa$	von Karman's constant
λ	wavelength
μ	water viscosity
ρ	water density
τ	shear stress
τU_*	stream power

"... sediments are a sort of epic poem of the earth. When we are wise enough, perhaps we can read in them all of past history. For all is written here."

- Rachel Carson

CHAPTER 1

INTRODUCTION

The major morphological features of coastlines are determined primarily by the tidal range. Davies (1964) and Hayes et al. (1973) have divided coasts into microtidal (mean range < 2 m), mesotidal (mean range 2-4 m), and macrotidal (mean range > 4 m).

All three types of coast have estuaries, defined by Pritchard (1967) as "a semi-enclosed coastal body of water which has a free connection with the open sea and within which the water is measurably diluted with fresh water derived from land drainage". Many studies exist of the hydraulics and sediments of micro- and mesotidal estuaries, but few of macrotidal estuaries; macrotidal estuaries are common and are the major loci of sediment accumulation on macrotidal coasts (Hayes, 1975).

PURPOSE

The main purpose of this study was to examine sediment dynamics on intertidal sand bodies within a macrotidal estuary; the particular one chosen for study was the Avon River estuary, Nova Scotia. Tidal range in the Avon is 15.6 m at spring tide (Canadian Hydrographic Service, 1974-1976). The hydraulic environment of the

Avon was investigated in conjunction with the distribution and morphology of sand bodies, bedforms and internal structures, and grain size distribution. The object was to determine the process - response relationships between the hydraulic and sedimentologic parameters. A secondary aim was to determine the process responsible for the original influx of sediment into the system.

Field work was conducted during the months of June, July and August in 1974 and 1975, from mid-June to the beginning of August 1976, and for five days in February 1976. Most field work was carried out using small boats. Other equipment and methods will be discussed in later chapters.

SCOPE

The study dealt with the major intertidal sand bodies in the Avon River estuary; minor intertidal sand bodies were not examined because they are subaerially exposed only for short periods of time. Subtidal sediments were not studied; echo sounding records indicate only one major subtidal sand body in the system (see Fig. 4-2). Swift et al. (1967) made a preliminary investigation of subtidal sediments in part of the study area; their results are shown in Figure 2-5. Fine sediments were not examined as there is but one significant accumulation in the study area and it is a direct result of a causeway constructed in 1970; this study attempted to deal with natural phenomena only.

Winter conditions were not studied in detail; four of the six major sand bodies are inaccessible in winter and the other two can be reached only for short time periods. Observations made during a brief period in February 1976 indicated few of the winter conditions noted in other parts of Minas Basin (Knight and Dalrymple, 1976). For example, no frozen ice-crust was observed on the surfaces of the sand bodies. However, temperatures were unseasonably high during the field visit; normal winter conditions may alter the sand bodies and produce the features observed by Knight and Dalrymple (1976).

Significance of the Study

This study represents one of the few investigations of sediment dynamics in macrotidal estuaries. Also, it completes a set of studies of the major intertidal sand body complexes in Minas Basin.

Sediments have been studied in many mesotidal estuaries on the eastern coast of the United States (Coastal Research Group, 1969; Meade, 1969; Schubel, 1971; Ludwick, 1974; Visher and Howard, 1974), in the North Sea (van Straaten and Kuenen, 1957; Postma, 1961; Reineck, 1967; Oomkens and Terwindt, 1960) and in other areas (Schou, 1967; Kulm and Byrne, 1967). This is an abb[illegible]iated list; none of the areas are macrotidal.

Relatively few macrotidal estuaries have been studied. Besides Cobequid Bay, such studies include the Wash, England (Evans, 1965), Mont Saint-Michel Bay, France (Larsonneur, 1975; Philiponneau, 1956; Bourcart and Boillot, 1960; Dolet et al., 1965), the River Tay, Scotland (Green, 1975), and the Ord River, Western Australia (Wright et al., 1973, 1975). Measurable salinity gradients exist in the River Tay, the Ord River and part of Mont Saint-Michel Bay; therefore they are estuaries according to the definition of Pritchard (1967); the Wash may be an estuary but Evans (1965) presents no salinity data. The present study adds to the literature an example of macrotidal estuarine sedimentation.

Most major intertidal sand body complexes in Minas Basin have been studied. These include Five Islands studied by Klein (1970) and Cobequid Bay studied by Swift and McMullen (1968) and Dalrymple et al. (1975). The Avon River estuary contains the only major sand body complex that had not been examined in detail; thus this study complements other investigations.

Previous Work

Intertidal sediments in Minas Basin have been studied by Klein (1963, 1964, 1968a, 1968b, 1970), Swift et al. (1967), Swift and McMullen (1968), Atlantic Tidal Power Engineering and Management Committee (1969), Knight (1971, 1972, 1977), Klein and Whaley (1972), Pelletier and McMullen (1972), Dalrymple (1973, 1977), Middleton (1972), Dalrymple et al. (1975), Knight and Dalrymple (1975). Many of these are concerned with general patterns of sediment distribution in the whole basin or large portions of it, others, especially Klein (1970), Knight (1971, 1972, 1977), Klein and Whaley (1972), and Dalrymple (1973, 1977) provide detailed descriptions of sediment distribution, current velocities, and bedforms and internal structures on specific intertidal sand bodies. In addition, Balazs and Klein (1972) have examined mineralogy and roundness of some intertidal sands from the Minas Basin.

Previous studies of Minas Basin intertidal sediments indicate that sand accumulates as sand bodies with asymmetric cross-sections (Klein, 1970; Dalrymple et al., 1975; Knight and Dalrymple, 1975); most sand bodies are located in Cobequid Bay and in the Avon River estuary and are parts of large ebb tidal deltas (see Fig. 2-2). Bedforms have been grouped into ripples, megaripples, and sand waves (terminology of Klein, 1970); each bedform type forms under different hydraulic conditions (Klein and Whaley, 1972; Dalrymple, 1977; Knight, 1977). Bedform flow regime decreases towards the eastern end of Cobequid Bay (Middleton et al. 1976). Grain size distributions generally reflect local hydaulic conditions (R. Dalrymple, 1976, pers. comm.); mean grain size decreases towards the eastern end of Cobequid Bay and towards the head of the Avon River estuary (Pelletier and McMullen, 1972).

There have been four previous studies of sediments in the Avon River Estuary. The earliest was by Kindle (1917) who studied bedforms. He distinguished three types of bedforms; from his descriptions (Kindle, 1917) these bedform classes correspond to the ripples, megaripples, and transverse bars described in the present study (see Chapter 5). Unfortunately, Kindle's study area was south of the causeway at Windsor (see Fig. 2-2); that area is now a man-made lake so it is impossible to replicate his observations and measurements.

Swift et al. (1967), Swift and McMullen (1968), and Pelletier and McMullen (1972) investigated sediment distribution and current velocity in the Avon River estuary. Swift, McMullen, and Lyall (1967) and Swift and McMullen (1968) described Western Bar and Middle Ground as part of a delta (see Fig. 4-1 and the discussion in Chapter 4) and recorded current velocities in the main channel at the estuary mouth and in the channel to the east of Middle Ground. Pelletier and McMullen (1972) have mapped mean grain size and sorting of bottom sediments in the Avon River estuary. Their results do not coincide with the results of the present study; comparison of the two sets of results is presented in Chapter 6.

Previous workers in the Minas Basin have described forms of sediment accumulation, bedforms, grain size distributions, and hydraulics, and have exposed relationships between the hydraulic environment and each of the sedimentological parameters; the present study extended this research into a macrotidal estuary. Prior to the present study, the Avon River estuary had not been studied in detail; sediment distribution had not been related to hydraulics. The major contributions of the present study include a detailed examination of hydraulics, sand body, grain size, and bedform distribution as well as an analysis of the process - response relationships of hydraulics and sediments in a macrotidal estuary.

Summary

The purpose of this study is to determine the process - response relationships between the hydraulic environment and the position and morphology of sand bodies, bedforms and internal structures, and grain size distribution in the macrotidal Avon River estuary, Nova Scotia. The study is limited to summer conditions and coarse sediments on the major intertidal sand bodies in the system; it represents one of the few investigations of sediments in a macrotidal estuary and complements studies of the other major sand body complexes in Minas Basin. Intertidal sediments in Minas Basin have previously been examined by several workers: four of these studies dealt with the Avon River estuary although not in detail.

CHAPTER 2

THE STUDY AREA

Location and Setting

LOCATION

The Avon River estuary is located in central Nova Scotia; the town of Windsor, at the southern end of the study area, has co-ordinates of 45°00' north latitude and 64°08' west longitude (Fig. 2-1). The Avon empties into the southwestern part of Minas Basin; the basin forms the northeastern arm of the Bay of Fundy (Fig. 2-1). The study area includes sand bodies that extend 8 km beyond the point where the Avon enters Minas Basin, and the first 16 km upstream of the river mouth. The reach within the Avon is roughly 2 km wide; the study area widens to 6 km at its northern end (Fig. 2-2).

Three major rivers, the Kennetcook, the Avon, and the St. Croix, discharge into the study area; discharge from the Avon is controlled by a sluice gate in the causeway across the river at Windsor (Fig. 2-2). (Discharge volumes will be discussed in Chapter 3.) The three rivers account for 1626 km^2 of the total 1835 km^2 drainage basin area of the Avon River System. A fourth river, the Cogmagun, has a drainage basin area of 142 km^2; the remaining 67 km^2 is drained by small creeks, (Fig. 2-4). Drainage basins ~~are depicted~~ on Figure 2-1.

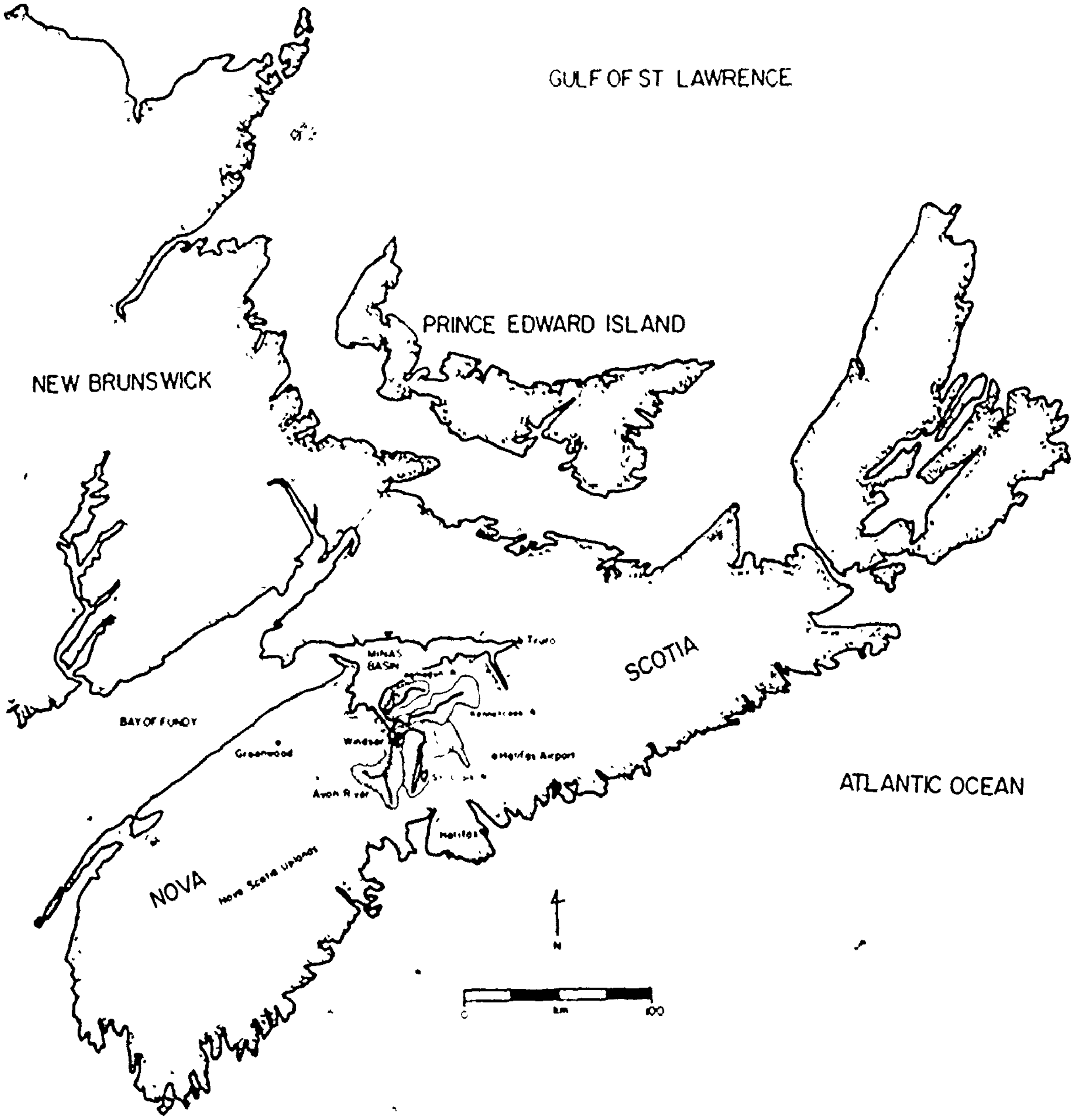
GULF OF ST LAWRENCE
PRINCE EDWARD ISLAND
NEW BRUNSWICK
MINAS BASIN
Truro
SCOTIA
BAY OF FUNDY
Greenwood
Windsor
Halifax Airport
Avon River
ATLANTIC OCEAN
Halifax
NOVA
Nova Scotia Uplands
N
0
km
100

Fig. 2-1. Location map of the Bay of Fundy and Minas Basin. Drainage basins of rivers discharging into the Avon River are hatched.

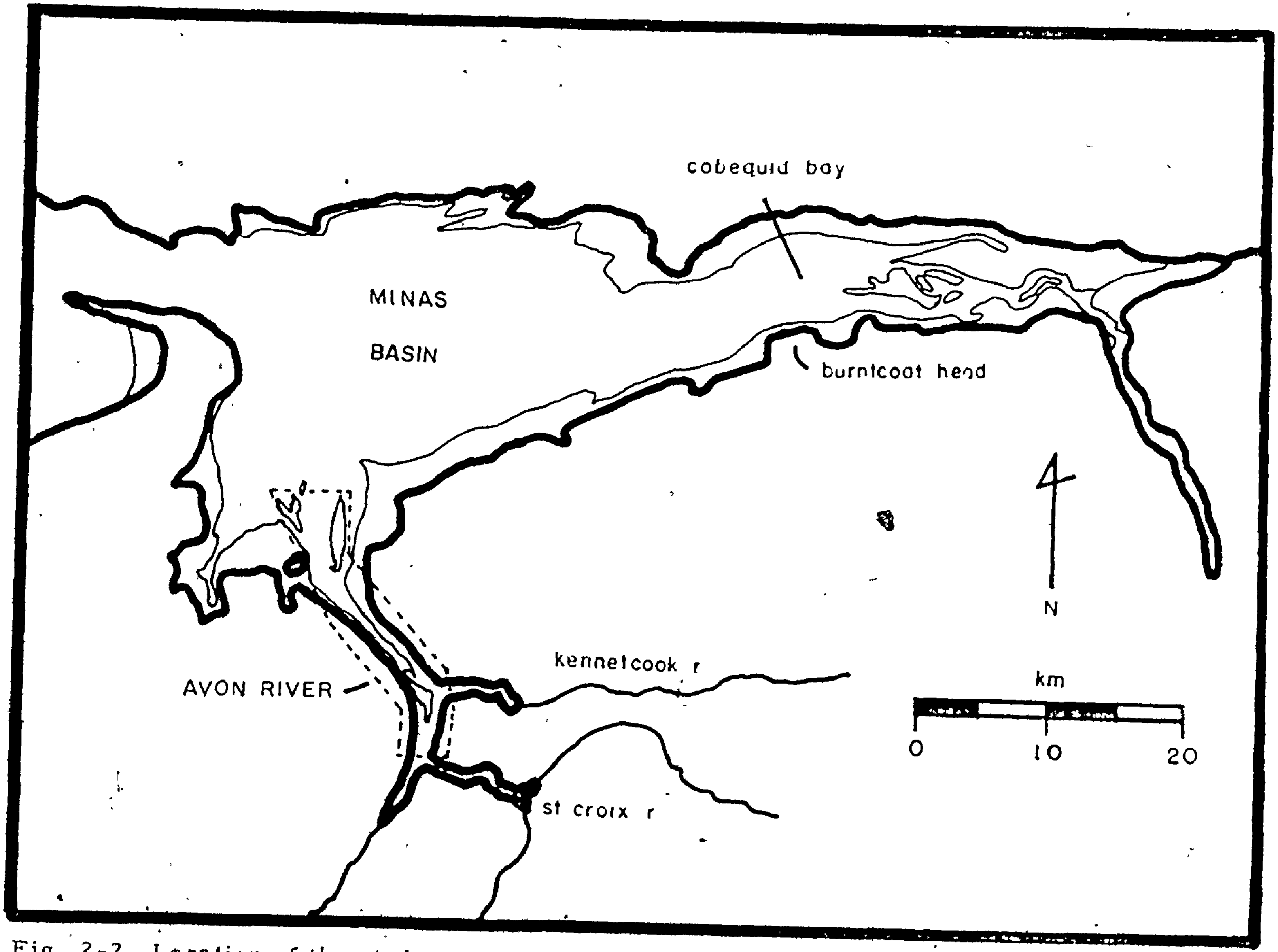
cobequid bay
MINAS
BASIN
burntcoat head
N
kennetcook r
km
0
10
20
AVON RIVER
st croix r

Fig. 2-2. Location of the study area; the study area is enclosed with a dashed line. The high tide line is the heavy line and the low tide line is the thin line.

BEDROCK GEOLOGY

Bedrock geology of the study area was mapped by Bell (1929) and Crosby (1962). Four major units underlie the study area and outcrop on the shores of the estuary. The oldest unit is the Mississippian Horton Group which Bell (1929) divides into the Horton Bluff Formation and the Cheverie Formation. The Horton Bluff Formation comprises part of the western shore of the study area (Fig. 2-3), and has been described as dark shales and sandstones by Bell (1960). The Cheverie Formation overlies the Horton Bluff Formation and forms the northeastern shore and part of the western shore of the Avon (Fig. 2-3); it is primarily red and grey shale with sandstones (Bell, 1929).

The Cheverie Formation is overlain by the Windsor Group, a Mississippian unit consisting of limestone, calcareous shale, gypsum, anhydrite, and red shale (Crosby, 1962). The Windsor Group outcrops along both shorelines in the southern part of the study area (Fig. 2-3). The Pennsylvanian (?) Scotch Village Formation occurs in the study area according to Crosby (1962) although Bell (1929) does not agree. It is composed of grey sandstone and occurs on the eastern shore of the Avon River just north of the Kennetcook River (Fig. 2-3). The Triassic Annapolis Formation is the youngest bedrock unit in the study area. It consists of red sandstone, conglomerate, and breccia (Bell, 1929), and its oldest member, the Wolfeville Sandstone, occurs in the northwest part of the study area (Fig. 2-3).

LEGEND

TRIASSIC

☐ WOLFVILLE SANDSTONE: red conglomerate and sandstone; minor red shale

PENNSYLVANIAN

▒ SCOTCH VILLAGE FORMATION: buff-weathering grey sandstone

MISSISSIPPIAN

░ WINDSOR GROUP: red shale, limestone, gypsum, anhydrite and salt

▧ PEMBROKE FORMATION: limestone conglomerate and limestone; minor sandstone and shale

■ MACUMBER FORMATION: thinly bedded arenaceous limestone

} ☐ red shale, limestone, gypsum, anhydrite and salt

░ HORTON GROUP: grey and red shale, siltstone, sandstone and arkose.

☐ HORTON GROUP: dark shale; sandstone conglomerate

ORDOVICIAN

▩ HALIFAX FORMATION: slate and minor siltstone

FAULT - - - - - - - ∿∿∿∿

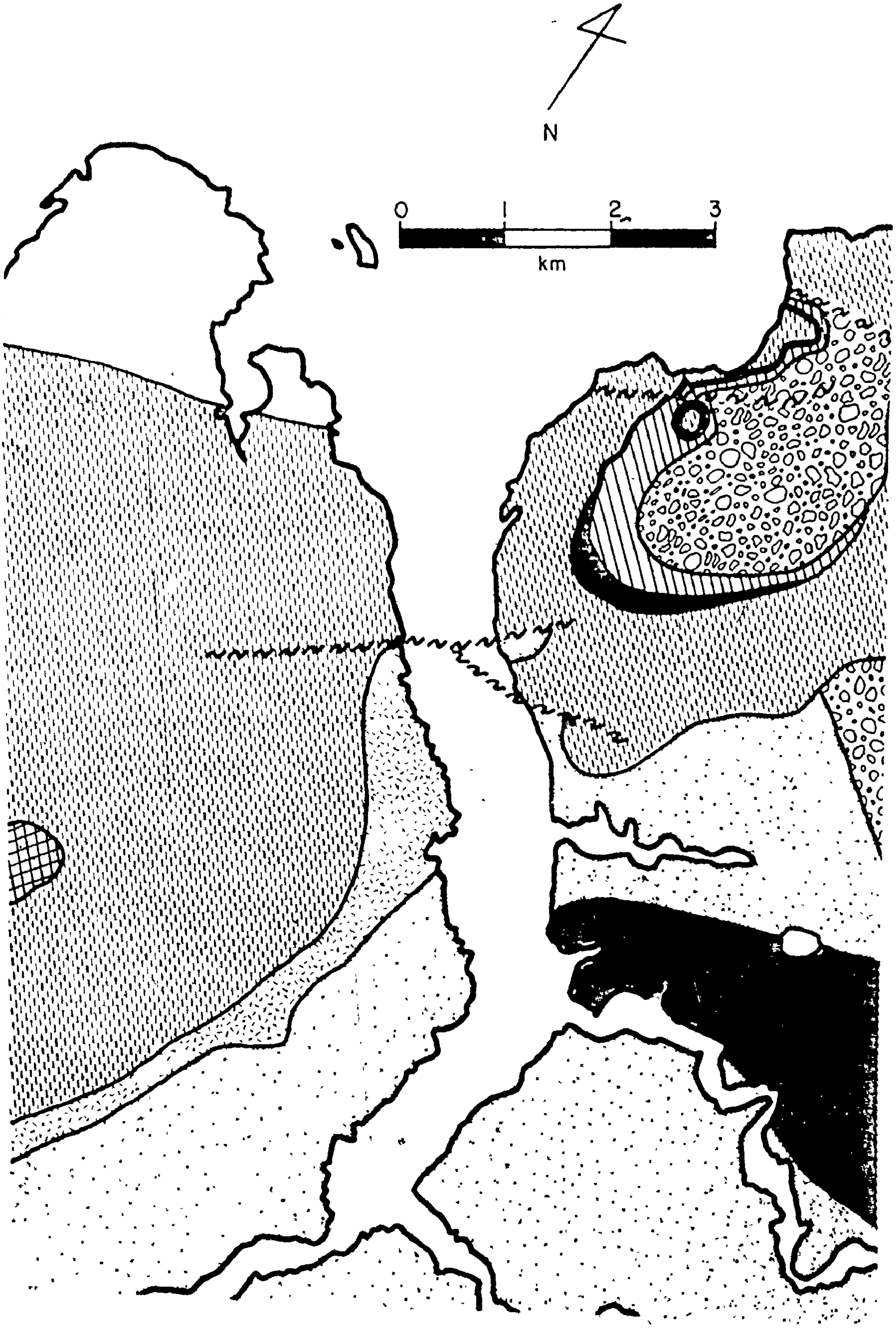

Fig. 2-3. Bedrock Geology

Bell (1929) and Crosby (1962) have mapped a fault that strikes perpendicular to the axis of the Avon River and forms the contact between the Horton Bluff Formation and the Cheverie Formation on the western shore of the river. The fault continues into the river where it branches and causes an offset on the eastern shore (Fig. 2-3). Another fault exists in the northeastern part of the study area (Fig. 2-3); neither Bell (1929) nor Crosby (1962) indicates that it extends into the Avon River.

SURFICIAL GEOLOGY

The map of surficial geology in the study area (Fig. 2-4) differs from the bedrock map (Fig. 2-3) because of Pleistocene till and supratidal salt marsh overlying the bedrock. The surficial map was constructed from aerial photographs and from a surficial map by Trescott (1969). Many areas of former salt marsh have been reclaimed as farmland; these are identifiable by the presence of dikes along the shore. Supratidal shorelines vary from low-lying salt marsh to cliffs up to 21.6 m high (Fig. 2-4); in general, the Horton Bluff Formation and Pleistocene till form the highest cliffs.

The intertidal zone of the study area, exclusive of sand bodies, is up to 2.5 km wide and includes several sedimentary facies. These include a wave-cut platform, gravel with a mud veneer, mud flats, gravel and cobbles, and beaches. A large wave-cut platform extends to the north and east of Boot Island (Fig. 2-5). The platform has been cut in

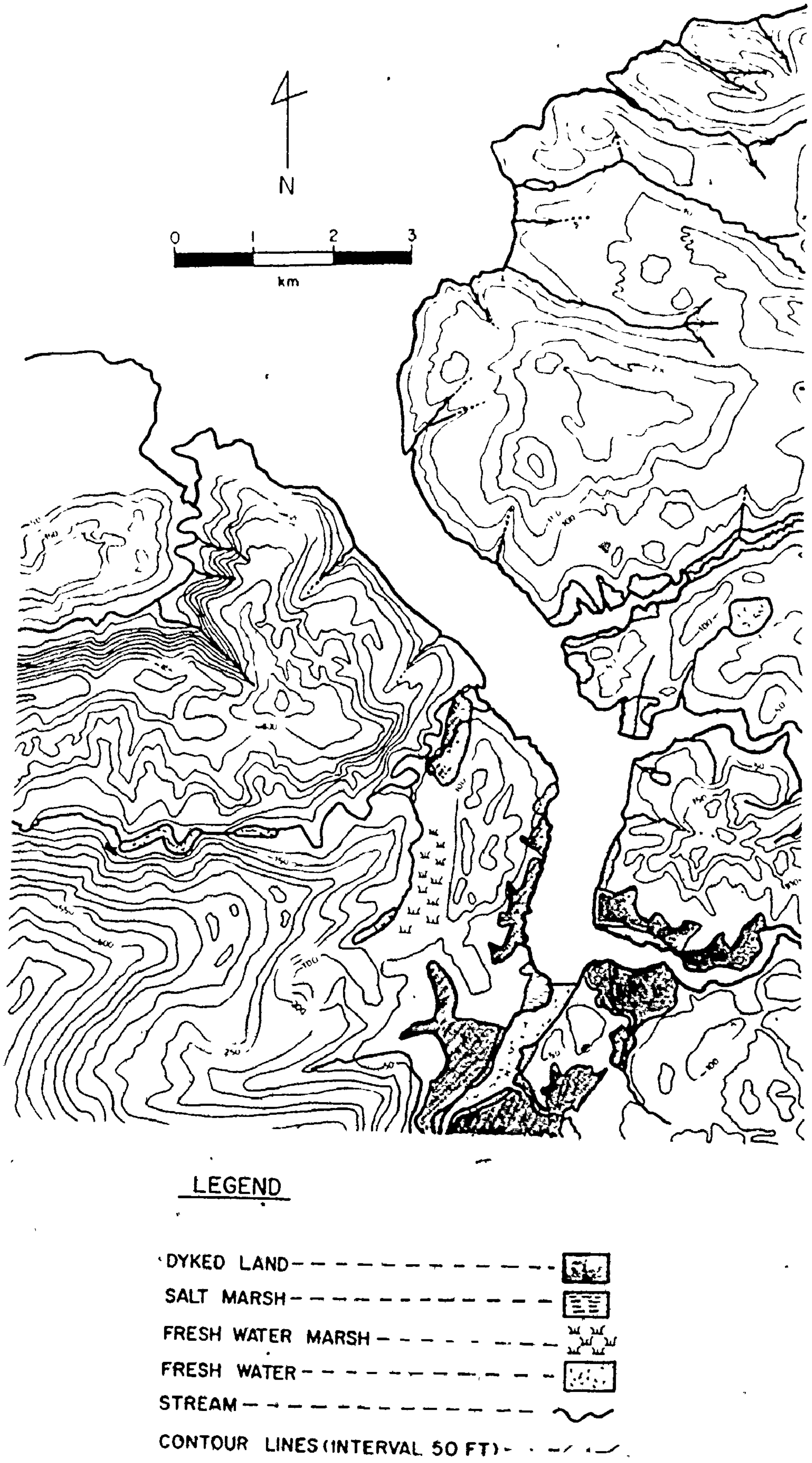
N
0
1
2
3
km
LEGEND
DYKED LAND
SALT MARSH
FRESH WATER MARSH
FRESH WATER
STREAM
CONTOUR LINES (INTERVAL 50 FT)

Fig. 2-4. Surficial Geology

red sandstone of the Triassic Wolfeville Sandstone and is covered by scattered cobbles and a patchy veneer of sand and gravel. Most locations have a higher and lower intertidal facies. In a few areas the highest intertidal facies is a beach of sand or shingle (Fig. 2-5); beaches consist of sediment accumulations just below the high water mark and generally have poorly developed berms. In many areas, the higher intertidal facies is gravel with a mud veneer (Fig. 2-5); the mud veneer generally is less than 10 cm thick. (Figure 2-5 was derived from field observations and aerial photograph interpretation.) Gravel and cobbles comprise the most common lower intertidal facies; it occurs almost everywhere and in most places extends to lower low water. A few areas have a sandy lower intertidal facies (Fig. 2-5). Harrow marks are common in areas of cobbles and sand.

Two mud flats are adjacent to the study area, one south of Boot Island and the other immediately north of the causeway at Windsor (Fig. 2-5). Prior to construction of the causeway in 1970 the latter mud flat did not exist (see Plates 4-3 and 4-4); by 1975 the mud had accreted vertically to a thickness of almost 5 m.

LATE-PLEISTOCENE AND HOLOCENE HISTORY

Most glacial remains in Nova Scotia stem from the Wisconsin glaciation; earlier Pleistocene glacial events are not well recorded (Greenwood and Arnott-Davidson, 1972). Prest and Grant (1969) present

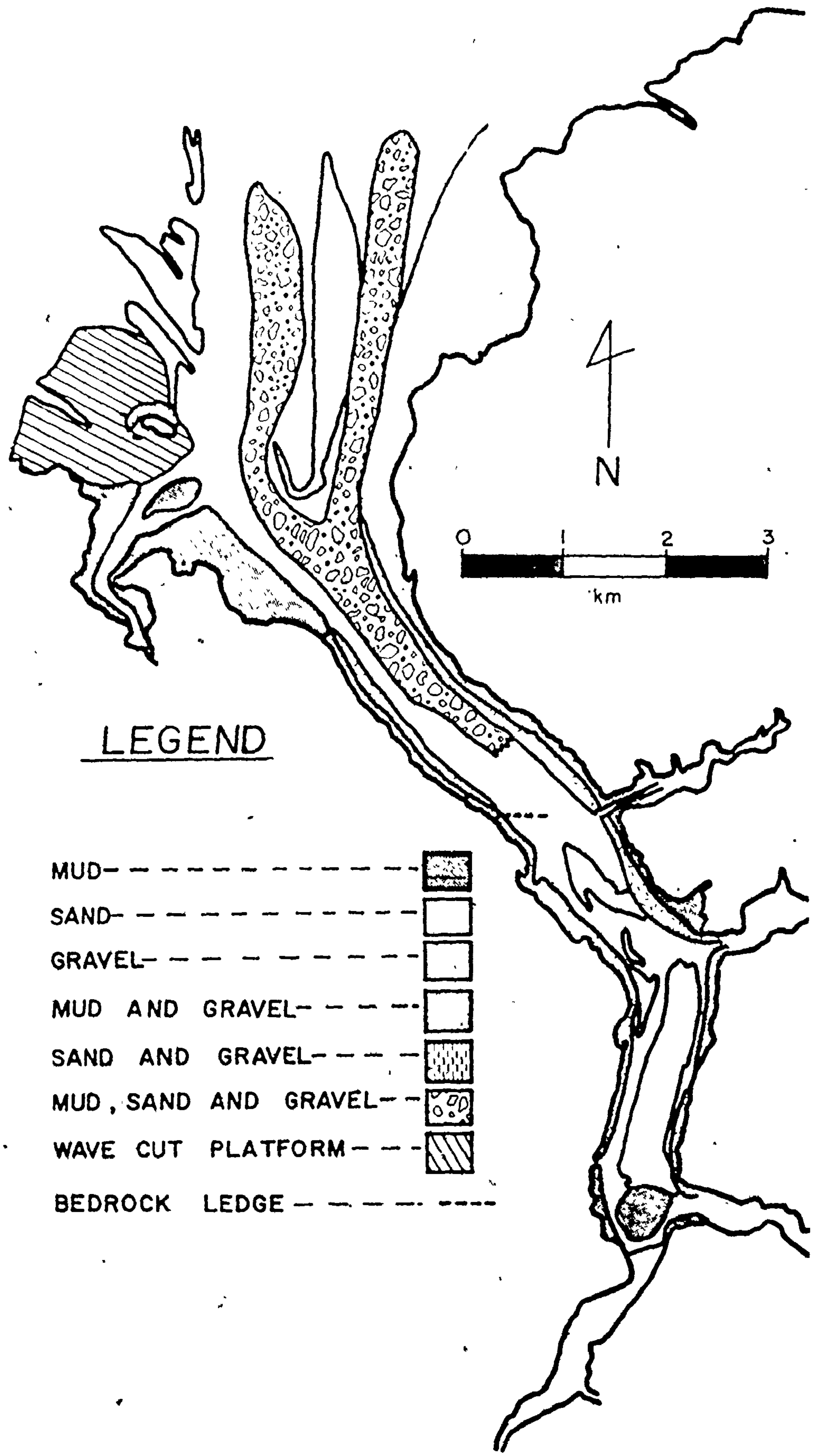
N
0
1
2
3
km
LEGEND
MUD
SAND
GRAVEL
MUD AND GRAVEL
SAND AND GRAVEL
MUD, SAND AND GRAVEL
WAVE CUT PLATFORM
BEDROCK LEDGE

Fig. 2-5. Intertidal Facies; subtidal facies from Swift et al. (1967)

evidence for two sets of retreating ice-flow features in the Bay of Fundy region. Flow direction of the older set was from the north; the more recent set results from a radiating flow pattern centered to the southwest of the Avon River. Prest and Grant (1969) believe that the more recent set was formed by an ice block stranded in the Nova Scotia uplands (Fig. 2-1). Thus, in the study area, flows from retreating glaciers originally were from the north and later came from the southwest. The latter flow direction probably existed by 14,000 BP; this post-dates the advance of the sea into the Bay of Fundy (Prest and Grant, 1969) since sea level rise began 15,000 to 20,000 BP (Milliman and Emery, 1968).

Grant (1970) found rates of sea level rise of 0.30 m per century for the Bay of Fundy during the last 4,000 to 6,000 years. At least 0.15 m per century is due to the increase in tidal range that Grant (1970) estimates to have begun about 6,000 years ago. The sea level rise of the past few thousand years is still continuing but calculations indicate that tidal range in the Bay of Fundy is no longer increasing (Grant, 1970). The Avon River, and the entire Bay of Fundy system, is experiencing a continued sea level rise of about 0.15 m per century (Grant, 1970).

Climate

The climate of Nova Scotia is humid and temperate. Trescott (1969) reports a mean annual temperature at Windsor, based on 77 years of records, of 6.8°C; the fifty year average for Windsor is 134 frost-free days (Canada Department of Transport, Met. Branch, 1967). Mean annual precipitation averages 1.07 m at Windsor based on seventy-seven years of records (Trescott, 1969). An annual mean snowfall of 1.64 m is included in the total precipitation. (Fresh water input into the Avon River estuary as a result of this precipitation will be discussed in Chapter 3.)

Wind data for the period 1968 to 1972 from Greenwood, Truro and Halifax International Airport (Fig. 2-1) has been compiled from Canada Department of Transport records by R.J. Knight and R.W. Dalrymple (Canada Department of Transport, Met. Branch, 1968-1972). Mean annual wind speed is 15.6 km per hour; winter speeds average 17.4 km per hour and summer speeds 14.8 km per hour. A rose diagram of wind direction frequencies is presented in Figure 2-6. A summary of wind, temperature, and precipitation data is listed in Table 2-1.

Bathymetry

The bathymetry of the study area is shown in Figure 2-7; the map was constructed from echo sounding records and Canadian Hydrographic Service Chart 4140 (Canadian Hydrographic Service, 1972). (See Appendix A for details of echo sounding and map-making methods.) The depth datum is higher high water. At the north end of the system, there are two deep channels with north-south oriented axes separated by an intertidal sand body named Middle Ground (Fig. 2-7). Maximum depth

TABLE 2-1. Mean Monthly Precipitation, Wind Speed, and Temperature

	Jan.	Feb.	Mar.	Apr.	May	June	July	Aug.	Sept.	Oct.	Nov.	Dec.	Mean Annual
Precipitation (cm)													
data from Trescott (1969)	10.4	7.9	8.4	7.6	8.1	8.1	6.9	7.1	10.9	10.7	11.2	9.7	107.1
Wind Speed (km/hr)													
compiled by R.J. Knight and R.W. Dalrymple	16.7	16.7	18.2	16.7	15.9	14.8	13.5	13.9	12.7	14.8	15.9	17.7	15.6
Temperature (°C)													
data from Trescott (1969)	-5.0	-5.6	-1.7	3.9	11.1	15.0	20.0	18.9	13.9	4.4	0.0	-2.8	6.8

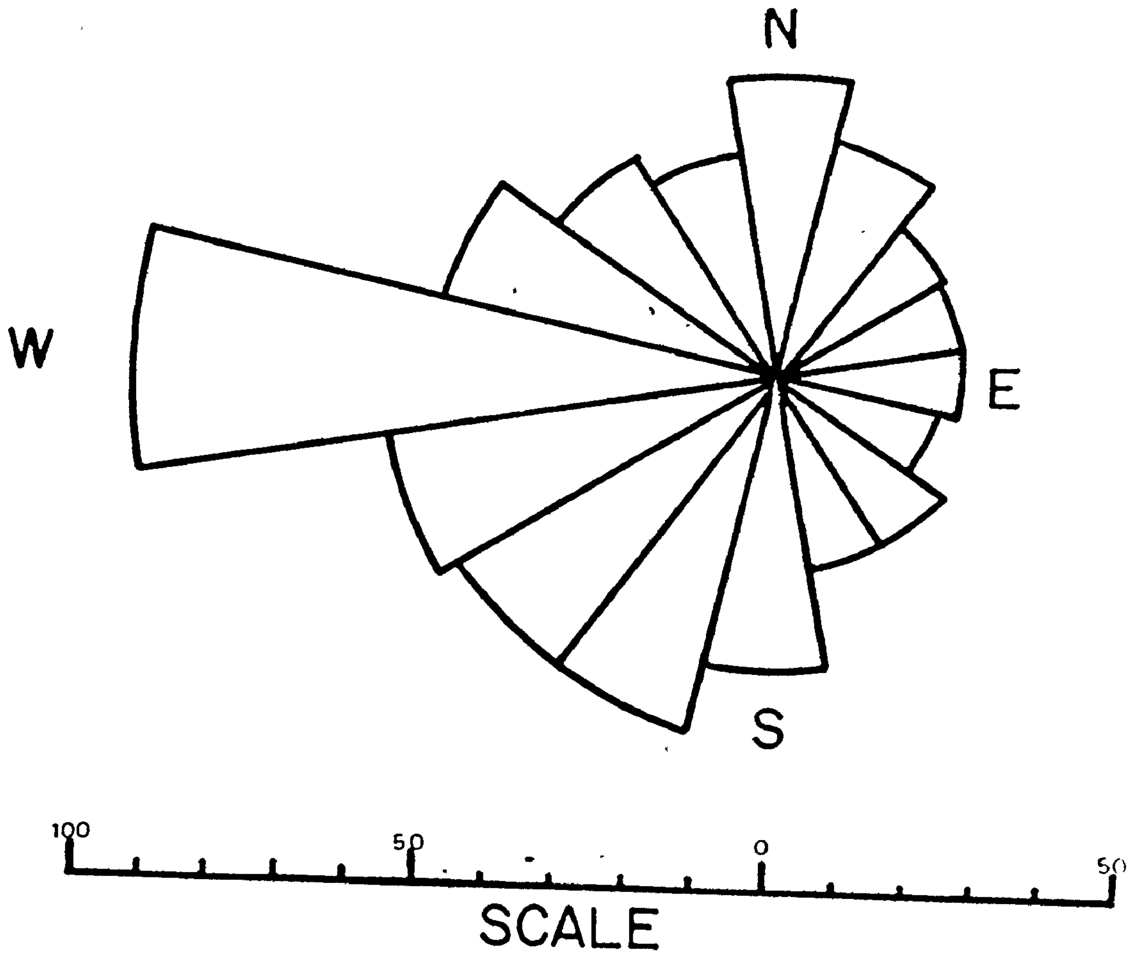

Fig. 2-6. Wind direction frequencies; the scale is frequency of occurrence per year

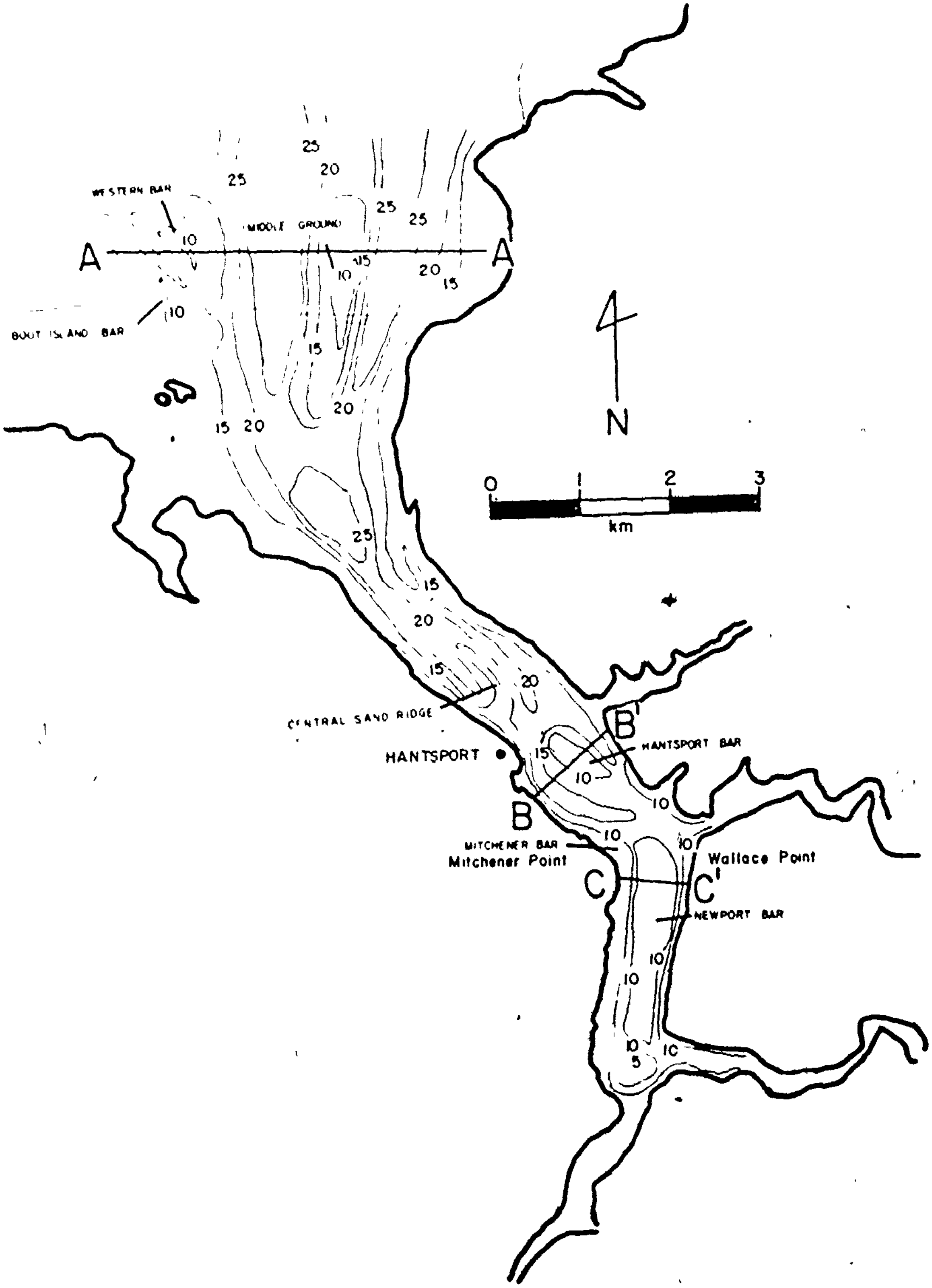
WESTERN BAR
MIDDLE GROUND
BOOT ISLAND BAR
A
A'
25
20
25
25
25
10
10
15
20
15
10
15
20
15
20
25
15
20
15
20
CENTRAL SAND RIDGE
HANTSPORT
B
B'
HANTSPORT BAR
15
10
10
10
10
MITCHENER BAR
Mitchener Point
C
C'
Wallace Point
NEWPORT BAR
10
10
10
5
10
N
0
1
2
3
km

Fig. 2-7. Bathymetry; the contour interval is 5 m. Depths are m below higher high water. The labelled cross-sections are illustrated in Figure 2-8 and also were used for hypsometric calculations (see Chapter 3).

is 25.4 m in the western channel and 24.5 m in the eastern; the two channels merge to the south of Middle Ground. Two smaller, shallower channels with northwest-southeast oriented axes are to the west of the deep channels (Fig. 2-7). From west to east, the north end of the study area is composed of intertidal sand bodies, Boot Island Bar and Western Bar, that are at depths of 8.8 m. There is a slope of 1° from these bars to 22.7 m of water in the thalweg of the western deep channel. The bottom rises at 0.5° to Middle Ground and then drops at 2.5° to the thalweg of the eastern deep channel. A slope of 1.5° exists from the cobbley eastern shore to the eastern deep channel. Figure 2-8A illustrates a typical east-west cross-section from the north end of the study area.

The greatest depths in the study area, 28.8 m, are found in the thalweg of the single large channel south of Middle Ground (Fig. 2-7). This channel shallows to the south and terminates north of Hantsport. A second, relatively deep channel lies to the east; the boundary between these channels is a thin ridge of sand (Fig. 2-7). Opposite Hantsport, as the eastern channel is followed upstream it bifurcates; one branch continues up the eastern side of the system and terminates 3 km to the south, the other swings to the west side of the river. The western branch continues upstream along the western side of Hantsport Bar. Depths in this reach are up to 19.1 m. A west-to-east cross-

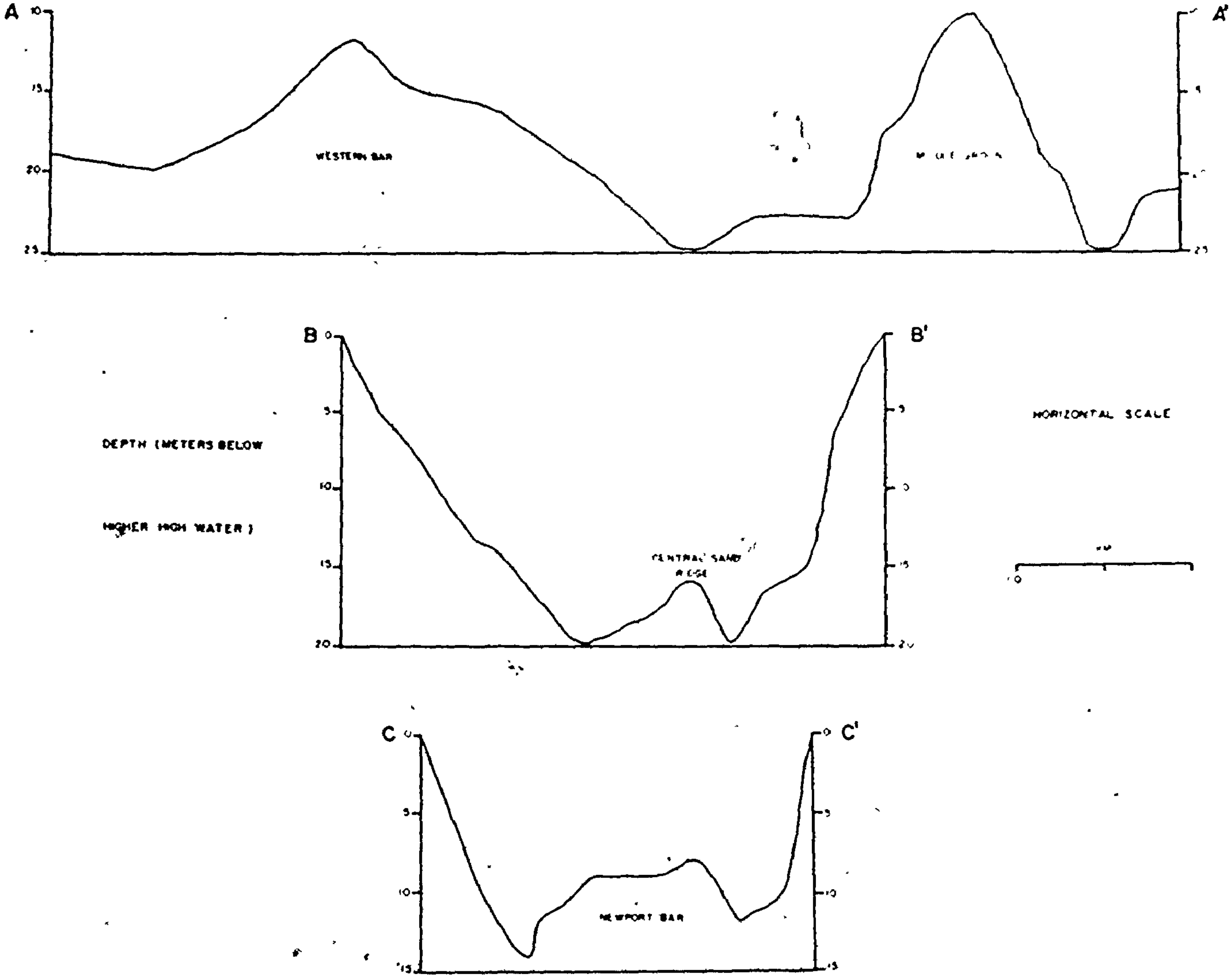

Fig. 2-8. Bottom profiles across the estuary. The cross-sections are located on Figure 2-7.

section north of Hantsport is shown in Figure 2-8B. The western shore slopes at 1° into the channel, the bottom climbs at 1° to the central ridge and then descends at 1.5° to the eastern channel. The eastern shore slopes down at 1.5° into the eastern channel.

The thalweg of the western channel bifurcates upstream near Mitchener Point, one branch turns south and follows the western shore of the river; ultimately it passes in front of the causeway at Windsor and into the St. Croix River (Fig. 2-7). Opposite Wallace Point, another bifurcation occurs; one branch extends into the Kennetcook River while the other swings south along the eastern side of the Avon and terminates north of the St. Croix River (Fig. 2-7). Another channel separates Newport Bar from the mud flat north of the causeway and extends into the St. Croix River. Depths in the channels south of Mitchener Point are less than 11.8 m; the study area shallows from north to south. The channels south of Mitchener Point contain only about 1 m of water at low tide; they do not dry only because of the delayed release of waters ebbing from tidal reaches of the river further upstream. The full spring tidal range in the estuary (15.6 m) is present only north of Hantsport. A west-east cross-section of the southern reach of the study area is illustrated in Figure 2-8C; slopes from the western shore to the western channel are 3.5° and 0.5° up to the crest of Newport Bar. The bottom drops at 10.0° to the eastern channel and climbs at 9.5° to the eastern shore.

In addition to the large channels described in the preceding discussion, there are several smaller channels in the study area including one that lies between the main part of Middle Ground and the large spit at its southern end and another along the eastern edge of Boot Island Bar. Also, there are several small channels, termed "swatchways" by Robinson (1960), that cut across sand bodies. A swatchway bisects Mitchener Bar, another cuts through the north-central part of Newport Bar, and a third crosses Western Bar with a northwest-southeast orientation. This discussion has concentrated on channel morphology as the topography of the intertidal sand bodies will be discussed in detail in Chapter 4.

Summary

The Avon River estuary is located in central Nova Scotia; it empties into the northeastern arm of the Bay of Fundy. Three major rivers discharge into the estuary of the Avon. Bedrock geology consists of Mississippian shale, sandstone and limestone, and Triassic sandstone; most surficial deposits are supratidal salt marsh and Pleistocene till. Adjacent intertidal facies include beaches, gravel veneered with mud, mud flats, gravel with cobbles, and a wave-cut platform. Sea level has been rising for 4000 to 6000 years and at present is rising at approximately 0.15 m per century.

Nova Scotia has a humid, temperate climate. Mean annual temperature is 6.8°C, mean annual precipitation is 1.07 m, and mean annual wind speed is 15.6 km/hr.

The estuary has a main channel that extends from the northern to the southern end of the study area; water depths along the channel thalweg tend to decrease towards the south. Several other channels branch from the main channel; slopes perpendicular to channel thalwegs tend to be consistent throughout the estuary.

CHAPTER 3

HYDRAULICS

Tides

The Bay of Fundy is reknowned for its large tidal ranges. At the Bay entrance, maximum tidal range is approximately 4.5 m; range increases towards the head of the Bay and reaches a maximum of 16.3 m at Burntcoat Head in the Minas Basin (see Fig. 2-2). The large tidal ranges generally are believed to be the result of resonant amplification of the semidiurnal (M_2) tidal component. Harleman (1966), Rao (1968), and Yuen (1969) point out that the resonant period of the Bay of Fundy is not equal to the semidiurnal period of 12.42 hours; they suggest a two-stage amplification, one across the continental shelf and the second within the Bay of Fundy. Duff (1970) and Garrett (1972) contend that the resonant period approaches 12.42 hours if the system is extended to include the continental shelf in the Gulf of Maine; resonance results in a quarter wavelength standing wave overlooking dynamic effects of the open end. Numerical model studies of Bay of Fundy tides and residual tidal currents were done by Tee (1975, reported in Greenberg, 1976) and Greenberg (1976); the models indicate that the system is in resonance but tidal currents in the Avon River estuary were not predicted.

Tidal range in the Avon River estuary varies between 8.2 m at neap tide and 15.6 m at lunar perigee spring tide; spring tide range at lunar apogee is 12.0 m (Canadian Hydrographic Service, 1974-1976, predictions for Hantsport; Fig. 3-2). Predicted tidal ranges during periods when observations were made are shown on Figure 3-1. Such large tidal ranges produce strong tidal currents which will be discussed later in this chapter. Tides are strongly semidiurnal with a small diurnal inequality that is almost always less than 0.6 m.

The large tidal ranges act over the approximately 25 km^2 surface area of the Avon River estuary (landward of the river mouth) producing a tidal volume of 2.1×10^9 m^3 at neap tide and 3.8×10^9 m^3 at spring tide. In order to allow for the large variation in tidal range, tidal coefficients (as described by Allen et al., 1969) have been calculated; the coefficient for a particular tide is calculated by dividing the range of that tide by the maximum range that occurs in the area (15.6 m).

Characteristics of the tidal curve were monitored by recording water depth every half hour for a complete tidal cycle at 29 stations with a direct reading depth gauge; times of local high and low water also were noted. Stations were located with horizontal sextant

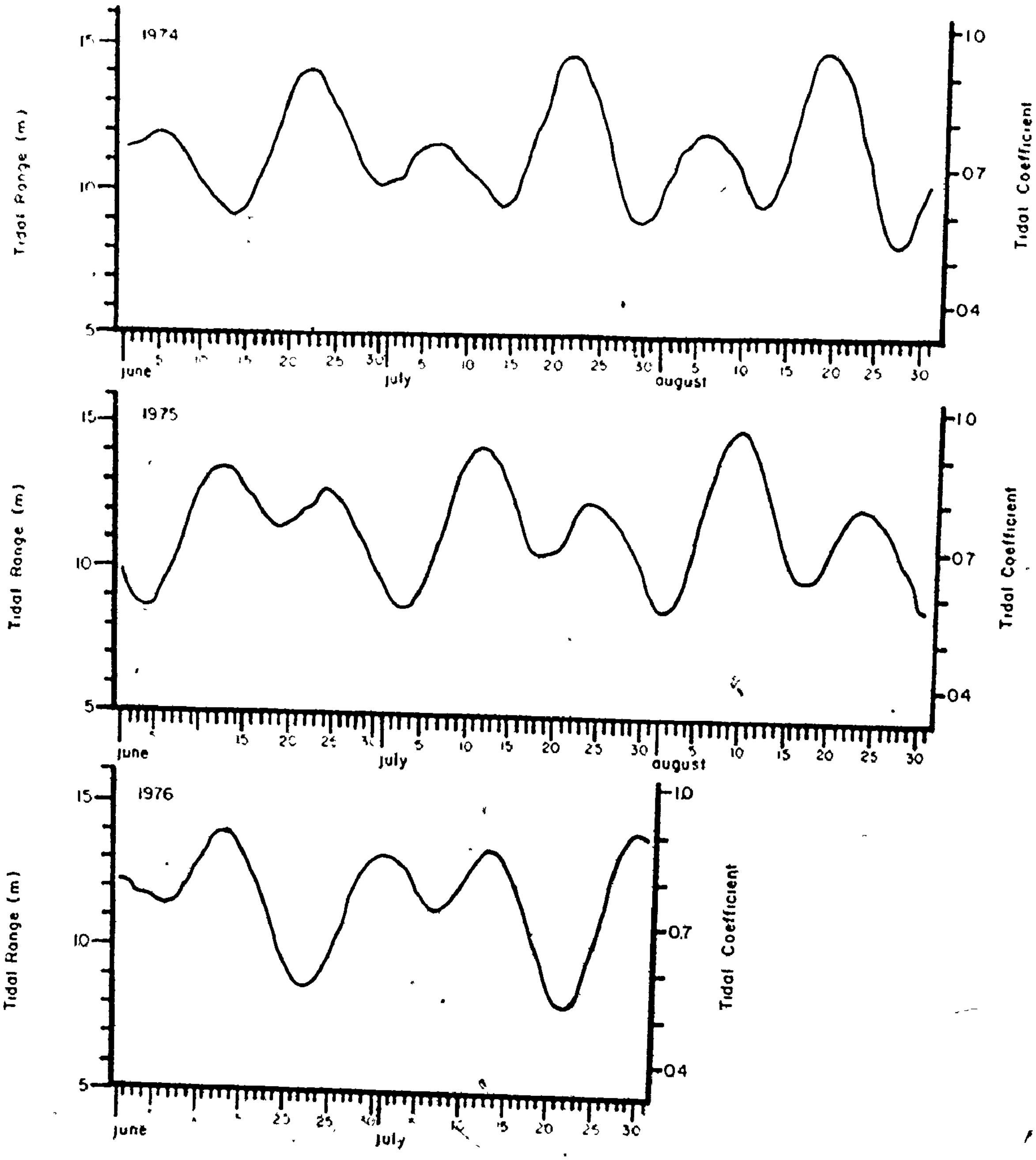

Fig. 3-1. Tidal ranges during field work

sightings. Because each station was occupied on a different day, tidal coefficients were used to determine changes in the tidal curve caused by the lunar cycle and position within the study area. Two additional stations in the study area have been monitored by Dr. Carl Amos of the Bedford Institute of Oceanography; raw data from all 31 stations are presented in Appendix B and station locations are shown on Figure 3-2.

Symmetry of the tidal curve is affected strongly by the lunar cycle; the magnitude of the effect varies with position in the estuary. In this discussion any tidal cycle with a tidal coefficient of less than 0.77 (the coefficient calculated for the mean tidal range of 12.0 m from data given by the Canadian Hydrographic Service, 1974-1976) is considered to be a neap tide; any cycle with a tidal coefficient greater than 0.77 is a spring tide. Tidal coefficients can range from 0.53 at low neap tides to 1.00 at high spring tides.

At neap tide the tidal curve is fairly symmetrical everywhere in the study area; ebb and flood flow each last approximately 6.25 hours. Near the head of the estuary ebb flow occasionally lasts slightly longer than flood flow (up to half an hour) when the tidal coefficient approaches 0.77. Figure 3-3 illustrates two examples of neap tidal curves, one from the mouth of the system and the other from near the head.

Fig. 3-2. Current station locations. Solid squares are current measurements only, solid triangles are currents and temperature, solid circles are currents, temperature, and salinity, and open circles are stations monitored by Bedford Institute of Oceanography. The station names corresponding to the numbers are:

1 Newport Bar 1
2 Newport Bar 2
3 Newport Bar 3
4 Newport Bar 4
5 Mitchener Bar 1
6 Kennetcook Mouth
7 Hantsport Bar 1
8 Hantsport Bar 2
9 Hantsport Bar 3
10 Hantsport Bar 4
11 Hantsport Bar 5
12 Summerville
13 Horton South
14 Horton North
15 Middle Ground 1
16 Middle Ground 2
17 Bedford Institute 2
18 Middle Ground 3
19 Middle Ground 4
20 Middle Ground 5
21 Main Channel
22 Western Bar 1
23 Western Bar 2
24 Western Bar 3
25 Western Bar 4
26 Boot Island Bar 1
27 Boot Island Bar 2
28 Boot Island Bar 3
29 Boot Island Bar 4
30 Boot Island Bar 5
31 Bedford Institute 3

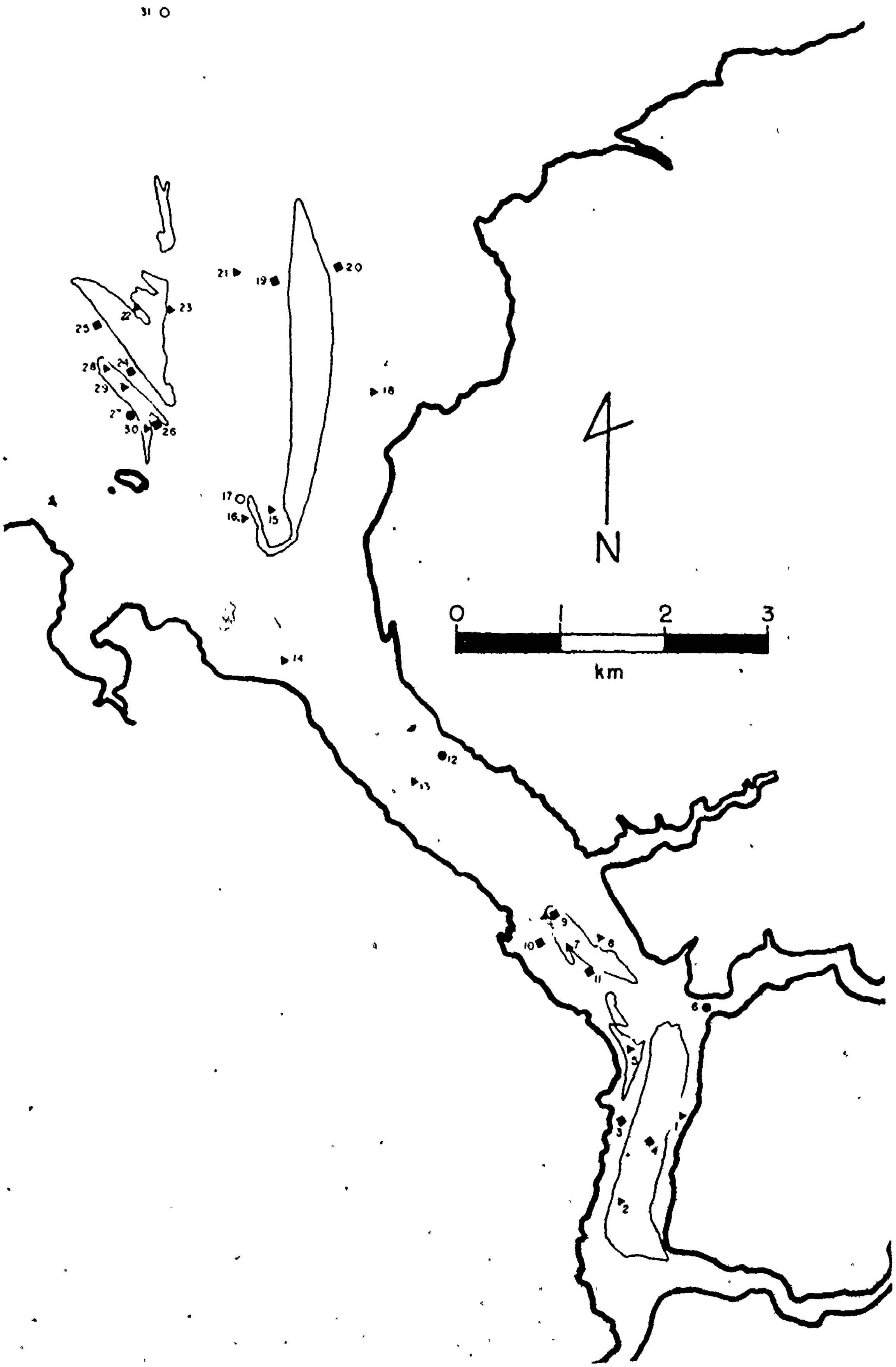
31
21
19
20
22
23
25
28
24
29
27
30
26
18
17
16
15
N
0
1
2
3
km
14
12
13
9
10
7
8
11
6
5
3
1
4
2

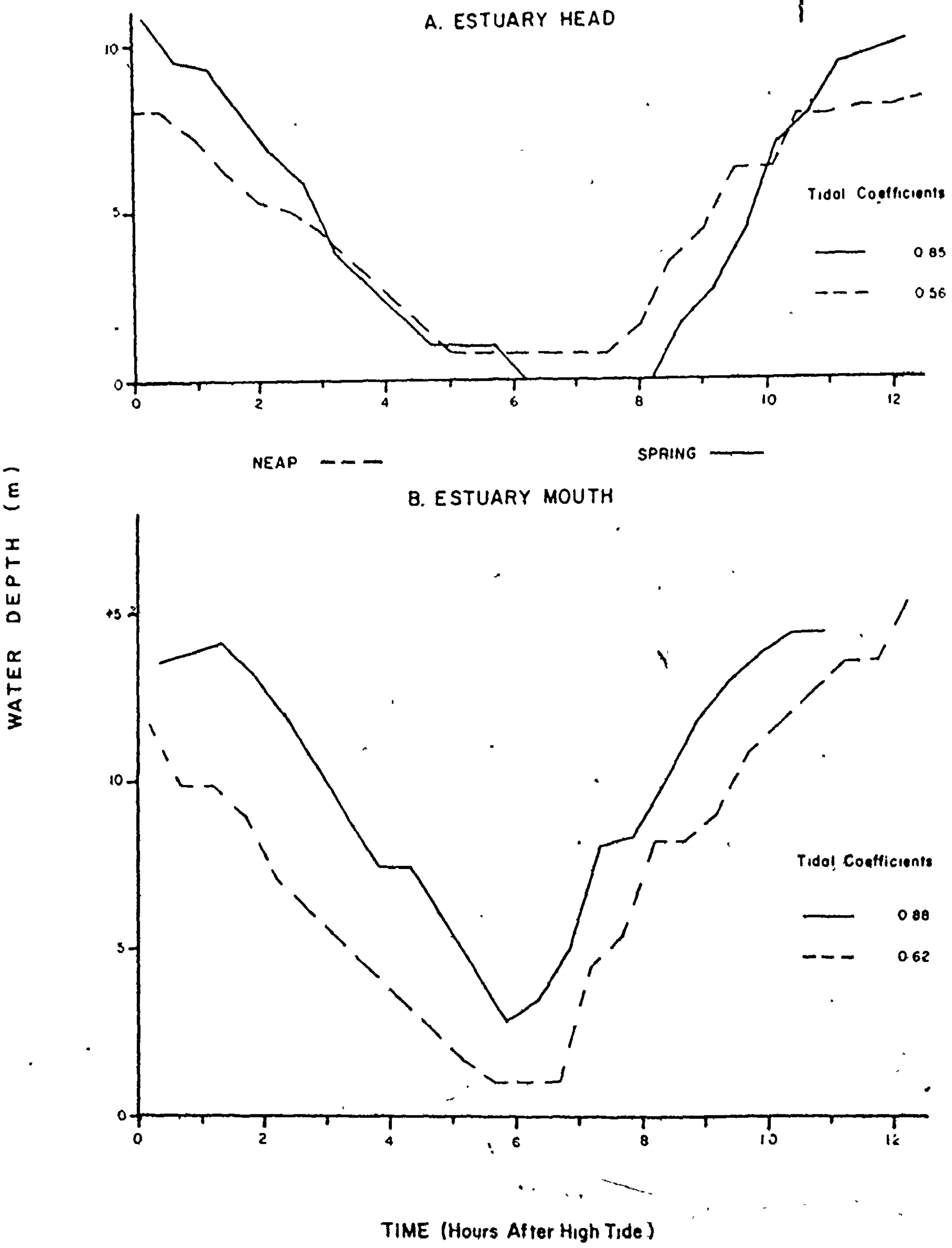

Fig. 3-3. Neap and spring tidal curves for A) the estuary head and B) the estuary mouth.

At spring tide the tidal curves are slightly asymmetric at the mouth of the estuary; ebb flow lasts approximately half an hour longer than flood flow. The asymmetry increases in the onshore direction; near Hantsport Bar one tidal cycle can have 7.25 hours of ebb flow and 5.25 hours of flood flow. At Newport Bar the asymmetry is even stronger; there can be as much as 8.5 hours of ebb flow with only 4 hours of flood flow. Figure 3-3 also depicts tidal curves from the mouth and head of the estuary at spring tide.

Dyer (1973) and Wright _et al_. (1975) state that asymmetry in a tidal cycle is developed by the crest and trough of the tidal wave travelling at different speeds. Wave celerity is a function of water depth as $C = \sqrt{gh}$ where C is celerity, g is the gravitational constant, and h is water depth. Since water depth is greater at the wave crest (high tide) than at the trough (low tide), celerity of the crest is greater than that of the trough. Thus it takes less time to move from low to high tide than from high to low (Dyer, 1973; Wright _et al_., 1975).

The above explanation assumes a progressive tidal wave; the observed tidal curve asymmetry suggests that there may be a progressive wave in the Avon River estuary even though the Bay of Fundy is believed to contain a standing wave (Duff, 1970). As previously discussed, the trough of the tidal wave (low tide) can take as long as 1 hour to advance approximately 6 km from Hantsport Bar to Newport Bar.

Using the relationship of $C = \sqrt{gh}$, average water depth would be 1.4 m; average water depths in the reach between Hantsport Bar and Newport Bar approximate this value at low tide (see Fig. 2-7).

Although high tide apparently occurs at the same time throughout the estuary (a characteristic of standing waves), a progressive wave would not be detected at high tide due to its rapid celerity. Assuming an average water depth of 10 m at high tide, the tidal wave would travel at 35 km per hour. Water surface level changes very little for roughly an hour near high tide (Fig. 3-3). Thus, the tidal wave could travel up to 35 km without being detected; since the study area is approximately 24 km long, high tide would appear to occur simultaneously throughout the system if a progressive wave were present. Thus, it appears that a progressive wave may exist in the Avon River estuary; Defant (1961, p. 464) believes that progressive waves develop in most estuaries because of increased friction as a result of shallow water depths.

If the Avon River estuary has a standing tidal wave, asymmetry in the tidal curve must have a different cause. It seems likely that inertia of the ebb tidal prism may cause the observed asymmetry. At spring tide, the momentum of the large ebb tidal prism may retard the flood tide; since the flood tide is forced by the rise of the tide in the Minas Basin, the entire tidal volume can be flooded quickly, resulting in no delay in the time of high tide. At neap tide, momentum of the smaller ebb tidal prism is insufficient to retard the flood tide.

At large spring tides (tidal coefficient ≥ 0.92), a tidal bore develops in the channel to the east of Newport Bar (Fig. 3-2). It attains an amplitude of approximately 0.15 m and advances upstream at nearly 1 m per second. The bore develops because the deeper part of the tidal wave (the flood tide) overtakes the shallower wave trough which steepens the wave front until the wave breaks (Defant, 1961, p. 472); this can happen only when the amplitude of the wave is comparable to the water depth so that, by $C = \sqrt{gh}$, the celerity of the incoming wave is large relative to the celerity of the wave trough. Bores can develop only in very shallow channels in the Avon River estuary as flood currents reach peak speeds of approximately 2 m per second; thus water depths must be less than 0.4 m for a bore to form.

Fresh Water Input

Considering the large tidal volumes described above, it was necessary to verify that the Avon River actually is an estuary by Pritchard's (1967) definition. If the Avon River is an estuary, tidal volume - fresh water ratios and salinity distribution can be used to relate it to Pritchard's (1967) estuary classification scheme.

The amount of fresh water entering the Avon River estuary was estimated by stream gauging and drainage basin area plus rainfall -

runoff ratios of nearby streams. The Kennetcook and St. Croix rivers were gauged for several months; fresh water input from the Avon River was estimated from Nova Scotia Department of Agriculture records of flow through the sluice gate in the causeway at Windsor (see Fig. 2-5). Rainfall - runoff ratios were calculated for each river; runoff for the remaining drainage basin area of the estuary was estimated using these ratios and ratios from nearby rivers. The method is described in detail in Appendix B. Fresh water discharge per tidal cycle was estimated to be between 6.86×10^3 m^3 and 1.00×10^8 m^3 based on estimates of minimum (once per 50 years) and maximum (once per 100 years) daily discharge. Monthly discharges range between 8.70×10^3 m^3 and 1.55×10^6 m^3 per tidal cycle; mean annual input is 1.18×10^7 m^3 per tidal cycle. All measured and estimated fresh water input rates are listed in Table 3-1.

Tidal volume - fresh water input ratios range between 1350 for minimum tidal range and maximum discharge per tidal cycle based on monthly averages and 4.37×10^5 for maximum tidal range and minimum monthly discharge. These values fall above the range of partially-mixed (type C) estuaries in Pritchard's (1967) classification as they are greater than 1000; therefore, salinity distribution in the Avon River estuary should generally be that of a well-mixed estuary. However, Pritchard (1967) doubts that well-mixed estuaries do exist in nature. If the

TABLE 3-1: Fresh Water Input

	Avon	Cogmagun	Kennetcook	St. Croix	Small Creeks	Total
Drainage Basin Area (km^2)	433	142	487	706	67	1835
Runoff (m^3/ tidal cycle)						
minimum daily (1/50 yr.)	2.07×10^3	4.15×10^2	2.07×10^3	2.07×10^3	2.50×10^2	6.86×10^3
maximum daily (1/100 yr.)	2.52×10^7	7.14×10^6	2.89×10^7	3.55×10^7	3.66×10^6	1.00×10^8
mean annual	8.88×10^5	2.96×10^5	8.68×10^6	1.47×10^6	4.29×10^5	1.18×10^7
minimum monthly	1.19×10^3	3.91×10^2	1.34×10^3	1.94×10^3	3.18×10^2	8.70×10^3
maximum monthly	3.65×10^5	1.20×10^5	4.10×10^5	5.94×10^5	5.65×10^4	1.55×10^6

estimated maximum daily discharge of 1.00×10^8 m^3 per tidal cycle were to occur, the tidal volume - fresh water ratio would be 21; stratification should develop temporarily as ratios between 10 and 100 are associated with stratified (type B) estuaries (Pritchard, 1967).

Salinity distribution was measured at 3 stations with an induction salinometer; vertical salinity profiles were recorded every half hour for a full tidal cycle at each station. Fresh water discharge was estimated to be lower than mean annual discharge during each day of salinity measurement; tidal volume - fresh water discharge ratios were over 1000 on each day.

Also, vertical water temperature profiles were recorded at all salinity stations and at 16 additional stations. All raw salinity data plus details of the measurement methods are included in Appendix B; all stations are located on Figure 3-2.

Vertical profiles reveal a slight salinity stratification in the southern part of the study area. At high tide near the head of the estuary, there is a vertical salinity difference of 0.3‰; a difference of equal magnitude exists at Summerville (Figs. 3-2 and 3-4). At low tide, the vertical salinity difference at the mouth of the Kennetcook River is 0.1‰ and there is no vertical difference at Summerville (Fig. 3-4). Near Boot Island there is no vertical salinity difference at high or low tide (Fig. 3-4); waters are mixed vertically at the mouth of the estuary.

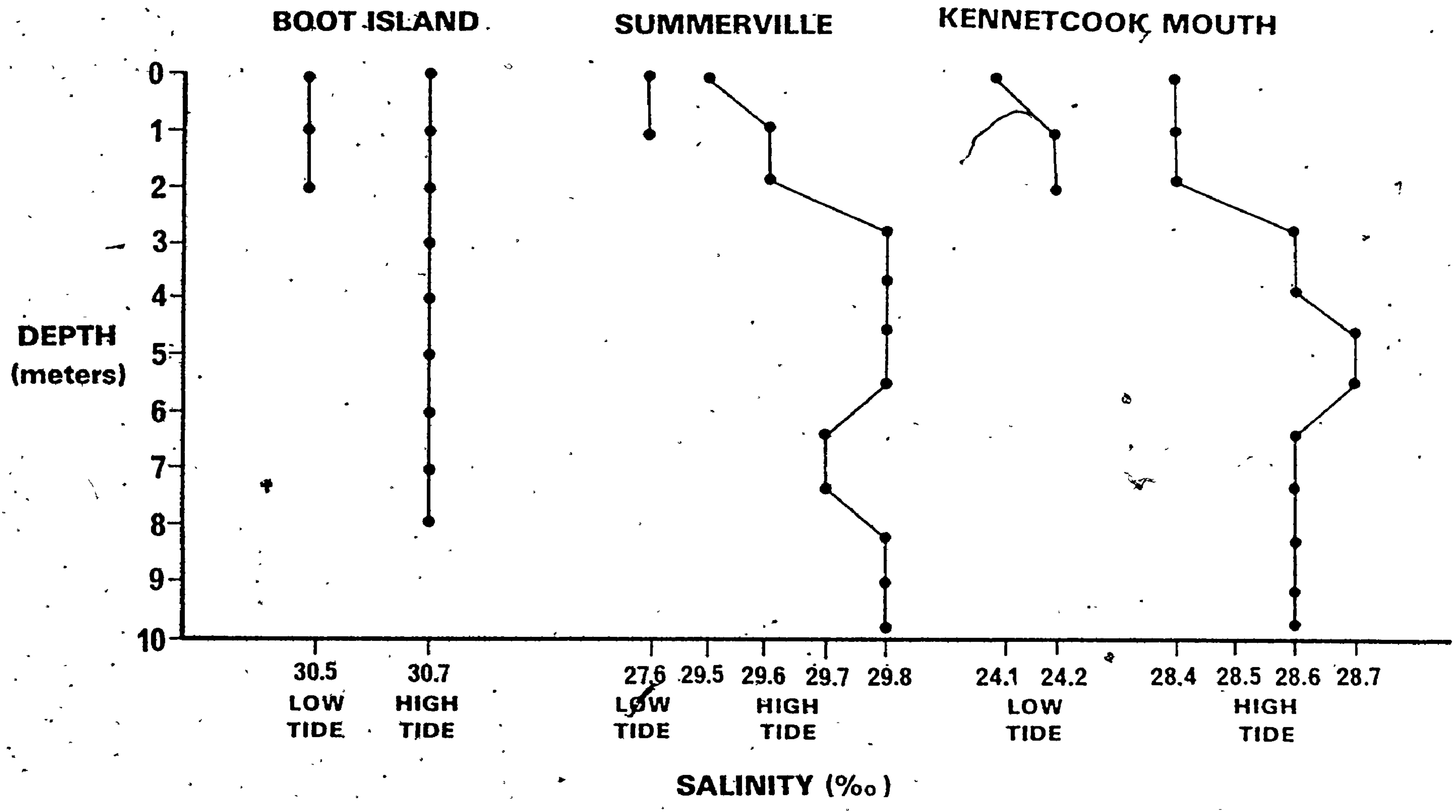

Fig. 3-4. Vertical salinity profiles; Boot Island (station 2) is at the estuary mouth, Kennetcook Mouth is near the estuary head, and Summerville has an intermediate location. Figure 3-2 depicts the location of each station.

There is a longitudinal salinity difference of approximately 2.0‰ from the head to the mouth of the estuary. At high tide, salinity is 28.5‰ at the mouth of the Kennetcook River and 30.5‰ near Boot Island (Fig. 3-4). The Summerville station recorded intermediate values.

These vertical and longitudinal salinity differences classify the Avon River as a partially-mixed (type C) estuary by Pritchard's (1967) classification despite high tidal volume - fresh water discharge ratios. Vertical salinity differences have a gentle slope rather than a steep interface and salinity increases towards the mouth of the estuary; both of these conditions are to be expected in a partially-mixed system (Pritchard and Carter, 1971).

Water temperatures were recorded with a direct reading thermometer; a vertical temperature profile was measured every half hour for a complete tidal cycle. Water temperature profiles at all 19 stations indicate that vertical temperature differences are usually 0.3°C or less. Surface waters are warmest due to solar heating; the remainder of the water column usually has a uniform, slightly cooler temperature (the raw data is in Appendix B). A few profiles have warmer water at the bottom of the water column than at the top. This occurs after submergence of intertidal sand bodies on sunny days.

There is a lateral temperature difference; temperatures are higher near the head of the estuary so that at each station, temperature is lower at high tide than at low tide. Heat transfer from sun-warmed intertidal sediments might produce the observed lateral temperature difference as there is more intertidal sediment relative to the total width of the system at the estuary head than there is at the mouth (see Fig. 2-7). Intertidal sediments generally are warmed to a depth of 5 cm or less; 1.43×10^4 cal/°C (Weast, 1973, p. F-68) are required to heat a 1 m^2 surface area. If the exposed sediment is 12°C warmer than the water, 1.72×10^5 cal would be available to heat the incoming water; the bottom 1 m of water could be heated by 0.17°C. The observed lateral temperature difference could be a function of heat transfer from intertidal sediments if, during each tidal cycle, lateral tidal convection of heat is minimal so that heat accumulates in each segment of the tidal prism. However, low tide at night probably would result in heat loss. In winter, the lateral temperature difference might be inverted as exposed sediments would be colder than the water; water temperature would be lower at the estuary head than at the mouth. Mean water temperatures increase during the summer from roughly 14°C in June to 20°C in August (see raw data in Appendix B).

Waves and Storms

WAVES: Waves are not an important hydraulic process on intertidal sand bodies in the Avon River estuary. Wave amplitudes tend to be small as a result a result of small fetch. Swells from other areas do not penetrate the system so that maximum wave height (H) can be predicted by hindcasting using published graphs (Coastal Engineering Research Center, 1973); wave height and period (P) are read from the graphs by inputing fetch, wind speed, and wind direction. The average wind speed of 20 km per hour (see Chapter 2) blowing across the maximum fetch of 26.3 km (see Fig. 2-2) would produce wave heights of only 0.5 m. For 1.3 m waves to be generated, winds would have to blow at 44 km per hour for 3 hours over the maximum 26.3 km fetch. The dominant westerly winds (see Fig. 2-6) are limited to 9.4 km of fetch (see Fig. 2-2); the average wind speed of 20 km per hour would generate waves 0.3 m high.

Observed wave heights did not exceed 1.3 m; waves greater than 1 m in height were seen rarely. On most days wave height was 0.3 to 0.6 m. As might be expected from fetch distances (see Fig. 2-2), wave height normally was greater at the mouth than at the head of the estuary.

Waves do not affect intertidal sand bodies significantly because each part of a bar is subject to wave attack for short time periods. Waves influence bottom sediments only while they "feel" bottom; this occurs when the ratio of water depth to wavelength is about 1/6 (Komar, 1976, p. 41).

Wavelength can be predicted from wave period with the formula $H^2 = 5.12(HP)^2$ (Coastal Engineering Research Center, 1973). The 0.5 m waves hindcasted for average wind conditions have wavelengths of 11.8 m; average waves would feel bottom in less than 2 m of water. Of course, waves with longer wavelengths and smaller heights would be superimposed on observed waves; these would feel bottom in deeper water, but their smaller heights would minimize the effect on bottom sediments.

Because the water surface level changes at approximately 2 m per hour, the normal waves, only 0.3 to 0.6 m high, only affect intertidal sand bodies for approximately one hour. Also, each part of an intertidal sand body is located within the breaker zone for a small fraction of the effective period, thereby reducing the effect of waves at each position.

No major changes in sand body configuration have been observed as a result of wave action. Minor changes in small-scale bedforms occur occasionally; these do not persist through one tidal cycle. Changes in surface features as a result of wave action will be described in Chapter 5.

STORMS: Storms do not appear to have a major effect on intertidal sand bodies in the Avon River estuary. Large storms could affect the study area by creating large waves and/or by significantly increasing the tidal range through storm surge. Abnormally large waves have not been observed during large storms; a hurricane during July, 1975 (recorded winds of 130 km per hour from the southeast at Halifax International Airport) produced waves with estimated amplitudes of 1.25 m (observed from shore).

Storm surge is relatively unimportant because of the large tidal range variation (6.9 m) between neap and spring tide. Freeman et al. (1957) report a storm surge of 1 m associated with Hurricane Edna of 1954 and MacMillan (1966, p. 112) lists a storm surge of 1.88 m in the Bay of Fundy; these values are well within the normal tidal range variation. Tidal volumes would not be extended beyond spring tide levels unless maximum storm surge coincided with a large spring tide.

Storms also could produce large fresh water discharges that could alter tidal currents and sediment discharge. However, maximum fresh water discharge of 1 x 10^8 m^3 (1/100 yr) results in an increase in ebb tidal volume of approximately 5%. It is unlikely that the corresponding increase in ebb velocities would produce a large change in sediment transport rates; smaller storms (1/yr) would have negligible effects as they would increase the ebb tidal volume less than 1%.

The July 1975 hurricane did not alter any of the intertidal sand bodies in the Avon River estuary. Observations resumed the day after the storm and revealed no changes in sand body morphology or surface features.

Tidal Currents

Current velocities were measured with a direct reading current meter at the 29 stations located on Figure 3-2. A vertical current velocity profile was measured each half hour for a complete tidal cycle at each station. (All the measured current data appears in Table B-1.) Additional current velocity data has been collected at 2 stations in the study area by Dr. Carl Amos of the Bedford Institute of Oceanography; this data is included in Table B-1.

Tidal currents have maximum speeds near the half-tides and minumum speeds at high and low water everywhere in the estuary. This supports the standing wave hypothesis for the Bay of Fundy system; a progressive wave would have maximum current speeds at high and low water and minimum speeds at the half-tides (Tricker, 1964, p. 29).

Tidal current speeds have the characteristic relationship with the tidal curve illustrated in Figure 3-5A. Following low tide, flood currents accelerate quickly to a peak, drop slightly and level off, and then decelerate slowly to high tide. Ebb currents accelerate slowly following high water, accelerate more quickly to a peak, and then decelerate rapidly to low water. The most rapid flow, during both ebb and flood stage, occurs while flow is channelized between sand bodies; deceleration of the flooding tide begins as sand bodies submerge and

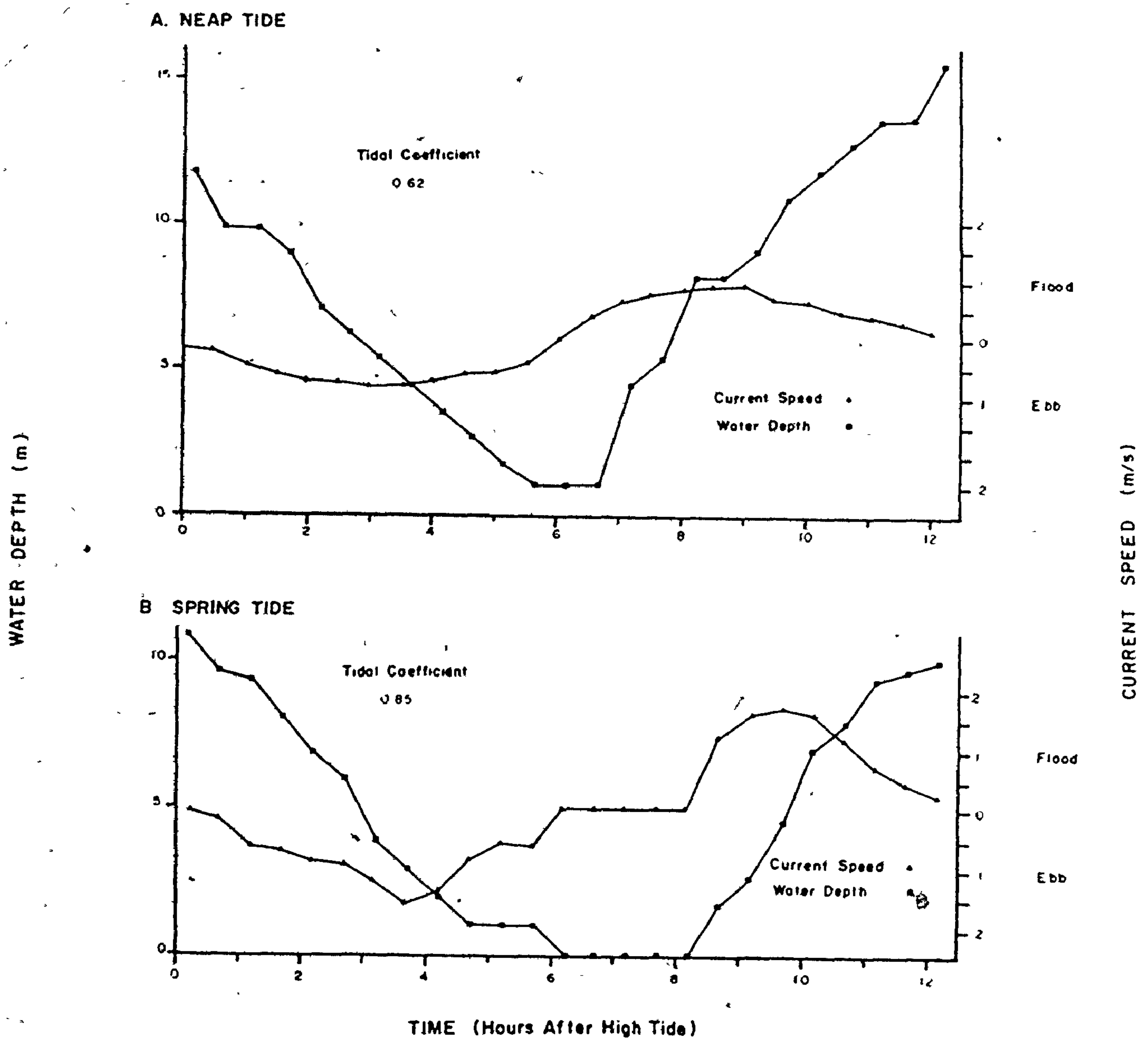

Fig. 3-5. Relation of tidal current speed to the tidal curve for A) neap tides and B) spring tides

ebb currents accelerate rapidly when sand bodies become emergent. The large tidal curve asymmetry at the head of the estuary during spring tide (Fig. 3-3A) causes an increase in flood current speed relative to ebb current speed (Fig. 3-5A&B); the normal acceleration - deceleration pattern is preserved.

At low tide, ebb current speeds drop to zero at the estuary mouth, but, at the head of the system, they continue to flow until they are reversed in direction by the incoming tide. At high tide flood current speeds drop to zero only within the Avon River. At the mouth of the system decelerating flood currents do not reach zero at high water; current direction swings slowly to the west until the flow has reversed. This results in a tidal ellipse as depicted in Figure 3-6; the observed ellipse is consistent with Coriolis force.

The observed relationship between the tidal curve and current speed is partly a function of the hypsometry of the estuary. At every location, the current speed required to change the water surface level by a fixed amount in a set period of time is affected by cross-sectional area and the volume of water that must be moved through the cross-section. Figure 3-2 shows the locations of three cross-sections that were examined with respect to hypsometry; Table 3-2 lists the results of the investigation. The data in Table 3-2 indicate that maximum current velocities should occur when intertidal sand bodies are sub-

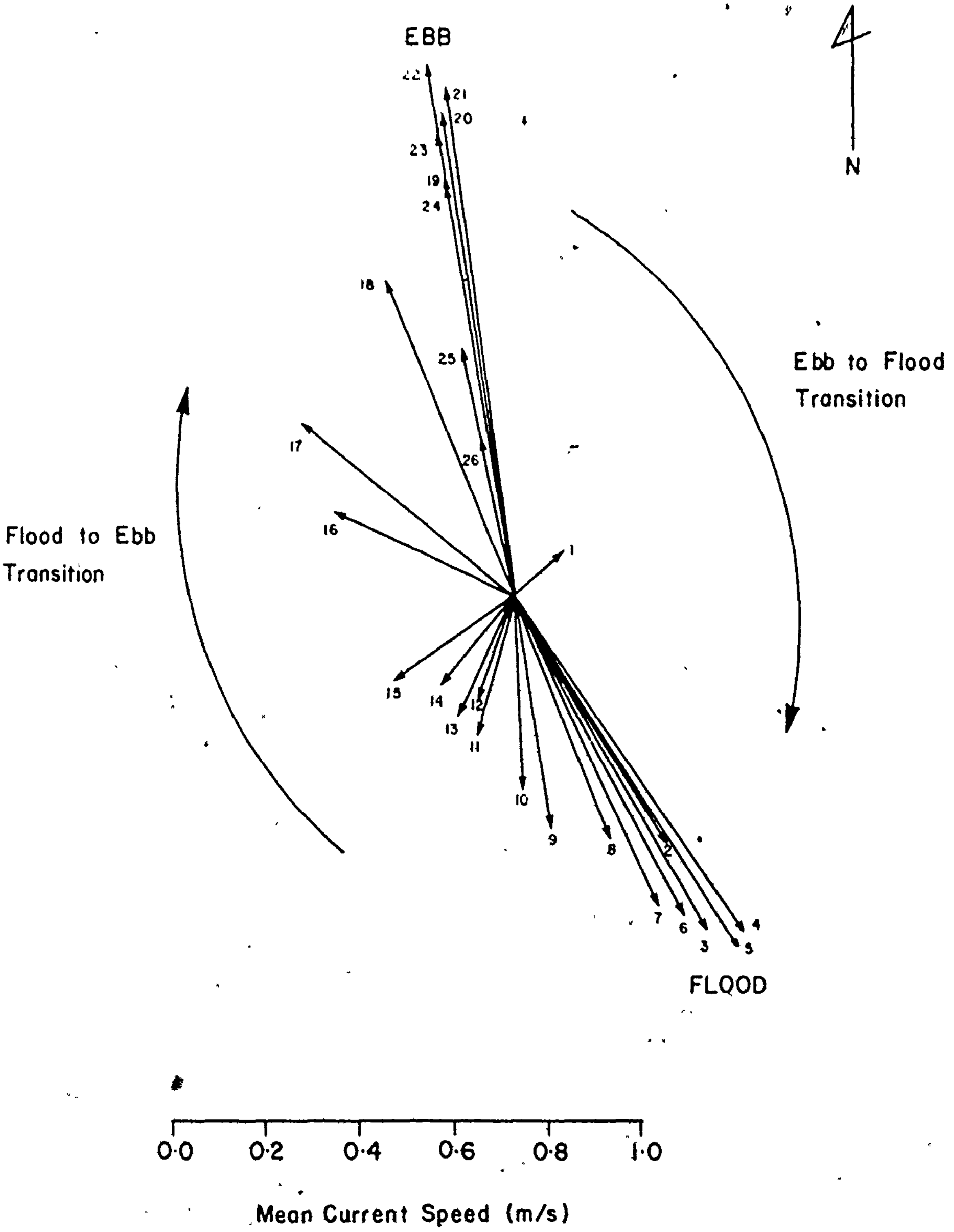

Fig. 3-6. Tidal ellipse at the estuary mouth; successive measurements are numbered sequentially beginning at low tide.

TABLE 3-2. Effects of Hypsometry at three Cross-sections; the cross-sections are located on Figure 3-2.

Cross-section	Water surface level (m below HHW)	Volume I Required (m^3)	Cross-sectional area (m^2)	Speed (m/s) required[1]	Speed (m/s) measured[3]
A	15.0	5.80×10^6	5.19×10^3	0.62	0.57
	12.5	8.03×10^6	6.55×10^3	0.68	0.81
	10.0	8.57×10^6	1.01×10^4	0.47	0.72
	--[2]				
	7.5	1.13×10^7	~~1.01×10^4~~	0.62	0.66
	5.0	1.22×10^7	1.01×10^4	0.67	0.51
B	12.5	1.45×10^6	7.65×10^2	1.05	0.89
	10.0	1.62×10^6	1.36×10^3	0.66	0.74
	--				
	7.5	1.82×10^6	1.70×10^3	0.59	0.68
	5.0	2.57×10^6	2.38×10^3	0.60	0.39
C	12.5	4.27×10^5	2.13×10^2	1.11	1.17
	10.0	4.83×10^5	5.95×10^2	0.45	0.60
	7.5	8.07×10^5	8.50×10^2	0.53	0.46
	--				
	5.0	1.27×10^6	1.70×10^3	0.41	0.45

[1] Required volume and speed are those needed to raise the water surface level 1 m in 1/2 hour; it is also assumed that speed is constant throughout the entire cross-section.

[2] Dashes indicate the maximum elevation of nearby intertidal sand bodies.

[3] Measured speed is recorded flood velocity at the appropriate water on the

aerially exposed because of the small cross-sectional area of the flow. At low water surface levels, current speeds often have less than peak values because the volume of water required to raise the water surface level is relatively small. When intertidal sand bodies are submerged, the large cross-sectional area decreases the required current speed (Table 3-2). Figure 3-7 illustrates the relationship between cross-sectional area, the volume of water that must pass through a cross-section, and current speed for cross-section A; current speeds reach maximum values while the intertidal sand bodies are subaerially exposed (water surface level more than 10.0 m below higher high water) (Fig. 3-7). The hyposometric curve for the estuary is illustrated in Figure 3-8.

Measured current speeds are comparable to predicted speeds (Table 3-2); several factors cause the observed differences. The predicted velocities in Table 3-2 were calculated assuming that the water surface level changes at a constant rate; the discussion of tidal curves earlier in this chapter indicates a variable rate of change. Also, the measured current speeds in Table 3-2 are not averages of the whole cross-section; they come from a single station in either a flood or ebb dominant zone (see the discussion later in this chapter).

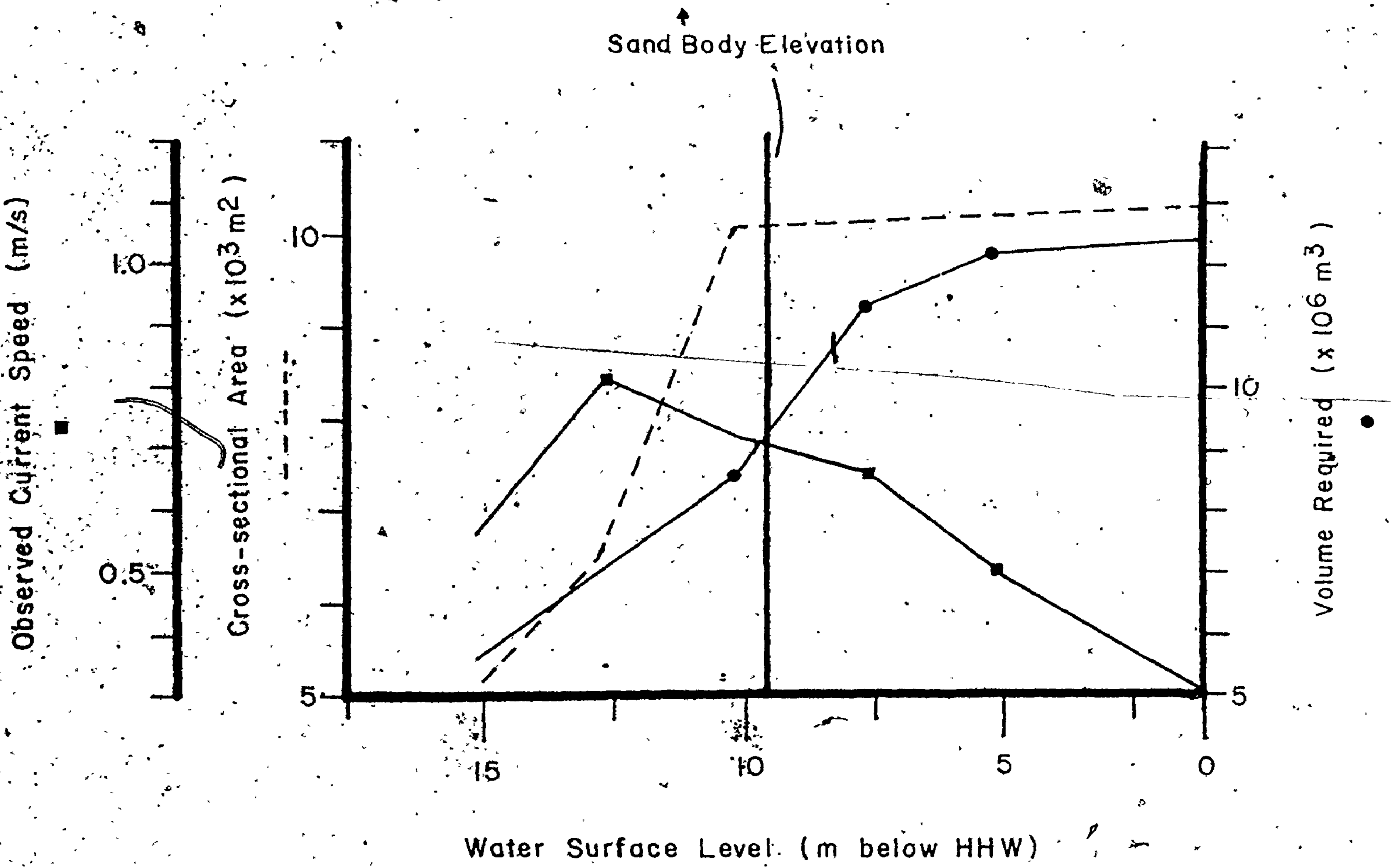

Fig. 3-7. Water surface level as a function of cross-sectional area, water volume, and current speed

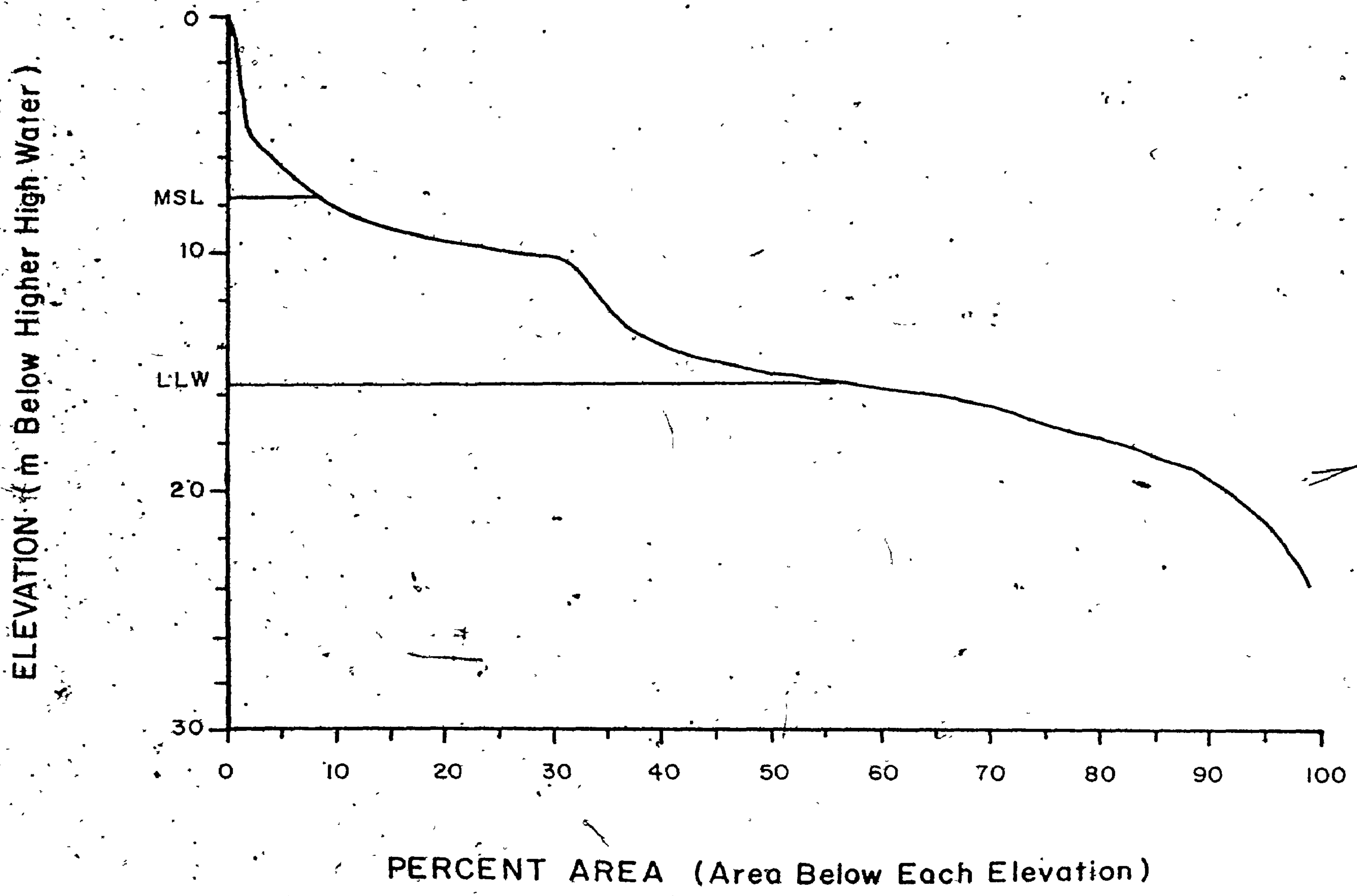

Fig. 3-8. Hypsometric curve; mean sea level and lower low water are marked

The predicted and observed current speeds for cross-sections B and C are in better agreement with each other than are those for cross-section A (Table 3-2). This probably is a result of the locations of the cross-sections. Cross-section A is at the mouth of the estuary (Fig. 3-2); cross-sectional area is relatively difficult to measure accurately because of the large width and varied topography (see Fig. 2-6). Also, there are several flood and ebb dominant zones along the cross-section so that measured speeds at one station, as presented in Table 3-2, may not correspond to average speeds across the whole section. Cross-sections B and C are within the Avon River (Fig. 3-2); there are few ebb and flood dominant zones on either cross-section so that measured speeds may be more representative of average conditions, and cross-sectional area is relatively easy to measure.

Near-bottom current speeds were measured as close to the bottom as possible; echo sounding indicated that the current meter usually was 0.75 m from the bottom. Maximum near-bottom current speeds range from 0.6 to 1.7 m per second; maximum speeds tend to be less than 1 m per second at the mouth of the estuary and greater than 1 m per second near the head. Maximum flood current speeds and ebb current speeds are unequal at each station (Fig. 3-9). Maximum mean ebb and flood current speeds also are shown on Figure 3-9; these, too, show

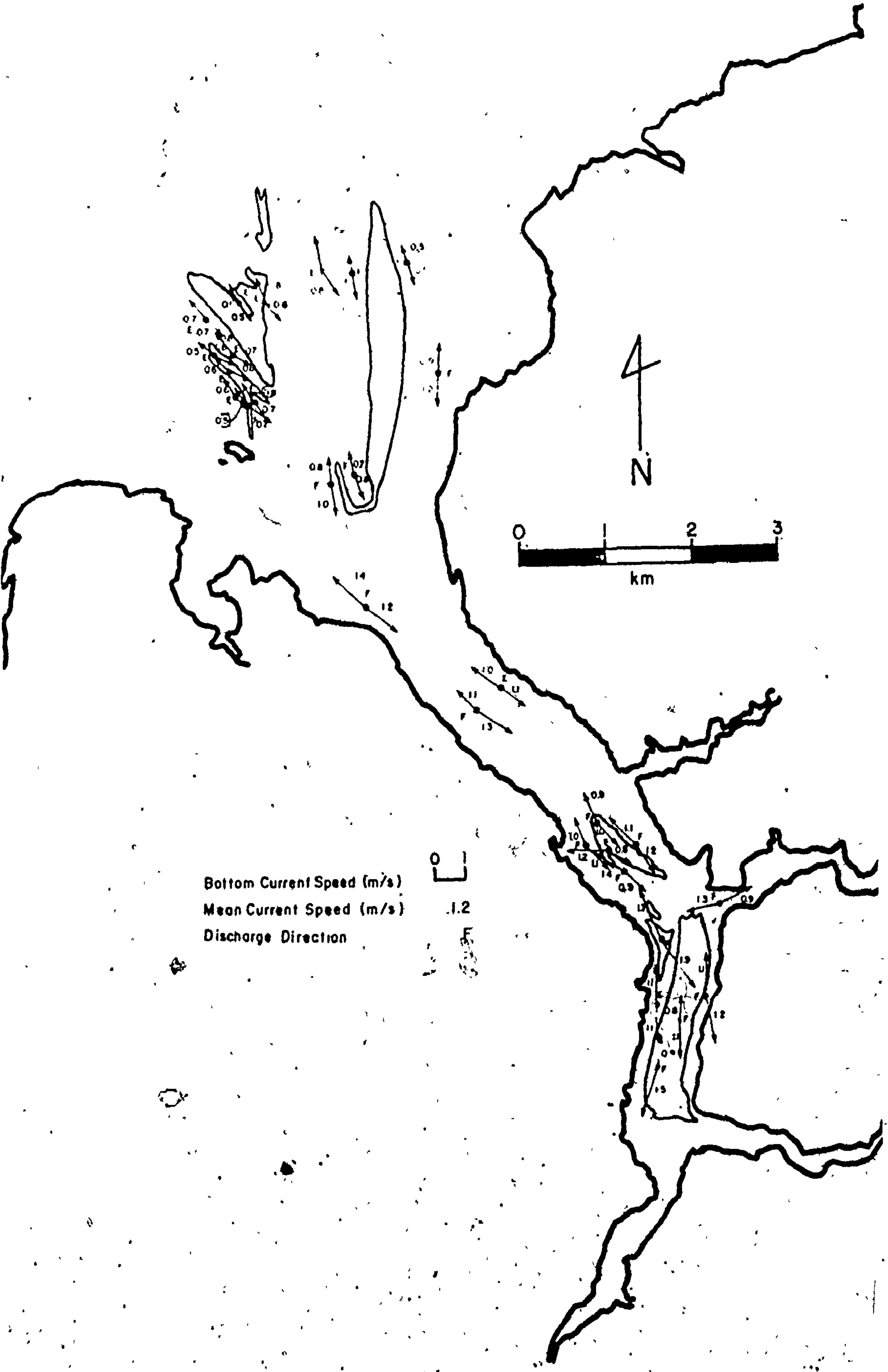
N
0 1 2 3
km
0 1
Bottom Current Speed (m/s)
Mean Current Speed (m/s) .1.2
Discharge Direction F

different ebb and flood values at each station. Maximum mean current speeds tend to be greater at the head of the estuary than at the mouth, and greater in channel areas than over intertidal sand bodies (Fig. 3-9).

Maximum near-bottom current speeds, maximum mean current speeds, and net discharge directions (Fig. 3-9) all indicate that tidal currents form "cells" with half of each cell dominated by ebb currents and the other half dominated by flood currents; the cells usually are centered on sand body crests. Distinct ebb and flood current areas have been observed in numerous tide-dominated locations (Kulm and Byrne, 1967; Schou, 1967; Houbolt, 1968; Coastal Research Group, 1969; Oertel, 1975). Similar ebb - flood systems also are common in Minas Basin (Klein, 1970; Dalrymple _et al._, 1975; Knight and Dalrymple, 1975).

Figure 3-10 depicts the tidal current cells derived from maximum near-bottom current speeds, net discharge directions, and maximum mean current speeds as well as the positions of the cells relative to sand body crests. The relationships between tidal current cells, sand bodies, and sediment transport will be discussed in Chapter 10.

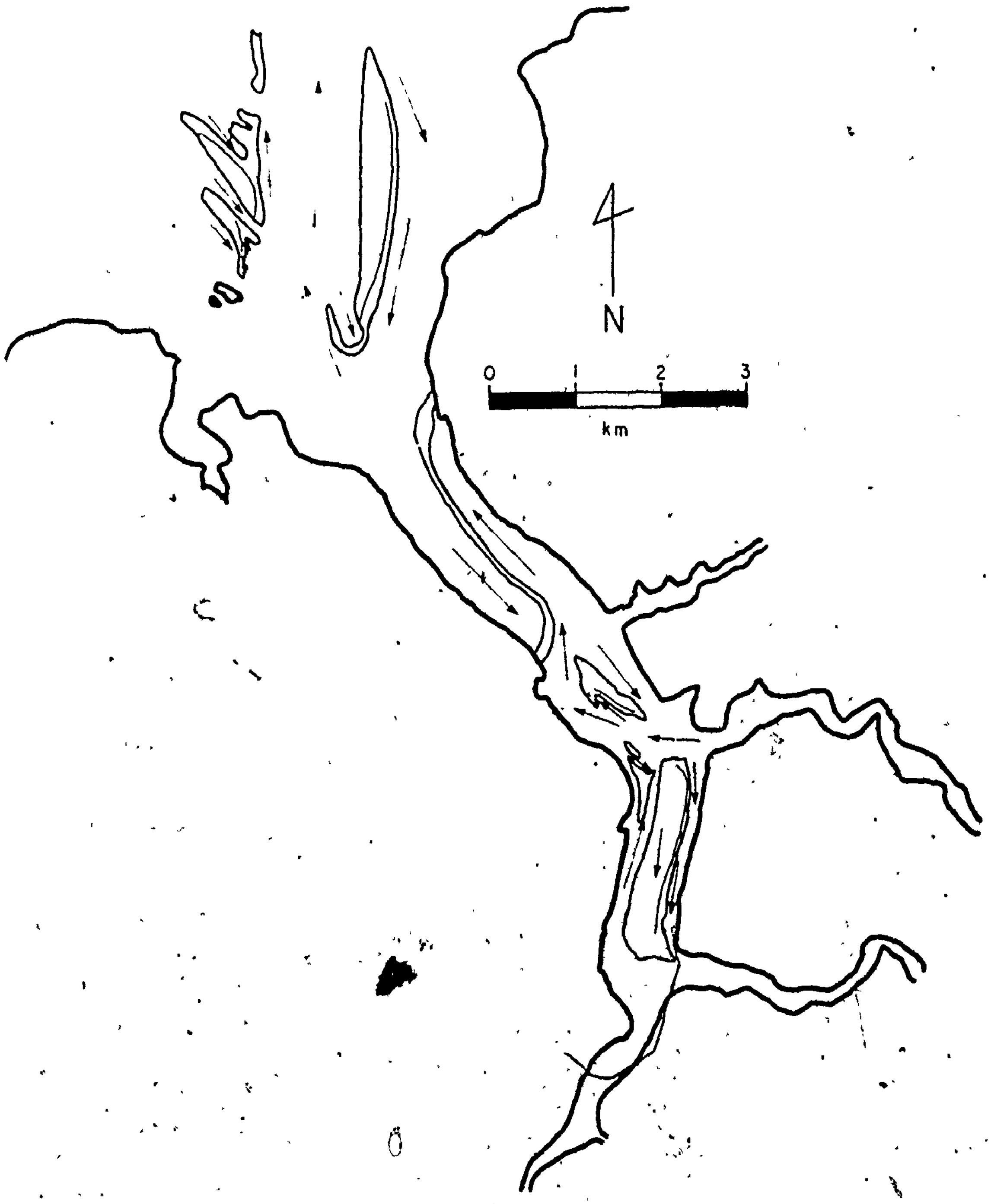

Fig. 3-10. Current cells; note that sand body crests usually form cell boundaries

Hydraulic Parameters

In addition to mean speed and discharge, the following hydraulic parameters were calculated for each velocity profile: "turbulence", speed .1 m from the bottom, shear velocity, shear stress, stream power, energy slope, the Darcy-Weisbach friction factor, roughness height, depth of zero velocity, Froude number, and Reynolds number. (All the computed values are presented in Table B-3.)

Hydraulic parameters were calculated from current velocity data with a computer program; input data consisted of current speed and direction plus water depth for each point of a velocity profile. Generally it is accepted that current velocities and water depth have a logarithmic relationship of the form

$$\frac{U}{U_*} = 8.5 + \frac{2.3}{K} \log \frac{y}{k} \qquad (3\text{-}1)$$

for rough boundaries (Blatt et al., 1972, p. 88); Sternberg (1968) found velocity profiles to be logarithmic 85% of the time. The best-fit line between the logarithm of the depth and current speed was calculated for each vertical profile using the method of Griffiths (1967, p. 441-444); the correlation coefficient was calculated to determine the goodness of fit of the line.

Most profiles are statistically logarithmic at the 95% level of confidence. Deviations from the theoretical logarithmic velocity distribution probably are caused by non-uniformity of flow due to the presence of large bedforms and by turbulence. Knight (1977) thoroughly discusses the shape of measured vertical velocity profiles. Profiles for which the linear regression is not significant at the 95% level may give computed values of shear stress or shear velocity that do not reflect true hydraulic conditions. Sediment transport rates computed from statistically insignificant profiles may not reflect actual conditions (see Chapter 7 and Appendix E).

The size of the deviations from the best-fit line was calculated from the sum of the squares of the velocity deviations (ΣU_{dev}) by the formula $T = \sqrt{\Sigma U_{dev}/n-2}/U_{*}$. This is the dimensionless parameter called "turbulence"; it is assumed that the major factor causing deviations from the theoretical semi-logarithmic velocity - depth distribution is large scale turbulence in the flow.

Turbulence values are remarkably consistent during a tidal cycle and with location. Most values lie between 0.5 and 3.0; during a tidal cycle, turbulence fluctuates between these limits. There is no apparent relation between turbulence values and the tidal curve or any computed hydraulic parameter; an example of turbulence during a tidal cycle is presented in Table 3-3. All computed turbulence values are

TABLE 3-3: Turbulence values through a tidal cycle

Time (hours from high tide)	Turbulence
0.00	1.68
0.50	2.01
1.00	2.49
1.50	0.74
2.00	0.92
2.50	1.04
3.00	1.69
3.50	2.81
4.00	0.90
4.50	2.11
5.00	1.24
5.50	1.87
6.00	0.83
7.00	2.61
7.50	1.80
8.00	0.86
8.50	2.01
9.00	1.95
10.00	1.10
10.50	1.17

Discussions in chapters 8 and 9 reveal that maximum shear velocity and shear stress are important for interpretation of grain size distributions, and that maximum stream power is useful for classifying bedforms. Because the computed values of shear velocity and shear stress fluctuate widely during a tidal cycle (Fig. 3-11), maximum shear velocity and shear stress are taken as the average of the 3 highest instantaneous values during a tidal cycle. Maximum stream power, shear velocity, and shear stress tend to be greater near the estuary head than at the mouth and greater in channels than over sand body surfaces. Table 3-4 contains all computed values of maximum mean velocity power, shear velocity, and shear stress.

The Darcy-Weisbach friction factor and roughness height also fluctuate during a tidal cycle in a similar manner to current speed (Fig. 3-12); most values of the friction factor are between 0.01 and 0.10 while roughness height generally ranges between 0.01 and 1.00 m. Froude number has a different relationship with the tidal curve than most other computed hydraulic parameters. Froude number is lowest at high tide and increases towards low tide; following low tide, values decrease to high tide (Fig. 3-12). In channel areas, there generally is a short time when Froude numbers are low near low tide. Froude numbers generally are between 0.01 and 0.15; few are larger than 0.25. All computed Froude numbers, friction factors, and roughness heights are listed in Table B-3.

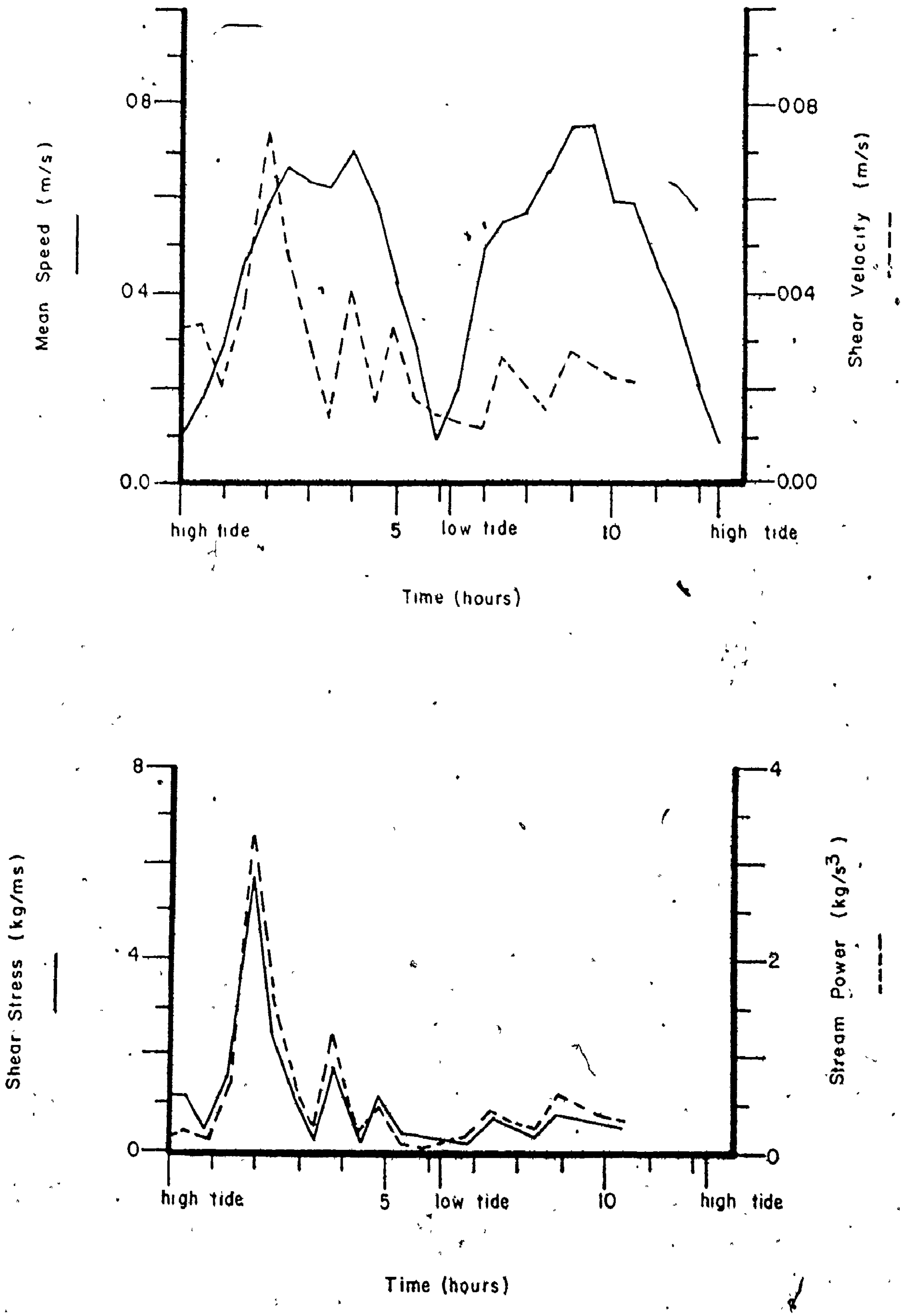

Fig. 3-11. Relation of shear stress, shear velocity, and stream

TABLE 3-4: Maximum mean velocity (m/s), shear velocity (m/s), shear stress (Kg/mS), and stream power (Kg/S^3)

Station	Mean Velocity	Shear Velocity	Shear Stress	Stream Power
Boot Island Bar 1	0.81	0.06	3.99	2.85
Boot Island Bar 2	0.72	0.04	1.84	1.04
Boot Island Bar 3	0.61	0.05	2.19	1.09
Boot Island Bar 4	0.64	0.05	2.73	1.42
Boot Island Bar 5	0.67	0.04	1.43	0.82
Hantsport Bar 1	1.13	0.08	7.08	7.60
Hantsport Bar 2	1.20	0.09	8.28	8.65
Hantsport Bar 3	1.02	0.07	5.64	4.57
Hantsport Bar 4	1.09	0.08	7.38	6.29
Hantsport Bar 5	1.20	0.11	13.77	11.74
Middle Ground 1	0.75	0.06	3.23	2.02
Middle Ground 2	0.95	0.07	5.33	3.54
Middle Ground 3	1.22	0.06	4.23	2.98
Middle Ground 4	0.61	0.06	3.41	1.74
Middle Ground 5	0.74	0.05	2.49	1.24
Mitchener Bar 1	1.91	0.08	6.92	11.95
Newport Bar 1	1.17	0.08	6.62	4.86
Newport Bar 2	1.02	0.07	1.56	1.31
Newport Bar 3	1.14	0.08	6.62	6.26
Newport Bar 4	1.09	0.06	3.51	2.54
Western Bar 1	0.65	0.05	2.50	1.43
Western Bar 2	0.66	0.05	2.26	1.34
Western Bar 3	0.76	0.07	4.76	2.74
Western Bar 4	0.74	0.04	1.85	1.20

TABLE 3-4 (continued)

Station	Mean Velocity	Shear Velocity	Shear Stress	Stream Power
Main Channel	1.04	0.05	2.53	2.26
Horton North	1.18	0.09	8.58	5.54
Horton South	1.27	0.08	7.50	8.07
Summerville	1.07	0.08	7.04	6.76
Kennetcook Mouth	1.28	0.08	5.93	6.70
B.I. Station 2	1.19	0.07	5.07	4.66
B.I. Station 3	0.98	0.06	3.73	3.10

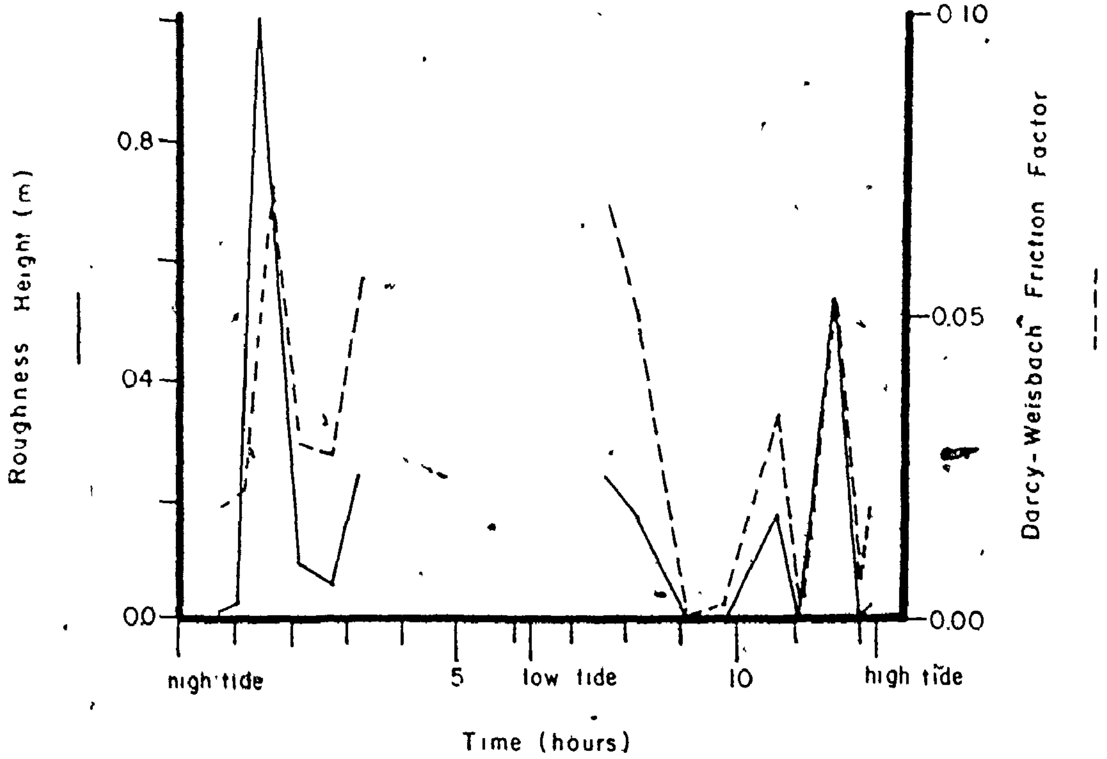
0.8
0.4
0.0
Roughness Height (m)
Darcy-Weisbach Friction Factor
0.10
0.05
0.00
high tide
5
low tide
10
high tide
Time (hours)

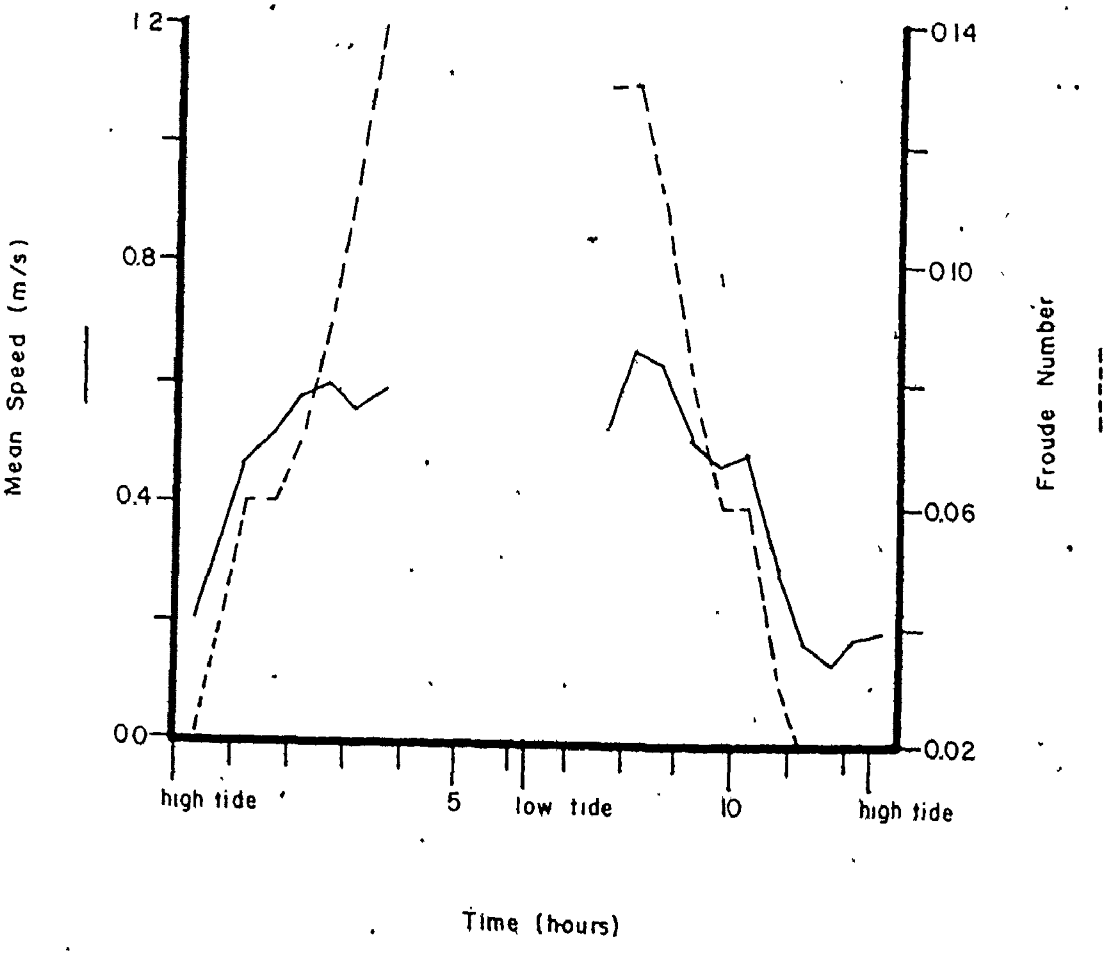
1.2
0.8
0.4
0.0
Mean Speed (m/s)
Froude Number
0.14
0.10
0.06
0.02
high tide
5
low tide
10
high tide
Time (hours)

Summary

Tidal range in the Avon River estuary varies between 8.2 and 15.6 m; tidal volumes range from 2.0×10^9 m^3 to 3.8×10^9 m^3. Tides are symmetric at neap tide and asymmetric at spring tide; the asymmetry increases from the mouth to the head of the estuary.

The ratio of tidal volume to fresh water input ratios ranges between 1350 and 4.37×10^5. These ratios are above the limit of partially-mixed (type C) estuaries in Pritchard's (1967) classification; nevertheless, vertical and longitudinal salinity gradients indicate that the system has some of the characteristics of a partially-mixed system.

Waves and storms are unimportant processes in the Avon River estuary. The small fetches do not allow generation of large waves and storm surge is small relative to the normal daily and monthly variation in tidal range.

Maximum near-bottom tidal current speeds tend to be greater near the head of the estuary and in channels than at the mouth of the system and over intertidal sand bodies; tidal current speeds have a characteristic relationship with the tidal curve that is produced by the hypsometry of the estuary. Maximum mean current speeds and maximum near-bottom current speeds are unequal for the flood and ebb stage at each station. Tidal currents form cells that are centered on sand body crests; half of each cell is dominated by ebb currents and half by flood currents. The relationship of shear velocity, shear stress, and stream power to the tidal curve is similar to that of maximum near-bottom current speeds.

CHAPTER 4

DISTRIBUTION AND MORPHOLOGY OF THE MAJOR INTERTIDAL SAND BODIES

Distribution

The six major intertidal sand bodies are identified on Figure 4-1; three of the bars are located at the mouth of the estuary and the other three towards the head. All six sand bodies are oriented parallel to tidal current flow directions. In addition to the six major sand bodies there is a minor sand body. This consists of a ridge of sand oriented parallel to the shoreline and in the center of the estuary near Summerville (Fig. 4-1). At its northern end, the ridge curves to the east and widens into a patch of sand that is joined to the shore near the low water mark (Fig. 4-1). The ridge terminates at its southern end on a bedrock ledge that projects into the estuary from the western shore (Fig. 4-1). The minor sand body is often unexposed at low tide as it does not extend much higher than lower low water (see Fig. 2-7).

Positioning of sand bodies seems to be influenced by tidal current flow patterns. Sand bodies always are located between channels, and channels on either side of a sand body generally have net discharges

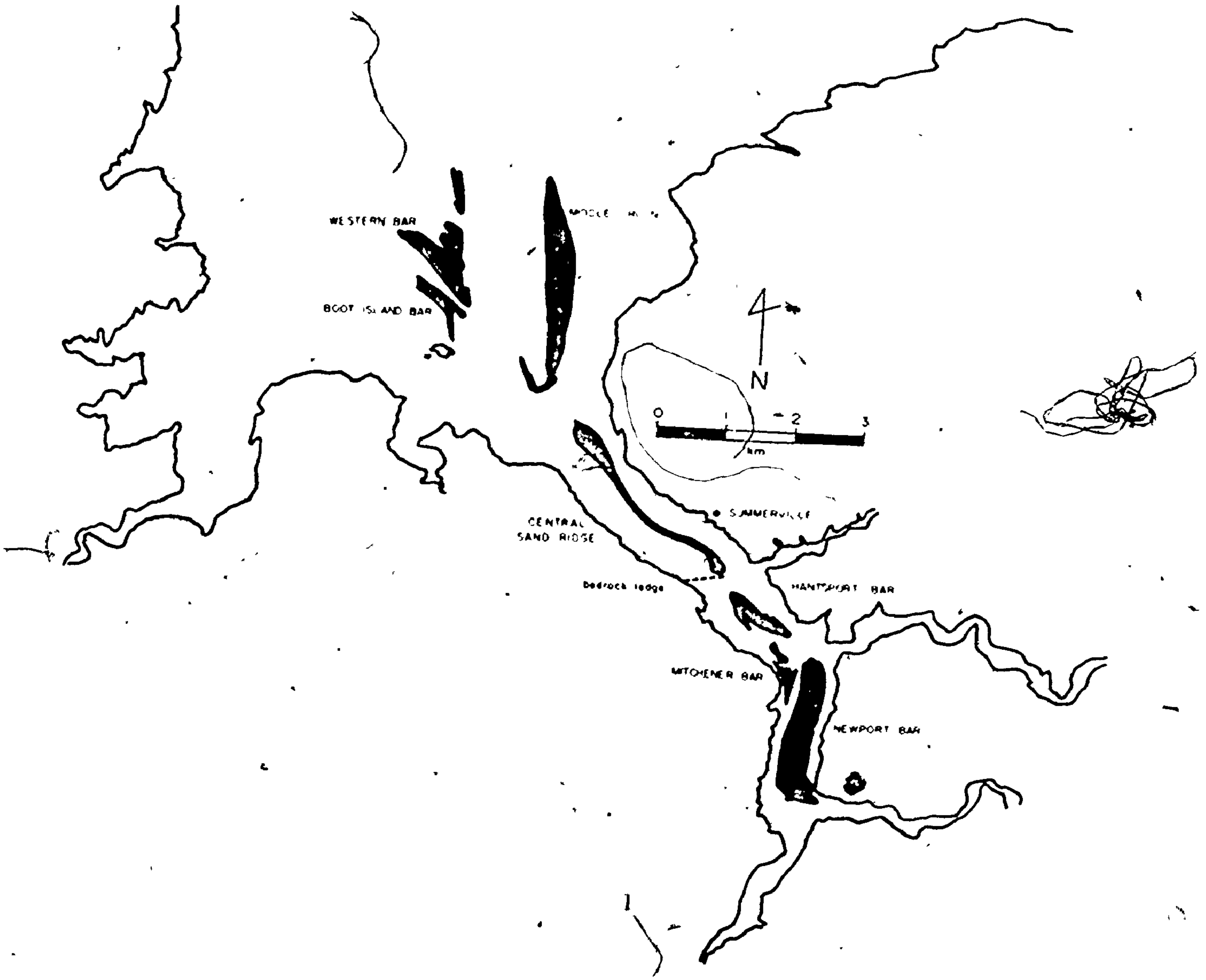
WESTERN BAR
BOOT ISLAND BAR
MIDDLE
N
0
1
2
3
km
SUMMERVILLE
CENTRAL SAND RIDGE
Bedrock ledge
HANTSPORT BAR
MITCHENER BAR
NEWPORT BAR

Fig. 4-1. Location of sand bodies; the central sand ridge is only exposed at low tide during spring tides

in opposite directions (see Fig. 3-9). The crest of a sand body generally is the boundary between the areas of opposing net discharge directions; this produces ebb and flood channel systems similar to those described by Robinson (1960) and illustrated in Figure 3-10. The relationship between sand body position and fluid flow patterns will be discussed in Chapter 10. Similar patterns of sand body distribution have been observed in other tidally dominated areas (Houbolt, 1968; Ludwick, 1974).

Boot Island Bar, Western Bar, and Middle Ground (Fig. 4-1) may be considered to form part of an ebb tidal delta (Coastal Research Group, 1969); ebb tidal deltas commonly are associated with estuaries (Coastal Research Group, 1969; Oertel, 1973, 1975; Hine, 1975; Hubbard, 1975; Finley, 1975). A model for the morphology of mesotidal ebb tidal deltas has been proposed by Hayes et al. (1973) (Fig. 4-2B). According to the model, Boot Island Bar, Western Bar, and Middle Ground are channel margin linear bars (Fig. 4-2A&B). The model calls for a terminal lobe at the seaward end of the delta (Fig. 4-2B); a corresponding lobe is present in the subtidal of the Avon River system (Fig. 4-2A). There are no swash bars present in the Avon River ebb tidal delta (Fig. 4-2A) as expected from the model of Hayes et al. (1973) (Fig. 4-2B). This is a result of the relative ineffectiveness of wave action in the macrotidal environment as previously discussed, since it is wave action that causes the formation of swash bars (Oertel, 1972).

Fig. 4-2. Comparison of the Avon River estuary to meso- and macrotidal estuary models.

A) The Avon River estuary mouth,

B) Mesotidal estuary ebb tidal delta model (from Hayes, 1975),

C) Macrotidal estuary model (from Hayes, 1975)

A

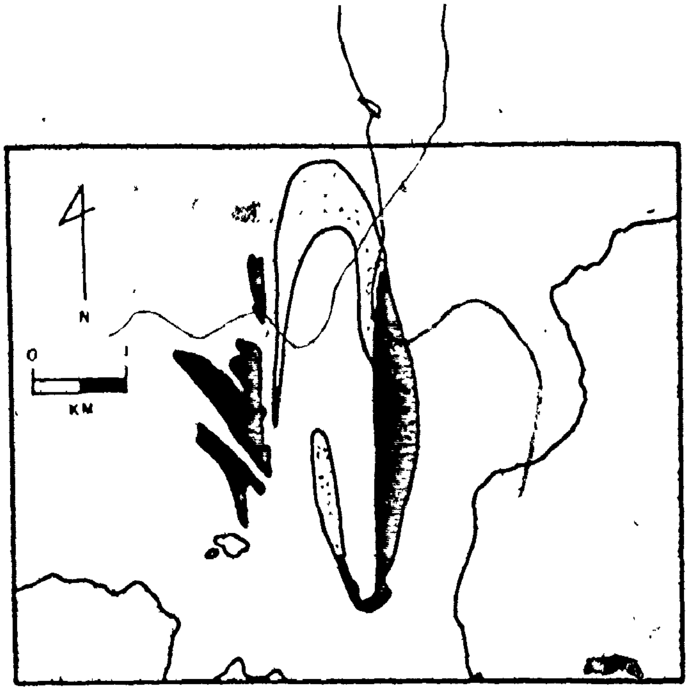
N
0
1
KM

B

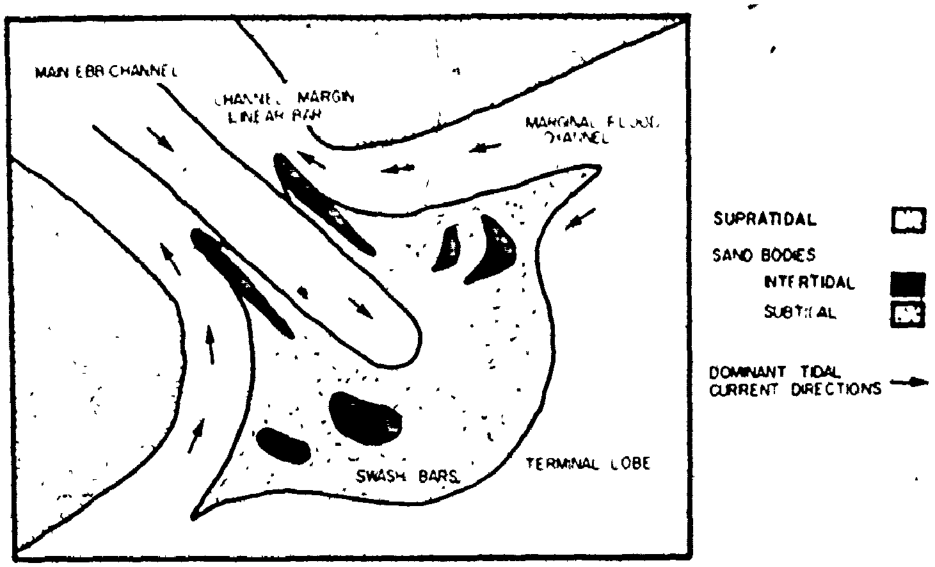
MAIN EBB CHANNEL
CHANNEL MARGIN LINEAR BAR
MARGINAL FLOOD CHANNEL
SWASH BARS
TERMINAL LOBE
SUPRATIDAL
SAND BODIES
INTERTIDAL
SUBTIDAL
DOMINANT TIDAL CURRENT DIRECTIONS

C

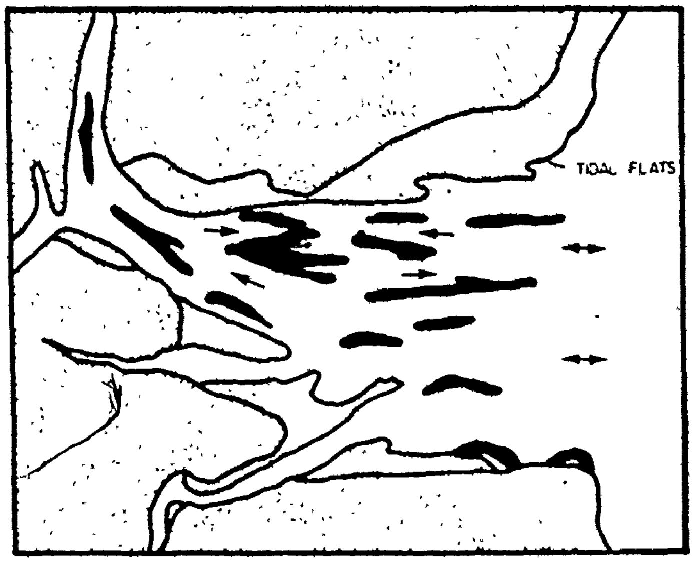
TIDAL FLATS

The model for ebb tidal deltas proposed by Hayes et al. (1973) is considered to be a model for mesotidal estuaries (tidal range 2 - 4 meters) (Hayes, 1975). This differs significantly from the model described by Hayes (1975) for macrotidal systems and illustrated in Figure 4-2C. The macrotidal model calls for a wide mouthed, funnel shaped system; the Avon River does not match this description even though it is macrotidal (Fig. 4-2A&C).

It seems likely that the configuration of sand bodies at the mouth of the Avon River resembles the mesotidal model more than the macrotidal because of the constraints to flow imposed by the cliffed bedrock shorelines (see Fig. 2-4). With unconsolidated shorelines, tidal currents might widen the estuary mouth until it approached the shape depicted in the macrotidal model (Fig. 4-2C). Bedrock shorelines confine the flow creating an expanding jet at the mouth during ebb flow, a condition that has been observed in mesotidal estuaries (Oertel, 1975) and is considered to be the reason for the formation of ebb tidal deltas (Todd, 1968).

Hantsport Bar seems to be positioned as a channel margin linear bar with respect to the Kennetcook River (Fig. 4-1). There is not a fully developed ebb tidal delta associated with the Kennetcook River probably because a corresponding channel margin linear bar on the south side of the Kennetcook would have to be perpendicular to the tidal currents, an atypical orientation in macrotidal areas (Hayes, 1975).

Mitchener Bar appears to be a tidal point bar since it lies at a turn in the estuary and it is joined to the shore (Fig. 4-1); tidal point bars are found in other tidal river systems (Land and Hoyt, 1966; Wright et al., 1975).

Morphology

Measurements of the surface morphology of the major intertidal sand bodies were made with echo soundings, surveying, and interpretation of aerial photographs. (See Appendix A for details of the method used to measure sand body topography.) Sand bodies range in length from 0.80 to 5.60 km. and in width from 0.40 to 0.95 km. Most sand bodies have a well developed crest running parallel to their length and they are all elongate parallel to the tidal currents. The highest point on each sand body varies from 7.2 to 9.2 meters below higher high water and in time of subaerial exposure from 3 to 6 hours per tidal cycle.

Sand bodies in Cobequid Bay generally are widest towards the head of the bay and taper to a point towards the mouth of the bay; the highest point on a sand body usually is at the eastern end (Knight, 1977; Dalrymple, 1977). None of the sand bodies in the Avon River estuary follows this pattern; only two sand bodies have their highest point near the head of the system, and none is wider nearer the head than it is towards the mouth of the system. The morphology of each sand body is described as follows:

NEWPORT BAR Newport Bar is 3.92 km long and 0.95 km wide at its widest point and is roughly rectangular in shape (Fig. 4-3A). The major topographic features of Newport Bar are its crest which is near the eastern edge, and a low relief channel in the north central part of the bar (Fig. 4-3A). This channel appears to be a dead-end flood channel as described by Robinson (1960).

The surface of Newport Bar is gently-sloped to the west of the sand body crest and steeply-sloped to the east. Slopes average approximately 0.5° on the western side of the crest and 10° on the eastern side. The highest point on Newport Bar is on the sand body crest and is 7.5 meters below higher high water; the sand body is subaerially exposed for 6 hours during each tidal cycle. The crest on Newport Bar is 5.9 meters above the bottom of the adjacent channel to the east implying a minimum thickness of at least that amount (Fig. 4-3B).

MITCHENER BAR Mitchener Bar is the smallest sand body in the system with a length of 0.80 km and a width of 0.40 km. The bar is joined to the shore and has a well-defined channel in the center that divides the sand body into two sections (Fig. 4-4A). Mitchener Bar is the only sand body without a well-defined crest. A poorly-defined crest is present in the position shown in Figure 4-4A but no abrupt slope changes are associated with it. To the west of the channel, the surface of Mitchener Bar slopes

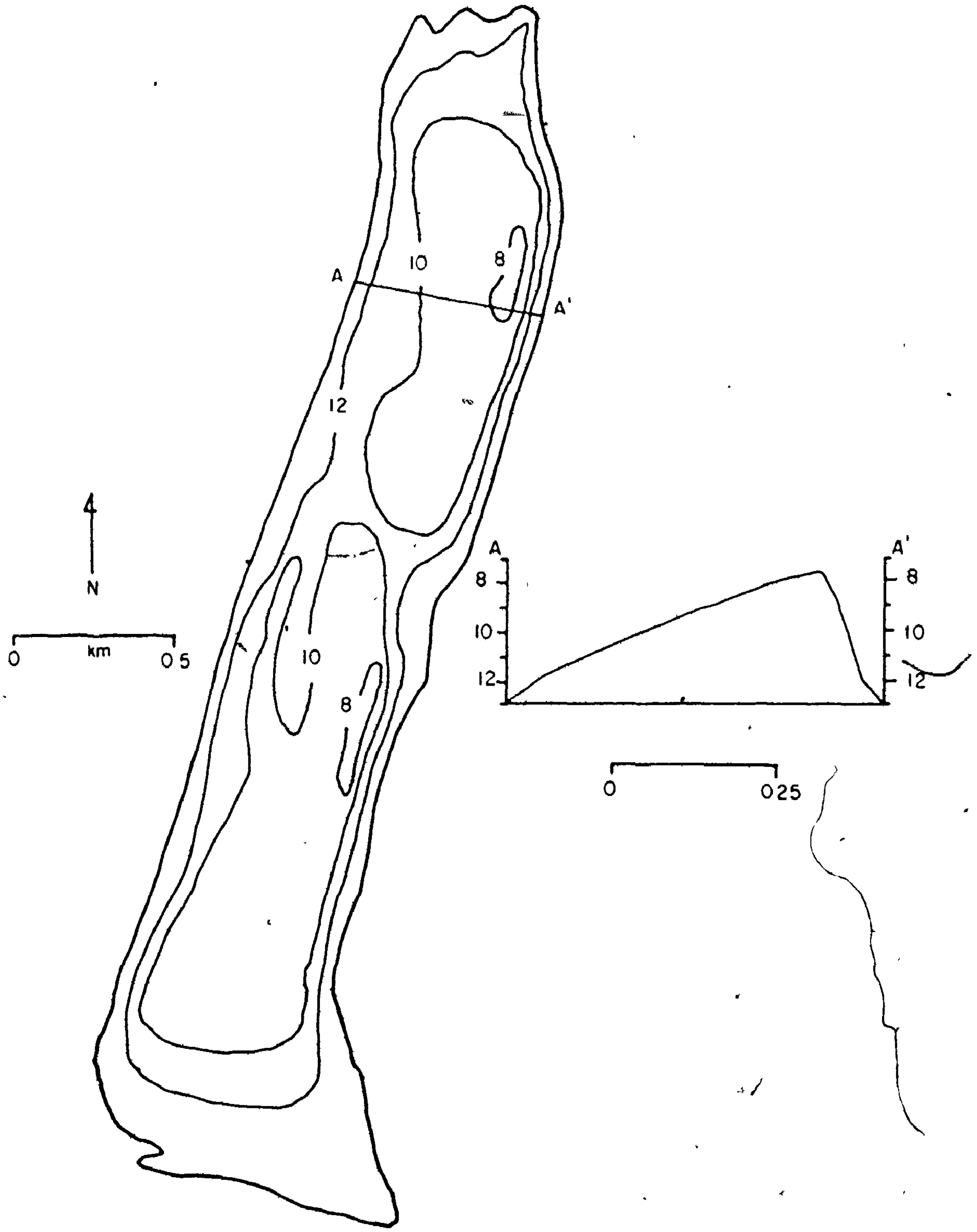
A
A'
10
8
12
10
8
N
0
km
0 5
A
A'
8
10
12
8
10
12
0
0 25

Fig. 4-3. Contour map and cross-section of Newport Bar. Depths are m below higher high water

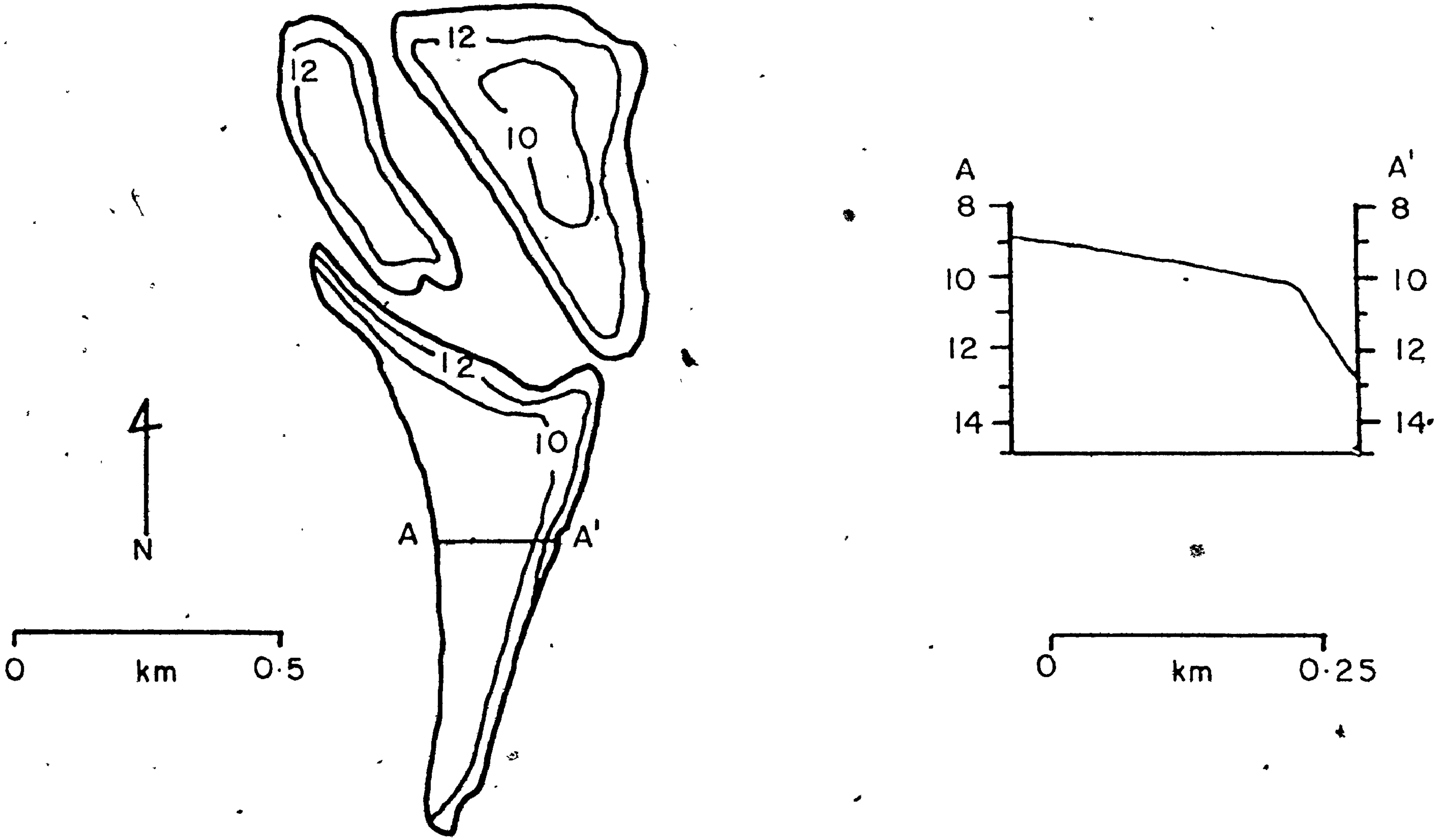
12
12
10
12
10
A
A'
N
0
km
0.5
A
A'
8
10
12
14
8
10
12
14
0
km
0.25

Fig. 4-4. Contour map and cross-section of Mitchener Bar. Depths are m below higher high water

down at 1° to the east. East of the channel the bar slopes upward at 0.75° to the sand body crest. A cross-section of Mitchener Bar is shown in Figure 4-4B.

The highest part of Mitchener Bar is where it attaches to the shore with an elevation of 8.6 m below higher high water. Most of the sand body is subaerially exposed for 3 hours during each tidal cycle; the highest point on the sand body is 4.2 m above the channel to the east of the sand body (Fig. 4-4B) yielding a thickness of 4.2 m for Mitchener Bar.

HANTSPORT BAR Hantsport Bar is 2.84 km long and up to 0.81 km wide and has a narrow southern end that is joined to the shore (Fig. 4-5A). The sand body widens to the north and terminates in a wide lobe; there is a spit projecting to the southwest from the western edge of the lobe (Fig. 4-5A). A well-developed crest lies near the western edge of Hantsport Bar; slopes are 1° to the east of the crest and 2° to the west. Figure 4-5B provides a cross-sectional view of Hantsport Bar.

Hantsport Bar is subaerially exposed for 4 hours of each tidal cycle. The highest point on the sand body is 4.5 m above the floor of the channel to the west of the bar and is 9.2 m below higher high water; Hantsport Bar is 4.5 m thick.

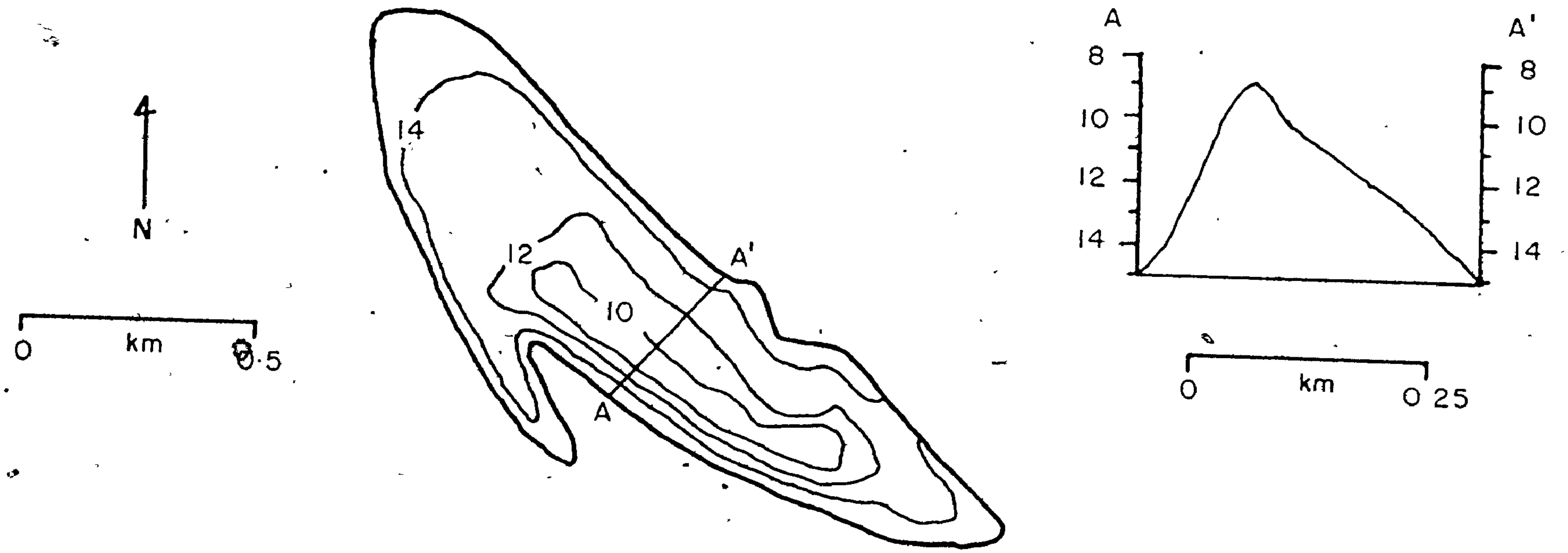
N
0
km
0.5
14
12
10
A'
A
A
A'
8
10
12
14
8
10
12
14
0
km
0 25

Fig. 4-5. Contour map and cross-section of Hantsport Bar. Depths are m below higher high water

MIDDLE GROUND Middle Ground is the longest sand body in the system at 5.60 km and is a maximum of 0.71 km wide; it is elliptical in shape, being narrow at either end and widest near the center (Fig. 4-6A). The most prominent topographic feature on Middle Ground is the large ebb spit at the southern end (Fig. 4-6A); the spit extends north of the position shown in Figure 4-6A in the subtidal (see Fig. 4-2). There is a well developed crest on Middle Ground. On most of the sand body the crest runs along the eastern side but towards the southern end it crosses to the west and terminates (Fig. 4-6A).

Slopes to the east of the crest are 2.5° and those to the west are 0.5°. A typical cross-section of Middle Ground is shown in Figure 4-6B. Middle Ground is at least 8.4 m thick and its highest point is 7.2 m below higher high water. Most of Middle Ground is subaerially exposed for almost 6 hours of every tidal cycle.

BOOT ISLAND BAR Boot Island Bar is 2.53 km long and 0.40 km wide as shown in Figure 4-7A. A spit projects to the southeast from the eastern side of the sand body (Fig. 4-7A). The southern part of Boot Island Bar has a crest along the eastern side; the crest terminates where the spit joins the sand body (Fig. 4-7A).

The surface of Boot Island Bar slopes 7° to the east of the crest and 1.5° to the west. In the northern part of the sand body, the surface of the sand body is slightly convex with slopes of 0.5° to the east and west of the sand body center. Two cross-sections are shown

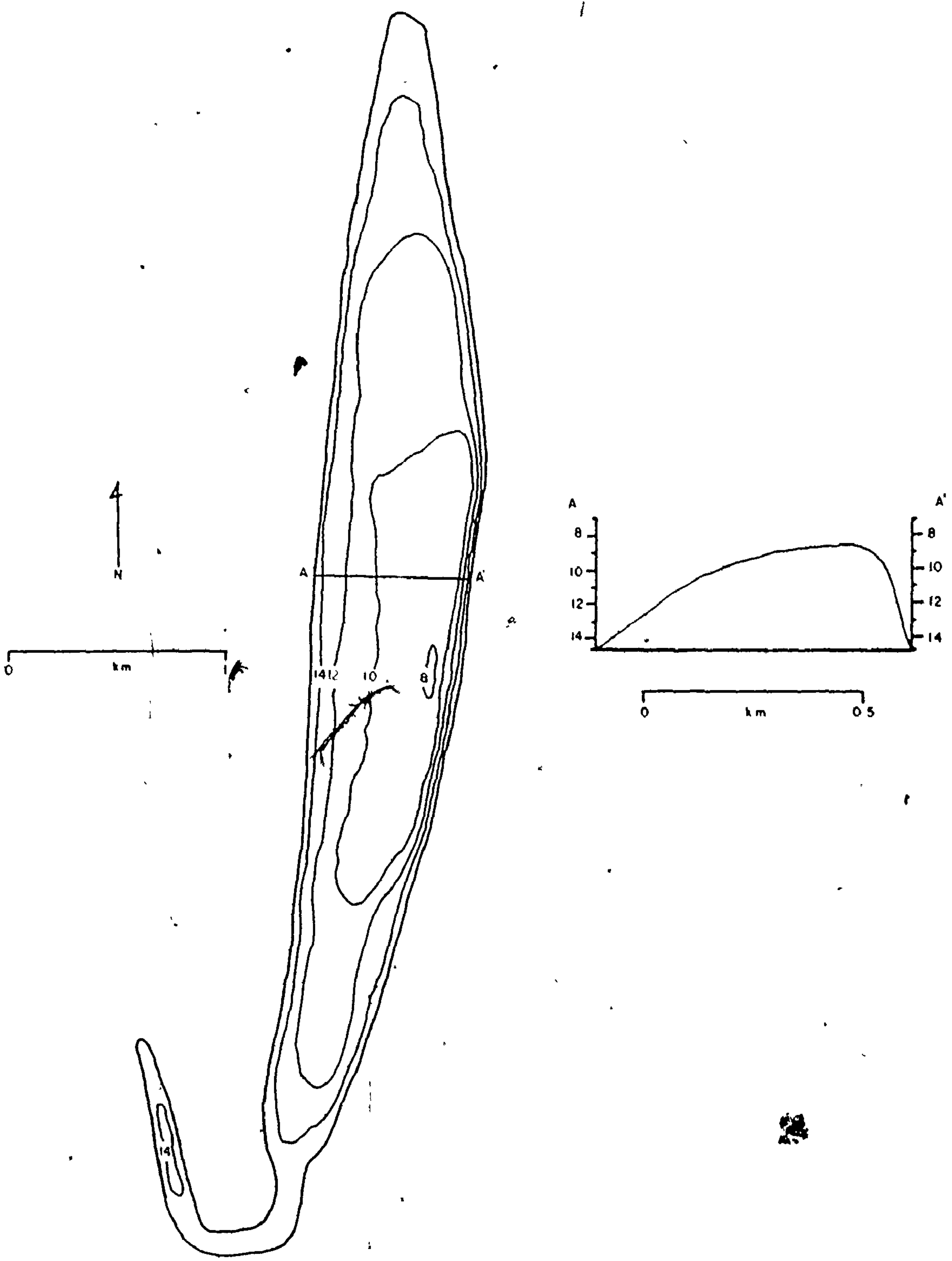
N
0
km
1
A
A'
14
12
10
8
14
A
A'
8
10
12
14
0
km
0.5

Fig. 4-6. Contour map and cross-section of Middle Ground. Depths are m below higher high water

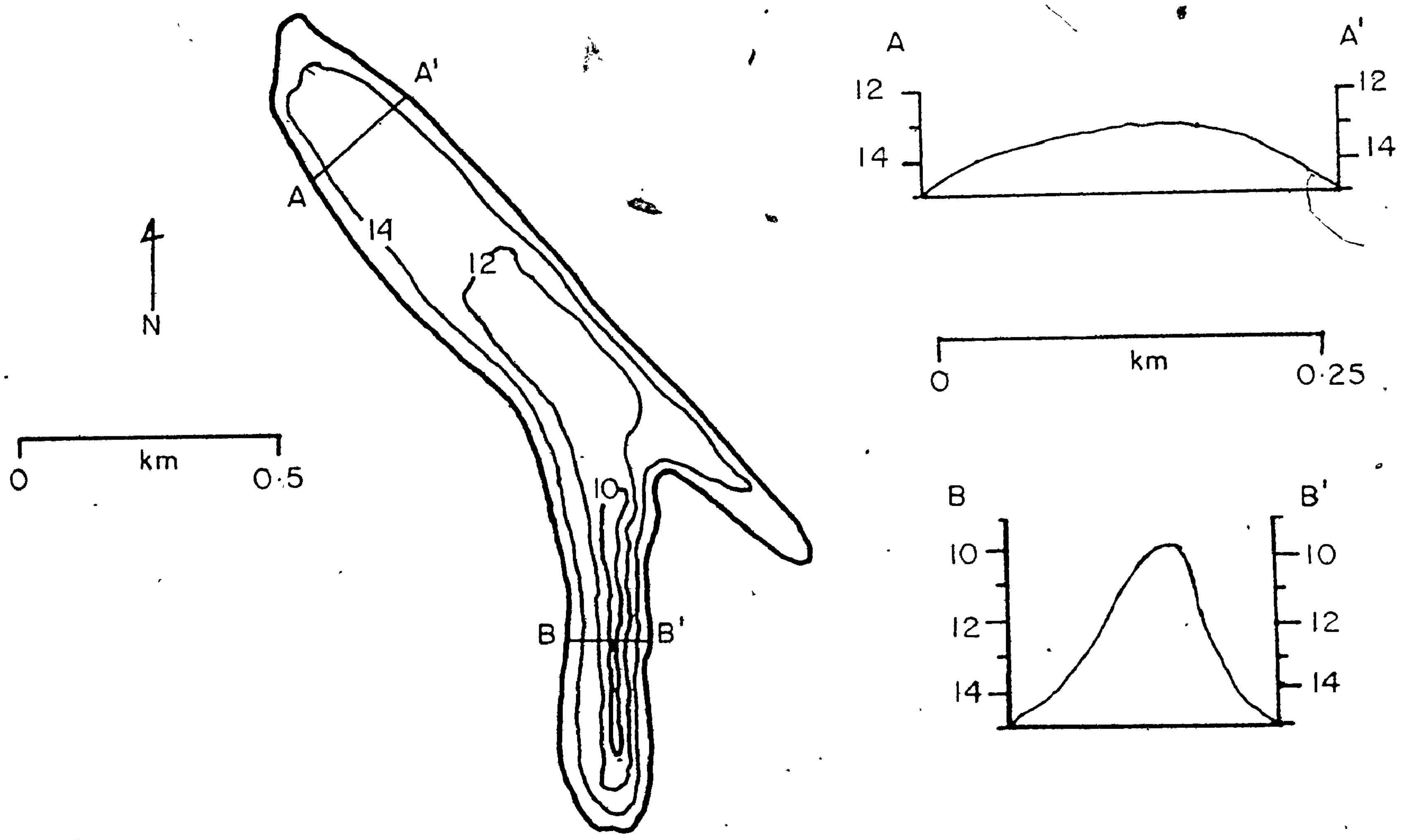
A'
A
14
12
10
B
B'
N
0
km
0.5
A
A'
12
14
12
14
0
km
0·25
B
B'
10
12
14
10
12
14

Fig. 4-7. Contour map and cross-sections of Boot Island Bar. Depths are m below higher high water

in Figure 4-7B. Boot Island Bar is subaerially exposed for 4 hours and its highest point is 8.9 m below higher high water. The wave cut platform to the west of the sand body is 2.6 m below the highest point on the sand body; this is a minimum thickness since it is not known if the platform underlies the entire sand body.

WESTERN BAR The larger part of Western Bar is 2.85 km long and 0.55 km wide; the smaller section to the northeast is 0.87 km long and 0.71 km wide and is separated from the main part of the sand body by a channel (Fig. 4-8A). There is another section of Western Bar to the north of that shown in Figure 4-8A but it is unexposed during most tidal cycles since it is only slightly higher than lower low water (see Fig. 2-7); it has not been examined due to its limited accessibility. The crest of Western Bar is on the western side of the sand body at the southern end. It crosses to the east near the center of the sand body and back to the west towards the northern end (Fig. 4-8A).

Slopes are 2.5° to the north and east of the crest of Western Bar and 1° to the south and west. Figure 4-8B shows a typical cross-section from Western Bar. The highest point on Western Bar is 8.9 m below higher high water and the sand body is at least 2.5 m thick. Western Bar is subaerially exposed for 4 hours.

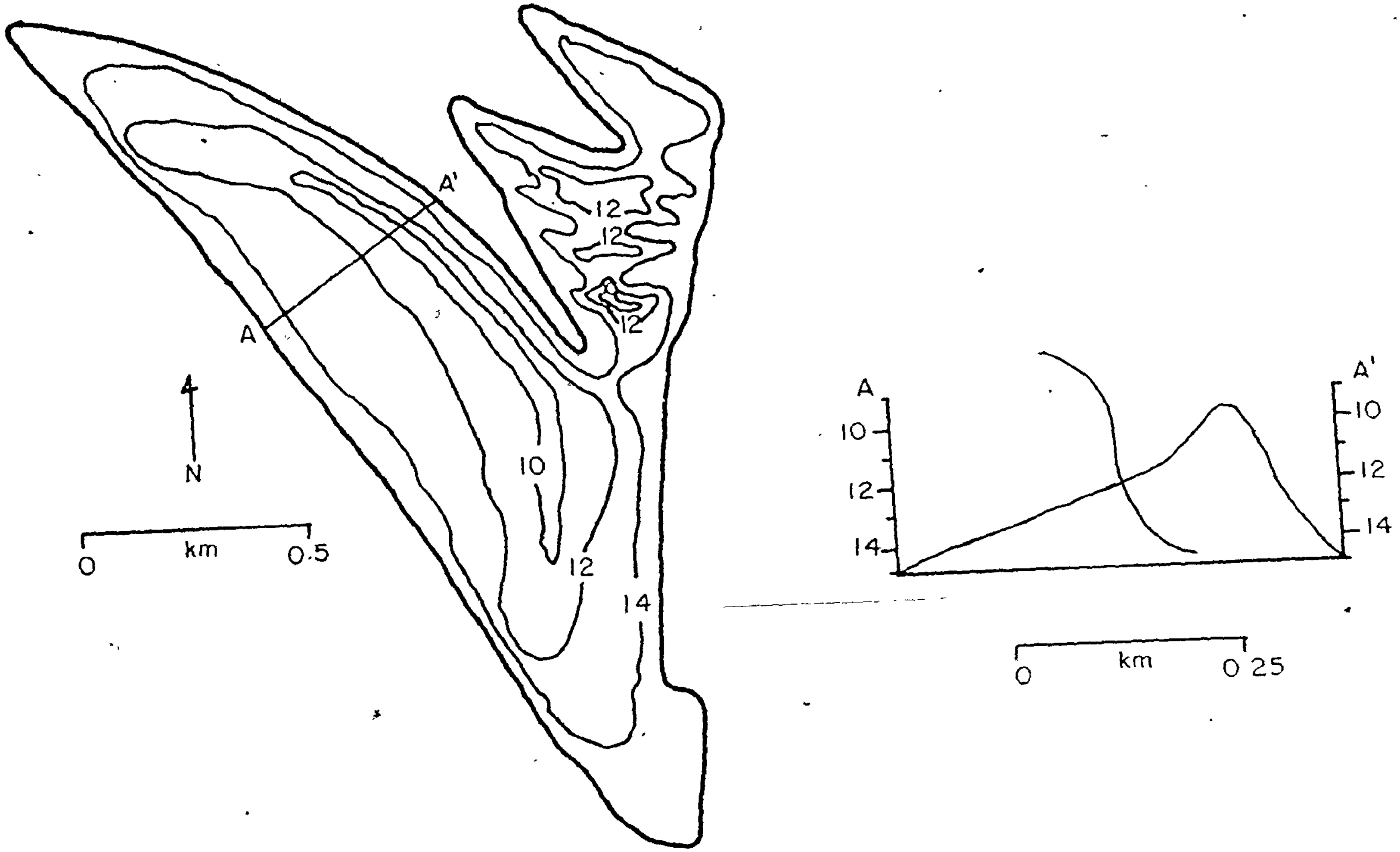
A'
12
12
12
A
N
0
km
0.5
10
12
14
A
10
12
14
A'
10
12
14
0
km
0 25

Fig. 4-8. Contour map and cross-section of Western Bar. Depths are m below higher high water

Sand Body Stability

Comparative measurements made between a British Admiralty Chart dated 1865 and sets of aerial photographs from 1963, 1964, 1973 and 1974 indicate that all six sand bodies in the Avon River estuary are remarkably stable. British Admiralty charts updated to 1908 and 1916, as well as a Canadian Hydrographic Service chart from 1972, also indicates that the sand bodies have been stable.There have been no major changes in any of the sand bodies since 1963; in each set of aerial photographs the sand bodies are the same size and shape, and are in the same positions. Plate 4-1 shows the sand bodies at the mouth of the system in 1963. If they are compared to the same sand bodies in 1974 (Plate 4-2), no differences are found. The same is true of the sand bodies at the head of the estuary; Plate 4-3 depicts them in 1963 and Plate 4-4, in 1974.

The British Admiralty Chart of 1865 shows that five of the six sand bodies have the same shape, size, and location that they have now (Figs. 4-1 and 4-9). The only exception is Newport Bar which appears as two sand bodies on the 1865 chart. These two sand bodies are in the same location and have the same length as Newport Bar but are split by a channel. The present day Newport Bar has a channel at its northern end that occupies a similar position to the one on the 1865 chart but it does not extend far enough south to divide the sand body (Fig. 4-3A). It seems likely that the southern end of this channel has filled since 1865. Aerial photographs reveal that the channel was filled prior to 1963; it has not been a conse-

Plate 4-1. 1963 Aerial photograph of the estuary mouth,

the scale is 1:45,000

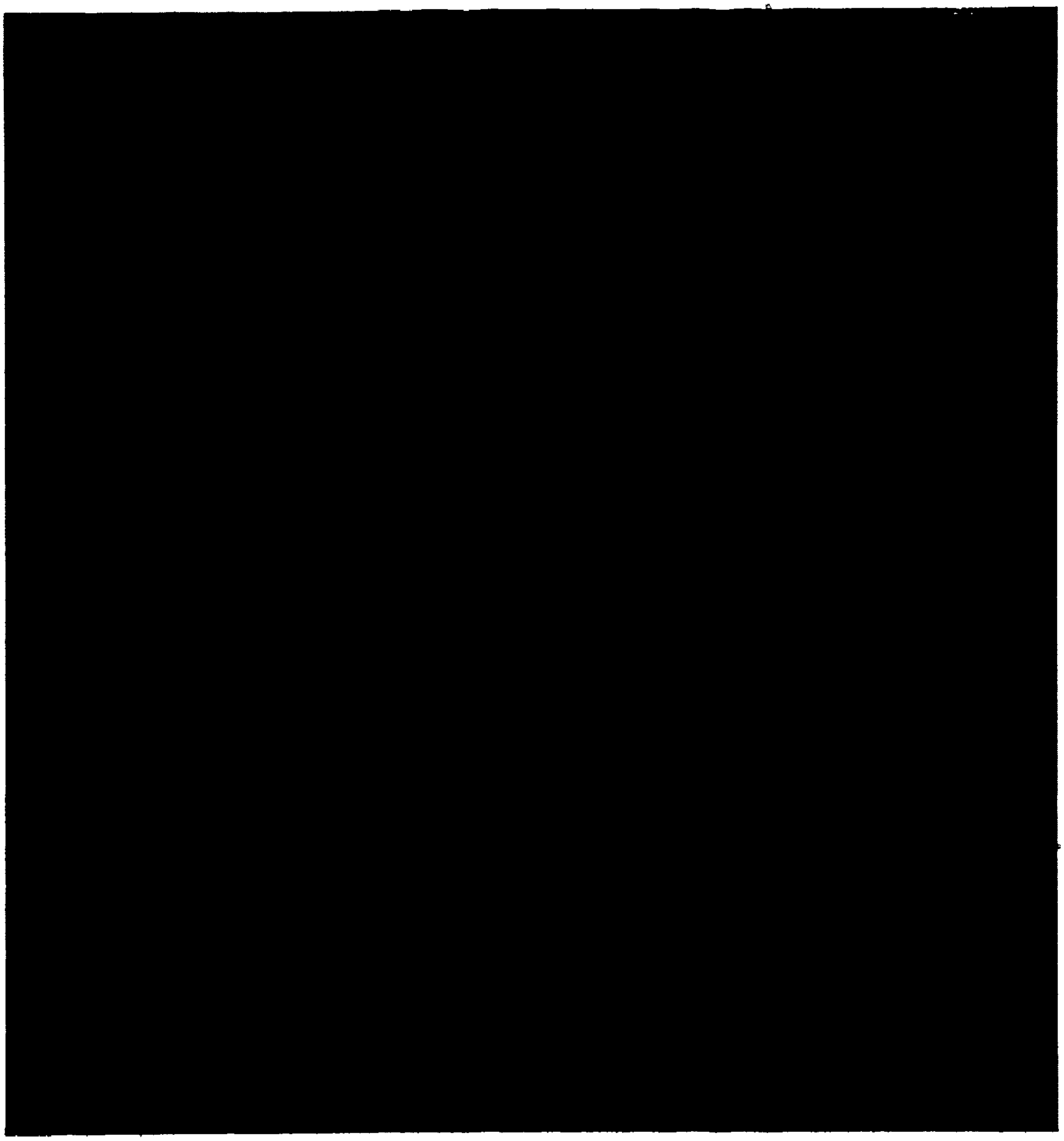

Plate 4-2. 1974 Aerial photograph of the estuary mouth,

the scale is 1:45,000

Plate 4-3. 1963 Aerial photograph of the estuary head;

the scale is 1:67,000

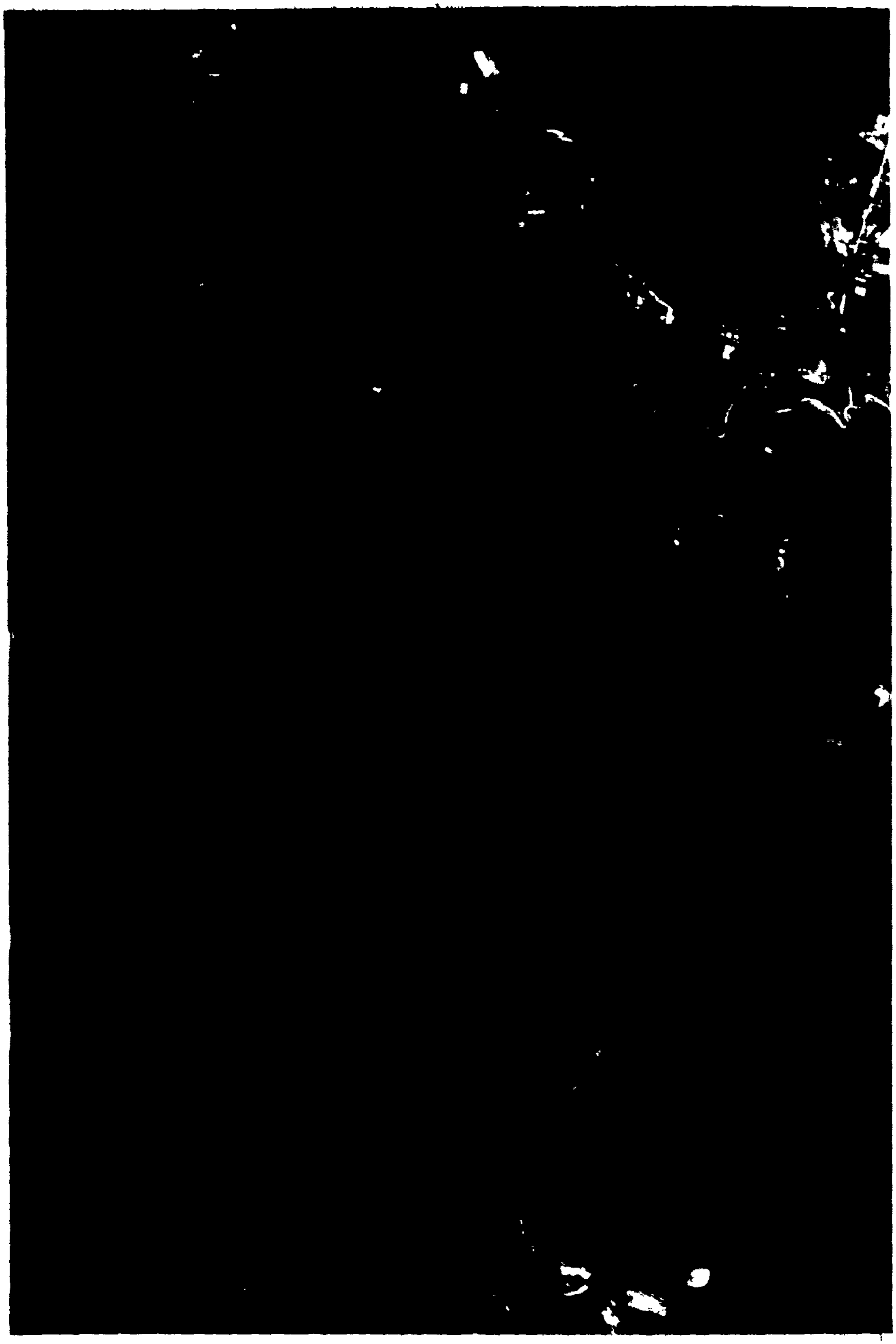

Plate 4-4. 1974 Aerial photograph of the estuary head;

the scale is 1:47,000

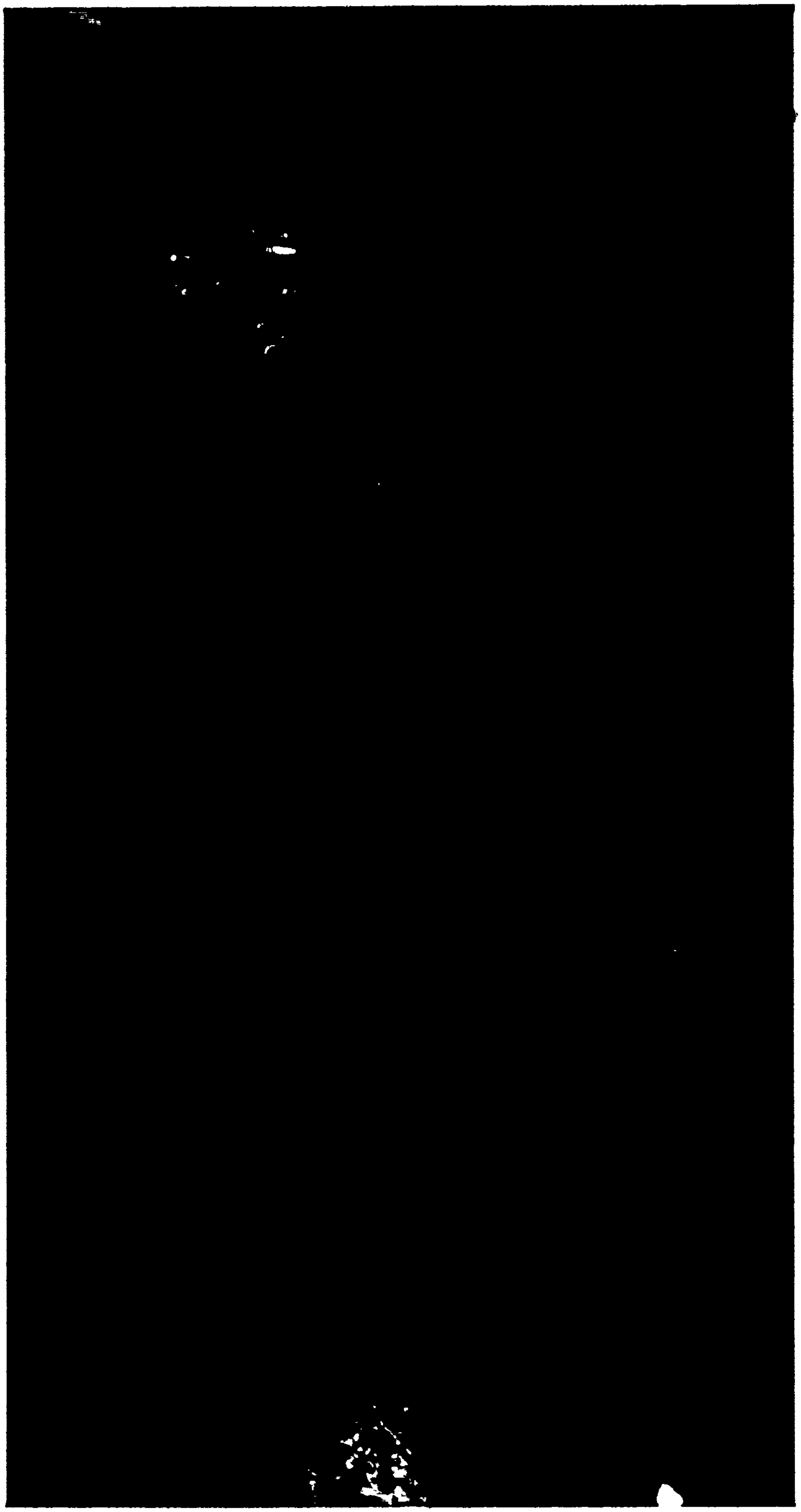

Fig. 4-9. 1865 British Admiralty map; soundings are in fathoms below lower low water; underlined readings are fathoms above lower low water.

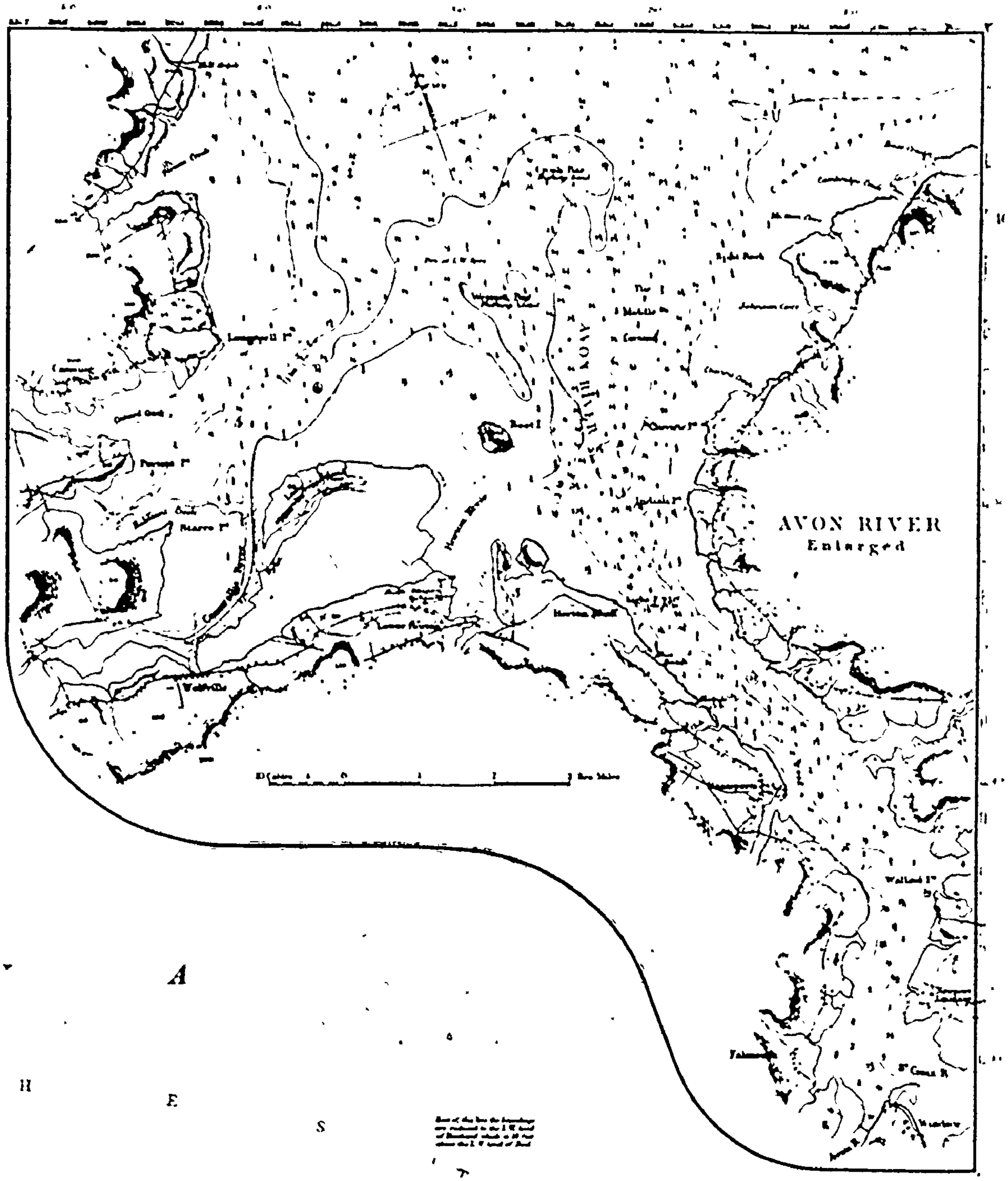
AVON RIVER
Enlarged
AVON RIVER
Boot I
Horton Bluff
Wolfville
Falmouth
Windsor
A
H
E
S

quence of construction of the causeway at Windsor in 1970.

Minimum thicknesses and highest elevation points were calculated for Newport Bar, Hantsport Bar, Middle Ground, and Western Bar from soundings displayed on the 1865 chart. Both thicknesses and elevations are similar to those surveyed in 1975; Table 4-1 compares 1865 and 1975 sand body thicknesses and highest elevations. Western Bar and Middle Ground seem to be thicker in 1975 than in 1865 and Hantsport Bar appears to have decreased in thickness since 1865. None of the apparent changes are larger than 1.2 m (Table 4-1).

Apparent differences in sand body thickness and elevation could be due to insufficient detail on the 1865 chart or they might represent actual changes in sediment distribution. Soundings marked on the 1865 chart are not closely spaced, and in some cases there are no soundings on what are now the highest parts of the sand bodies. (Compare Fig. 4-9 with Figs. 4-3A, 4-5A, 4-6A and 4-8A.) It seems likely that differences in sand body thicknesses and elevations may be the result of insufficient data from the 1865 chart; the possibility that sediment distribution has changed will be discussed further in Chapter 10. It appears that all the sand bodies in the Avon River estuary have remained almost constant in terms of size, shape, position, thickness, and elevation for 110 years; the system seems to have been in equilibrium since at least 1865.

TABLE 4-1. Thickness and Elevation of Sand Bodies in 1865 and 1975

	Minimum Thickness (m)			Elevation[1]		
Sand Body	1865	1975	Net Change[2]	1865	1975	Net Change[3]
Hantsport Bar	5.4	4.5	-0.9	10.1	9.2	+0.9
Middle Ground	8.2	8.4	+0.2	7.4	7.2	+0.2
Newport Bar	5.9	5.9	0.0	7.8	7.5	+0.3
Western Bar	2.3	2.5	+0.2	10.1	8.9	+1.2

[1] meters below higher high water

[2] a positive net change indicates an increase in thickness, a negative net is a decrease in thickness

[3] a positive net change means that the bar has grown higher with time

Minimum thickness and elevation for 1965 were calculated using the elevations recorded on the British Admiralty Chart of 1865; if their soundings were not at the base and crest of a sand body, the elevation and thickness is inaccurate.

Summary

All six major intertidal sand bodies lie between channels of opposing net discharge and are oriented parallel to tidal current flow. The three sand bodies at the mouth of the estuary form part of an ebb tidal delta that bears more resemblance to the mesotidal model than the macrotidal model of Hayes (1975); this is probably a result of confining bedrock shorelines. Hantsport Bar appears to form part of an ebb tidal delta at the mouth of the Kennetcook River, and Mitchener Bar seems to be a tidal point bar.

Sand bodies range in length from 0.80 to 5.60 km and in width from 0.40 to 0.95 km. Most sand bodies have a well-developed crest running parallel to their length; slopes on one side of the crest are gentle, typically 1°, and steep on the other side, usually about 2.5°. Subaerial exposure ranges from 3 to 6 hours as the highest point on each sand body varies from 7.2 to 9.2 m below higher high water.

Five of the six sand bodies appear to have been stable for at least 110 years; comparison of recent aerial photographs with a British Admiralty Chart from 1865 reveals no significant changes in sand body positions or shapes. A channel at the southern end of Newport Bar has been filled in since 1865. No major changes in sand body thickness or elevation are apparent.

CHAPTER 5

BEDFORMS, OTHER SURFACE FEATURES, AND INTERNAL STRUCTURES

Bedforms

Several bedform classification schemes relate surface morphology to hydraulic properties (Simons et al., 1965a; Boothroyd, 1969). In this discussion, the division of bedforms into classes is not based on hydraulics; it is purely descriptive and derives from observations and measurements. Hydraulic requirements for the bedforms described below and their relationship to other classification schemes will be discussed in Chapter 9. The terminology used in this study is identical to that of Klein (1970) and is compared to the terminology of other workers in Table 5-1.

There are four types of bedforms in the Avon River estuary. Three of these, ripples, megaripples, and sand waves, are fairly abundant, while the fourth, transverse bars, occurs only in one location. The three abundant bedform types occur in sets with individual bedforms regularly spaced, that is, they have easily recognizable wavelengths. Transverse bars seem to form individually; they are not found in sets with constant wavelengths.

TABLE 5-1. Comparison of Bedform Terminology

	Klein (1970) and the Present Study	Simons et al. (1965)	Boothroyd (1969)	Costello (1974)
Increasing Wavelength ↓	Ripples	Ripples	Ripples	Ripples
	Megaripples	Dunes	Megaripples	Dunes
	Sand Waves	-	Sand waves	Bars

Numerous megaripples, sand waves, and transverse bars were measured using a Brunton compass and a tape measure; ripples and other surface features were not examined systematically as only a few measurements were made. Wavelengths were calculated by measuring the total distance perpendicular to the crests of 3 adjacent bedforms and averaging the distance; recorded height was the averaged vertical distance from bedform crest to trough. Lee and stoss stopes, as well as crest strike, were measured using a Brunton compass. Measurements of all parameters were made on several days at each station. The raw data are listed in Appendix C; crest strike directions have been corrected for magnetic declination. Description and distribution of each bedform class is discussed below.

RIPPLES Ripples are the lowest order (smallest) bedform in the system with wavelengths commonly close to 0.30 m and heights of less than 0.05 m. Two types of ripples can be distinguished, sinuous ripples (Fig. 5-1) and linguoid ripples (Fig. 5-2). Sinous ripples cover large areas on Newport Bar and Mitchener Bar (Fig. 5-3) while linguoid ripples are common on Middle Ground and Boot Island Bar (Fig. 5-4); linguoid ripples also occur on parts of Newport Bar (Fig. 5-3). Wave-formed oscillatory ripples are found occasionally but are not considered to be important bedforms; their distribution will be discussed later in this chapter.

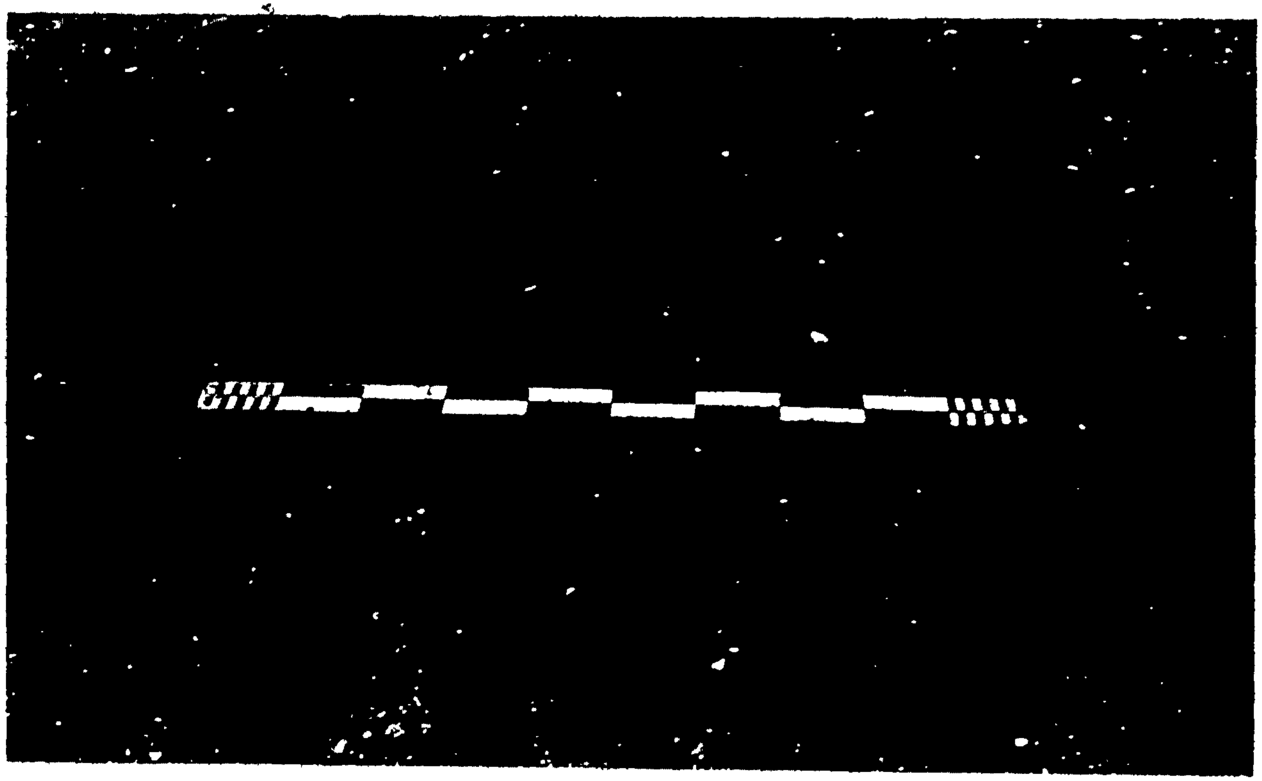

Fig. 5-1. Sinuous ripples; the scale is decimeters and centimeters

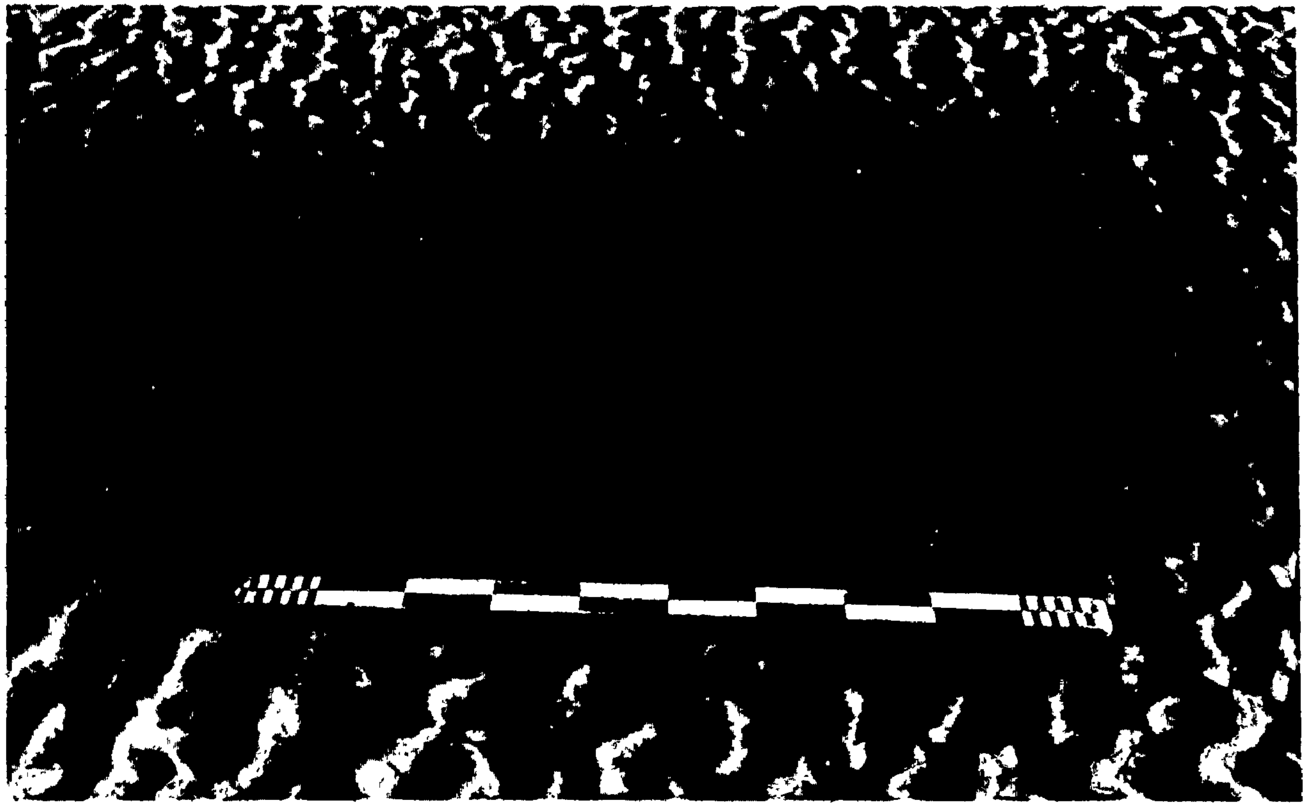

Fig. 5-2. Linguoid ripples; the scale is decimeters and centimeters

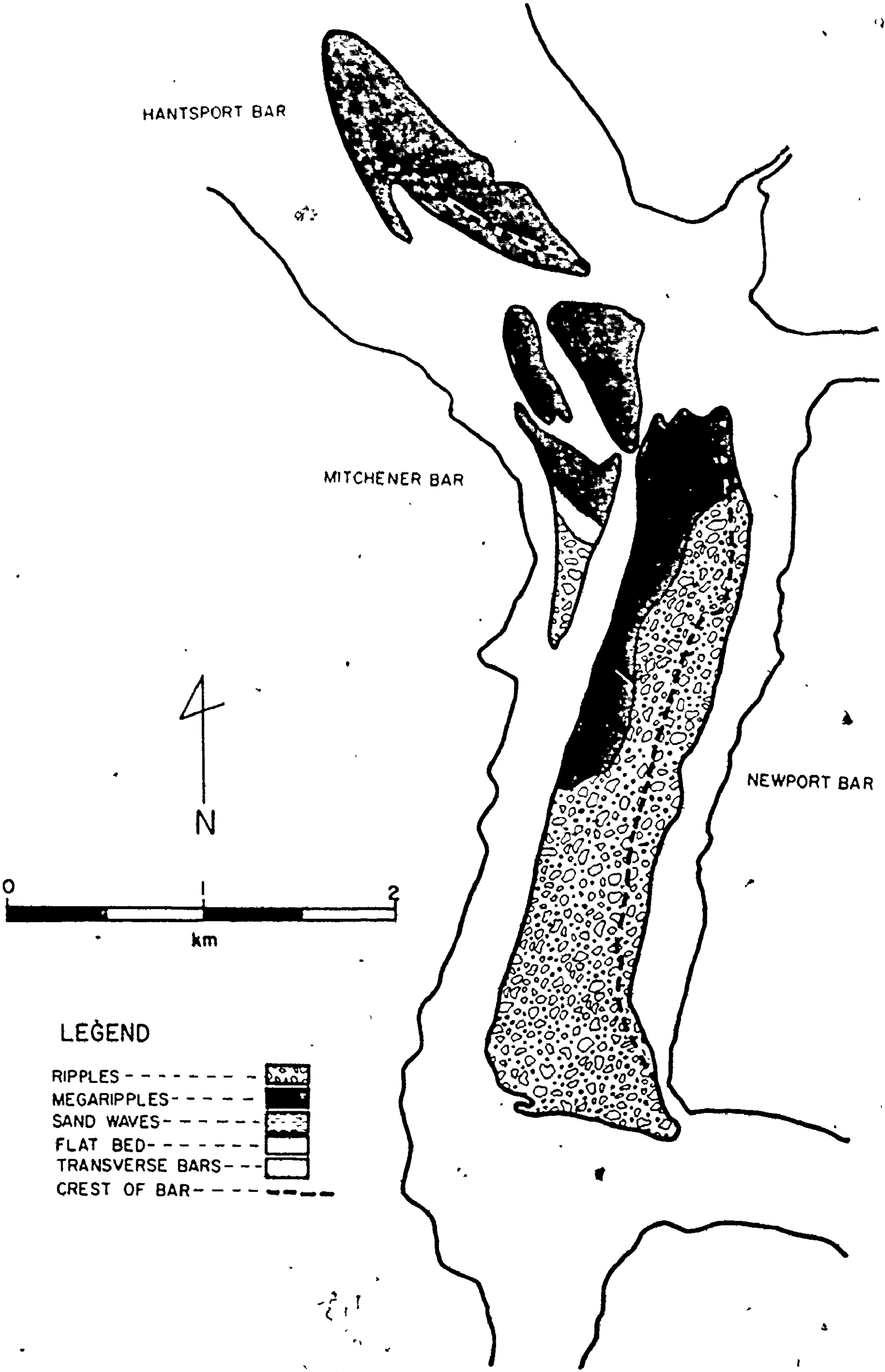
HANTSPORT BAR
MITCHENER BAR
NEWPORT BAR
N
0
1
2
km
LEGEND
RIPPLES
MEGARIPPLES
SAND WAVES
FLAT BED
TRANSVERSE BARS
CREST OF BAR

Fig. 5-3. Bedform distribution at the estuary head

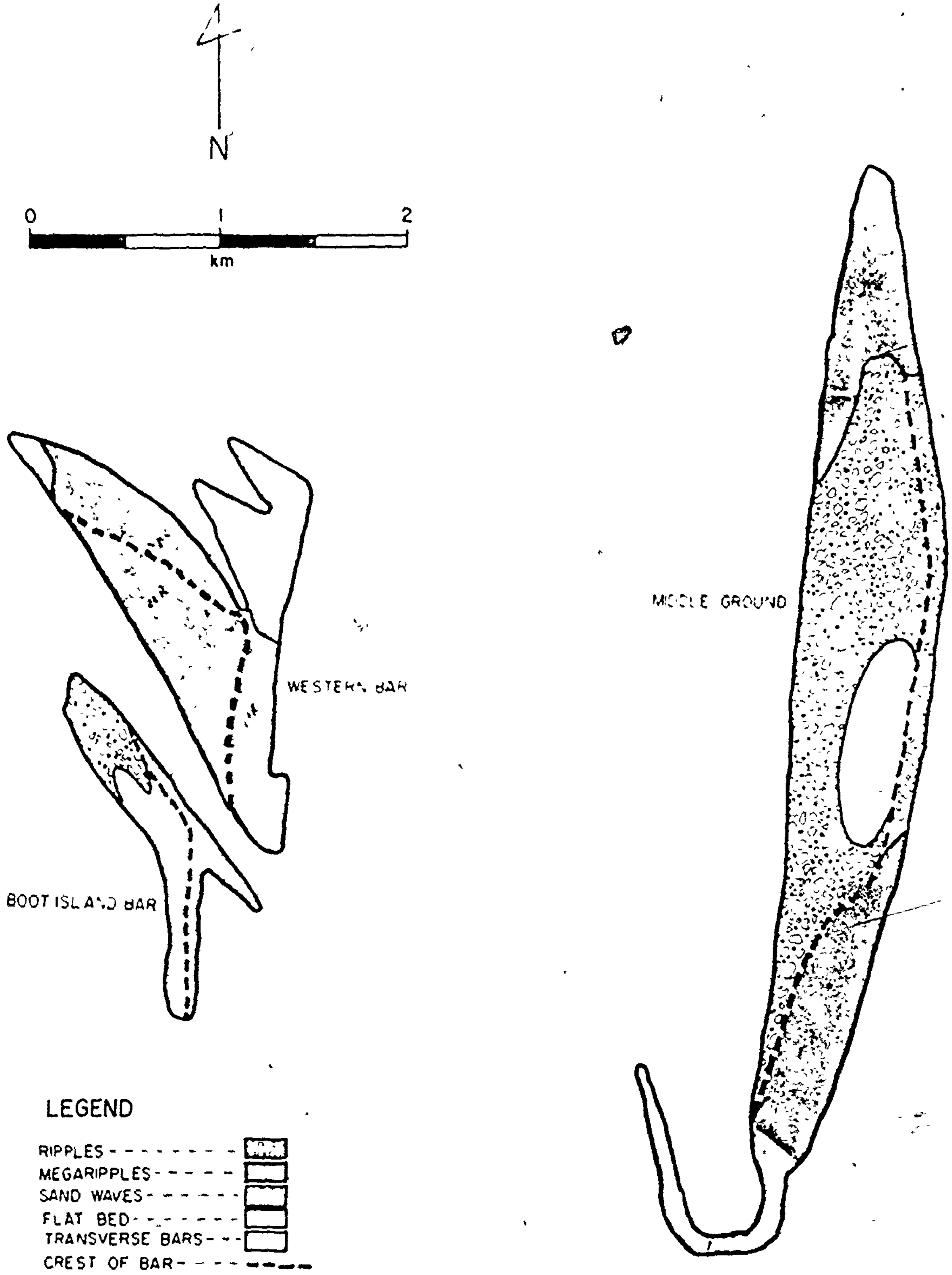
N
0
1
2
km
MIDDLE GROUND
WESTERN BAR
BOOT ISLAND BAR
LEGEND
RIPPLES
MEGARIPPLES
SAND WAVES
FLAT BED
TRANSVERSE BARS
CREST OF BAR

Fig. 5-4. Bedform distribution at the estuary mouth

MEGARIPPLES Megaripples are second order bedforms with wavelengths commonly less than 10 m and heights up to 0.85 m; a few wavelengths are greater than 10 m (Fig. 5-5). (See Table 5-2 for a summary of megaripple measurements; all the raw data are in Appendix C.) Lee slopes range from 23° to 29° and stoss sides from 2° to 20° with most values lying between 4° and 10° (Table 5-2); megaripples tend to have sinuous crests that are oblique to sand body crests but normal to tidal currents (Table 5-2). Two types of megaripples can be distinguished in the field by relative steepness of the stoss slope and relative height-to-wavelength ratios; the significance of the two types of megaripples will be discussed in Chapter 7, they are both illustrated in Figure 5-6.

Megaripples are found on all six sand bodies (Figs. 5-3 and 5-4). Each area tends to have consistent wavelengths and heights but there is a large variation in these parameters from area to area (Table 5-2). Megaripples on Boot Island Bar and Western Bar are small in both height and wavelength with mean height of 0.26 m and average wavelengths of 5.2 m (Table 5-2). On Middle Ground, the bedforms have mean heights of 0.37 m and wavelengths of 9.7 m. Newport Bar and Mitchener Bar have megaripples with long, mean wavelengths (11.1 m) and large average heights (0.61 m); mean wavelengths and average heights are 4.9 m and 0.30 m on Hantsport Bar (Table 5-2).

Fig. 5-5. Megaripples; the scale is decimeters and centimeters

TABLE 5-2. Summary of Megaripple Measurements

Location	Length (m)	Height (m)	Strike (°)	Lee Slope[1] (°)	Stoss Slope[2] (°)	Sand Body Crest Strike (°)
Boot Island Bar (east)	3.9	0.26	49	28	8	163
Boot Island Bar (west)	6.5	0.26	48	27	12	163
Hantsport Bar (east)	5.4	0.30	69	27	7	128
Hantsport Bar (west)	4.5	0.30	66	26	5	128
Middle Ground	9.7	0.37	82	25	6	7
Mitchener Bar	9.8	0.65	61	29	5	16
Newport Bar	12.3	0.57	82	20	15	23
Western Bar (south)	3.8	0.21	74	30	8	142
Western Bar (north)	3.6	0.29	85	20	14	142

[1] Lee slope is always in the ebb direction

[2] Stoss slope is always in the flood direction

Fig. 5-6. Comparison of the 2 megaripple types:

A) high height - length ratio and

B) low height - length ratio.

The scale is decimeters and centimeters

A

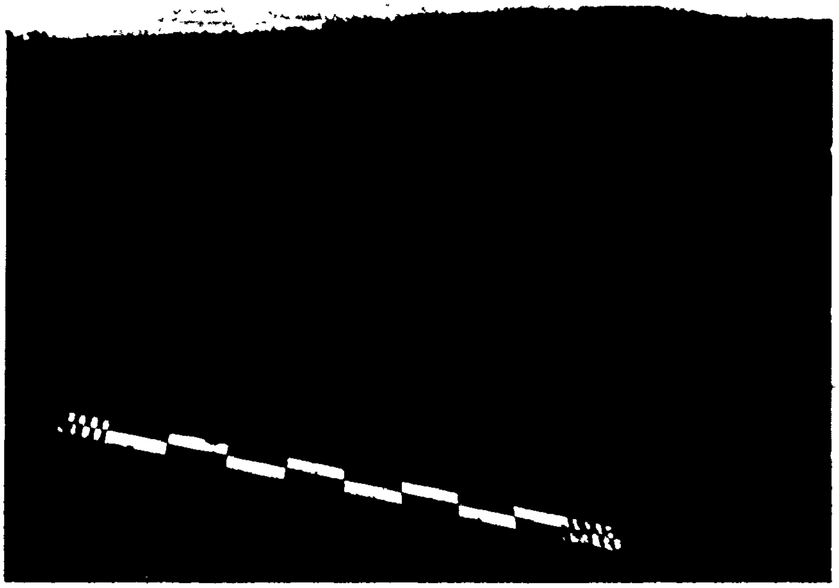

B

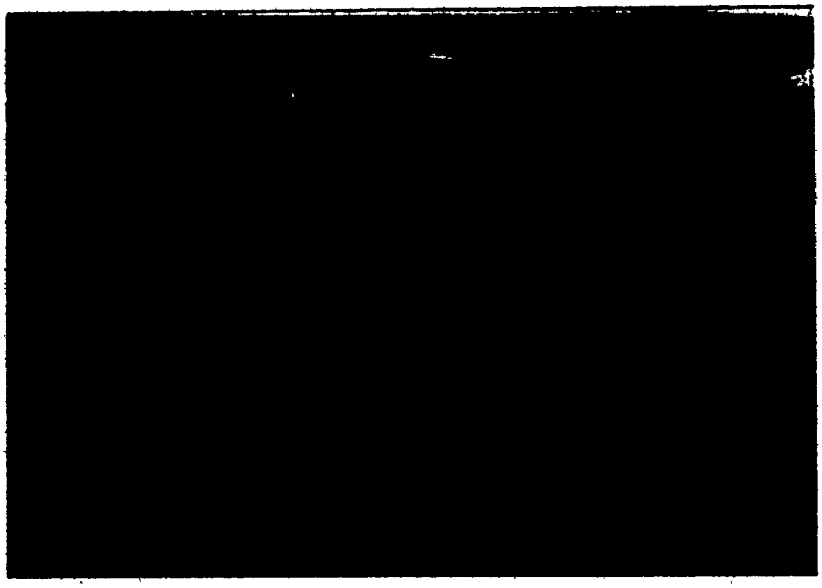

Other features are associated with megaripples including falling water marks, scours, spurs, and liquefaction surfaces. Falling water marks consist of a series of small parallel horizontal ridges along the lee face of a megaripple (Fig. 5-7); they are created by a falling water surface. Scours occurring in the troughs of megaripples, can have diameters of over a meter and their axis of rotation is in the vertical plane; there are often ripples within the scours that reflect the direction of rotation (Fig. 5-8). Spurs also form in megaripple troughs, they are oriented parallel to current direction and are widest at their upstream end (Fig. 5-9). The stoss surfaces of megaripples are almost always covered with ripples (Figs. 5-5, 5-6, and 5-7); liquefaction and fluid escape can flatten rippled surfaces producing the characteristic surface shown in Figure 5-10. During subaerial exposure, small run-off deltas often form in pools along megaripple troughs (Fig. 5-8).

The features described above are not found everywhere that there are megaripples; many megaripples do not have any of these features. Liquefaction surfaces, falling water marks, circular scours, and spurs are common on Hantsport Bar, Mitchener Bar and Newport Bar. None of the features is abundant on the sand bodies at the mouth of the estuary, possibly as a result of coarser grain size (see Chapter 6); falling water marks are observed occasionally and the other features are rarely seen.

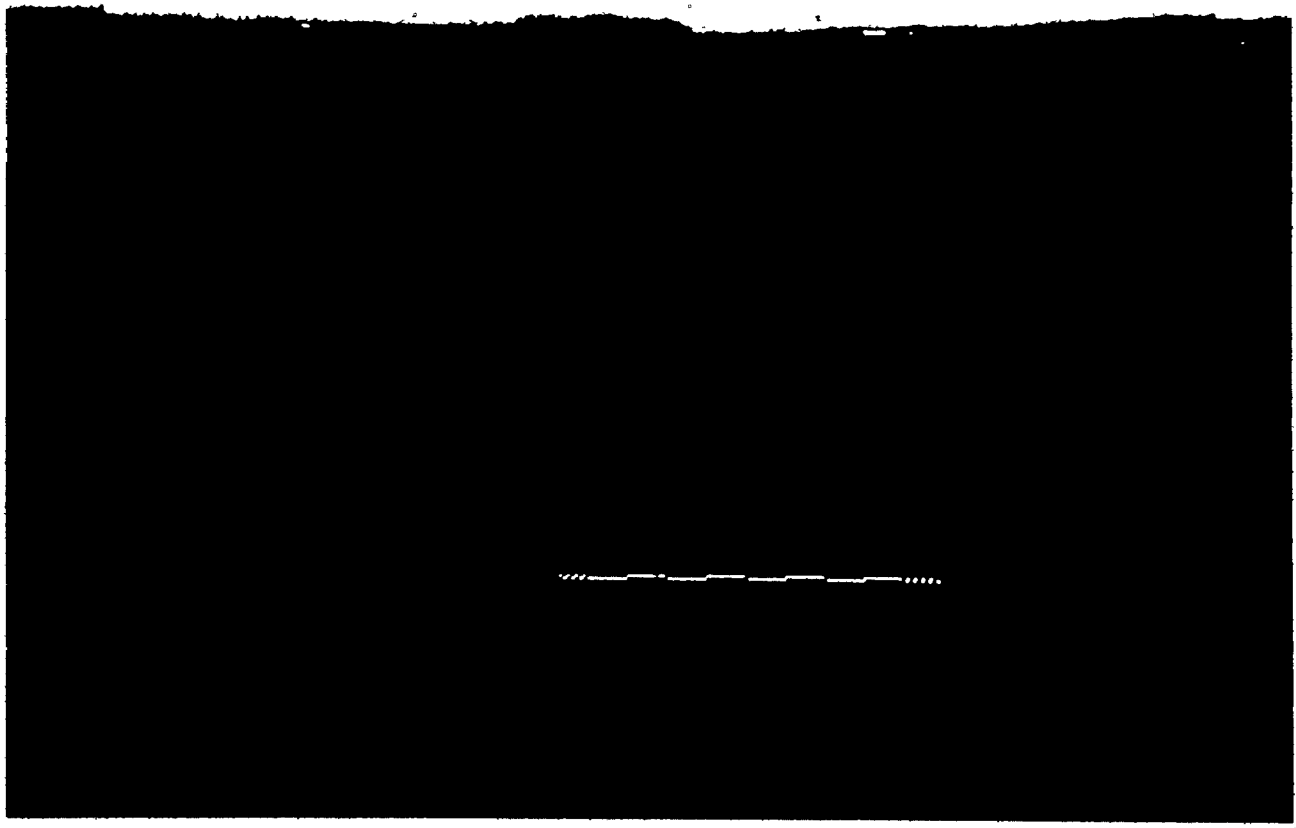

Fig. 5-7. Falling water marks on a megaripple; the marks are a series of horizontal lines along the slip face; they are left by successively lower water surface levels. The scale is decimeters and centimeters.

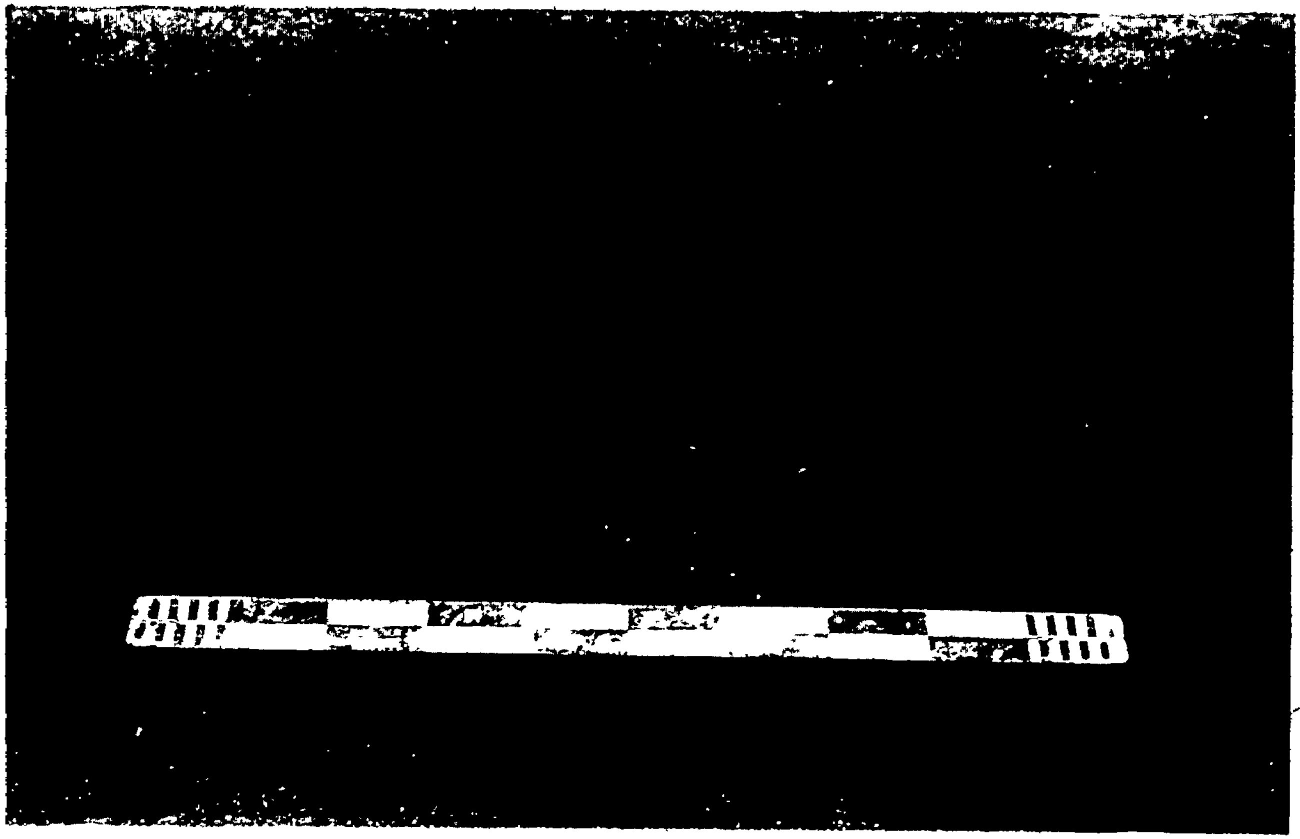

Fig. 5-8 r in a megaripple trough. The scour formed by a turbul ith a al axis of rotation, striking the bed; rotation was counte -stage runoff has built a micro-delta into the scour, the ers and centimeters.

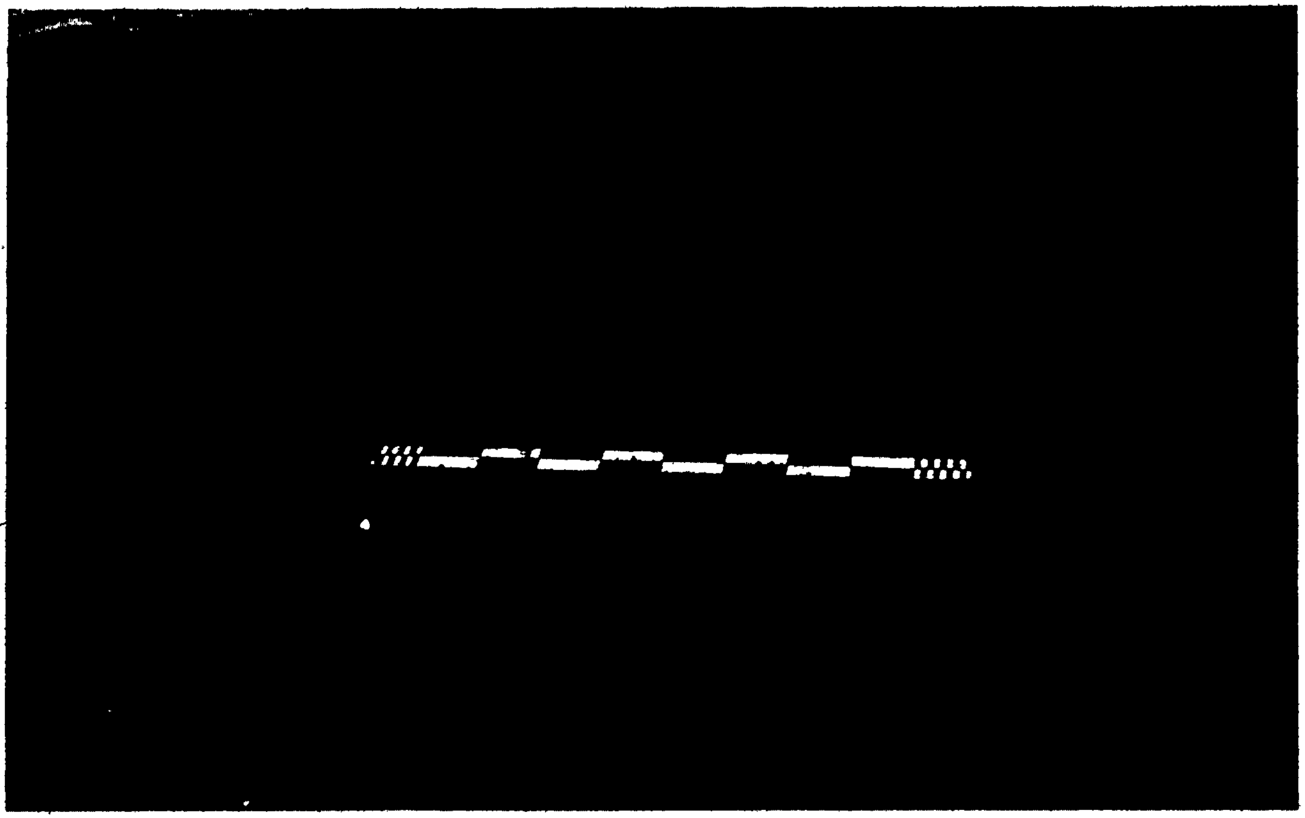

Fig. 5-9. Spur in a megaripple trough. The spur axis is perpendicular to the megaripple slip face, a scour and falling water marks are present also. The scale is decimeters and centimeters.

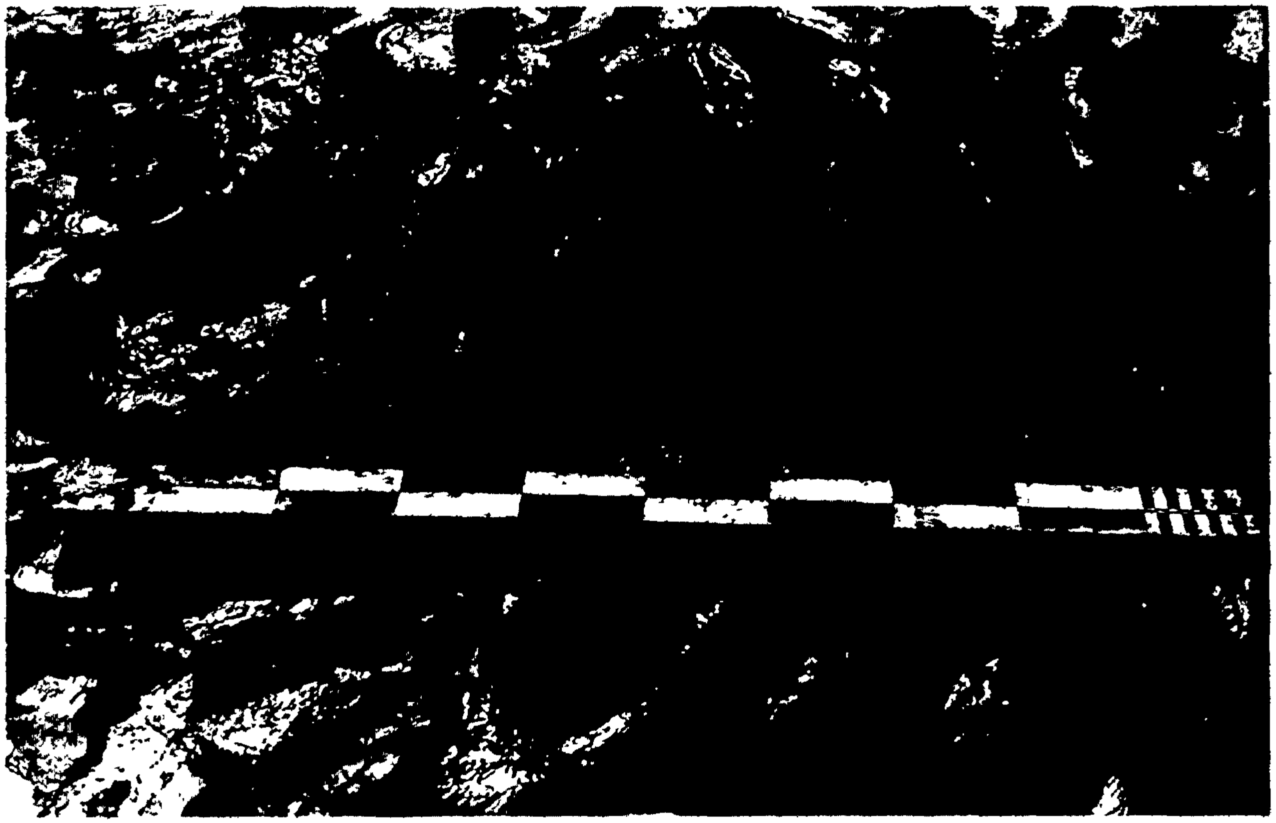

Fig. 5-10. Liquefaction surface on a megaripple; escaping fluid produced the surface. The scale is decimeters and centimeters.

Megaripples can be distinguished from sand waves (described below) by the presence of scour pits and relatively sinuous crests; sand waves tend to be straight-crested and do not have scour pits associated with them. Megaripples and sand waves fall into different fields on a plot of wavelength versus height (Fig. 5-11); sand waves have higher length to height ratios than megaripples; the boundary between the fields approximates the line with the equation height = 0.103 (length) - 0.570 (Fig. 5-11). Also, megaripples are more regularly spaced than sand waves.

SAND WAVES Sand waves are the highest order (largest) bedform in the study area, with heights up to 2 m and wavelengths up to 70 m; they are found in three places, Boot Island Bar, Western Bar, and at the northeastern end of the sand ridge in the center of the estuary (Fig. 5-4). Megaripples often cover the stoss surfaces of sand waves; Figure 5-12 is an aerial photograph of sand waves showing megaripples on their surfaces. Note that the megaripple crests are not parallel to the sand wave crests, and that current directions are perpendicular to the megaripple crests and therefore, oblique to the sand wave crests. A ground level view of a sand wave appears in Figure 5-13. On Western Bar, sand wave crests are not straight but curved; some have two curves resulting in an S-shaped crest (see Plate 4-2); heights of the sand waves increase towards the north. On Boot Island Bar height gradually in-

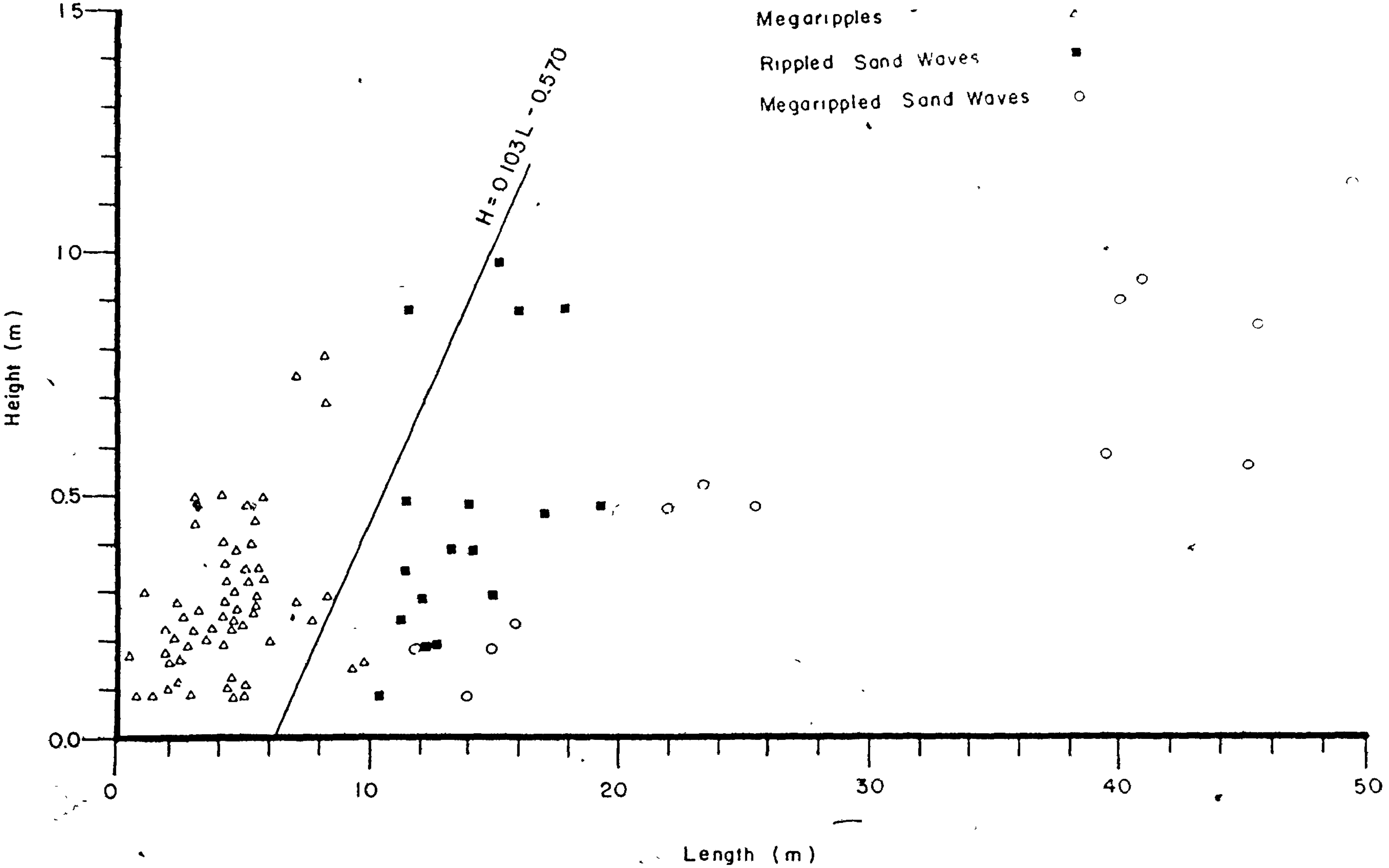

Fig. 5-11. Length versus height for megaripples and sand waves; the two fields are separated by the plotted line

Fig. 5-13. Ground view of sand waves. The scale is decimeters and centimeters.

creases from 0.22 m to 1.5 m from north to south. Slopes on sand waves range up to 27° for the lee face and up to 10° for the stoss.

TRANSVERSE BARS Transverse bars are the fourth, and rarest, bedform in the Avon River estuary; they are found only on part of Mitchener Bar (Fig. 5-3). Only a few are present and their average height is 0.45 m. Lee slopes average 26° and stoss slopes, 1°. They occur in steps resembling a series of terraces and their crests are sinuous (Fig. 5-14).

Transverse bars occur on Mitchener Bar probably because of its similarity to a point bar (see Chapter 4). They are common phenomena in braided rivers (Smith, 1971; D. Cant, 1976, personal communication) and have been observed on point bars in at least one other tidal river (G. Patton, 1975, personal communication). They appear to exist on, and to be restricted to Mitchener Bar because it is the only bar whose position is similar to that of point bars in a fluvial environment.

Other Surface Features

Several other surface features occur in the study area including symmetric wave-formed ripples, current crescents, ice-rafted blocks, mud pebbles, and mud drapes. Symmetric wave-formed ripples occur on days of greater than normal wave activity. Wave action can be sufficient to plane off current ripples and leave either a planed surface

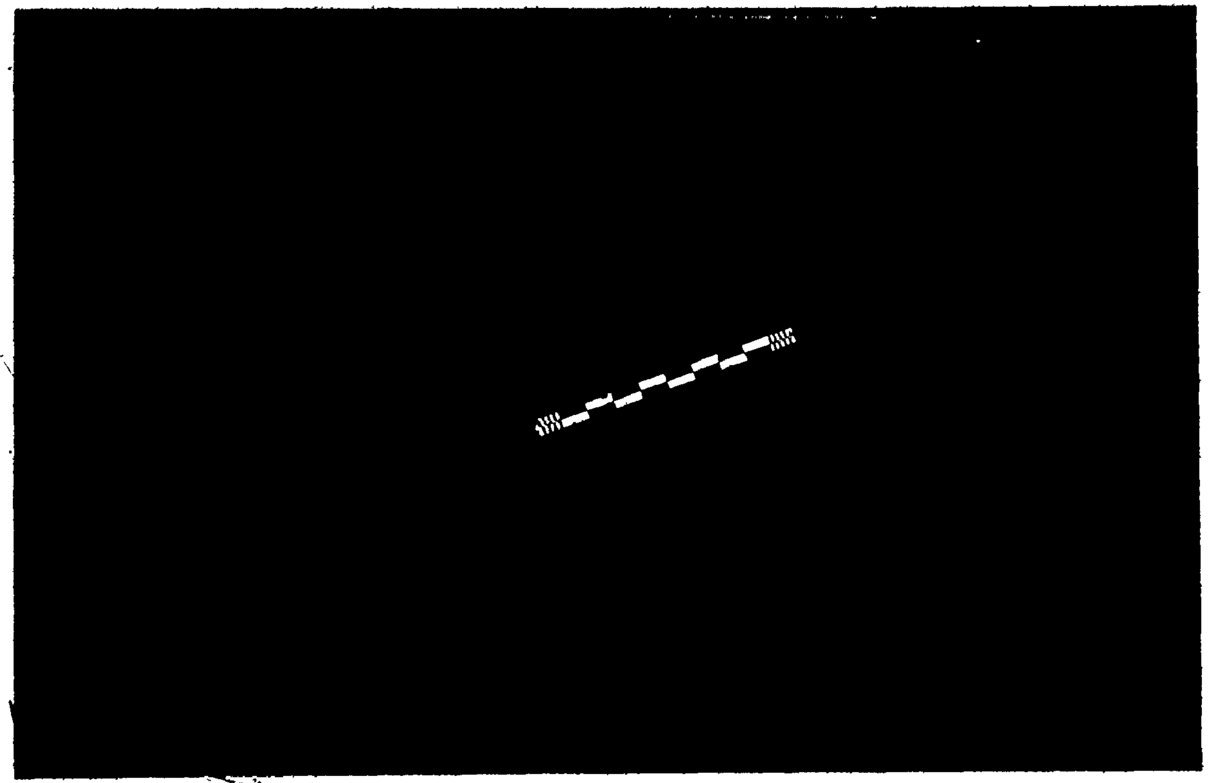

Fig. 5-14. Transverse bars; the scale is decimeters and centimeters.

or produce symmetric ripples (Fig. 5-15); in the Avon River estuary, wave action has never been observed to destroy higher order bedforms. The sand bodies at the mouth of the estuary display wave-formed ripples more often than those at the head of the system because wave action is stronger at the mouth. Wave-formed ripples are destroyed within one tidal cycle of their formation.

Ice-rafted blocks are scattered over the surfaces of all the sand bodies (Fig. 5-16); notable concentrations occur on the southern and western sides of Western Bar and on the western central area of Middle Ground (Fig. 5-4). Current crescents are found around many ice-rafted blocks, especially larger ones (Fig. 5-16). Other large objects have current crescents formed around them; this happens frequently with ice-rafted pieces of salt marsh.

The southern end of Newport Bar has a region where previously deposited muddy sediments are ripped out by scouring. This produces numerous mud pebbles that cover the surface of the sand body in that area (Fig. 5-17). Mud drapes are formed by fine sediment settling out of suspension during late-stage flow and covering the troughs of ripples with a layer of mud (Fig. 5-18). Almost all the ripples on Newport Bar have mud drapes; they also are very common on Mitchener Bar and on ripples on the stoss side of megaripples on Hantsport Bar. Mud drapes are rarely, if ever, found on any of the sand bodies at the mouth of

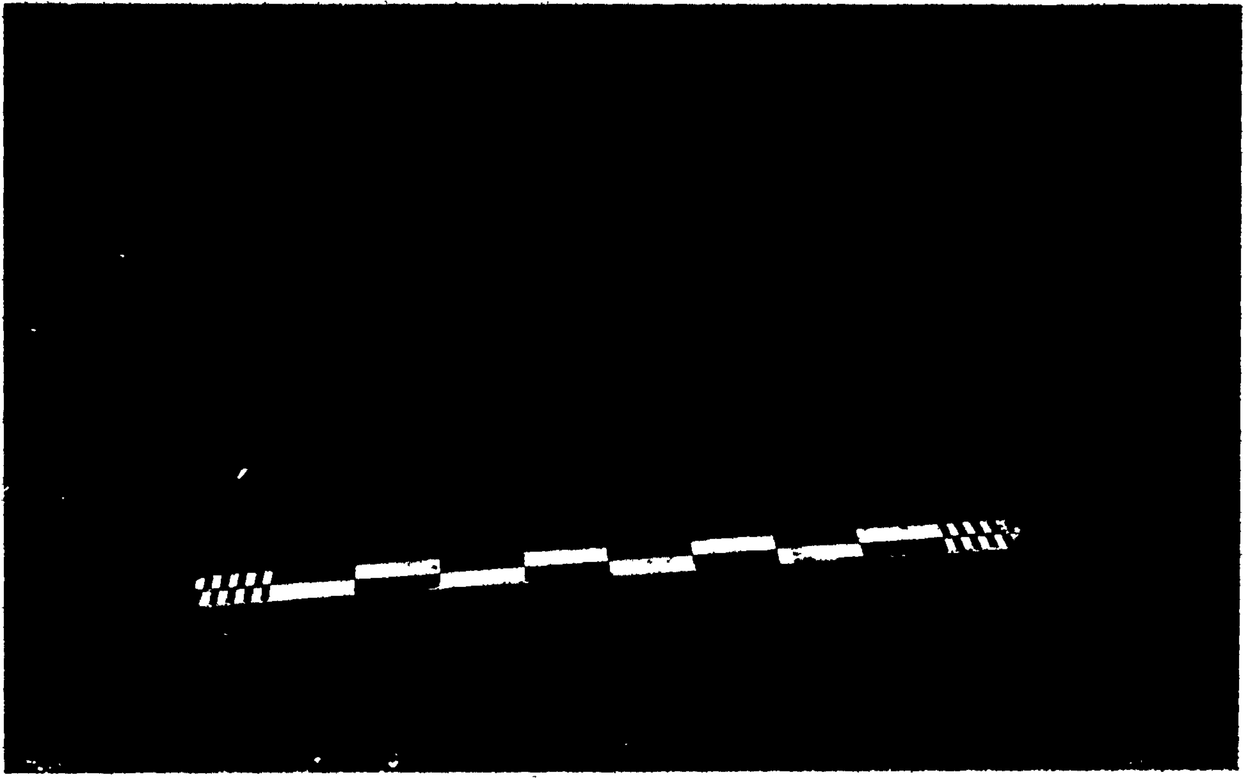

Fig. 5-15. Wave ripples and planed off surface; the bedform is a megaripple. The scale is decimeters and centimeters.

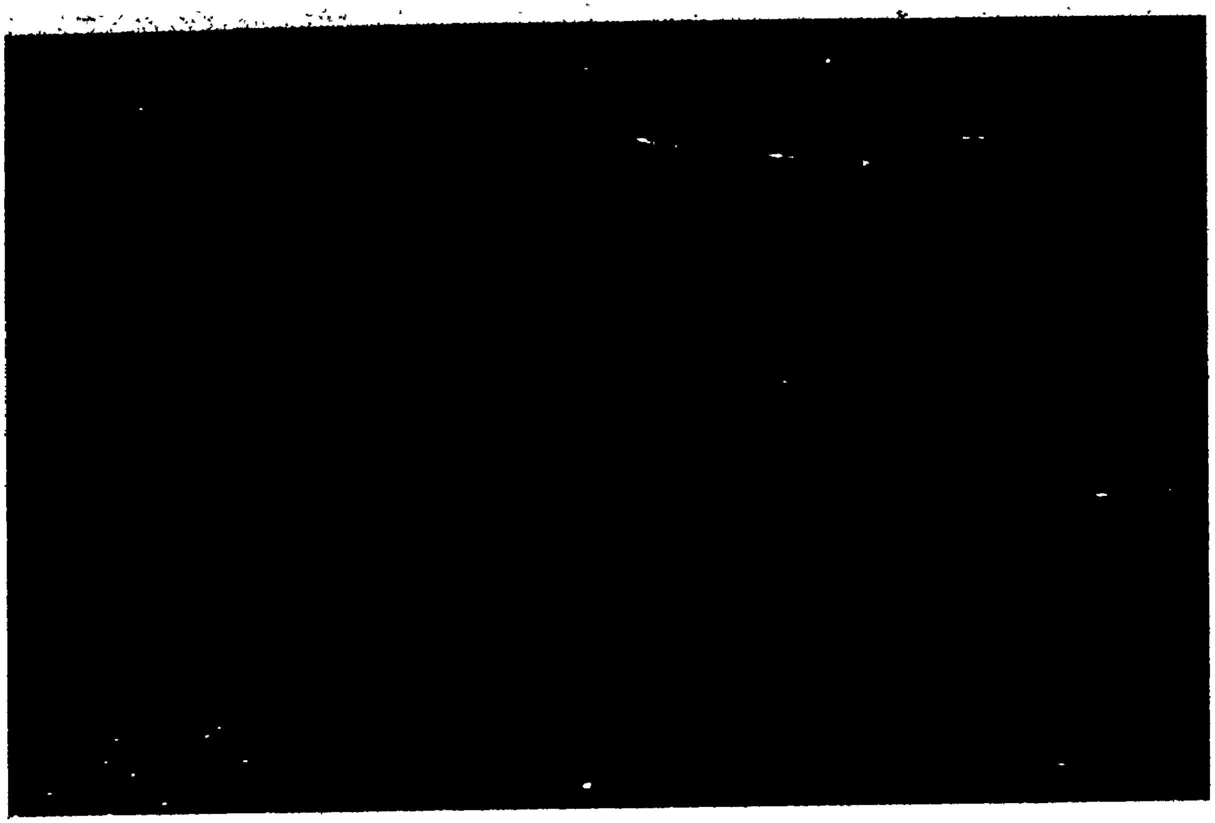

Fig. 5-16. Ice-rafted boulder with a current crescent; the scale is decimeters and centimeters

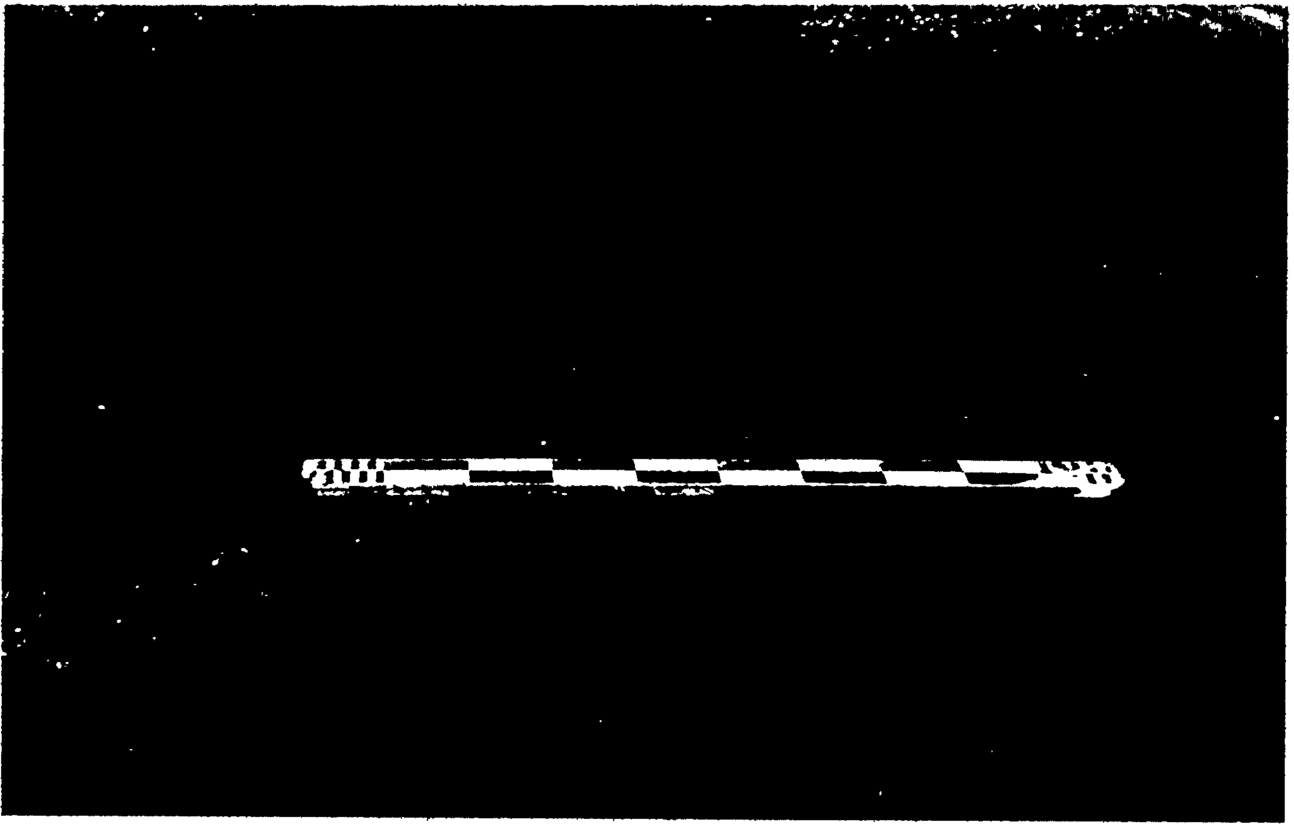

Fig. 5-17. Mud pebbles, the scale is decimeters and centimeters

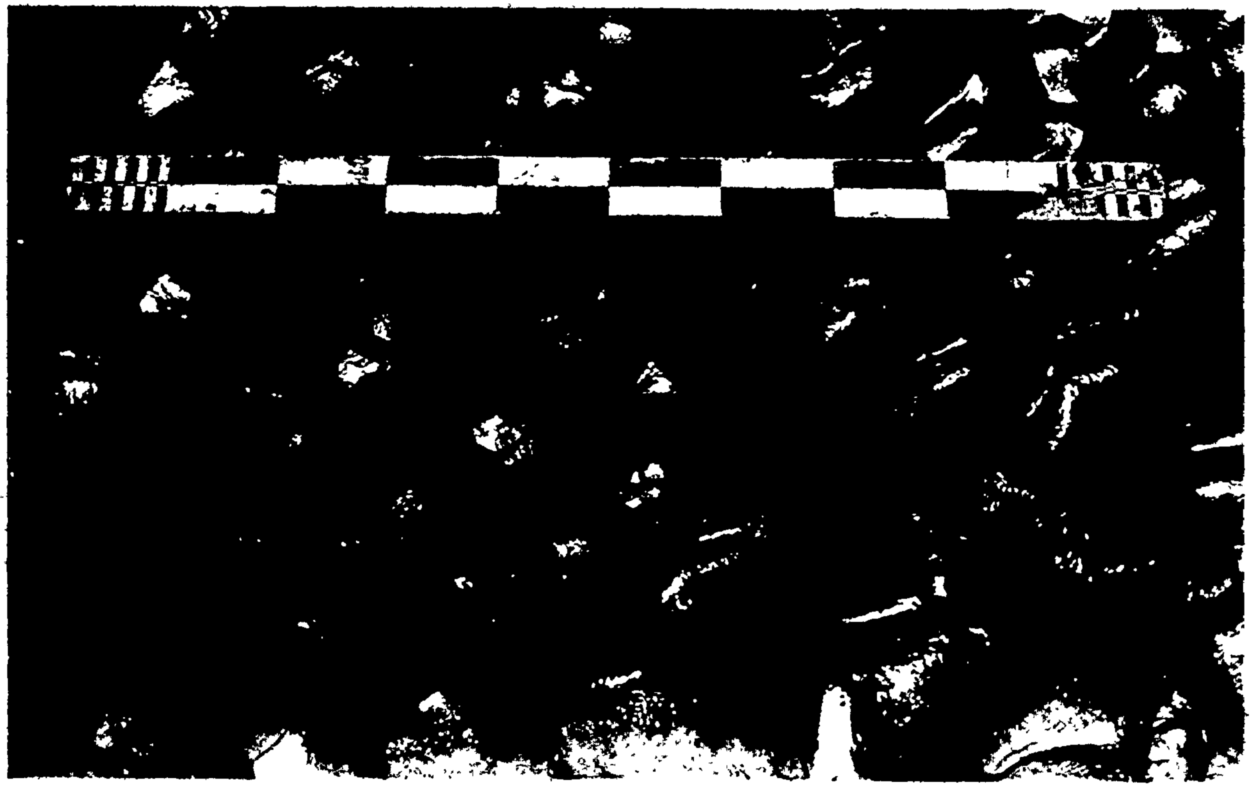

Fig. 5-18. Mud drapes on ripples; the scale is decimeters and centimeters

the estuary, probably because there is noticeably less mud in suspension at the mouth of the system than at the head.

Internal Structures

Internal structures were examined by digging trenches and by making epoxy peels. (See Appendix C for details of the methods used and for the raw data.) Small- and large-scale cross-bedding, parallel lamination, and reactivation surfaces are the most common structures; flaser bedding is found also. Large and small-scale cross-bedding can be either flood or ebb oriented. Small-scale cross-beds have average dip angles of 21° and set thicknesses of 4 cm; in some peels both ebb and flood oriented cross-beds are found together (Fig. 5-19). The occurrence of ebb and flood oriented structures at the same location is the result of bedform reversal; the mechanism for this will be discussed in Chapter 7. Most small-scale cross-beds sets are tabular to wedge-shaped, but a few trough sets are found. (A summary of the measurements of internal structures appears in Table 5-3.)

Large-scale cross-bedding, with average dip angles of 23° and set thicknesses of 16 cm, is the most common internal structure. Most of the sets are tabular to wedge-shaped with trough sets encountered in places. Commonly, flood and ebb oriented sets occur at the same location (Fig. 5-20). Reactivation surfaces are found in most peels and trenches that have large-scale cross-bedding (Fig. 5-20); they

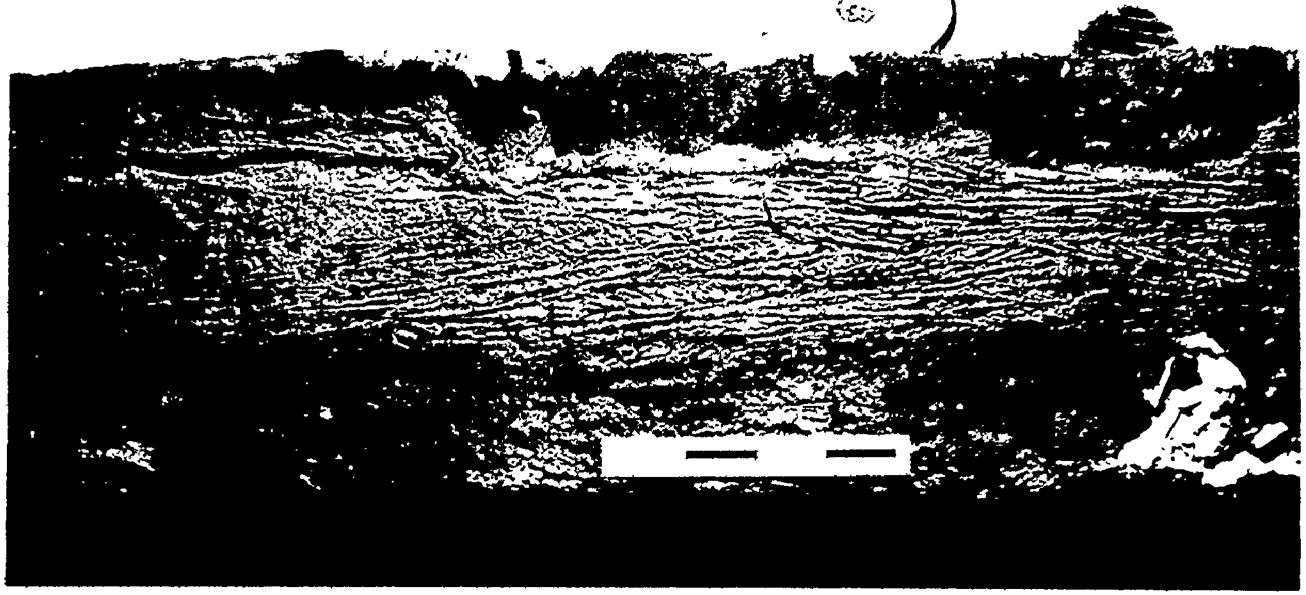

Fig. 5-19. Internal structures of ripples; the most abundant structure is small-scale cross-bedding. The scale is 20 cm long.

TABLE 5-3. Summary of Internal Structures

Structure	Average Dip Angle (°)	Average Set Thickness (m)	Associated Surface Features
small-scale flood cross-bedding	22	0.04	ripples, transverse bars with rippled surfaces
small-scale ebb cross-bedding	20	0.04	ripples, transverse bars with rippled surfaces
flaser bedding	-	-	ripples with mud drapes
small-scale trough cross-bedding	-	0.17	ripples
large-scale trough cross-bedding	-	0.12	megaripples
large-scale flood cross-bedding	24	0.14	sand waves, megaripples
large-scale ebb cross-bedding	22	0.17	sand waves, megaripples
parallel lamination	-	0.15	ripples, transverse bars
reactivation surfaces	9	-	sand waves, megaripples
low angle ebb cross-bedding	8	0.20	transverse bars

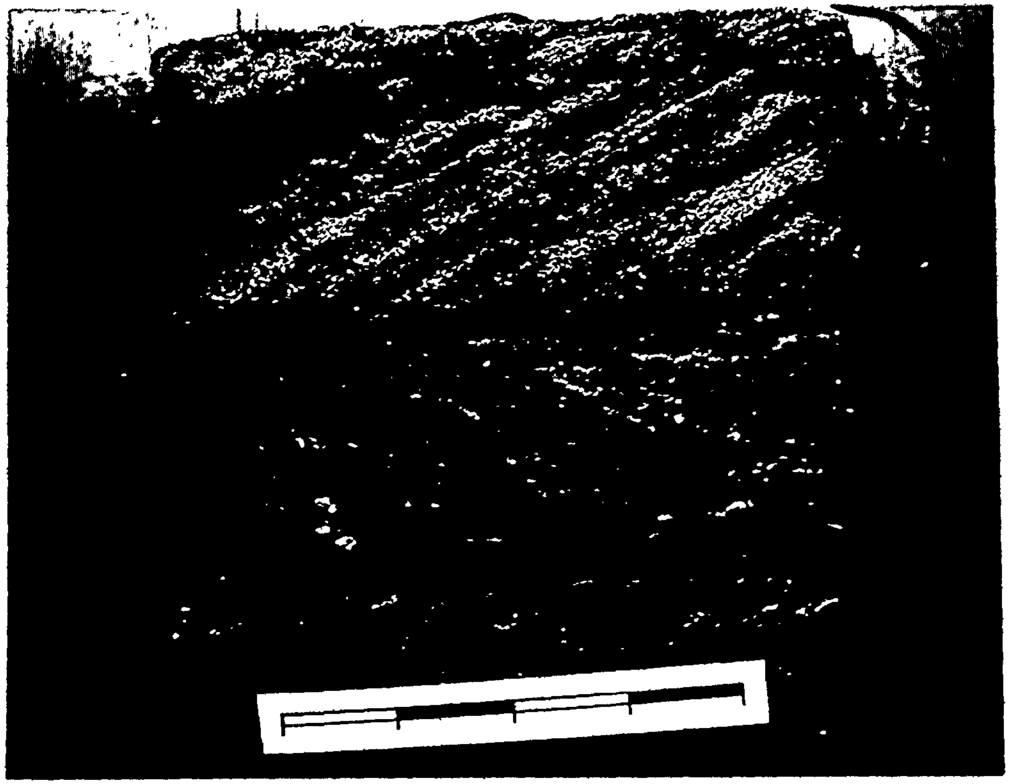

Fig. 5-20. Internal structures of megaripples. Sets of large-scale cross-bedding are separated by a shallow dipping reactivation surface. The scale is 20 cm long

consist of gently dipping coarse layers between sets of cross-beds and represent former bedform surfaces (Klein, 1970).

Flaser bedding (terminology of Reineck and Wunderlich, 1968) occurs only near the southern end of Newport Bar (Fig. 5-21). It appears to be formed as a result of burial of mud drapes by sand; very thick mud drapes are common in the area where flaser bedding is found (Table 5-3).

The distribution of internal structures is related directly to the distribution of bedforms since each type of structure is generated by specific kinds of bedforms (Blatt et al., 1972, p. 115). The overall distribution is revealed by comparing Figures 5-3 and 5-4 with the data in Table 5-3.

Small-scale cross-bedding is generated by ripples and is found underlying the rippled areas on Boot Island Bar and Middle Ground (Table 5-3). All rippled areas are not underlain by small-scale cross-bedding; most of the rippled surfaces of Newport Bar and Mitchener Bar are underlain by parallel lamination (Fig. 5-22; Table 5-3) that appears to be upper flow regime parallel lamination. The association of upper flow regime parallel lamination with rippled surfaces may indicate that ripples form during late-stage flow; this will be discussed further in Chapter 9. Parallel lamination also is associated with the transverse bars on Mitchener Bar (Table 5-3).

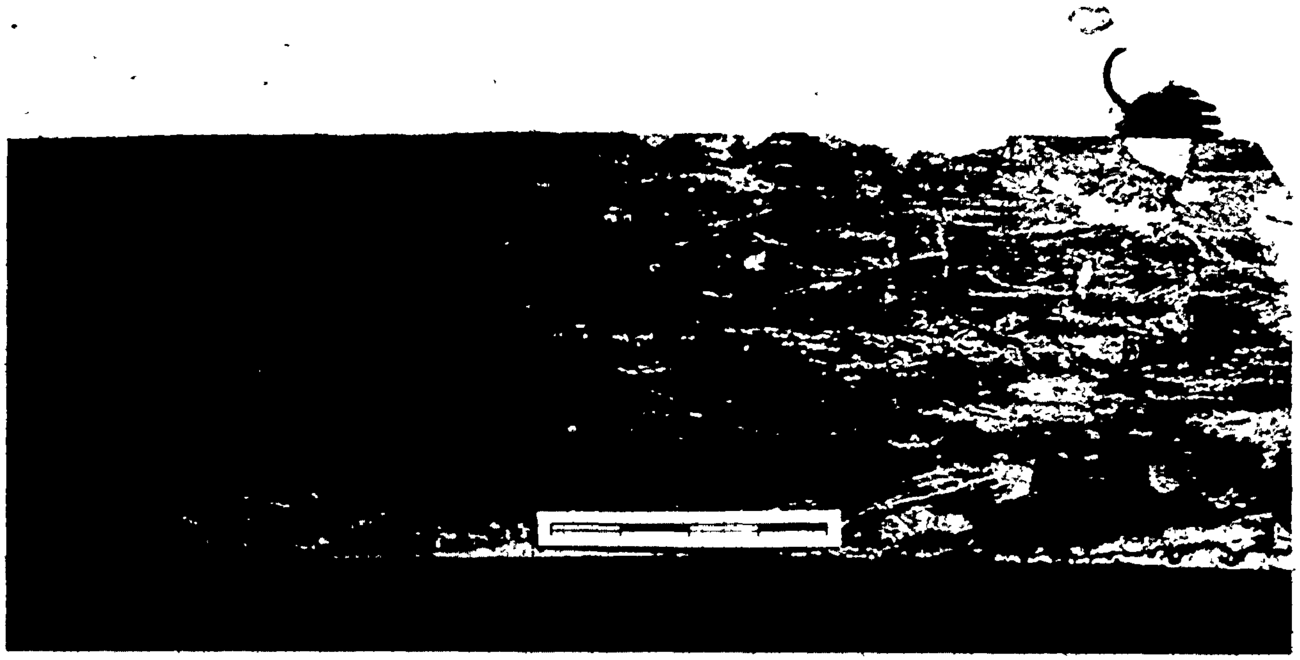

Fig. 5-21. Flaser bedding. The scale is 20 cm long.

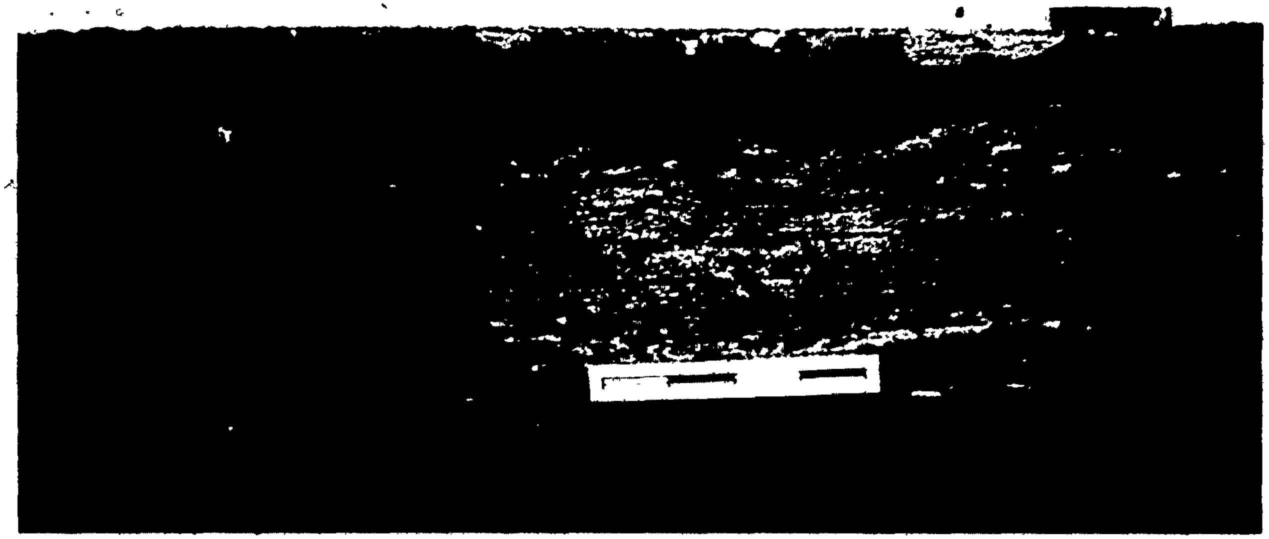

Fig. 5-22. Parallel lamination. The scale is 20 cm long.

Large-scale cross-bedding underlies the megarippled areas on all the sand bodies (Figs. 5-3 and 5-4; Table 5-3). The ratio of flood oriented sets to ebb oriented sets at a given location is greater in areas having megaripples with steep stoss sides. Large-scale cross-bedding also is associated with sand waves. Set thicknesses do not reflect the height of the sand wave but that of the megaripples on its surface (Fig. 5-23). It appears that the internal structures of sand waves are generated by migration of megaripples over the sand wave rather than by migration of the sand wave itself.

Generally, large-scale cross-bed sets are approximately 1/3 as high as the bedform that generates them although there is a lot of variation in bedform height - set thickness ratios. The observed variation does not appear to be related to position on a sand body, and there is no difference between sand bodies. Herringbone cross-bedding tends to be produced more commonly by sand waves than megaripples, and, generally, it occurs more often in areas that are neither strongly flood nor strongly ebb dominant such as near sand body crests; Dalrymple (1977, personal communication) observed similar distributions of herringone cross-bedding in Cobequid Bay.

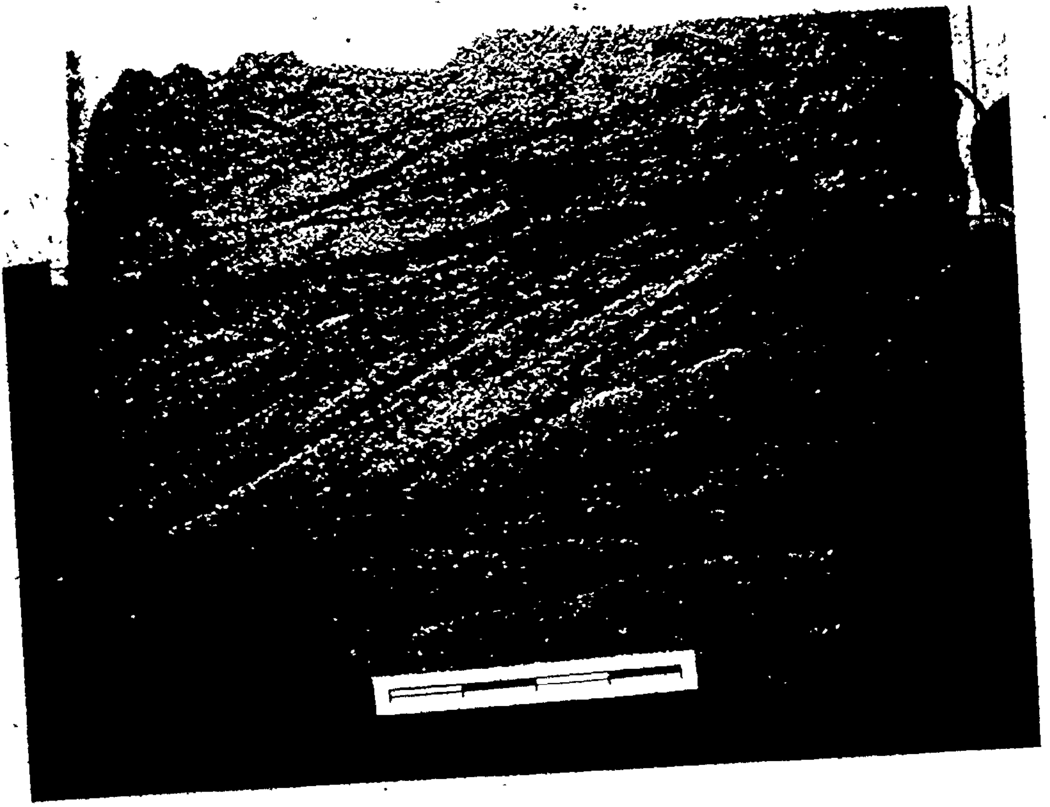

Fig. 5-23. Internal structures of a megarippled sand wave. The scale is 20 cm long.

Small-scale cross-beds are finer grained than large-scale cross-beds. This is a result of grain size control of bedform type (see Chapters 6 and 9) rather than a direct response of cross-bed scale to grain size.

Summary

Three of the four bedform types, ripples, megaripples and sand waves, occur in sets with easily recognizable wavelengths; transverse bars appear to form individually. Ripples are the smallest order bedform and are found on every sand body. Megaripples are second order bedforms and are found on each sand body also; ripple and megaripple crests are oriented perpendicular to current flow. Sand waves are found only at the mouth of the estuary and are oriented oblique to current direction; they are the largest bedform. Transverse bars occur on Mitchener Bar only. Other surface features include wave-formed ripples, current crescents, ice-rated blocks, mud pebbles, and mud drapes; none is abundant.

Small- and large-scale cross-bedding, parallel lamination, and reactivation surfaces are the most common internal structures; flaser bedding is also found. Internal structures reflect surface bedforms; small-scale cross-bedding and parallel lamination occur beneath rippled surfaces, large-scale cross-bedding and reactivation surfaces are associated with megaripples and sand waves. Ebb and flood cross-bed sets often are found at the same location; the relative amount of each varies with position on the sand bodies.

CHAPTER 6

GRAIN SIZE DISTRIBUTION

Textural Analysis

Four hundred and seventy-one sediment samples were collected from the surface of the six major intertidal sand bodies; 237 in 1974 and 234 in 1975.

Sediment sample positions were located using horizontal sextant sightings and pace and compass. A series of points parallel to the axis of each sand body, at approximately 400 m intervals, were fixed using horizontal sextant sightings. The points generally were near the sand body crest; samples were collected from each sighted point, and additional sample locations were fixed by pace and compass. Usually, one sample location was chosen on either side of the line of sighted points at a distance of approximately 400 m; if the sand body was too narrow, a sample location was established near its edge. If there was significantly more than 400 m between the sighted point and the sand body edge, additional sample locations were established;

this was done also if a noticeable grain size change occurred. Sample locations are shown on Figures 6-1 and 6-5.

Samples were collected by hand from as close to the sediment surface as possible in order to sample only sediment that was being actively transported. One sample was taken on rippled surfaces; points with megaripples, transverse bars, or sand waves were sampled both on the crest and near the bottom of the slip face of the bedform.

All samples were sieved, and textural parameters were calculated by moment statistics. (See Appendix D for methods of mechanical analysis and calculation of textural parameters.) Mean grain size, standard deviation and skewness have been examined in detail. Results of all grain size analyses are presented in Appendix D. All size grades are expressed in terms of the Udden-Wentworth scale (Wentworth, 1922).

GENERAL TRENDS: Several general trends emerge from textural analysis of the sediment samples. Textural parameters did not change between 1974 and 1975; average mean grain size, sorting, and skewness were consistent from year to year on each sand body (Table 6-1). Mean grain size decreases from the mouth to the head of the estuary; Boot Island Bar, Western Bar, and Middle Ground are noticeably coarser than Hantsport Bar, Mitchener Bar, and Newport Bar. Trough samples tend to be coarser than crest samples from the same bedform.

TABLE 6-1. Comparison of textural parameters from 1974 and 1975 (All sizes are in phi units)

	1974			1975		
	$\bar{x}$	σ	Sk	$\bar{x}$	σ	Sk
Boot Island Bar	1.29	0.80	-0.53	1.43	0.83	-0.73
Western Bar	1.08	0.99	-0.32	0.90	0.96	-0.21
Middle Ground	1.92	0.63	-1.14	1.81	0.63	-0.82
Hantsport Bar	1.96	0.52	0.20	1.85	0.49	0.31
Mitchener Bar	2.34	0.41	0.11	2.19	0.45	0.21
Newport Bar	2.92	0.51	0.24	2.89	0.48	0.27
TOTAL	2.03	0.64	-0.36	1.96	0.63	-0.21

Some of the difference between the two years results from different sample locations during each year; see Figs. 6-1 and 6-5.

Most sand bodies in Cobequid Bay (see Fig. 2-2) are coarsest near low water and finest at higher elevations (Dalrymple, 1977). Sand bodies at the head of the Avon River estuary exhibit this trend but those at the mouth do not; Boot Island Bar has the opposite relationship between mean grain size and elevation.

Standard deviation generally is consistent on the surface of each sand body; few trends were detected. There is a decrease in standard deviation towards the head of the estuary; sand bodies at the head of the system are better sorted than those at the mouth. Trough samples tend to be slightly better sorted than crest samples from the same bedform.

Sediment samples from sand bodies at the mouth of the estuary are almost all negatively skewed while most samples from the estuary head are positively skewed. Skewness values tend to be more positive towards the center and higher parts of a sand body than towards lower, marginal areas.

Textural parameters of the samples collected in the present study diverge from the results of Pelletier and McMullen (1972). Results of the present study probably are more reliable than those of Pelletier and McMullen (1972) as their results were based on significantly fewer samples.

BOOT ISLAND BAR: Locations of all 58 samples collected from Boot Island Bar are shown on Figure 6-1. Mean grain size ranges from very coarse sand (-0.08 phi) to fine sand (2.55 phi). Mean sizes are coarsest at the southern end of the sand body and finest at the northern end; there is a coarse to fine gradation from south to north with no discernible east - west trends in mean grain size. Figure 6-2 depicts mean grain sizes on Boot Island Bar.

Swift et al. (1967) indicated that Boot Island Bar was sand. Pelletier and McMullen (1972) mapped median grain sizes on Boot Island Bar as fine sand to very fine sand (2.00 to 4.00 phi); they collected only 90 samples (on a 2 km grid) from all over Minas Basin, so their results may not be as precise as those of the present study.

Standard deviation varies between moderately well sorted (0.54 phi) and poorly sorted (1.09 phi) with most values in the moderately sorted range (0.71 to 1.00 phi); verbal descriptions of sorting are from Folk (1974). Samples from the northern end of the sand body tend to be better sorted than those at the southern end; there are no east-west sorting trends. Figure 6-3 illustrates sorting values on Boot Island Bar. Pelletier and McMullen (1972) indicated that Boot Island Bar was moderately sorted (0.81 to 1.29 phi on their scale); this is essentially equivalent to the results of the present study.

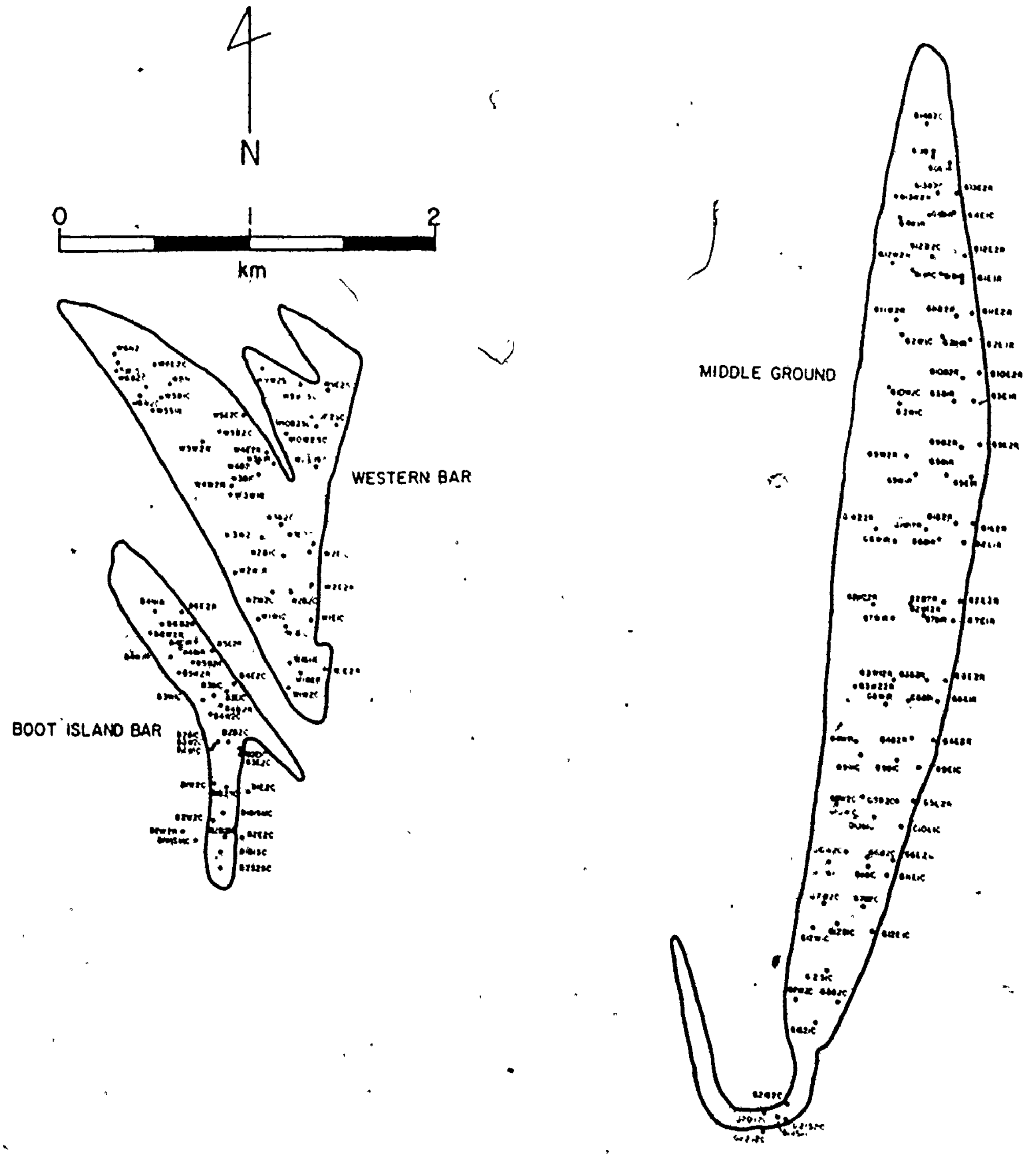
N
0
1
2
km
WESTERN BAR
BOOT ISLAND BAR
MIDDLE GROUND

Fig. 6-1. Estuary mouth sediment sample locations. Two samples were collected at each station ending with a "C"; the second sample label ends in "T". Textural parameters of both samples are listed in Table D-1.

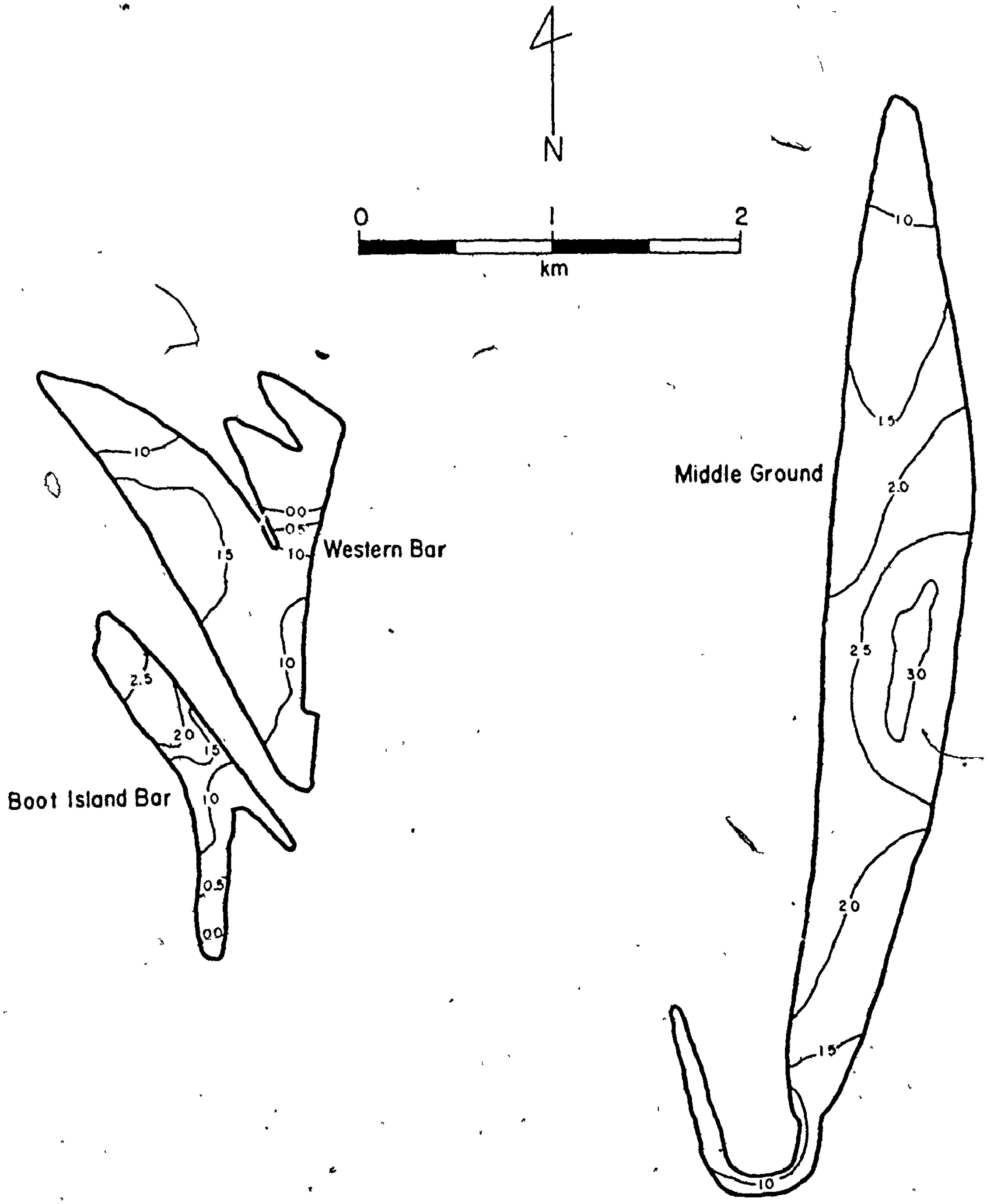
N
0
1
2
km
Middle Ground
Western Bar
Boot Island Bar
1.0
1.5
2.0
2.5
3.0
2.0
1.5
1.0
0.0
0.5
1.0
1.5
1.0
2.5
2.0
1.5
1.0
0.5
0.0

Fig. 6-2. Mean grain sizes at the estuary mouth. Contour values are phi units based on moment measure means for all samples on each sand body

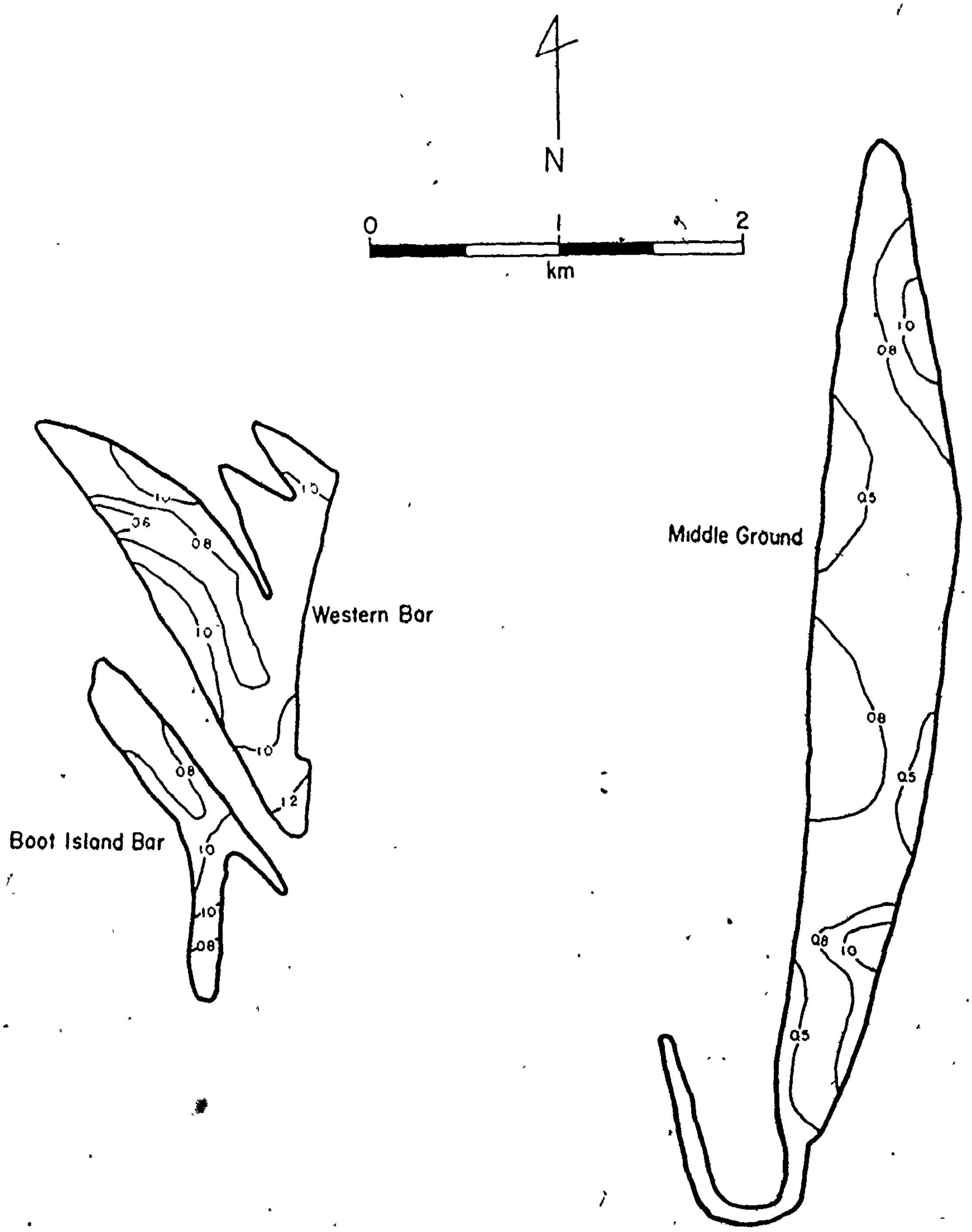
N
0
1
2
km
Western Bar
Boot Island Bar
Middle Ground
10
06
08
10
10
10
12
08
10
10
08
10
08
05
08
05
08
10
05

Fig. 6-3. Sorting at the estuary mouth. Contour values are phi units based on moment measure sorting of all samples on each sand body

Skewness values range between -2.39 and 0.51; most samples are negatively skewed and have values between 0.00 and -2.00. Samples at the northern end of Boot Island Bar tend to be more negatively skewed than those at the southern end (Fig. 6-4). All positively skewed samples were collected from the center of the sand body towards the southern end (Fig. 6-4).

WESTERN BAR: A total of 74 sediment samples were collected from Western Bar; their locations are shown on Figure 6-1. Mean grain size ranges from very coarse sand (-0.33 phi) to fine sand (2.02 phi); most samples are in the medium to coarse sand range (0.00 to 2.00 phi). The northern and southern ends of Western Bar are slightly coarser than the center; the northeastern section with sand waves is significantly coarser than the rest of the sand body (Fig. 6-2). Swift et al. (1967) considered Western Bar to be sand and Pelletier and McMullen (1972) reported it to be fine sand to very fine sand (2.00 to 4.00 phi).

Standard deviation varies from well sorted (0.48 phi) to very poorly sorted (2.13 phi) with most values in the moderately sorted range (0.71 to 1.00 phi). There are no obvious sorting trends although the center of the sand body tends to be slightly better sorted than the margins; Figure 6-3 depicts sorting on Western Bar. According to Pelletier and McMullen (1972), sorting varied from very well sorted to well sorted to moderately sorted (0.00 to 1.29 phi by their classification) from north to south.

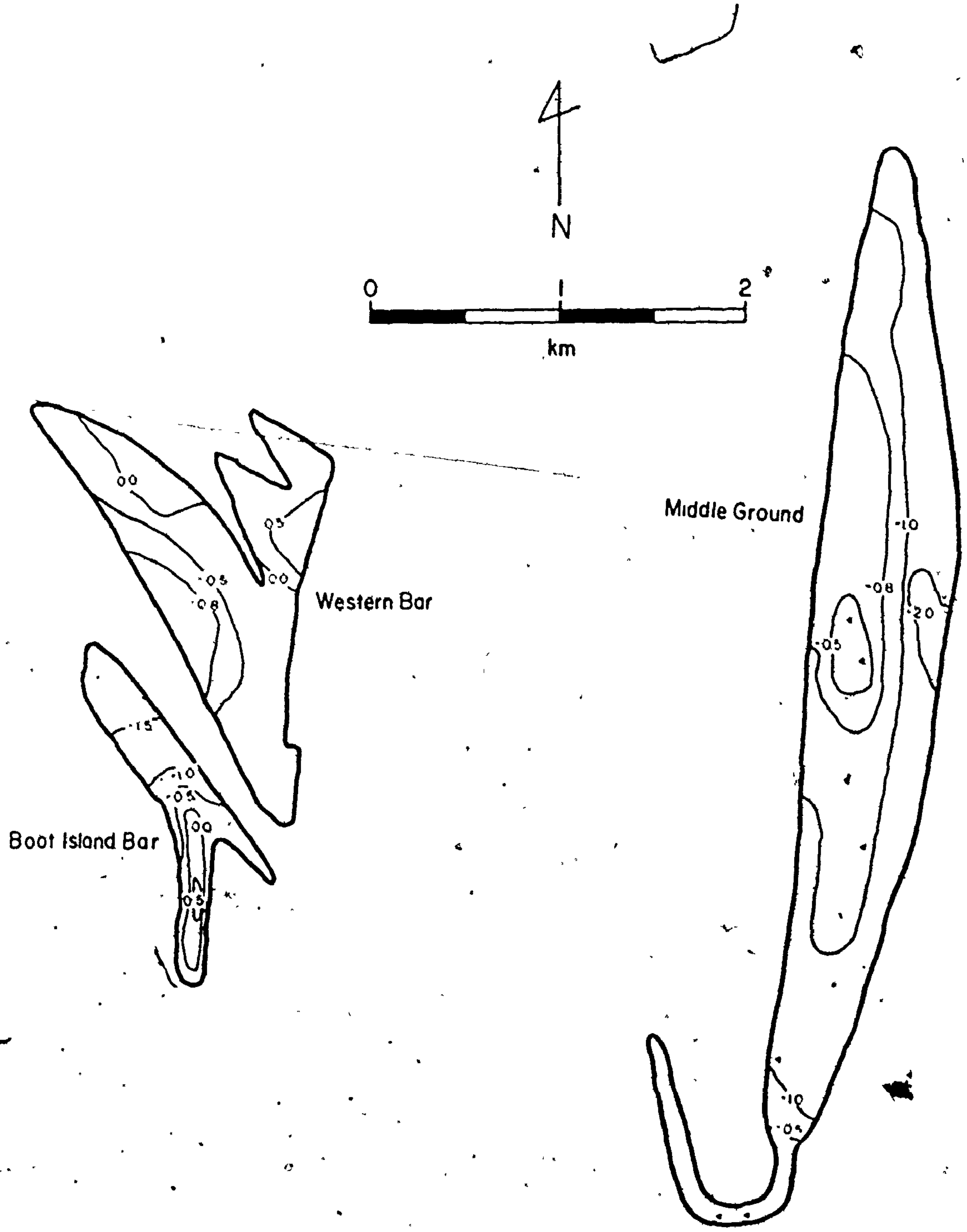
N
0
1
2
km
Middle Ground
Western Bar
Boot Island Bar
·00
·05
·00
·05
·08
·15
·10
·05
·00
·05
·10
·08
·05
·20
·10
·05

Fig. 6-4. Skewness at the estuary mouth. Contour values are based on moment measure skewness. Locations of samples with positive skewness are identified with triangles

Most samples from Western Bar are negatively skewed (Fig. 6-4); positively skewed sediments were collected from the northern and eastern parts of the sand body (Fig. 6-4). Skewness values range from -1.15 to 0.79; most are between 0.00 and -1.00. The western and southern sides of the sand body are more negatively skewed than are the eastern and northern sides (Fig. 6-4).

MIDDLE GROUND: Positions of the 112 samples collected on Middle Ground are marked on Figure 6-1. Mean grain size varies between coarse sand (0.35 phi) and very fine sand (3.50 phi); most samples have mean sizes in the medium sand or fine sand range (1.00 to 3.00 phi). The coarsest parts of Middle Ground are at the northern and southern ends and the finest part is near the center; there is a gradation from coarse to fine to coarse again from north to south (Fig. 6-2). Again, there are no distinct east-west trends in mean grain size. Swift et al. (1967) labelled Middle Ground as sand; Pelletier and McMullen (1972) indicated that median grain size increased towards the sand body center from either end from between 0.00 and 2.00 phi to between -2.00 and 0.00 phi, and then dropped sharply to less than 4.00 phi at the center.

Standard deviation ranges from very well sorted (0.32 phi) to poorly sorted (1.12 phi) with most samples being moderately well sorted (0.50 to 0.71 phi). There are no distinct sorting trends (Fig. 6-3); although the sand body center may be slightly better sorted than the ends. Pelletier and McMullen (1972) described Middle Ground as poorly sorted (1.30 to 2.29 phi) with a small area at the northern end that was moderately sorted (0.81 to 1.29 phi).

The only positively skewed sediment samples from Middle Ground were collected from the ebb spit at the southern end of the sand body and from the region of fine-grained sediment at the center of the sand body; all other samples are negatively skewed (Fig. 6-4). Sediment tends to be more negatively skewed on the east side of Middle Ground than on the west; skewness values range between -2.45 and 0.56 with most values between 0.00 and -2.00.

HANTSPORT BAR: 77 sediment samples were taken from Hantsport Bar; Figure 6-5 is a map of their locations. Mean grain size ranges from coarse sand (0.96 phi) to fine sand (2.41 phi). Coarsest samples are at the southern end of the sand body; mean grain size becomes progressively finer towards the northern end. No east-west tends in mean grain size are present (Fig. 6-6). Pelletier and McMullen (1972) mapped Hantsport Bar as coarse sand to medium sand (0.00 to 2.00 phi).

Two samples on Hantsport Bar are moderately sorted (0.74 and 0.78 phi), all the rest are well sorted to moderately well sorted (0.37 to 0.67 phi). Standard deviation seems to decrease towards the northern end of the sand body (Fig. 6-7). Pelletier and McMullen (1972) considered Hantsport Bar to be moderately sorted (0.81 to 1.29 phi in their classification).

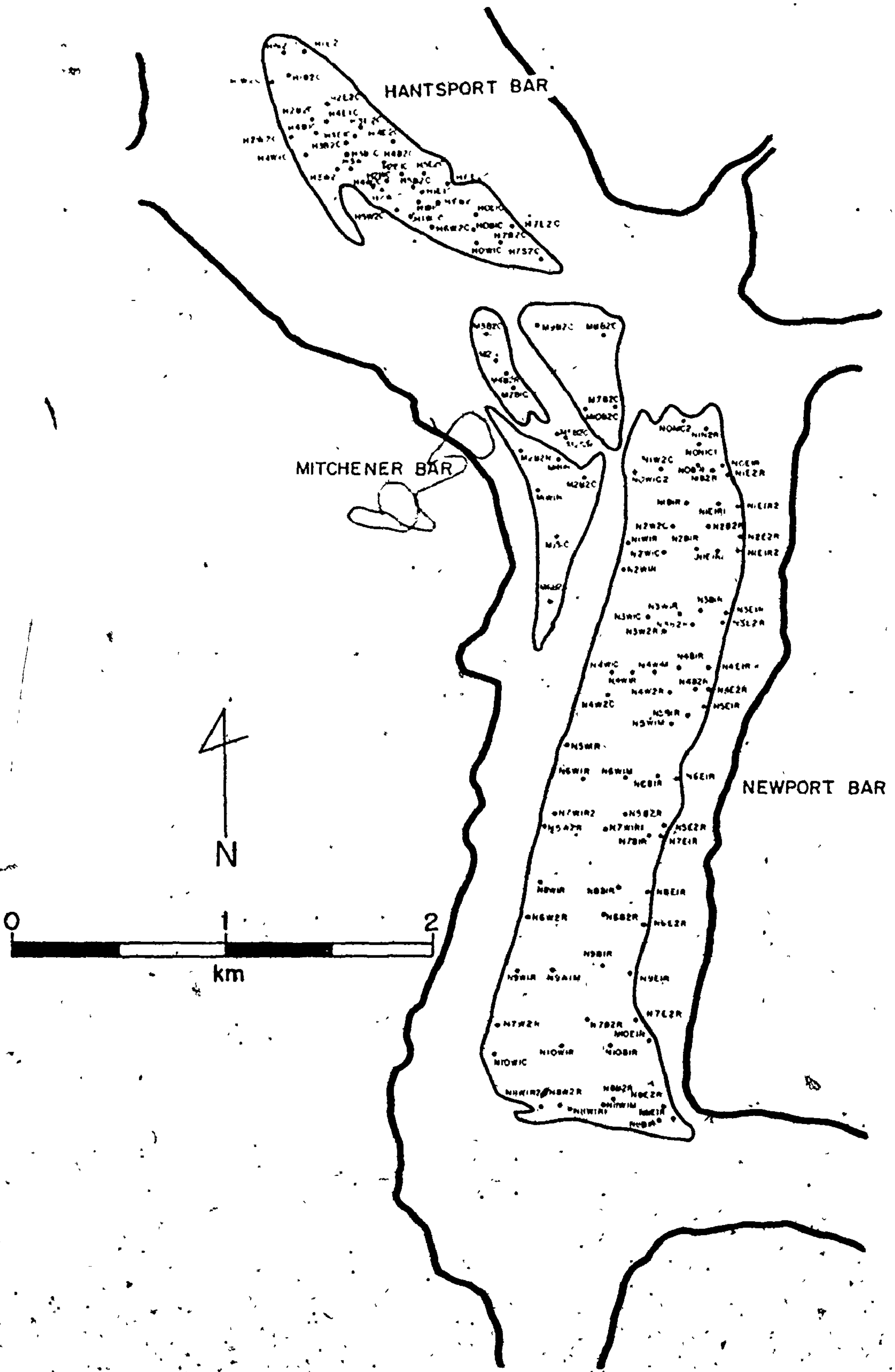
HANTSPORT BAR
MITCHENER BAR
NEWPORT BAR
N
0
1
2
km

Fig. 6-5. Estuary head sediment sample locations. Two samples were collected at each station ending with a "C"; the second sample label ends in "T". Textural parameters of both samples are listed in Table D-1.

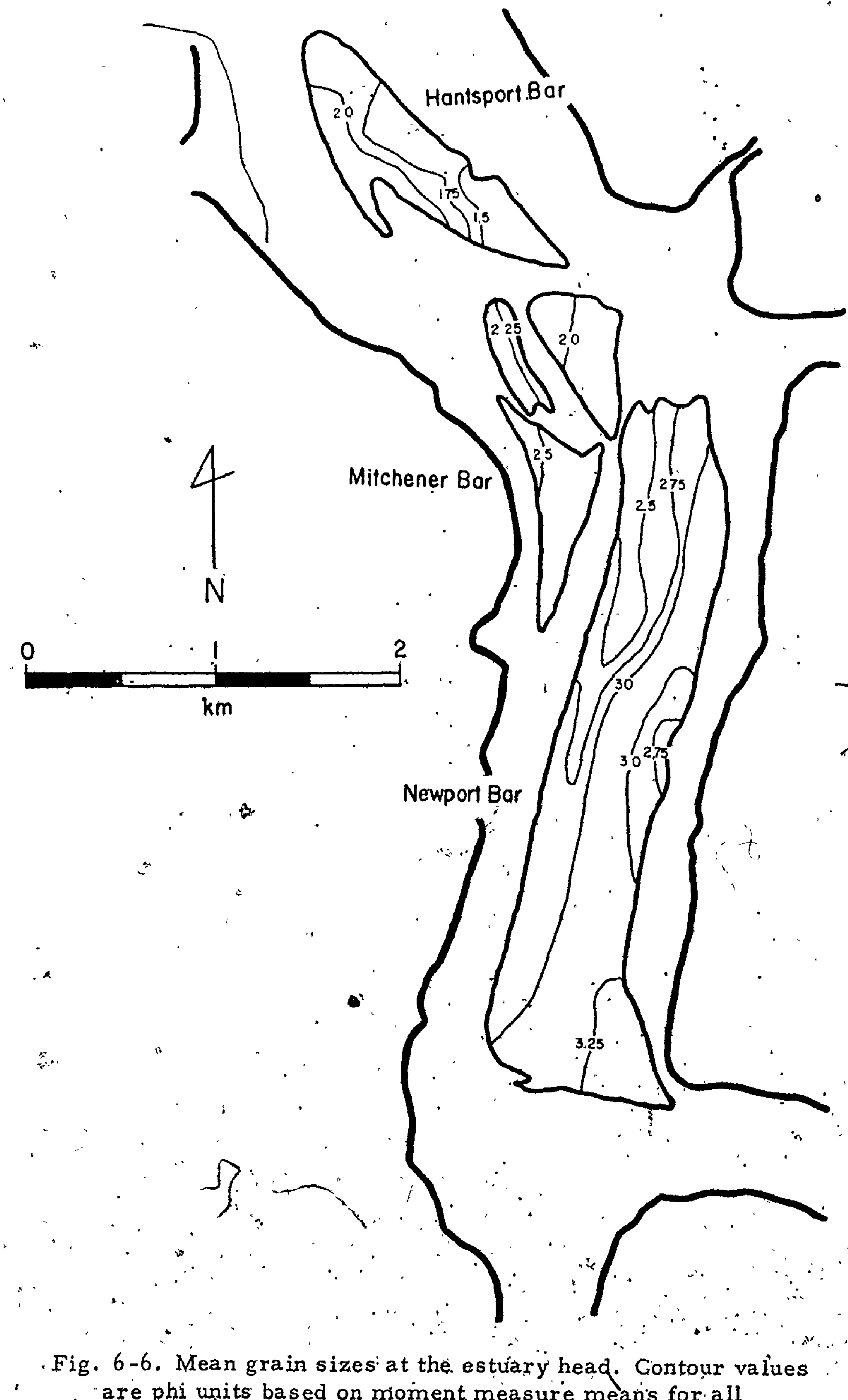
Hantsport Bar
2.0
1.75
1.5
2.25
2.0
2.5
Mitchener Bar
2.75
2.5
N
0
1
2
km
3.0
3.0
2.75
Newport Bar
3.25

Fig. 6-6. Mean grain sizes at the estuary head. Contour values are phi units based on moment measure means for all samples on each sand body

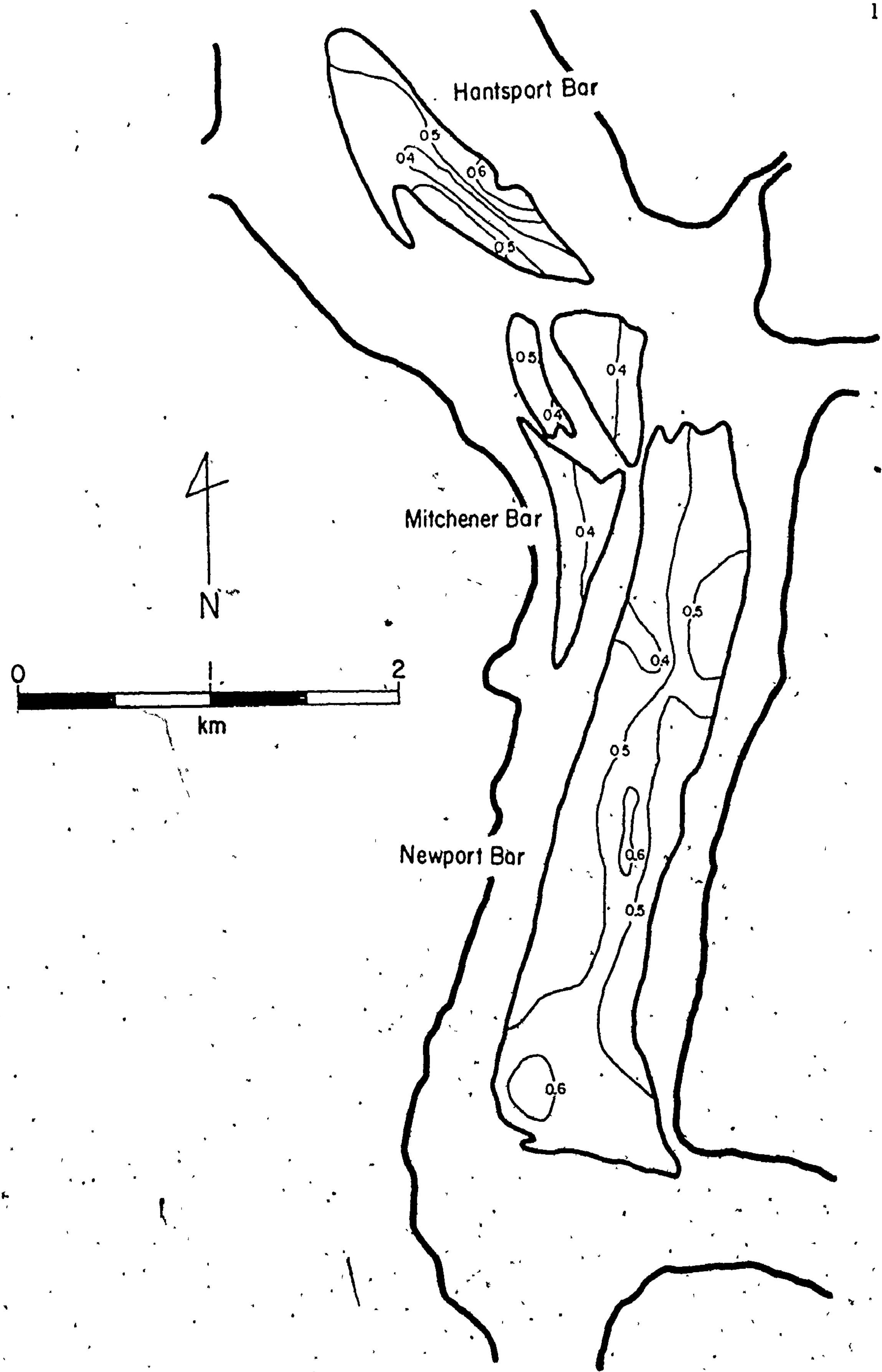
Hantsport Bar
0.5
0.4
0.6
0.5
0.5
0.4
0.4
Mitchener Bar
0.4
N
0.5
0.4
0
1
2
km
0.5
Newport Bar
0.6
0.5
0.6

Fig. 6-7. Sorting at the estuary head. Contour values are phi

Almost all sediment samples collected from Hantsport Bar are positively skewed; a few negatively skewed samples were collected at scattered locations (Fig. 6-8). Skewness values range between -2.04 and 1.27 and most values are between 0.00 and 1.00; there are few trends in skewness values (Fig. 6-8).

MITCHENER BAR: The 39 sediment samples collected on Mitchener Bar are located on Figure 6-5; mean grain size varies between medium sand (1.63 phi) and very fine sand (3.06 phi) with all except these two samples in the fine sand range (2.00 to 3.00 phi). No trends in mean grain size are discernible (Fig. 6-6). Pelletier and McMullen (1972) plotted median grain size on Mitchener Bar as 2.00 to 4.00 phi.

With the exception of one moderately sorted sample (0.67 phi), all standard deviations on Mitchener Bar fall into the well sorted category (0.35 to 0.50 phi). Again, no trends in the sorting distribution are apparent (Fig. 6-7). Pelletier and McMullen (1972) also labelled Mitchener Bar as well sorted (0.51 to 0.80 phi in their scheme).

Sediment samples from most of Mitchener Bar as positively skewed; several negatively skewed samples were collected from the southern end of the sand body (Fig. 6-8). Skewness values range from -1.27 to 1.36 and are more positive towards the north and east of the sand body.

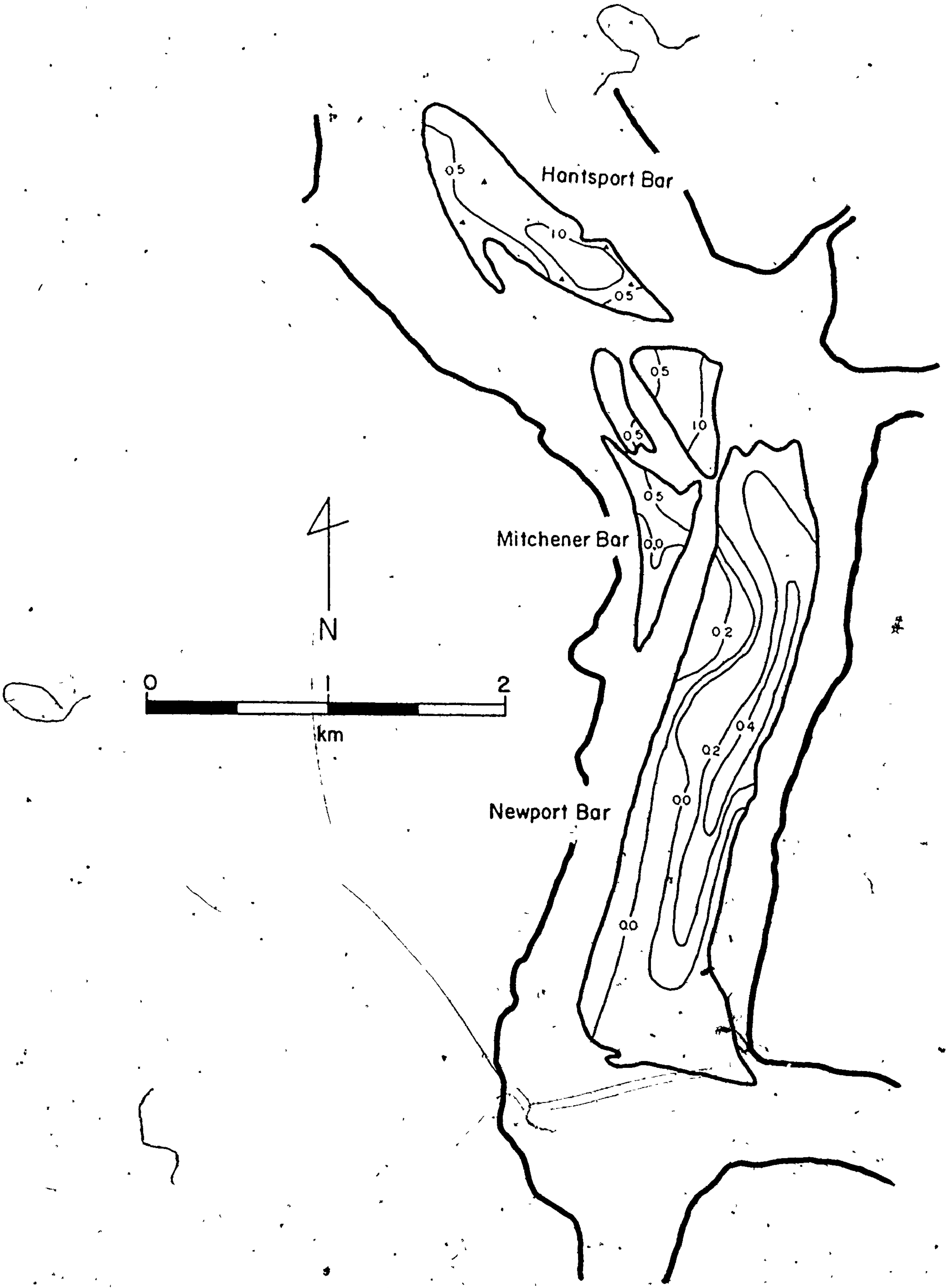
Hantsport Bar
0.5
1.0
0.5
0.5
1.0
0.5
0.5
Mitchener Bar
0.0
N
0
1
2
km
0.2
0.4
0.2
0.0
Newport Bar
0.0

Fig. 6-8. Skewness at the estuary head. Contour values are based on moment measure skewness. Locations of negatively skewed samples are identified with triangles

NEWPORT BAR: A total of 111 sediment samples were collected on Newport Bar; locations of these samples are shown on Figure 6-5. Mean grain size ranges from fine sand (2.30 phi) to very fine sand (3.49 phi); most samples are in the fine sand range (2.00 to 3.00 phi). There seems to be a decrease in mean grain size from west to east at the northern end of the sand body; no other trends are recognizable (Fig. 6-5). Pelletier and McMullen (1972) mapped median grain size on Newport Bar as 2.00 to 4.00 phi.

The standard deviations of two samples are in the moderately sorted range (0.72 to 0.89 phi); most of the other samples are well sorted (0.35 to 0.50 phi), the remainder are moderately well sorted (0.50 to 0.71 phi). This is markedly different from the plot of Pelletier and McMullen (1972) which showed the southern end of Newport Bar as poorly sorted (1.30 to 2.39 phi) becoming moderately sorted (0.81 to 1.29 phi) and then well sorted towards the northern end (0.51 to 0.81 phi). The results of the present study do not reveal any distinct sorting trends (Fig. 6-7).

Most sediment samples collected from Newport Bar are positively skewed although a few negatively skewed samples were taken from the southern and western parts of the sand body (Fig. 6-8). Skewness values range between -2.84 and 0.75; most are between 0.00 and 0.50. Few other trends are apparent (Fig. 6-8).

Textural Parameters and Bedforms

A strong correlation exists between mean grain size and bedform type. Sediment samples from sand waves are the coarsest in the study area; mean grain size on sand waves is almost always coarse sand or very coarse sand (-1.00 to 1.00 phi). Megaripples overlap this range; they have mean grain sizes from coarse sand to fine sand (0.00 to 3.00 phi). Sediment samples from rippled areas have mean grain sizes from medium sand to very fine sand (1.00 to 4.00 phi). Although there is appreciable overlap in the ranges of mean grain size for different bedform types, the majority of samples fall into distinct classes (Fig. 6-9).

There is a relationship between bedform type and standard deviation. Ripples are better sorted than megaripples which are better sorted than sand waves (Fig. 6-9). However, this is not solely a function of bedform type but is a result of the decrease in mean grain size that accompanies a transition from sand waves to megaripples to ripples. In many studies, sorting has been observed to be better in finer sand grades than coarser. Inman (1949) has explained this by hydraulics; it also may account for the decrease in standard deviation from the mouth to the head of the estuary as mean grain size also decreases in that direction. This point will be discussed in more detail in Chapter 8.

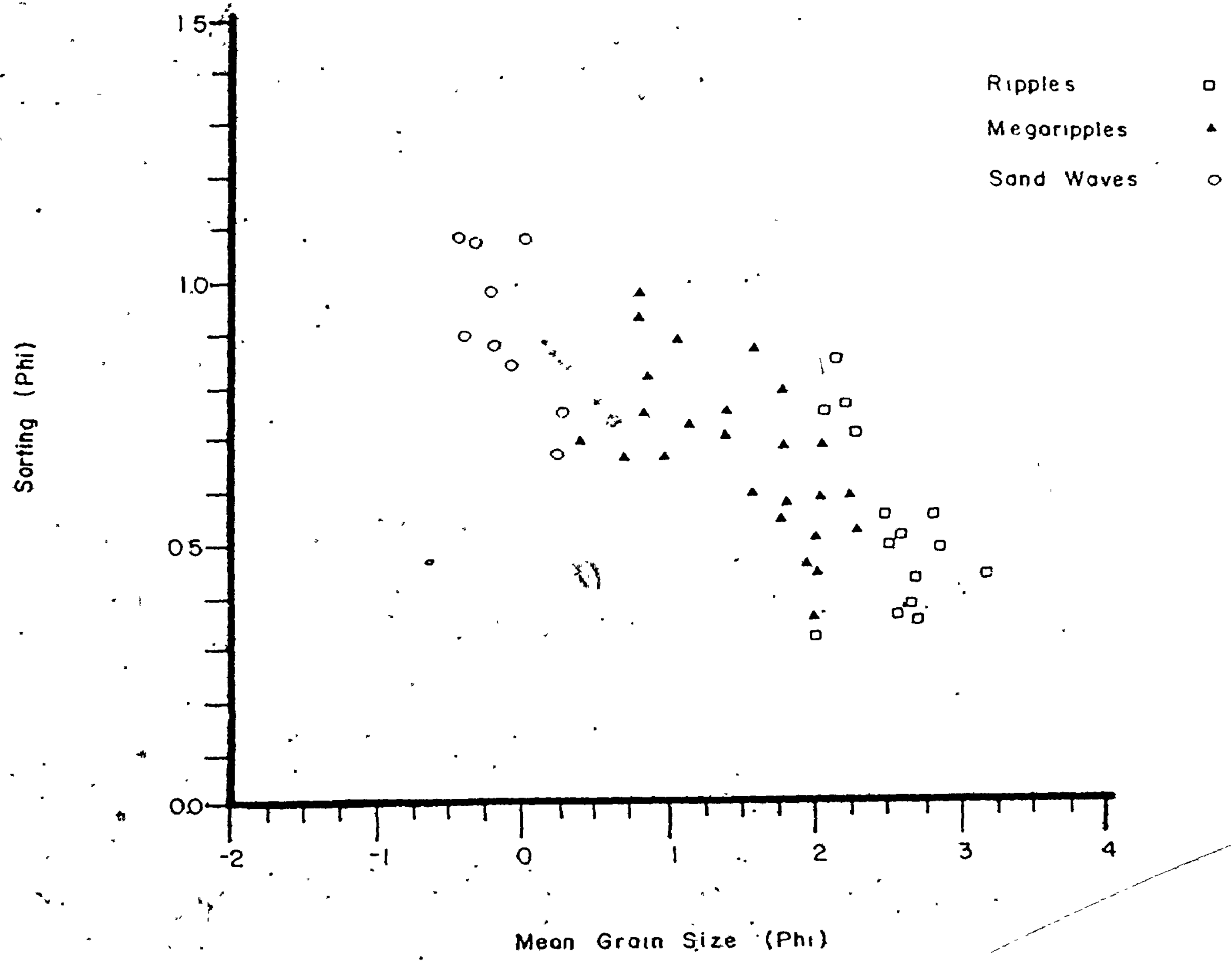

Fig. 6-9. Mean size versus sorting of 3 bedform types. Not all measured points are plotted; points were selected to illustrate the entire range of sorting and mean size while eliminating overlapping points

Cumulative Curve Analysis

Naturally occurring grain size distributions can reflect sediment source (Shea, 1974), depositional processes (Visher, 1969), or both. Grain size parameters have been used to distinguish depositional environments; Friedman (1961) plotted skewness versus sorting and Passega (1964) plotted the coarsest one percentile versus median grain size. Neither approach is entirely successful.

Numerous authors have noted that many grain size distributions have marked discontinuities. Visher (1969) suggested that the whole population actually is composed of a number of truncated log-normal components, and interpreted each grain population as a reflection of a different sediment transport mechanism.

However, Tanner (1959, 1964), Spencer (1963) and others believe that cumulative curves are composed of overlapping normal distributions; Middleton (1976) has shown that the two methods yield different results, and that dissected overlapping normally distributed grain populations can be interpreted with respect to hydraulics.

In this study, the purpose of cumulative curve analysis is to relate grain size distribution to hydraulics. This discussion will deal only with the results of cumulative curve analysis; hydraulics will be related to grain size distribution in Chapter 8.

Cumulative curves of all 471 sediment samples were plotted on probability paper. Each curve was examined; several trends emerged. Over ninety percent of the curves have marked discontinuities. There is no apparent relationship between location and the presence of discontinuities in cumulative curves although most curves without marked discontinuities are from samples collected at the mouth of the estuary.

Cumulative curves can be divided into three groups based on the relative amounts of the coarse (C), intermediate (A), and fine (B) populations. A population was considered small if it constitutes less than 10% of the total sample, moderate if 10-30%, and large if more than 30%. The three groupings are:

(1) large intermediate population, small fine, and small coarse;

(2) moderate or large intermediate, small fine, and moderate or large coarse;

(3) moderate or large intermediate, moderate or large fine, and small coarse.

Group 1 accounts for approximately 30% of all samples, group 2 for not quite 25%, and the remaining 45% belong to group 3. Figure 6-10 illustrates typical Group 1, Group 2 and Group 3 cumulative curves.

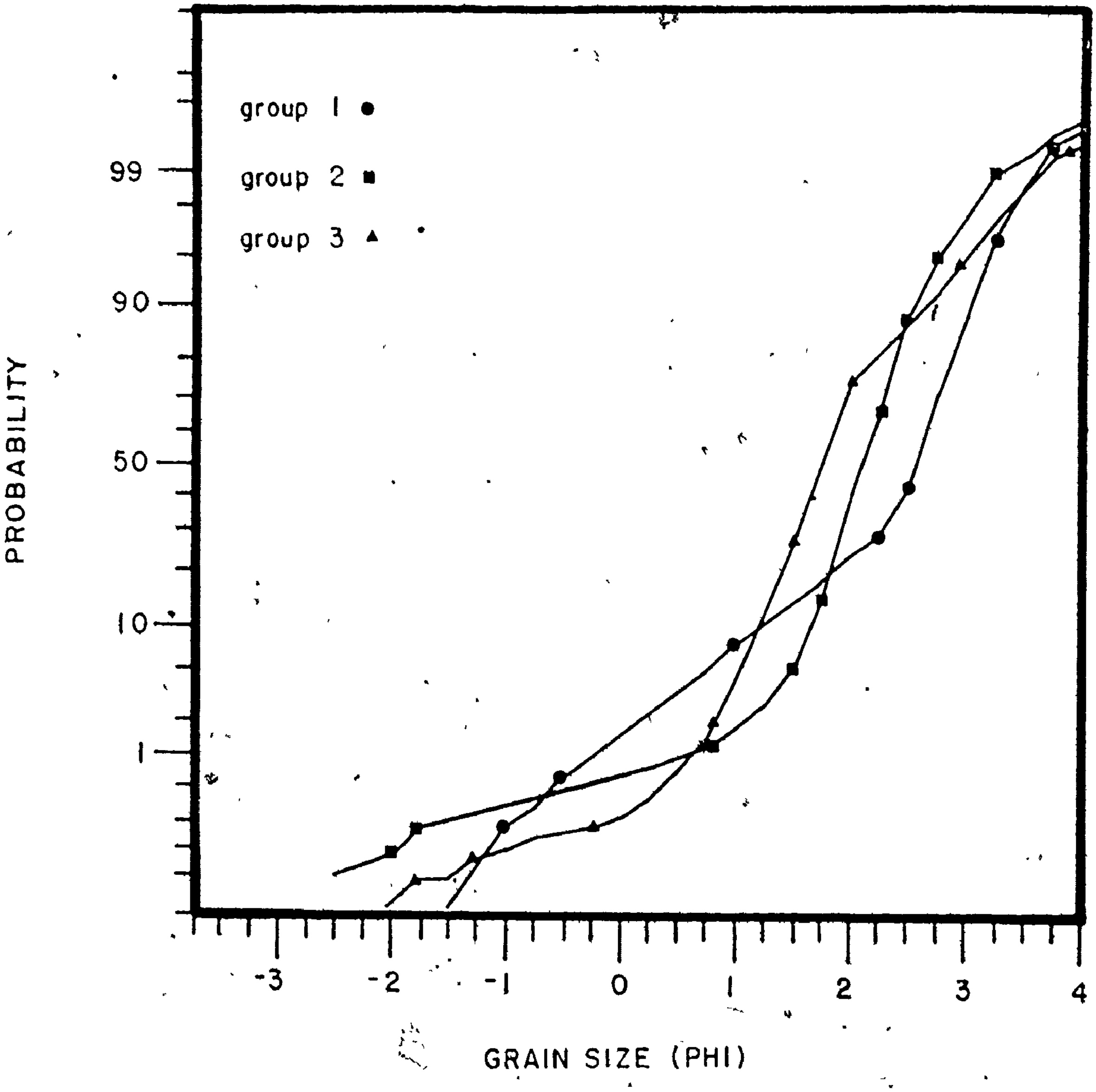

Fig. 6-10. Typical group 1, 2, and 3 cumulative curves

There is a strong correlation between location and cumulative curve group. No group 2 curves are from sand bodies at the head of the estuary; the only samples with 10% or more of population C are from the mouth of the estuary; and most curves from the estuary mouth belong to this group. Almost all group 3 samples come from sand bodies at the head of the estuary; the few exceptions are from the finest part of Middle Ground (Fig. 6-2). Group 1 curves occur on all sand bodies but they do not dominate except on Middle Ground. Group 3 curves are dominant on sand bodies at the head of the system; Western Bar and Boot Island Bar have mainly group 2 cumulative curves.

Cumulative curve variation with location is reflected in the average grain size distribution of each sand body. The average grain size distribution of the whole system is presented in Table 6-2; the distribution is bimodal. Comparison of this curve with the average grain size distribution of each sand body reveals broad trends in grain size distribution (Table 6-2). At the estuary mouth, coarse size fractions contain greater than average amounts of sediment; the opposite is true at the estuary head (Table 6-2). There is a third, coarse mode (1.25 phi) at the estuary mouth that is not present at the head, and the average fine mode (3.00 phi) is shifted to 2.75 phi at the estuary mouth (Table 6-2). All these trends reflect the areal distribution of cumulative curve groups. Also, skewness values vary with cumulative curve group 1

TABLE 6-2. Average Grain Size Distribution for each Sand Body and the Whole System (All values are percents)

* denotes a mode

Size (phi)	Hantsport Bar	Mitchener Bar	Newport Bar	Boot Is. Bar	Western Bar	Middle Ground	Aver. Head	Aver. Mouth	Total
-3.25	0.00	0.12	0.00	0.14	1.03	0.01	0.02	0.35	0.20
-3.00	0.01	0.05	0.00	0.16*	0.15	0.00	0.01	0.09	0.05
-2.75	0.01	0.02	0.00	0.14	0.14	0.18	0.01	0.17	0.10
-2.50	0.03*	0.06	0.00	0.33	0.27	0.05	0.02	0.19	0.11
-2.25	0.02	0.08*	0.00	0.33	0.40	0.05	0.02	0.23	0.13
-2.00	0.02	0.07	0.00	0.45	0.48	0.07	0.02	0.28	0.16
-1.75	0.02	0.09	0.01*	0.52	0.63	0.09	0.03	0.35	0.20
-1.50	0.03	0.10	0.00	0.81	1.05	0.15	0.03	0.55	0.31
-1.25	0.03*	0.10	0.00	0.95	1.35	0.22	0.03	0.70	0.39
-1.00	0.02	0.10	0.00	1.09	1.63	0.23	0.03	0.80	0.44
-0.75	0.03	0.11	0.00	1.35	2.29	0.32	0.04	1.07	0.59
-0.50	0.04	0.11	0.01	1.55	2.57	0.33	0.04	1.17	0.65
-0.25	0.06	0.14	0.01	2.12	3.51	0.53	0.05	1.66	0.92
0.00	0.08	0.16	0.01	2.78	4.51	0.69	0.06	2.19	1.21
0.25	0.13	0.19	0.02	3.56	5.60	0.92	0.09	2.81	1.56
0.50	0.24	0.25	0.03	4.44	6.63	1.22	0.15	3.47	1.94
0.75	0.47	0.29	0.04	4.77	6.77	1.45	0.24	3.72	2.11
1.00	1.27	0.45	0.07	5.55	7.47	1.93	0.58	4.34	2.61
1.25	4.28	1.15	0.16	6.85*	8.96*	3.32	1.86	5.81*	3.99
1.50	6.81	1.96	0.16	5.35	7.06	3.77	2.94	5.22	4.49
1.75	14.58	5.98	0.40	7.08	8.77*	6.74	6.63	7.74	6.19
2.00	17.83	12.59	1.08	7.55	7.58	8.96	9.29	8.72	8.98
2.25	18.77*	20.95*	4.20	8.25*	5.97	15.24*	12.50*	11.32*	11.86*
2.50	8.82	12.10	5.31	4.35	2.32	12.53	7.81	7.65	7.72
2.75	10.24*	15.40*	12.03	7.10	3.18	16.92*	11.99	10.45*	11.16
3.00	8.58	13.59	23.81*	12.82*	5.16*	11.98	16.37*	9.92	12.90*
3.25	3.77	6.04	16.50	5.53	2.63	4.94	9.95	4.28	6.90
3.50	2.12	4.13	15.42	2.53	1.11	3.51	8.52	2.50	5.28
3.75	0.82	1.86	8.22	0.75	0.29	1.62	4.37	1.00	2.55
00	40	1.02							

tively skewed, and group 3 curves are positively skewed. Implications of areal grain size differences will be discussed in Chapter 8.

CUMULATIVE CURVE DISSECTION: Cumulative curves from 59 sediment samples were dissected graphically using the method of Cassie (1954, 1963) which assumes that cumulative curves result from the summation of overlapping normal populations. Each population dissected by Cassie's method was tested against the observed cumulative curve with a chi-squared statistic; 176 of 177 populations were found to be significant. The remaining population is the coarse tail of a sample and has an anomalously high weight in one size fraction; the population was found to be significant if this one fraction was not included in the test.

After a cumulative curve had been dissected and each population tested for significance, the mean and standard deviation of each population was computed graphically using the method of Inman (1952); means were computed using the formula $(\text{phi}_{84} + \text{phi}_{16})/2$ and standard deviations with $(\text{phi}_{84} - \text{phi}_{16})/2$. Average characteristics of dissected populations for each sand body are presented in Table 6-3; implications of differences in the dissected populations are discussed in Chapter 8.

TABLE 6-3. Results of Cumulative Curve Dissection (all values are means; sample size is in parentheses after location names)

2

Location	C			Size of equal overlap (phi)	A			Size of equal overlap (phi)	B		
	$\bar{x}$ (phi)	s (phi)	%		$\bar{x}$ (phi)	s (phi)	%		$\bar{x}$ (phi)	s (phi)	%
Boot Island Bar (10)	0.72	0.61	48.9	1.84	2.44	0.41	50.3	3.43	3.91	0.12	0.78
Middle Ground (14)											
group 1	0.48	0.74	4.5	1.44	2.19	0.43	94.2	3.25	3.65	0.51	1.51
group 2	0.69	0.50	43.6	1.35	1.76	0.58	55.6	2.54	3.69	0.57	0.80
group 3	1.10	0.56	3.2	1.55	2.35	0.34	59.2	2.74	3.33	0.50	39.50
total	0.66	0.61	21.1	1.42	2.03	0.48	72.7	2.87	3.61	0.53	6.60
Western-Bar (8)	0.36	0.71	70.2	1.49	1.87	0.37	26.5	2.77	3.21	0.28	3.25
Hantsport Bar (11)	0.31	0.41	0.8	0.63	1.57	0.27	66.4	2.05	2.47	0.31	32.80
Mitchener Bar (4)	-0.10	0.68	0.3	0.83	1.69	0.31	65.2	2.08	2.36	0.34	34.30
Newport Bar (12)	1.04	0.43	0.6	1.47	2.36	0.28	60.1	2.86	3.17	0.29	39.30
estuary mouth (32)	0.60	0.64	42.1	1.57	2.12	0.43	54.2	3.02	3.61	0.34	3.90
estuary head (27)	0.57	0.46	0.7	1.03	1.94	0.28	63.4	2.41	2.76	0.31	35.90

Curves were selected to represent all the samples on each sand body; the proportions of all 3 curve groups were maintained and typical members of each group were chosen for dissection. Fifty-five of the 59 curves could be dissected into 3 populations and one into 4 populations; the remaining 3 samples are composed of 2 populations. Results of cumulative curve dissection are as follows for each sand body.

Boot Island Bar: Nine of the 10 cumulative curves from Boot Island Bar samples that were dissected are group 2 samples; the tenth is a group 1 sample. The proportion of the C population tends to decrease slightly from north to south and averages 48.9% for the whole sand body. Also, the size of equal overlap between the C population and the A population increases from north to south; average equal overlap size is 1.84 phi. The proportion of C tends to be less in ebb dominant areas than in flood dominant zones; the lone group 1 sample is from an ebb dominant zone. Population C has an average mean size of 0.72 phi and an average standard deviation of 0.61 phi.

The B population is small in all Boot Island Bar cumulative curves comprising, on the average, 0.78% of each sample; in 3 samples there is no B population. The coarse end of the B population equally overlaps the A population at an average of 3.43 phi; its average mean size is 3.92 phi and its average standard deviation is 0.12 phi. There do not appear to be any trends in the B population distribution.

On Boot Island Bar the A population averages 50.3% of each sample. Since the B population is constant in size, the A population distribution is the inverse of the C distribution; the proportion of A tends to increase from north to south and to be larger in ebb dominant areas than in flood dominant regions. The average mean size of A is 2.44 phi and the average standard deviation is 0.41 phi; A equally overlaps C at 1.84 phi and B at 3.43 phi.

Western Bar: All eight cumulative curves from Western Bar that were dissected are group 2 curves. There are no trends in the proportions of the A or C populations; B population percentages are small everywhere.

The C population averages 70.2% of each sample and has an average mean size of 0.36 phi with an average standard deviation of 0.71 phi; it equally overlaps the A population, on the average, at 1.49 phi. The average mean size of the A population is 1.87 phi and its average standard deviation is 0.37 phi; it equally overlaps the C population at 1.49 phi and the B population at 2.77 phi, and comprises an average of 26.5% of each sample. Percentages of the B population average 3.25; on the average it equally overlaps the A population at 2.77 phi. The B population has an average mean size of 3.21 phi and an average standard deviation of 0.28 phi (see Table 6-3).

Middle Ground: Fourteen cumulative curves from samples on Middle Ground were dissected; two of them are group 3 curves, six belong to group 1, and six are group 2 curves. The group 3 curves are associated with the area of fine sediment near the center of the bar (Fig. 6-2); there is no distinct trend in the distribution of group 1 and 2 curves although more group 2 curves are from the north end of the bar than the south end. Within each curve grouping there are no apparent trends in the relative proportions of populations A, B and C.

Average mean grain size of the C population is 0.48 phi, 0.69 phi, and 1.10 phi and the average standard deviation is 0.74 phi, 0.50 phi, and 0.56 phi for group 1, 2 and 3 curves respectively; 0.66 phi and 0.61 phi are the average mean size and average standard deviation of the C population for the whole sand body. Population A has an average mean size of 2.19 phi for group 1 curves, 1.76 phi for group 2, and 2.35 phi for group 3; the average mean size for the whole sand body is 2.03 phi. Average standard deviations are 0.43 phi for group 1, 0.58 phi for group 2, 0.34 phi for group 3, and 0.48 phi for the whole sand body. Population B has an average standard deviation of 0.51 phi, 0.57 phi, and 0.50 phi for group 1, 2 and 3 curves respectively. Average mean size is 3.65 phi, 3.69 phi, and 3.33 phi for the three groups. For the entire sand body, the average mean size of population B is 3.61 phi and the average standard deviation is 0.53 phi.

Population C equally overlaps population A at 1.44 phi, 1.35 phi, and 1.55 phi for group 1, 2 and 3 curves respectively; population A terminates at 3.25 phi, 2.54 phi, and 2.75 phi for the three groups.

For the entire sand body, the average equal overlap size of population C is 1.42 phi; it is 1.87 phi for population A. The average proportions are 21.1% of population C, 6.6% of population B, and 72.7% of population A.

Hantsport Bar: Ten of the 11 cumulative curves from Hantsport Bar samples that were dissected are group 3 curves; the eleventh belongs to group 1. The only trend in relative population proportions is that population B tends to decrease from north to south. The average percentage of population C in each sample is 0.8%; it is 66.4% for population A, and 32.8% for population B.

The average mean size of population C is 0.31 phi and the average standard deviation is 0.41 phi; population C equally overlaps population A at an average of 0.63 phi. Population A extends, on the average, to 2.05 phi and has an average mean size of 1.57 phi and an average standard deviation of 0.27 phi. The average standard deviation of the B population is 0.31 phi and its average mean size is 2.47 phi.

Mitchener Bar: All four cumulative curves from Mitchener Bar samples belong to group 3; there are no trends in relative population proportions. Average proportions of the three populations are: population C 0.33%, population A 65.2%, and population B, 34.3%. Population C equally overlaps population A at 0.83 phi; population A extends from 0.83 phi to 2.08 phi.

The average mean grain size of population C is -0.10 phi and its average standard deviation is 0.68 phi; population A has an average mean grain size of 1.69 phi and an average standard deviation of 0.31 phi. Average standard deviation of population B is 0.43 phi and average mean grain size is 2.63 phi (see Table 6-3).

Newport Bar: Eleven of the 12 cumulative curves from Newport Bar samples belong to group 3; the other is a group 1 curve. The proportion of population B tends to increase from north to south; it averages 39.3%. Population C averages 0.62% of each sample and equally overlaps the A population at 1.47 phi; the A population extends to 2.86 phi and averages 60.1%.

Average mean size of population B is 3.17 phi and its average standard deviation is 0.29 phi. Population A has an average standard deviation of 0.28 phi and an average mean size of 2.36 phi; the average mean size of population C is 1.04 phi and its average standard deviation is 0.43 phi.

Synthesis: Earlier in this chapter, it was noted that sediment samples at the head of the estuary are finer than those at the mouth. Cumulative curve dissection reveals the cause of this difference - the presence of a large coarse population at the mouth of the estuary. The average percentage of population C at the estuary mouth is 42.1% and its average equal overlap size with the A population is 1.57 phi (Table 6-3); an average of only 6.3% of each sample from the head of the system is coarser than 1.57 phi (Table 6-3). The mean size of the C population is consistent throughout the estuary; it is better sorted at the head than at the mouth (Table 6-3).

Table 6-3 shows that the A population changes with location; both the coarse and fine points of equal overlap between the A and adjacent populations occur at coarser grain sizes at the estuary head than at the mouth. The A population is coarser and better sorted at the estuary head than at the mouth (Table 6-3); samples at the estuary head have a slightly larger A population than samples at the mouth. The B population also changes with location; it equally overlaps the A population at a coarser size at the estuary head than at the mouth, is coarser and better sorted towards the estuary head, and comprises a larger percentage of each sample near the estuary head (Table 6-3).

Summary

Textural analysis indicates that sediment is finer and better sorted at the head of the estuary than at the mouth; sorting is relatively uniform on each sand body. Each sand body has a unique trend in mean grain size; Boot Island Bar grades from fine sand at the north to coarse sand at the south while Middle Ground is fine sand at the center and medium sand at either end, and Western Bar is medium to coarse sand everywhere. Hantsport Bar grades from fine sand to medium sand from north to south; Mitchener Bar is fine sand and Newport Bar is fine sand to very fine sand. Sand waves tend to be coarser and more poorly sorted than megaripples which are coarser and more poorly sorted than ripples.

Cumulative curve analysis reveals a large coarse population at the estuary mouth that is not present at the head. The estuary mouth has much more sediment that is coarser than 1.57 phi than the head does. Both the intermediate and fine populations are coarser at the estuary head than at the mouth. The fine population increases in percentage from the mouth to the head while the intermediate population is fairly constant in proportion throughout the estuary.

CHAPTER 7

SEDIMENT TRANSPORT

Sediment Transport Paths

Numerous studies in tide-dominated areas have reported distinct zones of ebb and flood sediment transport (Coastal Research Group, 1969; Ludwick, 1974; Oertel, 1972; Houbolt, 1968; among others); similar patterns also occur in Minas Basin (Klein, 1970; Dalrymple et al., 1975; Knight and Dalrymple, 1975). The Avon River estuary can be divided into zones of ebb and flood sediment transport using sand body and channel morphology, sandwave and megaripple morphology and migration directions, and cross-bed orientation.

Zones of ebb and flood sediment transport were inferred from sand body and channel morphology using the techniques of Robinson (1960); flood and ebb channels are mutually evasive, flood channels have a closed end in the onshore direction and ebb channels are closed in the offshore direction. Several "dead-end" flood channels can be identified as well as a few dead-end ebb channels (Fig. 7-1). The major flood channels are be-

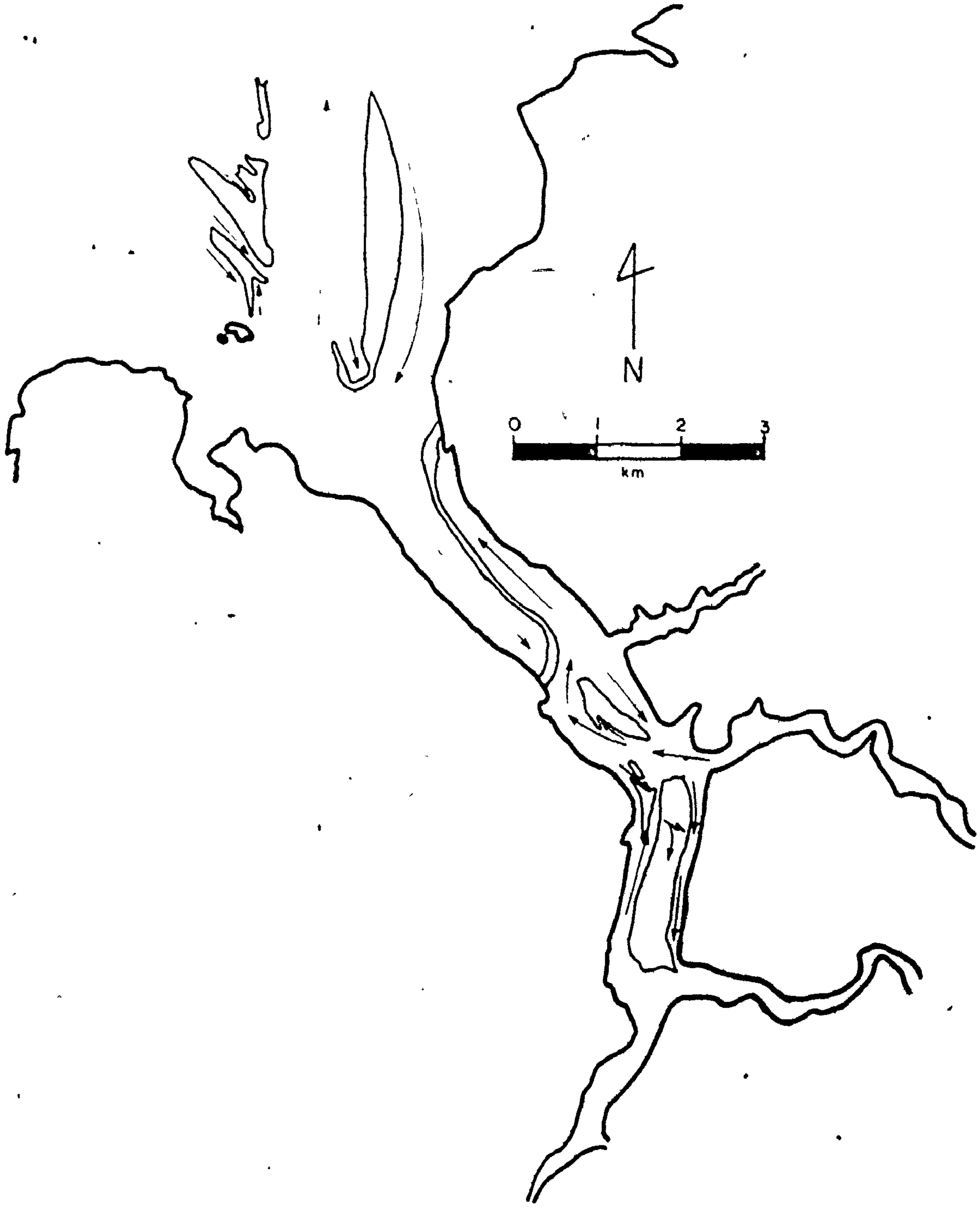

Fig. 7-1. Ebb and flood channels. Arrow direction reflects dominant transport direction

tween Western Bar and Boot Island Bar, the small channel bisecting Western Bar, between the spit and the main portion of Middle Ground, between the western shore of the Avon and the central sand ridge, to the east of Hantsport Bar, through Mitchener Bar, along the eastern side of Newport Bar, and down the center of Newport Bar (Fig. 7-1). Ebb channels occur along the western side of Newport Bar, at the northeastern edge of Newport Bar, on the western edge of Hantsport Bar, along the eastern shore of the Avon River near Summerville, along the eastern edge of Boot Island Bar, and the main channel at the estuary mouth (Fig. 7-1).

Megaripple morphology and bedform migration directions were used to verify the sediment transport directions inferred from sand body and channel morphology. Megaripples can be divided into two groups by their wavelength - height ratios and stoss angle steepness (see Chapter 5). Each type of megaripple is related to a different net migration direction; megaripples with low wavelength - height ratios and steep stoss angles are associated with flood migration directions and megaripples with high wavelength - height ratios migrate in the ebb direction.

The two megaripple morphologies result from reversal of bedform orientation. During each tidal cycle, bedforms reverse their orientation as illustrated in Figure 7-2; bedform reversal has been documented on many sand bodies in Minas Basin (Klein, 1970; Dalrymple

Fig. 7-2. Stages in bedform reversal. The arrow depicts the flow direction causing the changes in surface shape and internal structures shown in stages 1 to 4.

BEDFORM REVERSAL

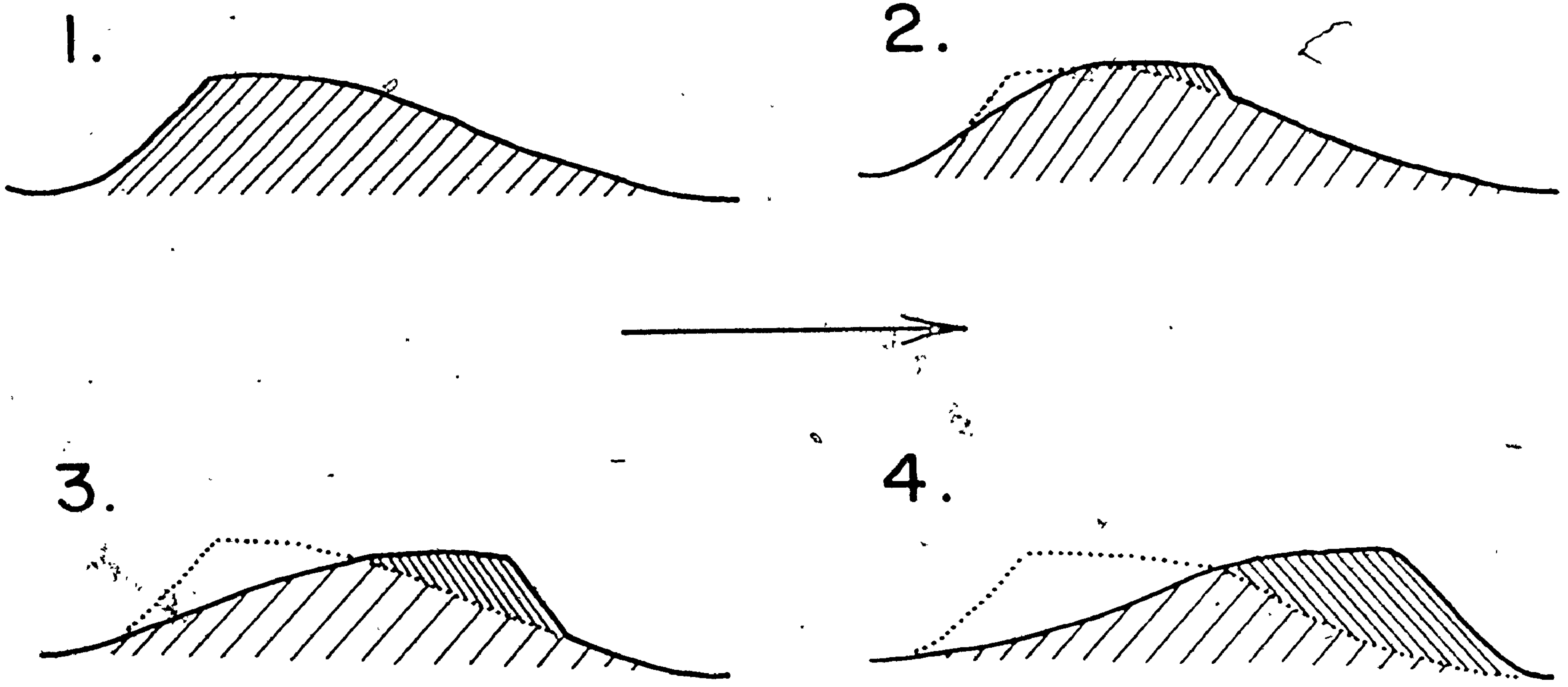

et al., 1975, Knight and Dalrymple, 1975). Stage 1 on Figure 7-2 shows a bedform in equilibrium with the most recent flow direction. After the flow has reversed, the morphology of the bedform begins to reverse as in Stage 2, the process continues until the bedform is completely reversed (Stage 4). Reactivation surfaces are formed by burial of the old bedform surface. If the previous flow direction is dominant, however, the reversal may not be completed and the bedform morphology may resemble an intermediate stage (e.g. Stage 3).

At low tide, megaripples in flood-dominant areas resemble Stage 3, or in extreme cases, Stage 2 of Figure 7-2. Thus flood-dominant megaripples have lower wavelength - height ratios and steeper stoss slopes than ebb-dominant megaripples. Also, remnants of the upstream end of the previous bedform often are present; Figure 7-3 compares the morphology of an ebb-dominant megaripple with that of a flood-dominant megaripple.

Orientation of preserved cross-beds also is dependent on net sediment transport direction. Figure 7-2 illustrates the relationship between bedform orientation and cross-bed orientation; bedforms in flood-dominant areas have more flood-oriented cross-beds than ebb-oriented cross-beds. Interpretation of preserved cross-beds must only consider sets that are below the most recently formed set as subsequent tidal cycles may alter the uppermost set. Figure 7-4 depicts the internal structures of both an ebb and a flood dominant megaripple; a reactivation

Fig. 7-3. Flood and ebb dominant megaripples.

A) are flood and B) are ebb;

the scale is decimeters and centimeters.

A

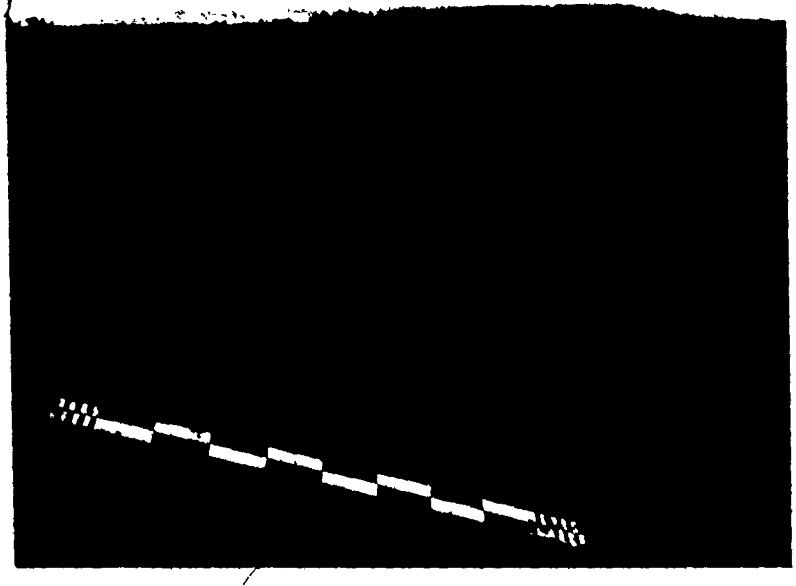

B

Fig. 7-4. Internal structures of flood and ebb megaripples.

A) are flood and B) are ebb;

the scale is 20 cm. long.

A

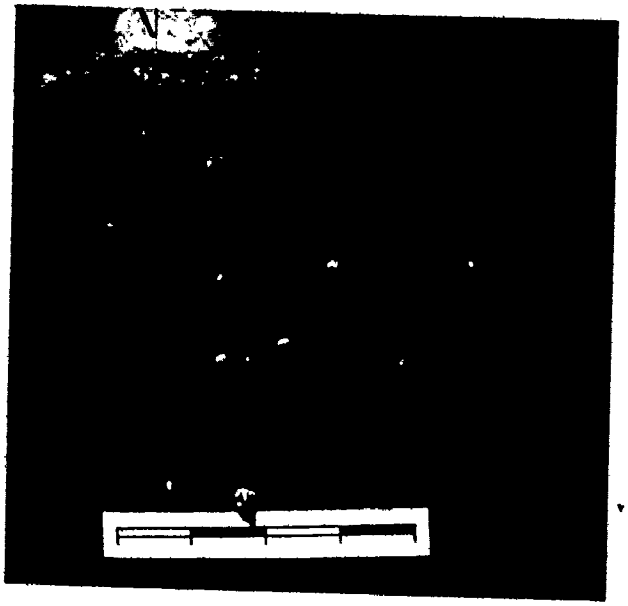

B

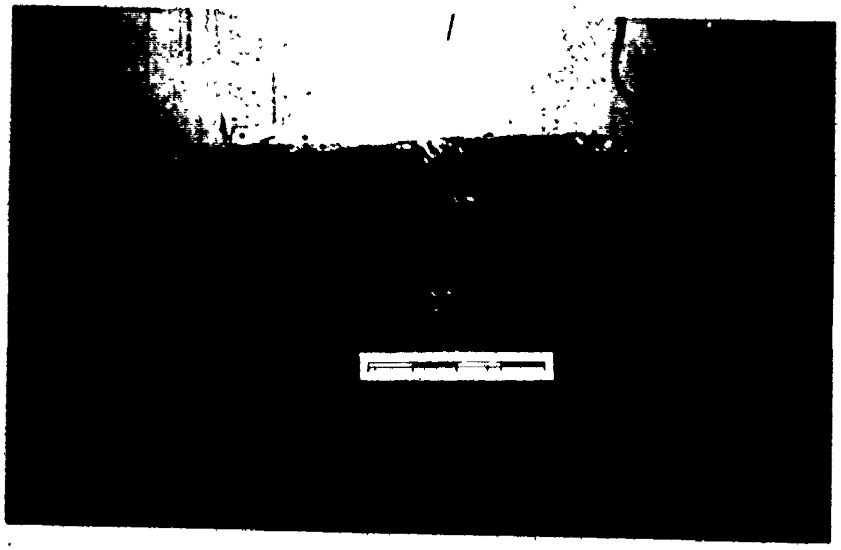

Bedform migration directions also were used to indicate sediment transport directions; see Appendix E for the method of bedform migration measurement. Sediment transport directions derived from megaripple morphology, cross-bed orientation, and bedform migration directions are consistent with directions inferred from sand body and channel morphology, the net sediment transport directions on sand body surfaces and in channels are shown on Figure 7-5.

The net sediment transport directions shown on Figure 7-5 reveal several trends. Sediment transport tends to occur in elliptical cells that are centered on intertidal sand body crests; elliptical transport cells have been recognized on many intertidal sand bodies in Minas Basin (Klein, 1970; Dalrymple et al., 1975; Knight and Dalrymple, 1975) and in other tidally-influenced areas (Houbolt, 1968; Reineck, 1963; Smith, 1969). Sediment is transported by flood currents along one side of a sand body and then dumped across the sand body crest where it enters an ebb dominant zone. The grains are then carried in the ebb direction along the opposite side of the sand body, and are returned finally to the flood dominant area. Transport paths on Hantsport Bar (Fig. 7-5) provide an excellent illustration of this process. Sediment is transported to the south along the eastern side of the sand body by flood currents, across the sand body crest near the southern end, and to the north along the west side by ebb currents (Fig. 7-5). The cycle is completed by west to east transport at the northern end of the sand body by ebb currents (Fig. 7-5).

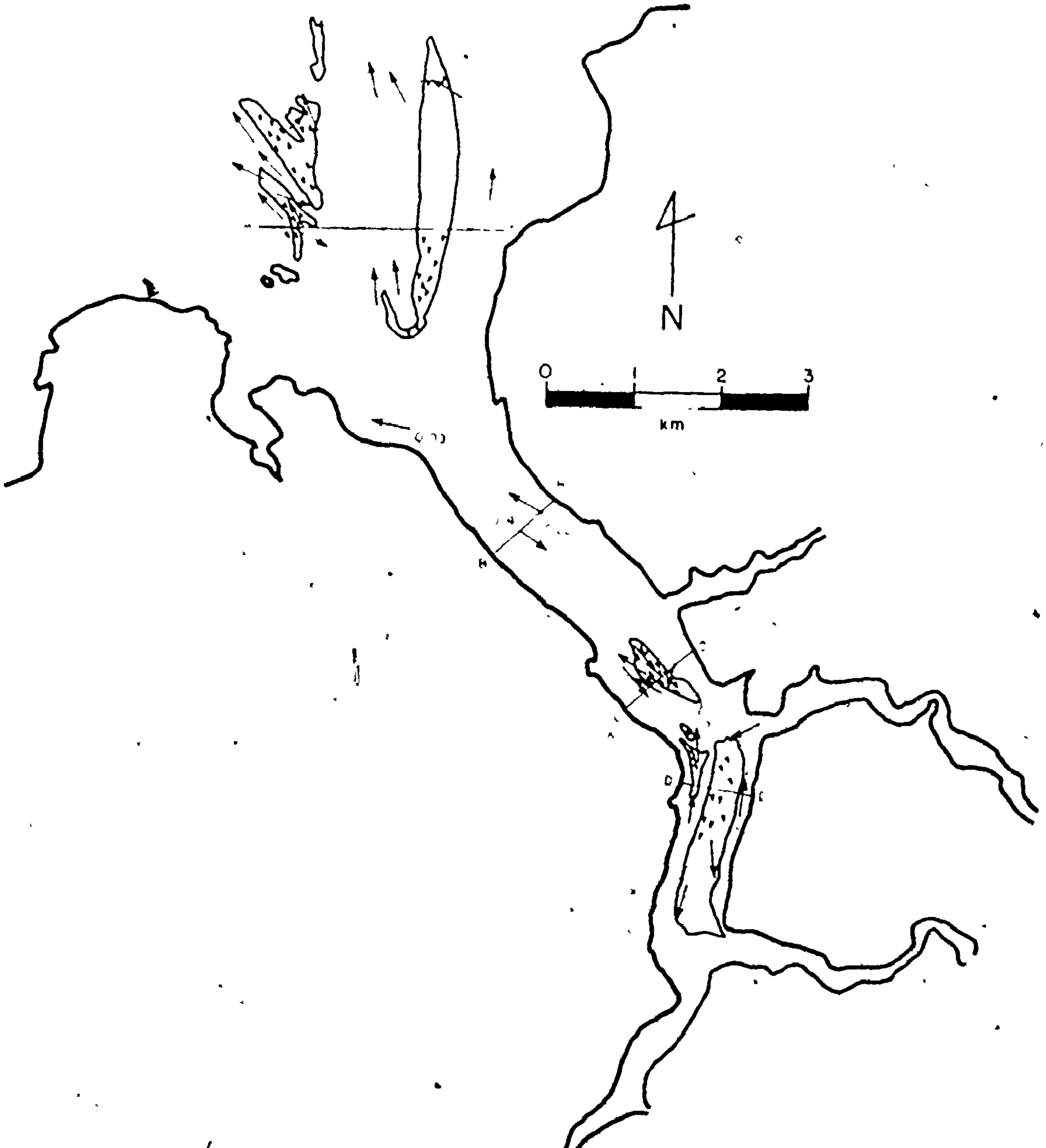

Fig. 7-5. Net sediment transport directions. Arrow heads are directions from bedform migration studies; long arrows are net transport directions computed with Engelund and Hansen's equation. Net sediment transport rates (m^3/m width/tidal cycle) are shown for 3 stations near the center of the estuary. The 4 cross-sections used for integrated net sediment transport rates are located.

Sediment transport paths at the estuary mouth correspond with those expected in an ebb tidal delta. The central channel has transport in the ebb direction, the intertidal sand bodies have both ebb and flood zones, and the outer margins of the system are flood dominant (Fig. 7-5). This is similar to the pattern described in the ebb tidal delta model of Hayes et al. (1973) depicted in Figure 4-2; numerous mesotidal ebb tidal deltas have similar patterns (Coastal Research Group, 1969; Oertel, 1972, 1973; Wright and Sonu, 1975; Finley, 1975; Hubbard, 1975).

Within the Avon River, most flood dominant areas are shallower in water depth than ebb areas. Most net ebb transport is confined to a long, relatively deep channel that meanders between shallow flood dominant zones (Fig. 7-5). Similar patterns were described in Denmark by van Veen (1950; reported in Schou, 1967) and from Yaquina Bay, Oregon (Kulm and Byrne, 1967).

Sediment Transport Rates

BEDFORM MIGRATION: Net sediment transport rates were computed by calculating the volume of sediment transported past a point during one tidal cycle. The formula used is that of Simons et al. (1965b); net sediment transport rate per unit width per tidal cycle equals bedform height times migration distance during one tidal cycle times grain concentration. The method and its limitations are described in detail in

Appendix E. Computed transport rates range from 0.003 to 1.26 m^3 per unit width per tidal cycle. Sediment transport rates calculated from bedform migration measurements on intertidal sand bodies at the estuary mouth are displayed on Figure 7-6; transport rates at the head of the system are shown on Figure 7-7. These are minimum sediment transport rates; only sediment moving on the bed can be monitored using bedform migration rates as other transport mechanisms can cause sediment to bypass bedforms. Note that sediment transport directions tend to be oblique to sand body crests (Figs. 7-6 and 7-7); this will be discussed further in Chapter 10.

Net sediment transport rates in the Avon River estuary show a few general trends. Rates tend to be higher near the head of the estuary than at the mouth. The average rate is 0.06 m^3 per meter width per tidal cycle on Middle Ground, 0.02 m^3 on Boot Island Bar, and 0.10 m^3 on Western Bar; it is 0.67 m^3 per meter width per tidal cycle on Newport Bar and 0.48 m^3 on Mitchener Bar; Hantsport Bar has an intermediate mean net sediment transport rate of 0.19 m^3 per meter width per tidal cycle.

Three sand bodies have areas of both ebb and flood net transport: Hantsport Bar, Boot Island Bar, and Western Bar. There is no significant difference between average net transport rates in the flood area and those in the ebb zone on Boot Island Bar. Flood rates

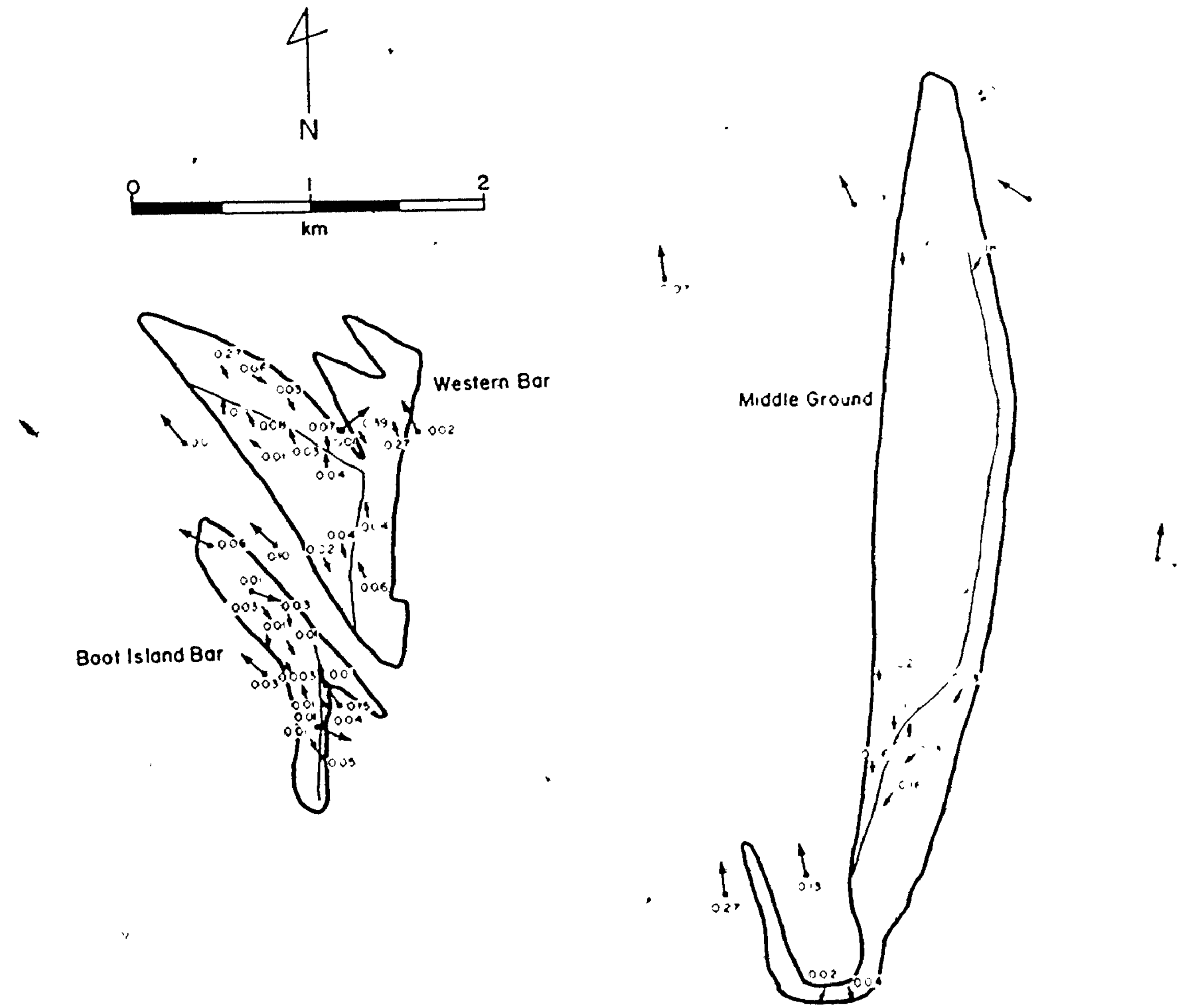
N
0
1
2
km
Western Bar
Middle Ground
Boot Island Bar
002
027
004
006
003
013

Fig. 7-6. Sediment transport rates at the estuary mouth. All rates are net transport rates for a complete tidal cycle in m^3/m width. Arrows indicate net transport directions. The longer arrows projecting from a square depict rates computed with Engelund and Hansen's equation; the smaller arrows represent rates calculated from bedform migration rates. The sand body crest is illustrated with a thin line.

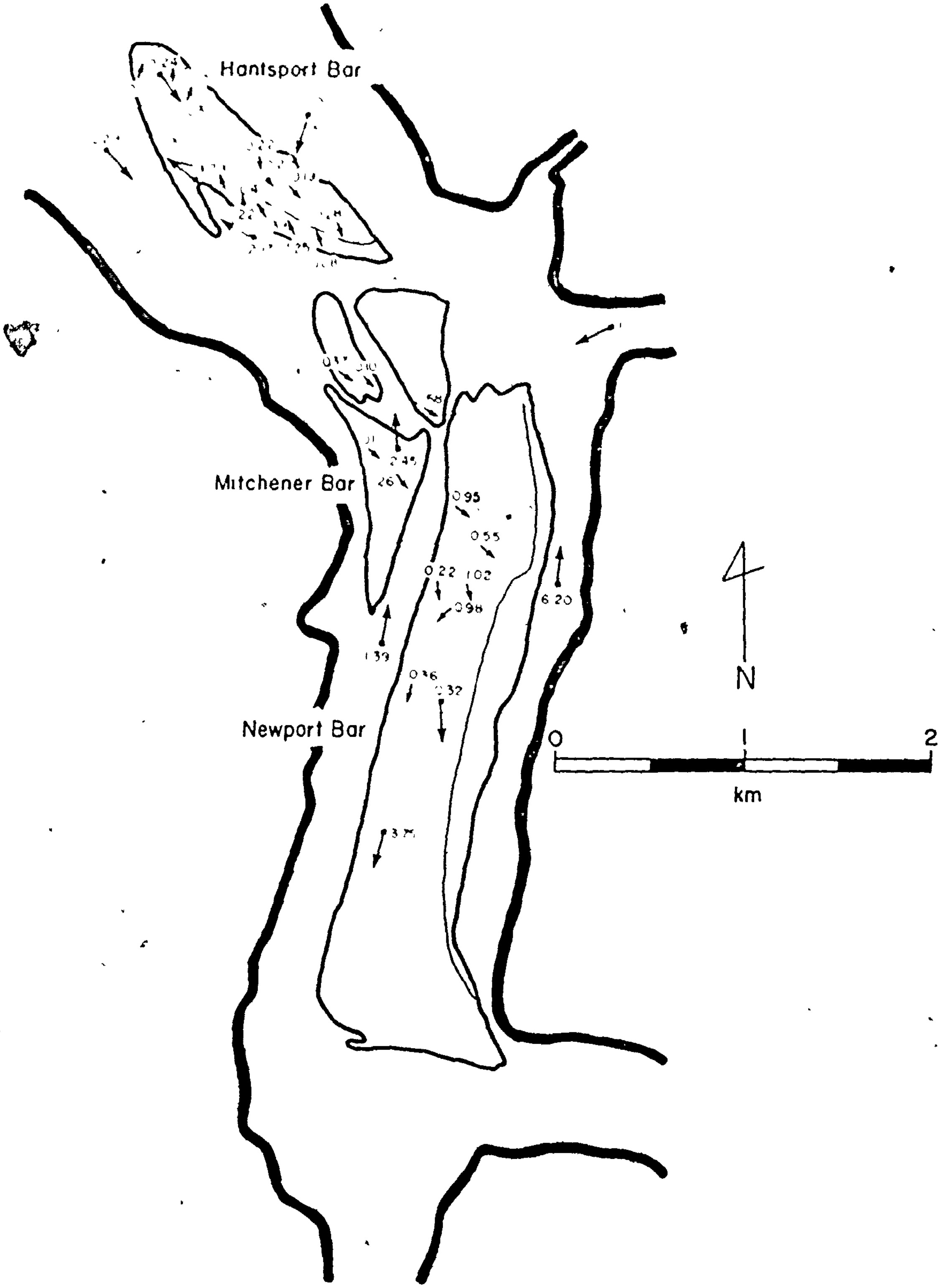
Hantsport Bar
Mitchener Bar
Newport Bar
2 45
26
0 95
0 55
0 22
1 02
0 98
6 20
1 39
0 32
N
0
1
2
km

Fig. 7-7. Sediment transport rates at the estuary head. All rates are net transport rates for a complete tidal cycle in m^3/m width. Arrows indicate net transport directions. The longer arrows projecting from a aquare depict rates computed with Engelund and Hansen's equation; the smaller arrows represent rates calculated from bedform migration rates. The sand body crest is illustrated with a thin line.

are higher than ebb rates on both Hantsport Bar and Western Bar. On Hantsport Bar, average transport rates are 0.21 m^3 per meter width per tidal cycle in the flood area and 0.17 m^3 in the ebb region; average net sediment transport rates are 0.16 and 0.07 m^3 per meter width per tidal cycle on the flood and ebb side of Western Bar respectively. Boot Island Bar has mean net transport rates of 0.02 m^3 in the flood zone and 0.03 m^3 per meter width per tidal cycle in the ebb region.

Differences in net transport rates between adjacent ebb and flood areas may be due partly to differences in the width of each zone. If each sand body is essentially a closed sediment system with elliptical transport as suggested by Klein (1970), transport rates per unit width must be greater in narrower zones. Transport rates on Western Bar and Hantsport Bar support this idea. On each sand body, the ebb transport volume obtained by multiplying the ebb transport rate by the width of the ebb zone nearly equals the flood transport volume computed in the same manner. However, transport zones on sand body surfaces often are parts of larger transport zones that include channels; a balance between transport rate and zone width must consider the entire transport zone. This problem will be discussed later in this chapter.

There is no relationship between net sediment transport rate as determined from bedform migration rates and down-current location within a flood or ebb transport area; net transport rates neither increase nor decrease systematically in the transport direction. Also, there is no consistent relationship between net sediment transport rate and bedform type.

Megaripples are smaller than sand waves (see Chapter 5) and form under higher flow strengths (see Chapter 9) so that they might be expected to migrate and transport sediment more quickly than sand waves, but net transport rates for the two bedform types are similar. The net rates are similar because megaripples migrate further than sand waves in both the flood and ebb direction so that their net migration is small; despite their slower migration rate in each direction, sand waves can have as large net transport rates as megaripples because net rate is the residual of flood migration minus ebb migration.

Bedform migration studies do not indicate any relationship between net sediment transport rate and mean grain size or sediment sorting on any sand body. The trends that exist in mean grain size and sorting on each sand body (see Chapter 6) are not reflected in the net sediment transport rates displayed on Figures 7-6 and 7-7. Relationships between sediment transport rates and grain size distribution will be discussed in Chapter 8.

TRANSPORT EQUATIONS: Sediment transport rates were calculated with a computer program written by R. W. Dalrymple; the program utilizes the transport equations of Einstein (1950), Bagnold (1956), Engelund and Hansen (1967), Toffaleti (1969), and Ackers and White (1973). Appendix E contains a brief description of the computation method and the limitations of applying transport equations to the Avon River estuary.

The Einstein transport equation considers bed load transport as a stochastic process; each grain has an equal probability of motion. The equation relates fluid flow to this probability. Transport rates are computed separately for each grain size (1/2 phi intervals) and then summed to give the total transport rate; correction factors are added for form resistance, velocity distribution, and "hiding" of small grains by larger ones. The formula is derived in Einstein (1950); Yalin (1972) discusses limitations of the equation.

Bagnold's transport equation relates sediment transport rate to the efficiency of available energy in doing work. The total amount of work, derived from physics, is multiplied by an efficiency factor. The formula is applied to median grain size only and uses a critical shear stress for motion derived by Bagnold. Yalin (1972) and Raudkivi (1967) discuss Bagnold's equation; a full derivation is given in Bagnold (1956).

Engelund and Hansen (1967) use an approach similar to that of Bagnold by relating sediment transport to available energy; the difference is that Engelund and Hansen are concerned with surfaces with dunes (megaripples) and consider the lift required to lift a grain to the height of a bedform. Engelund and Hansen's equation is simple in form; sediment discharge (Q_s) is calculated with the formula

$$Q_s = 0.1 \left[\left(\frac{\tau}{(\gamma_s - \gamma) D_f} \right)^{2.5} \left(\frac{4 \sqrt{\frac{\gamma_s - \gamma}{\gamma} g (D_f)^3}}{f} \right) \right]$$

The complete derivation is in Engelund and Hansen (1967).

Toffaleti (1969) uses a more empirical approach than the others; his reasoning is similar to that of Einstein in that probabilities of grain motion are considered. Also, Toffaleti's equation considers transport of individual grain sizes (one phi intervals) as does Einstein's. The formula shows good agreement with measured sediment transport rates for rivers; this data plus the derivation is presented in Toffaleti (1969).

The Ackers and White transport function is another Bagnold-like model; it relates particle motion to available energy. Ackers and White (1973) developed their formula for flumes but their tests in natural systems gave results that are comparable to other formulae. The function is derived in Ackers and White (1973). The rates predicted by each equation were compared to rates calculated with the other equations and with transport rates computed from bedform migration rates.

Each of four transport equations has at least one major flaw. The Ackers and White (1973) equation produced unreasonably high transport rates that were up to one, or more, orders of magnitude larger than rates calculated from bedform migration rates. Bagnold's (1956) transport function gave inconsistent results; at some stations computed rates were much greater than measured while at others the inverse was true. White et al. (1975, 1976) report that Bagnold's formula does not yield equivalent results for different grain size ranges. Toffaleti's (1969) equation also produced inconsistent results; its accuracy also has been found to vary with grain size (White et al., 1975).

Although Einstein's (1950) transport equations probably are the most widely used (Yalin, 1972) and are considered by some to be the most reliable (Shen, 1971), they produced transport rates that are consistently lower than measured rates; transport rate was calculated to be zero for many profiles even though τ values are above Shield's critical values. White et al. (1975, 1976) also found that Einstein's transport equations tend to underestimate transport rate.

Engelund and Hansen's (1967) equation gave the most consistent results when compared to bedform migration rates (Fig. 7-8). White et al. (1975, 1976) also found Engelund and Hansen's equation to be

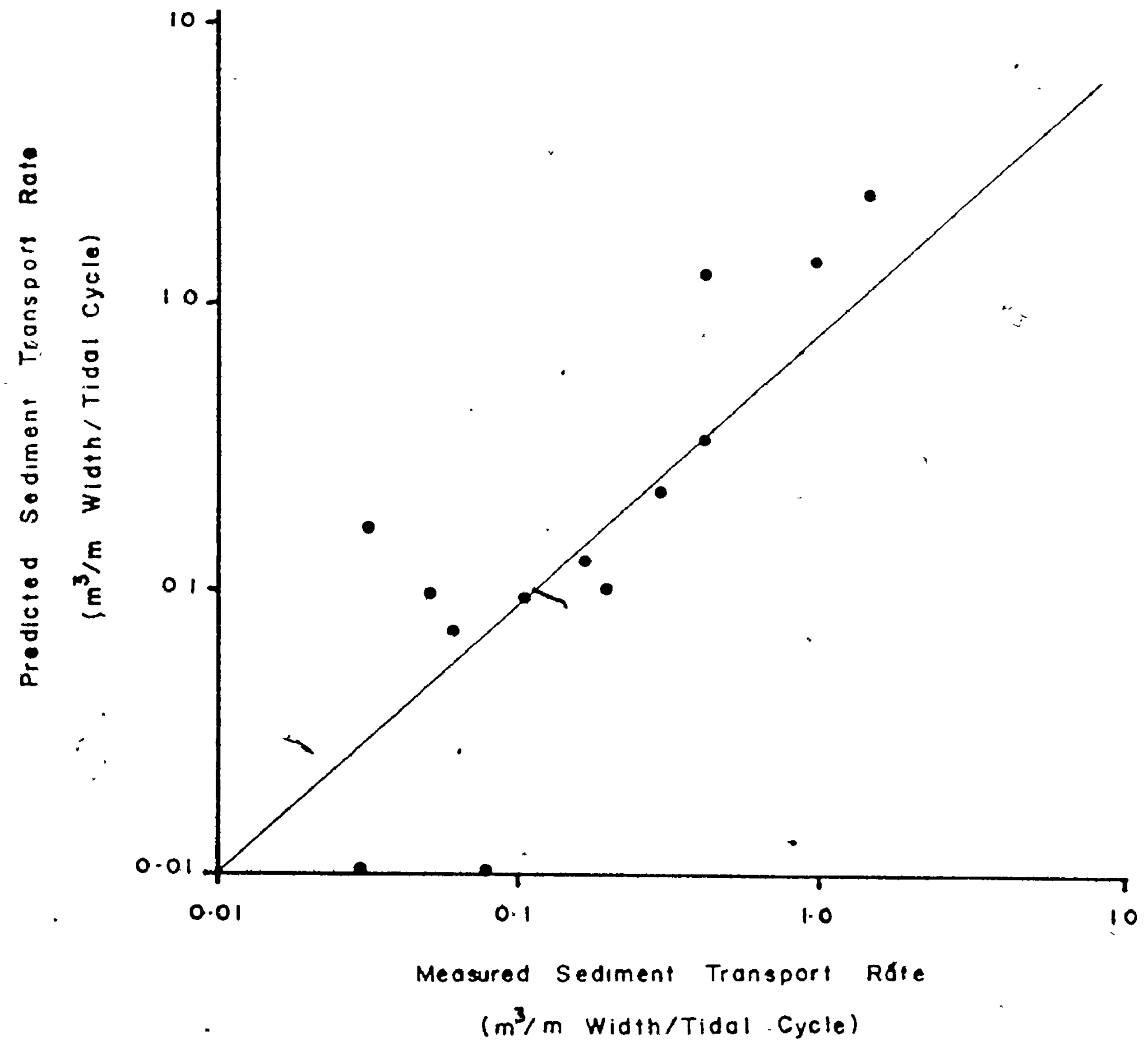

Fig. 7-8. Comparison of measured and predicted sediment transport rates. Predicted rates are those computed with Engelund and Hansen's equation; measured rates were derived from bedform migration studies. The line of predicted equal to measured is plotted.

reliable and to work well for all grain sizes although it tended to overestimate transport at low shear velocities.

Dalrymple (1977) computed sediment transport rates in a macrotidal environment (Cobequid Bay, see Fig. 2-2) using fluorescent tracers and bedform migration rates; he compared these rates to the products of several transport equations and found that Engelund and Hansen's formula agreed most closely with the measured rates. The single disadvantage of this transport equation is that it does not yield transport rates for individual grain size fractions. Since Engelund and Hansen's transport equation proved to be the most consistent of the five equations, all computed transport rates used in this study are products of that equation. The results of Einstein's equations were used to compare relative transport rates of different grain size fractions.

In most cases, sediment transport rates and directions computed with Engelund and Hansen's formula agree with rates and directions calculated from bedform migration rates and with dominant current directions (Figs. 7-6 and 7-7 and Chapter 3). Rates tend to be greater near the estuary head than at the mouth and tend to decrease laterally from channel thalwegs to sand body crests (Figs. 7-6 and 7-7); this corresponds with trends in current velocities (see Chapter 3).

During a tidal cycle, sediment transport rates vary in a similar manner to current speeds (see Chapter 3), although transport rates vary as the fourth to sixth power of current speed. Following low tide, transport rates accelerate rapidly to a peak, level off, and decelerate to high tide. After high tide, transport rates accelerate slowly to a peak late in the ebb stage and then drop rapidly to low water (Fig. 7-9). Most tidal cycles follow this pattern with few inconsistencies; peaks tend to be higher at the estuary head than at the mouth.

The highest values of sediment transport for each tidal cycle always occur with flow in the dominant direction. The highest values only occur for short time periods and often are several times larger than any other values. In some cases it is the volume of sediment moved by the highest single transport rate that determines net transport direction. Stations Newport Bar No. 2 and Mitchener Bar No. 1 are good examples of this phenomenon (Table 7-1). The large rate of 9.07 m^3/tidal cycle at 4.17 hours at Mitchener Bar No. 1 and the rate of 7.36 m^3/tidal cycle at -2.83 hours at Newport Bar No. 2 determines the net transport direction in each case (Table 7-1). (Table E-1 lists all sediment transport rates computed with Engelund and Hansen's formula.)

SEDIMENT TRANSPORT RATES NEAR EACH SAND BODY AND IN THE MAJOR CHANNELS: Sediment transport rates and directions in the following discussion were derived from bedform migration studies and

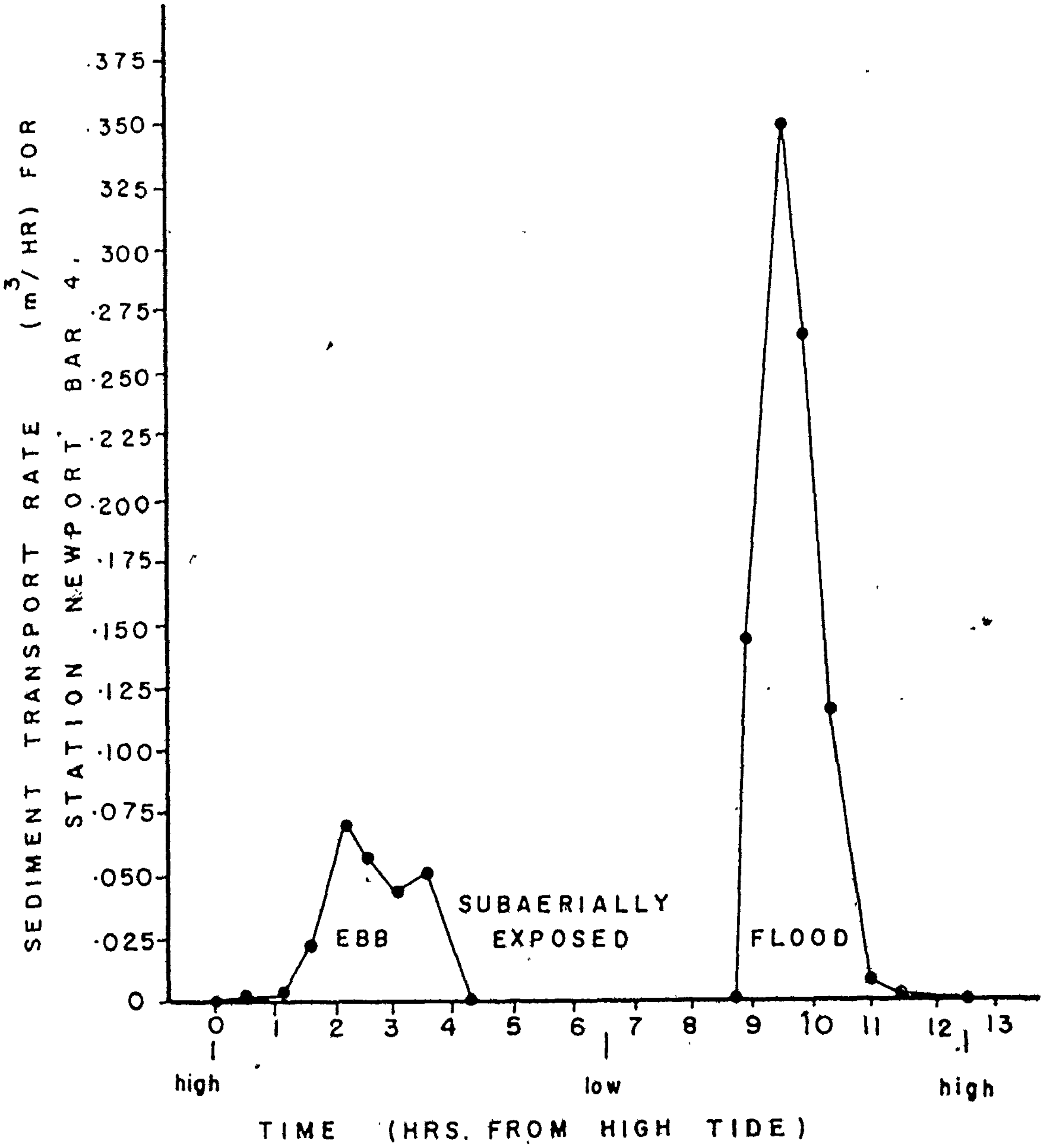

Fig. 7-9. Predicted sediment transport rate through a tidal cycle. Rates are per meter width and were computed with Engelund and Hansen's equation.

TABLE 7-1. Sediment Transport Rates for two stations where net Transport Direction is determined by the results of one Profile; all rates are m^3/meter width/hour, time is in hours from high tide and direction is flood (F) or ebb (E); net rates are m^3/meter width/tidal cycle

MITCHENER BAR 1			NEWPORT BAR 2		
Time	Dir.	Rate	Time	Dir.	Rate
-2.83	F	2.49	-10.08	E	0.01
-2.33	F	3.25	-9.58	E	0.03
-1.83	F	0.22	-9.08	E	0.06
-1.33	F	0.26	1.17	E	0.00
-0.83	F	0.02	1.67	E	0.00
-0.33	F	0.00	2.17	E	0.03
0.17	F	0.00			
8.67	F	0.06	-2.83	F	7.36*
9.17	F	0.09	-2.33	F	0.24
			-1.83	F	0.00
0.67	E	0.00	-1.33	F	0.01
1.17	E	0.03	-0.83	F	0.00
1.67	E	0.04	-0.33	F	0.00
2.17	E	0.00			
2.67	E	0.27	Net	F	3.75
3.17	E	0.97			
3.67	E	0.41			

rates calculated with Engelund and Hansen's transport formula.

Newport Bar: Net sediment transport rates on Newport Bar range from 0.22 to 3.75 m^3 per tidal cycle; all transport rates in this discussion are per unit (one meter) width. In channels adjacent to Newport Bar rates vary between 1.39 and 6.20 m^3 per tidal cycle. All net transport on the sand body surface is in the flood direction; it is in the ebb direction in both adjacent channels (Fig. 7-7).

Transport rates seem to be lower near the center of Newport Bar than at the ends; there are no other trends on the sand body surface. The high transport rate at Newport Bar station 2 probably is not related to rates calculated from statistically insignificantly current velocity profiles since the only insignificant profiles are low velocity profiles. (See the discussion of statistical significance of velocity profiles in Chapter 3, and the discussion of the effect of statistically insignificant profiles on sediment transport rate in Appendix E; all sediment transport rates are listed in Table E-1.) One profile accounts for most sediment transport at Newport Bar station 2 (Table 7-1); it is impossible to determine the accuracy of the magnitude of this value.

High transport rates in the channels adjacent to Newport Bar may be due to relative width of ebb and flood dominant zones. Since Newport Bar does not appear to be accreting or eroding (see Chapter 4), and since sediment transport rates imply little or not net transport through 4 cross-sections of the estuary (see the discussion later in this section), total ebb transport must nearly equal total flood transport. Flood transport areas are approximately 5.3 times as wide as ebb areas; ebb transport rates should be proportionately higher. (The relationship between transport rates and channel and sand body stability will be discussed in Chapter 10.)

Mitchener Bar: Transport rates near Mitchener Bar range from 0.10 to 1.26 m^3 per tidal cycle on the bar surface and reach 2.45 m^3 per tidal cycle in the adjacent channel (Fig. 7-7). On the bar surface all net transport is in the flood direction while in the adjacent channel net transport is in the ebb direction. Again, the high ebb transport rate in the channel probably is due to a flood to ebb area ratio of approximately 2.8; there are no other trends in sediment transport rates near Mitchener Bar.

Hantsport Bar: The lowest net transport rate on Hantsport Bar is 0.03 m^3 per tidal cycle and the highest is 0.39 m^3 per tidal cycle; in the channels to the east and west of the sand body, net transport rates range between 0.10 and 2.17 m^3 per tidal cycle (Fig. 7-7). Rates are higher in ebb dominant channels than in flood dominant channels; flood areas comprise 76 percent of the width of the Avon River at Hantsport Bar.

The anomalously high rate of 2.17 m^3 per tidal cycle at Hantsport Bar station 5 may be due to high ebb transport rates calculated for several current velocity profiles that are not significant at the 95% level (see the discussion in Appendix E and Table E-1); lower rates for these profiles would reduce the net transport rate to a level consistent with nearby stations (Fig. 7-7). Hantsport Bar station 4 has one flood profile that appears to have an anomalously low transport rate (Table E-1); a more accurate value would increase the net flood transport at Hantsport Bar station 4.

Middle Ground: Net transport rates on Middle Ground range from 0.01 to 0.16 m^3 per tidal cycle; most rates on the sand body surface are less than 0.10 m^3 per tidal cycle and all are in the flood direction. In the adjacent channels rates vary between 0.01 and 0.51 m^3 per tidal cycle (Fig. 7-6). Flood rates are similar in magnitude to ebb rates.

At two current velocity stations the net sediment transport directions predicted by Engelund and Hansen's formula do not agree with directions derived from bedform migration measurements and sand body and channel morphology. Middle Ground station 1 has a calculated net transport in the ebb direction (Fig. 7-6) although channel morphology and nearby bedform migration rates predict flood transport for this region. Four profiles are statistically insignificant at the 95% level (Table E-1); in addition, profiles had to be eliminated because of negative slopes or because they consisted of only one point (see the discussion in Appendix E). Since the net transport rate at this station is small (Fig. 7-6), a small change in the computed rates for one or more of these profiles could change the net transport direction.

Middle Ground station 3 also has a computed net ebb transport in an area that would be expected to be flood dominant (Fig. 7-6). Five profiles are insignificant at the 95% level including 3 flood profiles with anomalously low transport rates (Table E-1); a slight increase in the transport rate for these profiles would reverse the net transport direction. Results for Middle Ground stations 4 and 5 are inconclusive since small changes in transport rates for the statistically insignificant profiles from each station could reverse the net transport direction (Table E-1). The difference in the calculated net transport rates between Middle Ground station 2 and Bedford Institute station 2 (Fig. 7-6) probably is related to the inclusion of statistically insignificant profiles; the close proximity of the stations, and the nearly equivalent tidal coefficients (Table E-1), reduce the possibility that the difference is real.

Boot Island Bar: The lowest net sediment transport rate on Boot Island Bar is 0.003 m^3 per tidal cycle; the highest is 0.05 m^3 per tidal cycle. In the adjacent channels rates vary between 0.02 and 0.15 m^3 per tidal cycle. Flood and ebb rates do not differ significantly in magnitude (Fig. 7-6).

Boot Island Bar station 2 has a calculated ebb net transport in a region where flood transport is expected (Fig. 7-6). As in the case of the Middle Ground stations, the low net transport rate at Boot Island Bar station 2 could be reversed in direction with a small change in calculated rates for statistically insignificant profiles; there are 11 profiles from Boot Island Bar station 2 that are insignificant at the 95% level. Boot Island Bar station 3 produced inconclusive results; sand body and channel morphology do not indicate a probable transport direction and there are no nearby bedforms that are suitable for migration measurements (see Chapter 5). The net ebb transport rate of 0.06 m^3 per tidal cycle could reverse direction easily with small changes in the 8 statistically insignificant profiles recorded at this station (Table E-1).

Western Bar: Net sediment transport rates on the surface of Western Bar range from 0.01 to 0.39 m^3 per tidal cycle; most rates are between 0.03 and 0.08 m^3 per tidal cycle. Rates are highest on the sandwave zone (see Chapter 5 and Fig. 7-6) and are slightly higher on the northwestern end of the sand body than on the southeastern end. In the adjacent channels rates vary between 0.01 and 0.10 m^3 per tidal cycle; there are no significant differences in magnitude of ebb and flood transport rates.

Western Bar station 1 has a surprisingly low net transport rate; there are several statistically insignificant flood profiles with low transport rates that may account for the low transport rate (Table E-1). The net ebb transport computed for Western Bar station 3 disagrees with sand body and channel morphology. Again, several profiles that are insignificant at the 95% level were recorded at Western Bar station 3, and a small change in the rates calculated for these profiles could reverse the net transport direction (Table E-1).

Major Channels: Sediment transport rates were calculated for six stations in the major channels of the Avon River estuary; the six stations are Bedford Institute station 3, Main Channel, Horton North, Horton South, Summerville, and Kennetcook Mouth (Figs. 7-6 and 7-7). Absolute transport rates were not computed since sediment samples could not be collected as a grab sampler was not available. The same sediment sample was used to compute sediment transport rate at each of the six stations so that relative rates could be established among the six stations.

All six stations have calculated net sediment transport directions that agree with sand body and channel morphology. At the mouth of the system Bedford Institute station 3 has a small net ebb transport rate; Main Channel and Horton North also have small net transport rates in the ebb direction. Horton South has a moderate transport rate in the flood direction while Summerville, on the opposite side of the central sand ridge (see Chapter 3), has a moderate net ebb transport rate. Kennetcook Mouth has a large net sediment transport rate in the ebb direction. (See Table E-1 for calculated sediment transport rates of the six stations in the major channels; the stations are located on Figure 3-2.)

NET SEDIMENT TRANSPORT IN THE ESTUARY: Net sediment transport for a tidal cycle was calculated for four cross-sections of the study area; the cross-sections are located on Figure 7-5. On each cross-section, transport rates were considered to decrease with water depth from maximum values at channel thalwegs to near zero at the crest of Hantsport Bar; net transport rates computed from bedform migration rates were combined with estimates for the channels to produce an average sediment transport rate for each transport zone. The average rate for each zone was multiplied by the width of that zone to yield the total volume of sediment transported during a tidal cycle in each transport zone; flood and ebb zones were subtracted giving the net volume of sediment transported across the cross-section during a tidal cycle.

Results indicate very little net sediment transport; rates range between 0.93 m^3/tidal cycle in the ebb direction and 0.33 m^3/tidal cycle in the flood direction (Table 7-2). The implications of net sediment transport rates on sand body stability will be discussed in Chapter 10.

TABLE 7-2. Net Sediment Transport Rates for Four Cross-Sections

(All the cross-sections are located on Figure 7-5)

Cross-Section	Transport Rate (m^3/tidal cycle)	Direction
A	0.33	Flood
B	0.38	Ebb
C	0.03	Ebb
D	0.93	Ebb

Summary

Sediment transport paths were determined using internal structures, bedform migration directions, and sand body and channel morphology. Transport paths form elliptical cells centered on sand body crests; transport on either side of a crest has sediment transport in opposite directions. Near the estuary head ebb transport is confined mainly to channels and most sand body surfaces are flood dominant.

Sediment transport rates were calculated with Engelund and Hansen's transport formula and with bedform migration rates; transport rates are greater at the estuary head than at the mouth and are higher near channel thalwegs than sand body crests. During a tidal cycle the highest flood transport rates occur early in the flood stage and the highest ebb rates occur late in the ebb stage. Net transport rates computed with Engelund and Hansen's equation are, in most cases, consistent with rates and directions determined from bedform migration rates. However, statistically insignificant current velocity profiles appear to influence net sediment transport rate; this problem is discussed in Appendix E. All net sediment transport rates are displayed on Figures 7-6 and 7-7.

CHAPTER 8

INTERPRETATION OF GRAIN SIZE DISTRIBUTIONS

As discussed in Chapter 6, some authors believe that grain size distributions are related to source material (Shea, 1974) while others attribute observed grain size distributions to depositional processes (Visher, 1969; Friedman, 1961; among others). This chapter attempts to relate the grain size distributions described in Chapter 6 to hydraulics; results indicate that grain size distributions in the Avon River estuary can be interpreted with respect to hydraulic processes. Sediment transport mechanisms are reflected in the observed sediment distribution; textural parameters and cumulative curve shapes are influenced by hydraulic processes and can be interpreted in terms of these processes.

Initiation of Motion

Both cumulative curve shape and textural parameters are affected by the coarsest grain size present at any location. If grain size distributions reflect local hydraulics, then the coarsest sediment at any location should be the coarsest size that can be transported by the local currents.

A criterion for competence of a given flow was established by Shields (1936) and has been examined by the Committee on Sedimentation (1966) who compared the results of several workers; Shields' criterion was found to be reasonably accurate. Sternberg (1966, 1967, 1971) verified that Shields' criterion is applicable to tidal currents in a shallow marine environment.

Using Shields' criterion, the maximum grain size that can be transported by the largest shear stress values recorded during a tidal cycle was calculated for each current velocity station; stations at which sediment samples were not collected were eliminated (see Chapter 7). At most stations near the estuary mouth, the coarsest grain size present corresponds with competence predicted by Shields' criterion (Table 8-1; Fig. 8-1). A few exceptions occur on Boot Island Bar, Western Bar, and Middle Ground where a few percent of some samples are too coarse to be transported (Table 8-1); this could represent locally derived material since Boot Island Bar sits on a wave cut bedrock platform (see Chapter 2). Tidal cycles with larger tidal coefficients than those recorded may generate sufficient shear to transport most, or all, of the "lag" sediment. At most estuary mouth stations, Einstein's transport equations indicate that the coarsest grain size present is transported slowly. This agrees with Shields' criterion and provides evidence that hydraulics control the coarsest grain size present.

TABLE 8-1. Initiation of Movement

T.C. is theoretical competence

C.S.P. is coarsest size present (sieve containing coarsest sediment)

Station		Tidal Coeff.	τ(dynes /cm^2)	T.C. (phi)	C.S.P. (phi)	% Lag	Ein. (phi)*
Boot Island Bar	1	0.76	48	-2.50	-2.50	0.0	-2.75
	2	0.76	20	-1.50	-2.00	0.2	-1.75
	3	0.79	32	-2.00	-2.50	0.1	-1.75
	4	0.79	43	-2.25	-2.00	0.0	-2.25
	5	0.62	16	-1.25	-1.75	9.0	-
Middle Ground	1	0.65	56	-2.50	-1.50	0.0	-0.75
	2	0.65	67	-2.75	-2.50	0.0	-2.25
	3	0.91	53	-2.50	-2.50	0.0	-2.25
	4	0.76	44	-2.50	-1.50	0.0	-1.75
	5	0.81	28	-1.75	-3.50	1.5	-2.25
Western Bar	1	0.64	27	-1.75	-3.00	1.5	-1.75
	2	0.64	28	-1.75	-1.50	0.0	-1.75
	3	0.88	63	-2.75	-2.25	0.0	-2.25
	4	0.81	24	-1.75	-1.75	0.0	-1.75
Hantsport Bar	1	0.77	99	-3.25	-0.50	0.0	-0.25
	2	0.77	89	-3.25	-1.00	0.0	-0.75
	3	0.77	62	-2.75	0.00	0.0	0.75
	4	0.75	102	-3.50	-1.75	0.0	-1.75
	5	0.81	174	-4.25	0.00	0.0	0.25
Mitchener Bar	1	0.88	227	-4.50	-1.25	0.0	-1.25
Newport Bar	1	0.77	527	-5.75	0.75	0.0	0.75
	2	0.72	132	-3.75	0.00	0.0	0.25
	3	0.58	67	-2.75	-1.00	0.0	-0.25
	4	0.70	45	-2.50	0.00	0.0	0.25

* Ein. is the coarsest size transported as predicted by Einstein's equation

Fig. 8-1. Predicted competence versus coarsest observed grain size. Observed maximum grain size is the coarsest sieve fraction; predicted competence is Shields' criterion computed for maximum shear stress. The line of predicted = observed is plotted.

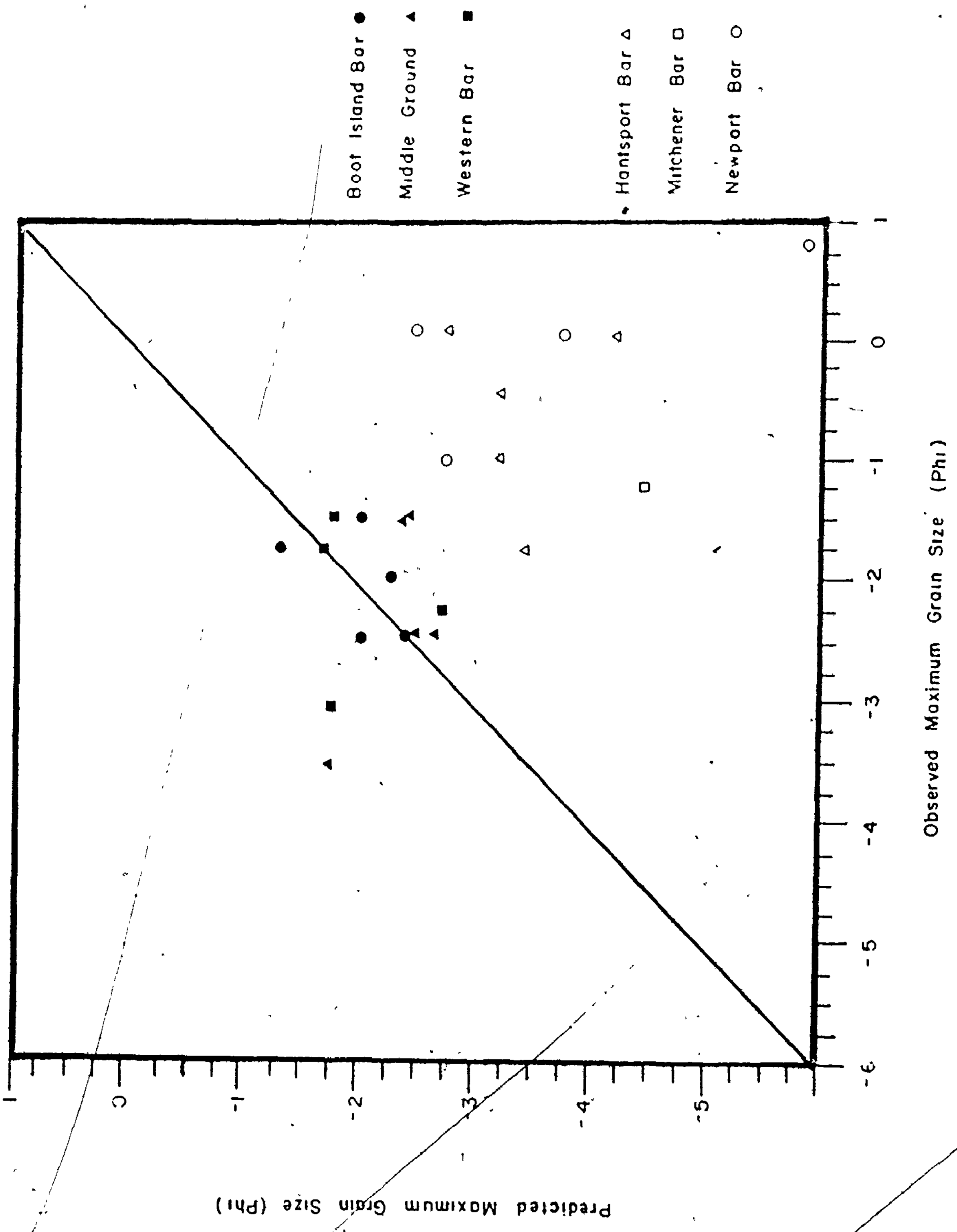
Boot Island Bar ●
Middle Ground ▲
Western Bar ■
Hantsport Bar △
Mitchener Bar □
Newport Bar ○
Observed Maximum Grain Size (Phi)
-6
-5
-4
-3
-2
-1
0
1
Predicted Maximum Grain Size (Phi)
1
0
-1
-2
-3
-4
-5

At the estuary head, the coarsest grain size present always is much finer than the coarsest size that could be transported by the local currents (Table 8-1). Thus, while the coarsest grain size present at each location at the estuary mouth appears to be controlled by hydraulics, near the estuary head the coarsest grain size present is not determined by the local hydraulic environment. The reason for this apparent discrepancy will be discussed later in this chapter.

Virtually all sediment on the surfaces of the intertidal sand bodies can be transported by their respective local hydraulic regimes. The relationships between hydraulics and cumulative curve shape and those between hydraulics and textural parameters will be examined separately in the following sections.

Cumulative Curve Shape

RELATION OF TRANSPORT MECHANISMS TO CUMULATIVE CURVES

Several authors have advanced the idea that each normally distributed grain population contributing to a cumulative curve is related to a depositional mechanism (Fuller, 1961; Moss, 1962, 1963, 1972; Spencer, 1963; Visher, 1969; Middleton, 1976); other workers believe that grain populations are a function of source material or mechanical breakage of original material (Shea, 1974). Visher (1969) has associated the coarse (C) population with surface creep or traction, the intermediate (A) population with saltation, and the fine (B) population with suspension. Middleton (1976) argues that since saltation is unimportant in water (Kalinske, 1943), the A population actually is transported by intermittent suspension rather than saltation; Francis (1973) verified experimentally that grains are transported by intermittent suspension.

If grain size populations reflect transport mechanisms, then each "break" in a cumulative curve should represent a transition from one mechanism to another. Middleton (1976) examined the break between populations C and A and was able to relate the break to a transition from traction to intermittent suspension transport for a number of modern rivers.

Hydraulic theory predicts that the coarsest sediment that can be suspended will have a settling velocity, w, that is approximately equal in magnitude to the root mean square of the vertical velocity fluctuations; the criterion for suspension is then

$$w = \sqrt{\bar{v}'} \qquad (8\text{-}1)$$

Since turbulent velocity fluctuations are difficult to measure, some workers have related the magnitude of $\sqrt{\bar{v}'}$ to the magnitude of the shear velocity U_*; Bagnold (1973) found the relationship

$$\sqrt{\bar{v}'} \,/\, U_* = 1.1 - 1.3 \qquad (8\text{-}2)$$

McQuivey (1973) found ratios up to 1.74 for small flume data and Bowden (1962) measured turbulence in tidal currents and found $\sqrt{\bar{v}'}$

to be 1.2 times as large as U_*. Middleton (1976) combined equations 8-1 and 8-2 to form a criterion for suspension of $w/U_* \simeq 1$; (8-3) this criterion has been verified experimentally by Francis (1973).

Since U_* is one of the hydraulic parameters that have been calculated for the measured velocity profiles (see Chapter 3), the relationship between the C - A break in a cumulative curve and the initiation of suspension could be tested for samples from the Avon River estuary; the C - A boundary is defined as the point of equal overlap between the C and A populations (see Chapter 6). For each current station the settling velocity of the grain size at the C - A population boundary of the appropriate sediment sample was taken from Graf and Acaroglu (1966). The settling velocity values first were compared to values of time-average U_*; time-average U_* values are too small to indicate suspension of the appropriate grain size.

If maximum U_* for each tidal cycle is compared to the appropriate w, w/U_* ratios fit the suspension criterion of equation 8-3 (Fig. 8-2). w/U_* ratios range between 0.38 and 1.70 with an average of 0.90; the average value of 0.90 is close to the criterion of $w/U_* = 0.8$ established by Engelund (1973). All w, maximum U_*, and w/U_* ratios are listed in Table 8-2.

Sediment transport rates calculated with Einstein's transport equations support the theory that the break between the C and A

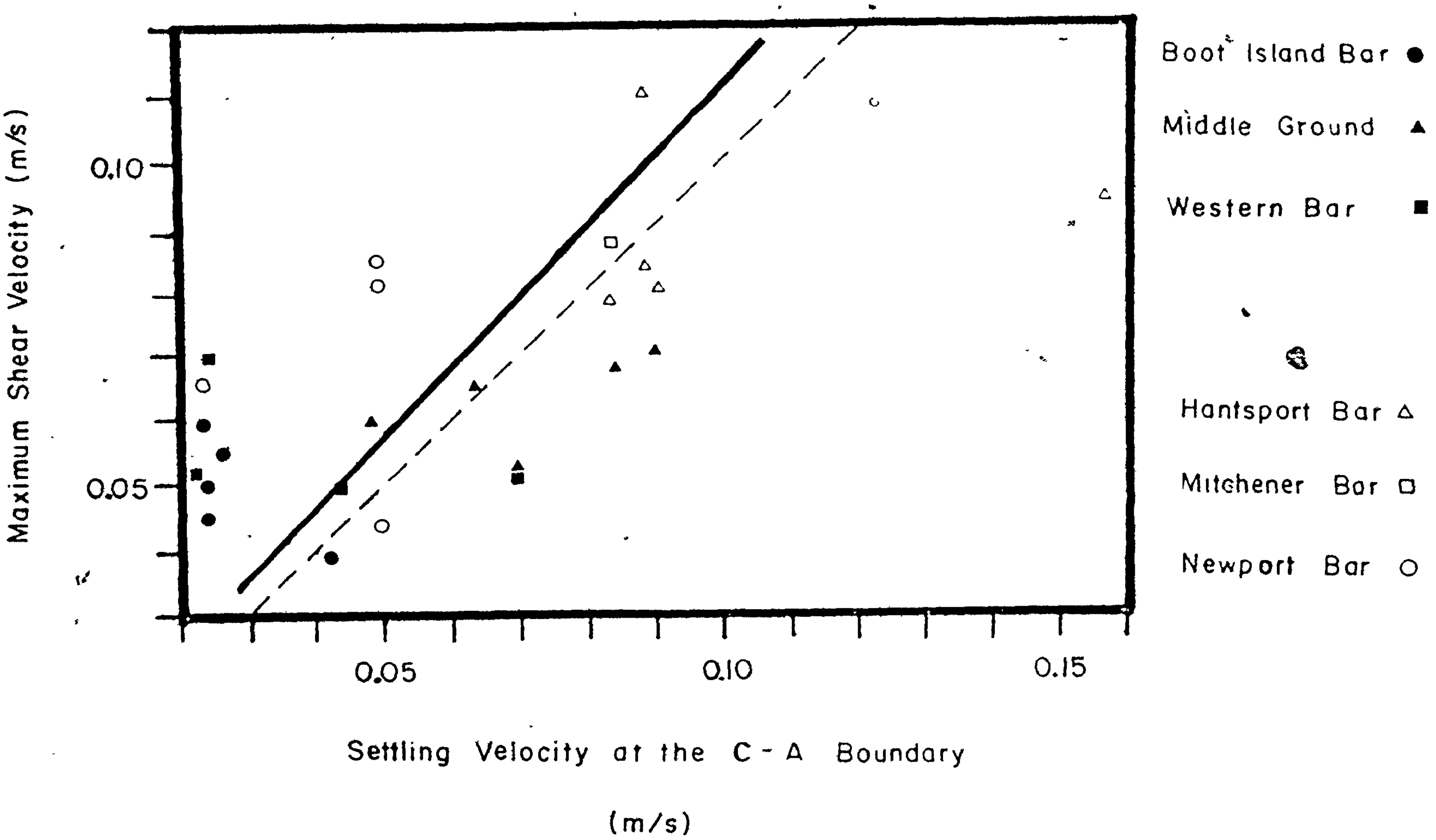

Fig. 8-2. Settling velocity at the C - A boundary versus maximum shear velocity. The dashed line is $U_* = w$; the solid line is the average w/U_* ratio of 0.9.

TABLE 8-2. Initiation of Intermittent Suspension

Station		Tidal Coeff.	C - A Break (phi)	w (cm /sec)	Max. Ū (cm /sec)	w/U	Susp. Ein. (phi)[1]
Boot Island	1	0.76	2.00	2.5	6.0	0.42	0.25
Bar	2	0.76	2.00	2.5	4.5	0.56	0.75
	3	0.79	2.20	2.7	5.6	0.48	1.25
	4	0.79	2.00	2.5	5.0	0.50	0.25
	5	0.62	1.70	4.2	4.0	1.05	0.25
Middle	1	0.65	1.40	4.8	6.0	0.80	1.25
Ground	2	0.65	0.70	9.2	7.0	1.31	0.75
	3	0.91	1.20	6.5	6.4	1.02	0.75
	4	0.76	0.90	8.5	6.8	1.25	0.75
	5	0.81	1.00	7.0	5.2	1.35	0.75
Western Bar	1	0.64	2.30	2.3	5.2	0.44	0.75
	2	0.64	1.00	7.0	5.2	1.35	0.25
	3	0.88	2.00	2.5	7.0	0.36	-0.25
	4	0.81	1.60	4.4	4.9	0.90	0.25
Hantsport Bar	1	0.77	0.70	9.2	8.0	1.15	0.25
	2	0.77	0.35	15.8	9.3	1.70	0.25
	3	0.77	0.90	8.5	7.8	1.09	0.75
	4	0.75	0.75	9.0	8.2	1.10	0.75
	5	0.81	0.75	9.0	11.0	0.82	0.75
Mitcherier Bar	1	0.88	0.90	8.5	8.6	0.99	0.75
Newport Bar	1	0.77	1.35	5.0	8.4	0.60	1.25
	2	0.72	1.25	6.0	4.3	1.40	1.25
	3	0.58	1.35	5.0	8.1	0.62	0.75
	4	0.70	2.00	2.5	6.6	0.38	1.75
					Mean	0.90	

---

[1] Susp. Ein. is the coarsest grain size transported by suspension as calculated by Einstein's transport formula.

populations represents the transition from traction to intermittent suspension transport on four of the six sand bodies. The coarsest grain size that Einstein's formula predicts will be suspended at a given station corresponds to the grain size at the C - A break in the appropriate cumulative curve for samples from Middle Ground, Newport Bar, Mitchener Bar, and Hantsport Bar (Fig. 8-3). Boot Island Bar and Western Bar do not fit the pattern established by the other sand bodies (Fig. 8-3); Einstein's formula predicts suspension at coarser grain sizes than those at which the C - A transition occurs (Table 8-2). The reason for this discrepancy is not apparent.

Thus, the break between cumulative curve populations C and A probably reflects a transition from traction to intermittent suspension transport. Also, examination of the coarsest sediment present and the relation of the C - A population boundary indicates that grain size distribution reflects maximum, rather than average, flow conditions.

The boundary between cumulative curve populations A and B has not been related to hydraulics; Einstein et al. (1940) contend that a gradual transition occurs from suspended bed material load (population A) to wash load (population B) and that population B is a function of sediment supply. However, since the C and A populations are related to sediment transport mechanisms, it seems probable that population

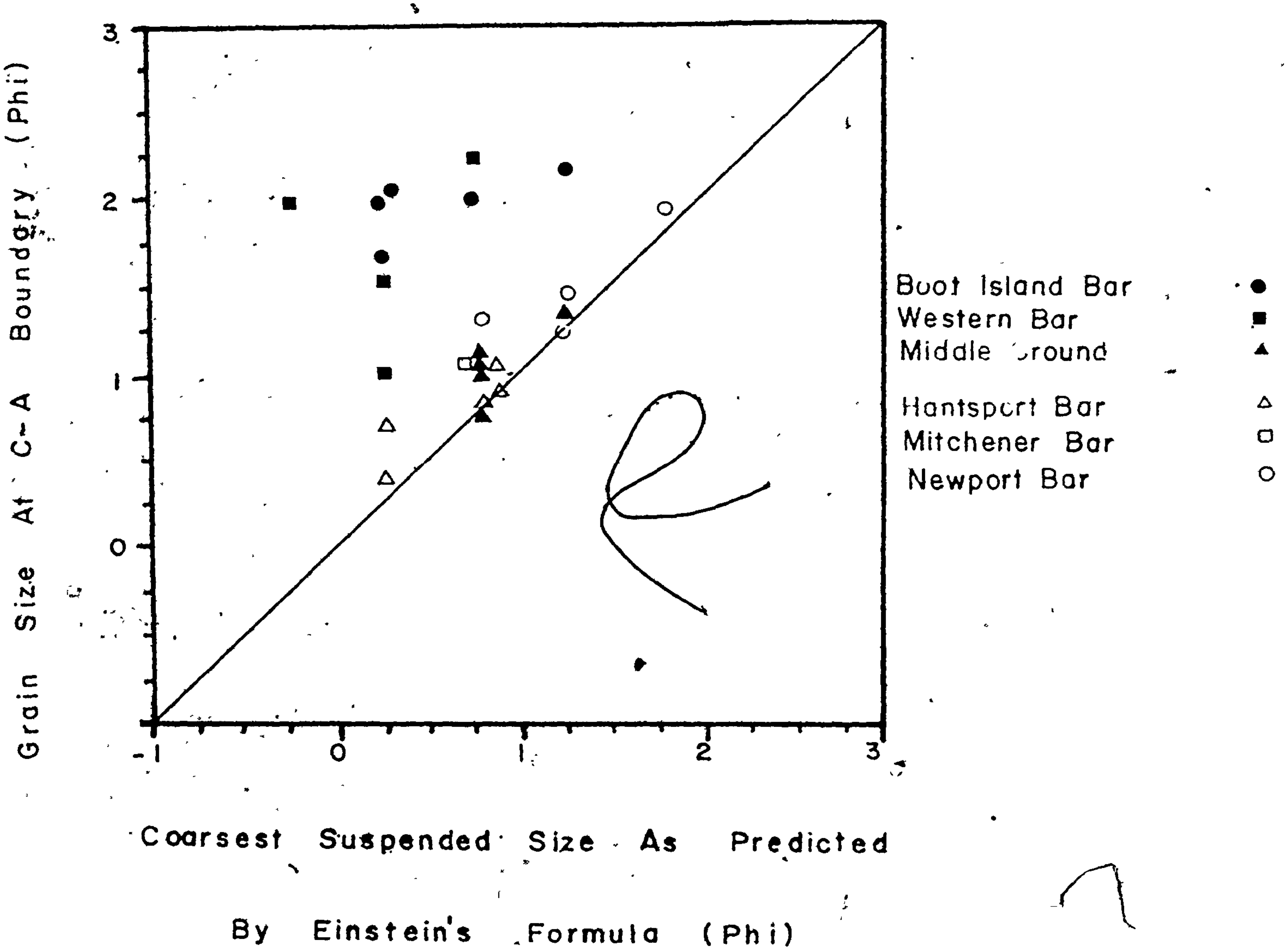

Fig. 8-3. Predicted coarsest suspended grain size versus grain size at the C - A boundary. The line of predicted = observed is plotted.

B also should be associated with a transport mechanism, as proposed by Visher (1969). Also, the results of this study suggest that population B can be related to hydraulics.

Grain size at the A - B break varies directly with maximum U_*. The A - B break occurs at coarser grain sizes at stations with higher maximum U_* values (Table 8-3); average grain size at the A - B break is 3.43 phi at the estuary mouth and 2.37 phi at the head. This suggests that population B is controlled by flow intensity; stronger flows are capable of suspending coarser sediment. Also, the ratio between maximum U_* at a station to settling velocity of the grain size at the A - B break is reasonably consistent (Table 8-3; Fig. 8-4). Hantsport Bar and Mitchener Bar deviate from this trend for no apparent reason. The ratio U_*/w has been calculated instead of w/U_* because of the small numbers yielded by w/U_*.

U_*/w ratios average 5.13 with a standard deviation of 2.40. The variation of U_*/w ratios listed in Table 8-3 reflects factors such as the statistical nature of turbulence and unequal tidal coefficients for the measured tidal cycles; however, the data suggest that a criterion for the transition from intermittent suspension to suspension transport is

$$U_*/w \simeq 5 \qquad (8\text{-}4)$$

TABLE 8-3. Criterion for Transition to Suspension

Station		Tidal Coeff.	A - B Break (phi)	w (cm /sec)	Max. U_* (cm /sec)	U_*/w
Boot Island	1	0.76	< 4.00	-	6.0	-
Bar	2	0.76	< 4.00	-	4.5	-
	3	0.79	3.60	0.5	5.6	11.20
	4	0.79	3.25	0.8	5.0	6.25
	5	0.62	< 4.00	-	4.0	-
Middle Ground	1	0.65	2.75	1.5	6.0	4.00
	2	0.65	< 4.00	-	7.0	-
	3	0.91	3.00	1.2	6.4	5.33
	4	0.76	2.60	1.7	6.8	4.00
	5	0.81	2.80	1.3	5.2	4.00
Western Bar	1	0.64	3.25	0.8	5.2	6.30
	2	0.64	3.30	0.8	5.2	6.50
	3	0.88	3.50	0.7	7.0	10.00
	4	0.81	< 4.00	-	4.9	-
Hantsport Bar	1	0.77	2.00	3.0	8.0	2.67
	2	0.77	1.87	3.6	9.3	2.60
	3	0.77	2.00	3.0	7.8	2.60
	4	0.75	2.80	1.3	8.2	6.31
	5	0.81	2.00	3.0	11.0	4.30
Mitchener Bar	1	0.88	2.00	3.0	8.6	2.87
Newport Bar	1	0.77	2.75	1.5	8.4	5.60
	2	0.72	2.65	1.7	4.3	2.53
	3	0.58	2.85	1.3	8.1	6.20
	4	0.70	2.75	1.5	6.5	4.30
					Mean	5.13

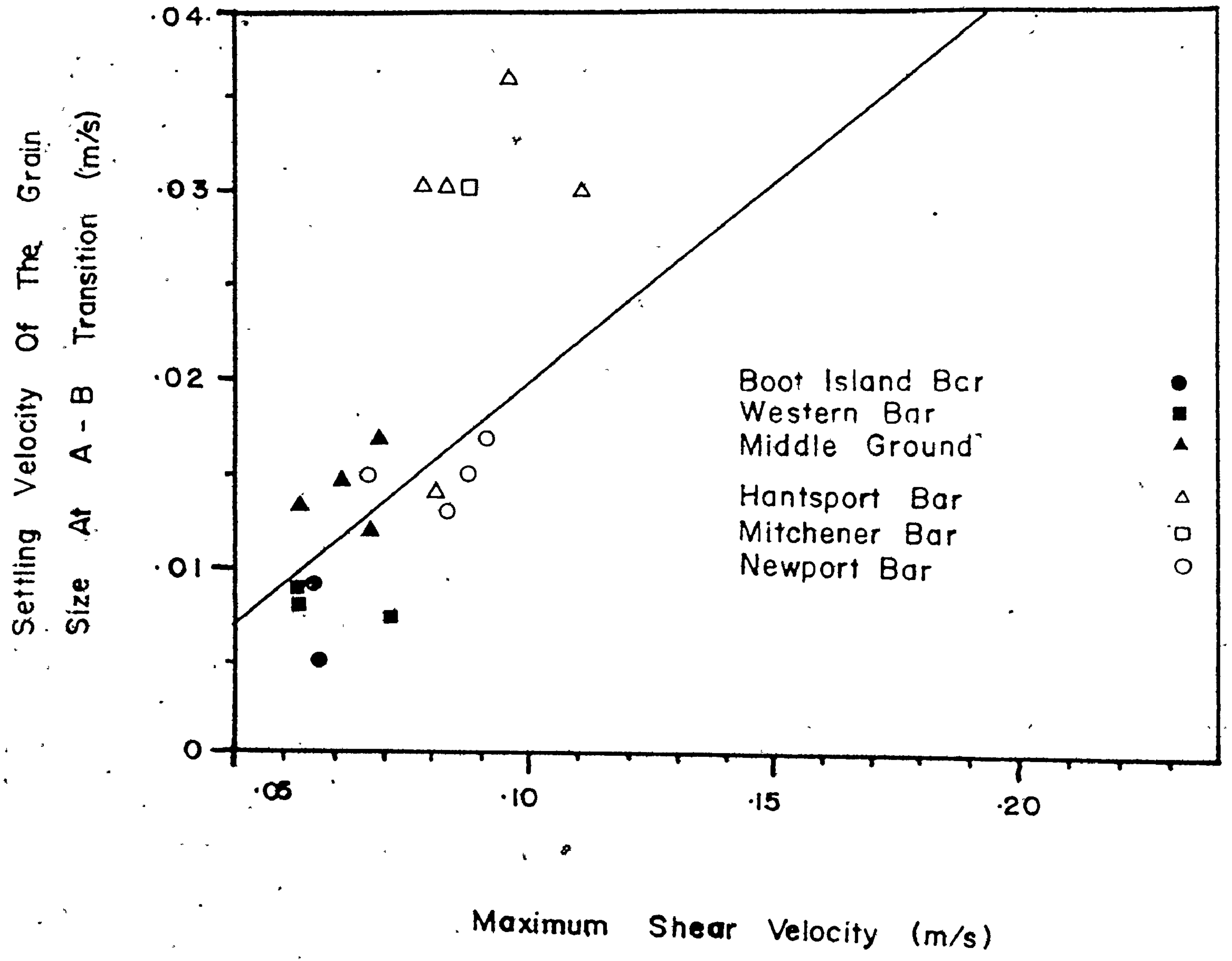

Fig. 8-4. Settling velocity at the A - B boundary versus maximum shear velocity. The average condition of $U_*/w = 5$ is plotted.

This is approximately 4.5 times higher than the $U_*/w = 1.11$ (the reciprocal of the mean w/U_* ratio) criterion for the initiation of intermittent suspension. Francis (1973) reports rapid change in transport mechanism with small changes in U_*/w ratios of similar magnitude; this supports the criterion for suspension in equation 8-4 as representing a real change from equation 8-3 and signifying a change in transport mechanism.

Relative transport rates of different grain size fractions calculated with Einstein's transport formula (see Chapter 7 and Appendix E) reveal trends that affect cumulative curve shape. As previously discussed, Einstein's formula predicts the initiation of sediment suspension at the C - A population boundary (Table 8-2); the rate of transport also increases dramatically as transport shifts from traction to intermittent suspension as expected in such a transition (Table 8-4). There is no corresponding rapid increase in transport rate at the A - B boundary.

HYDRAULIC SORTING: The relationship between cumulative curve shape and hydraulics, relative transport rates for different grain size fractions, and the results of cumulative curve analysis (see Chapter 6) suggest that hydraulic sorting is operating in the Avon River estuary. The observed head to mouth variation in cumulative curves can be explained by hydraulic sorting; the effect of hydraulic sorting on textural parameters will be discussed later in this chapter.

TABLE 8-4. Relative Transport Rates of Grain Size Fractions (kg/hr/% sample)

Station[1]	Load Type	-2.75	-2.25	-1.75	-1.25	-0.75	-0.25	0.25	0.75	1.25	1.75	2.25	2.75
		Grain Size (phi)											
Newport	Bed	0.00	0.00	0.00	0.00	0.00	0.00	0.17	0.26	0.14	0.13	0.71	1.63
Bar 2	Susp.	0.00	0.00	0.00	0.00	0.00	0.00	0.00	0.00	0.24•	0.63	18.7	369.9†
(-2.83)	Total	0.00	0.00	0.00	0.00	0.00	0.00	0.17	0.26	0.38	0.76	19.5	371.5
Mitchener	Bed	0.00	0.00	0.00	0.14	0.00	0.33	0.28	0.18	0.18	0.19	0.19	0.19
Bar 1	Susp.	0.00	0.00	0.00	0.00	0.00	0.00	0.00	0.34	0.76•	2.67	16.6†	120.4
(4.17)	Total	0.00	0.00	0.00	0.14	0.00	0.33	0.28	0.53	0.94	2.85	16.8	120.6
Hantsport	Bed	0.00	0.00	0.33	0.00	0.00	0.00	1.00	0.10	0.11	0.11	0.12	0.12
Bar 4	Susp.	0.00	0.00	0.00	0.00	0.00	0.00	0.00	0.15•	0.27	0.94	7.83	85.0†
(7.33)	Total	0.00	0.00	0.33	0.00	0.00	0.00	1.00	0.24	0.38	1.05	7.95	85.1
Middle	Bed	0.00	0.00	0.25	0.17	0.04	0.05	0.06	0.07	0.07	0.08	0.08	0.08
Ground 4	Susp.	0.00	0.00	0.00	0.00	0.00	0.00	0.00	0.05	0.09•	0.24	1.82	28.3†
(2.42)	Total	0.00	0.00	0.25	0.17	0.04	0.05	0.06	0.12	0.16	0.32	1.90	28.4
Boot Island	Bed	0.00	0.00	0.07	0.07	0.03	0.01	0.02	0.03	0.02	0.02	0.03	0.03
Bar 2	Susp.	0.00	0.00	0.00	0.00	0.00	0.00	0.00	0.01	0.01	0.02	0.09•	1.15*
(2.75)	Total	0.00	0.00	0.07	0.07	0.03	0.01	0.02	0.04	0.04	0.04	0.12	1.18
Western	Bed	0.00	0.00	0.05	0.01	0.01	0.03	0.04	0.05	0.06	0.06	0.06	0.06
Bar 2	Susp.	0.00	0.00	0.00	0.00	0.00	0.00	0.01	0.02	0.04•	0.08	0.36	4.97
(2.50)	Total	0.00	0.00	0.05	0.01	0.01	0.03	0.05	0.07	0.09	0.14	0.42	5.04

[1] For each station, transport rates for the profile with maximum shear velocity are listed; the time of the profile is in parentheses

C - A Transition •

A - B Transition †

* A - B Transition at 2.75 phi

Several lines of evidence point to hydraulic sorting of an original grain population at the estuary mouth as a result of different transport rates for different transport mechanisms and, therefore, different grain size populations. The process develops from the relatively coarse sediment at the estuary mouth (see Chapter 6) being subjected to a relatively low current regime (see Fig. 3-9) which prevents coarse sediment from being suspended.

Sediment transport paths near the central sand ridge appear to limit the penetration of coarse sediment into the Avon River. Intertidal sand waves exist on the northeast part of the central sand ridge and echo sounding records indicate that sand waves also are present in the subtidal to the west of the central sand ridge. Since sand waves are associated with coarse sediment (see Chapter 9), coarse sediment must extend into the Avon River as far as the central sand ridge; observations indicate that coarse sediment exists in the intertidal near the bedrock ledge north of Hantsport and on the intertidal sand waves at the northeast end of the central sand ridge. Thus, the limit of coarse sediment penetration into the Avon River must lie between the central sand ridge and Hantsport Bar.

Most coarse sediment is transported by traction; current velocities recorded in the flood channel west of the central sand ridge (station Horton South in Table B-1 and on Figure 3-9) cannot suspend sediment coarser than 0.75 phi and Einstein's transport equations indicate that suspension occurs at grain sizes finer than 0.25 phi (Table 8-5). Table 8-5 also indicates that grain size fractions that are transported exclusively by traction move at a much slower rate than grain fractions that travel mainly by suspension.

The width and position of the ebb channel south of Hantsport seems to prevent coarse sediment from reaching Hantsport Bar (Fig. 8-5); the channel is too wide for sediment moving by traction to cross before being entrained in the ebb transport system (Fig. 8-5). Table 8-5 indicates that traction load moves much more slowly than suspended load so that during each tidal stage the distance traveled by each grain is a function of transport mechanism.

Figure 8-5 illustrates how different transport rates for different transport mechanisms produce hydraulic sorting and limit the penetration of coarse sediment into the Avon River. The step length of distance traveled during a tidal stage is sufficiently different for traction and suspended transport that suspended sediment is able to cross the ebb channel while the traction load is not (Fig. 8-5). The crucial point in the transport path occurs where the ebb transport zone curves around the bedrock ledge and aligns with the river axis; sediment still in the ebb channel at this point cannot reach Hantsport Bar.

TABLE 8-5. Flood Sediment Transport Rates for Station Horton South (see Fig. 3-2) as calculated by Einstein's Formula; all rates are $m^3/10^4$ tidal cycles/ percent sample

Load Type	-2.75	-2.25	-1.75	-1.25	-0.75	-0.25	0.25	0.75	1.25	1.75	2.25	2.75
	Grain Size (phi)											
Bed	0.00	0.00	0.01	0.04	0.10	0.18	0.28	0.37	0.41	0.44	0.54	0.54
Susp.	0.00	0.00	0.00	0.00	0.03	0.08	0.16	0.31	0.61	2.23	24.89	390.84
Total	0.00	0.00	0.01	0.04	0.13	0.26	0.44	0.68	1.02	2.67	25.43	391.38
				mostly traction					mostly suspension			

Travel distances computed from the above transport rates for 0.3 m high bedforms ($m/10^4$ tidal cycles/% sample)

0.00	0.00	0.03	0.13	0.43	0.87	0.15	2.27	3.40	8.90	8.48	1300.00
		traction						suspension			

average traction = 0.87

average suspension = 350.00

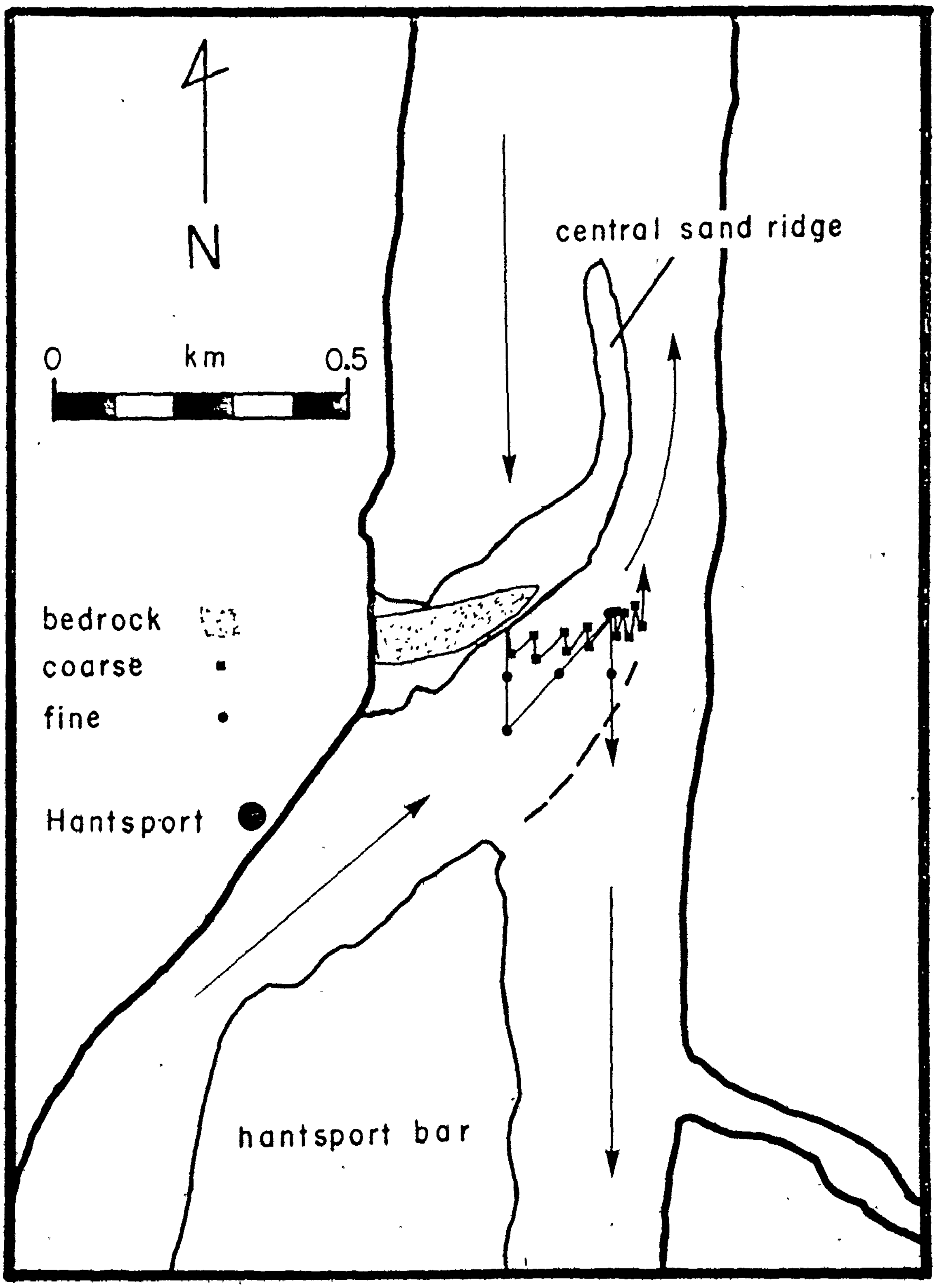
N
0
km
0.5
central sand ridge
bedrock
coarse ■
fine ●
Hantsport
hantsport bar

Fig. 8-5. Hydraulic sorting as a function of differential transport rates. For the fine (intermittent suspension) and coarse (traction) populations, arrow length is proportional to travel distance during a tidal cycle. Other arrows net transport directions; see the text for an explanation of the sorting process.

Since current velocities were not measured in the center of the ebb channel near Hantsport, it was assumed that the net distance traveled in the ebb channel is approximately 1.5 times greater than net flood travel distance on the western side of the central sand ridge; transport rates for the ebb channel were chosen to be typical of other stations near Hantsport Bar. Sediment transport rates presented in Table 8-5 were transformed into travel distances, also listed in Table 8-5, by calculating migration distance for bedforms with heights of 0.3 m; echo sounding records indicate that bedforms of this height exist in the ebb channel near Hantsport. Thus, penetration of coarse sediment into the Avon River is limited by hydraulic sorting caused by the positions of ebb and flood transport zones that are functions of local physiography and relative transport rate of traction and suspended grain populations; hydraulic sorting is not necessarily a general characteristic of macrotidal estuaries.

Figure 8-6 illustrates the different transport paths of coarse (traction) and fine (suspended) sediment in the Avon River estuary.

The process of hydraulic sorting plus hydraulic control of position of breaks in the curve explains many of the observed characteristics of cumulative curve shape. As discussed in Chapter 6, sediment near the estuary head is deficient in grains coarser than 1.5 phi. Hydraulic sorting accounts for the lack of coarse grains near the estuary head; grains coarser than 1.5 phi are transported slowly by traction and cannot penetrate to the estuary head.

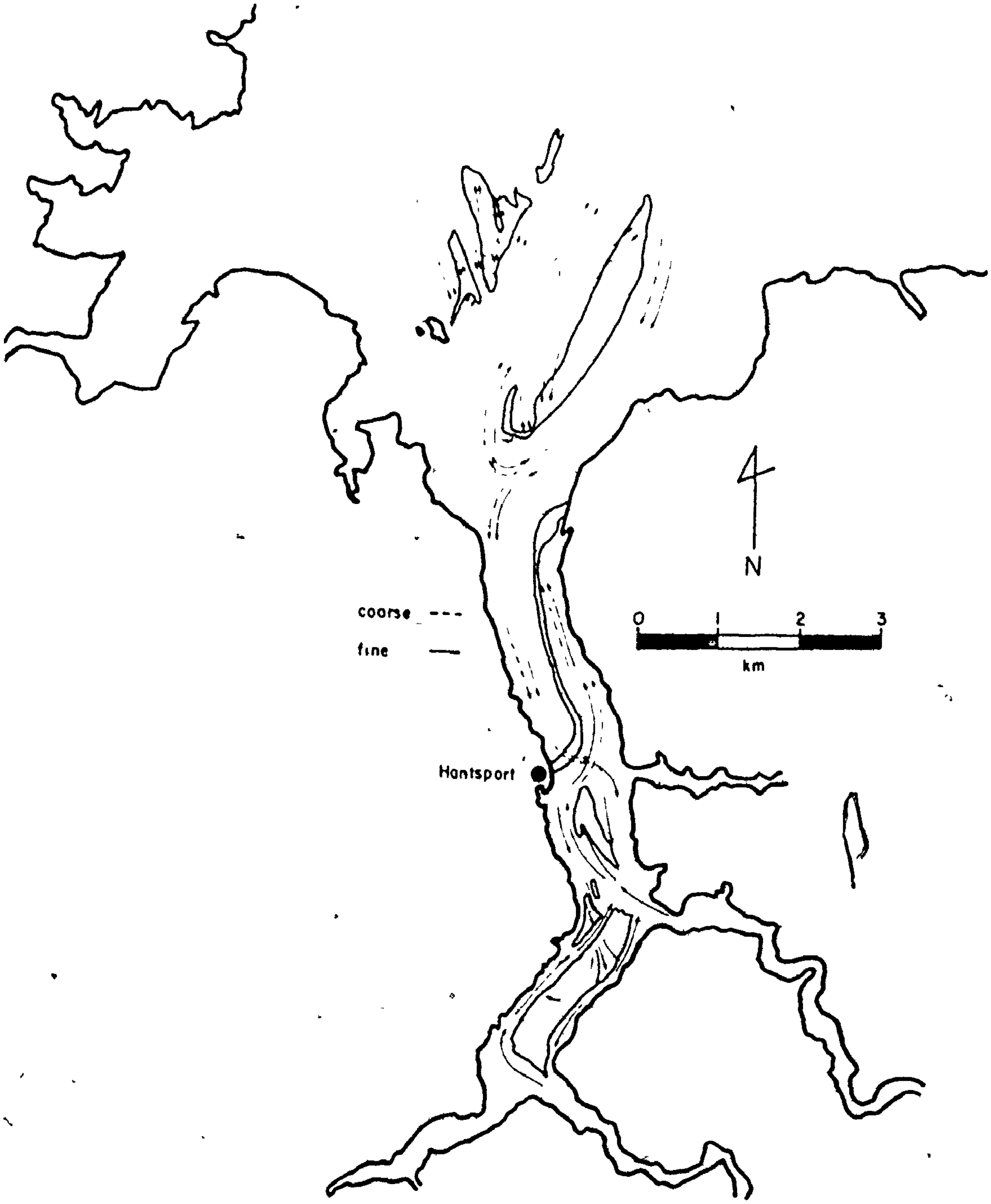
coarse
fine
N
0
1
2
3
km
Hantsport

Fig. 8-6. Transport paths of different grain size fractions. The coarse fraction is transported by traction and the fine is transported by intermittent suspension.

Exclusion of coarse material from the estuary head by hydraulic sorting also explains the apparent discrepancy between critical shear stress and the largest grain size present at the estuary head. At the estuary mouth, the largest grain size present always is close to the competence of the flow as predicted by Shields' criterion; the same should occur at the estuary head. As previously discussed, the coarsest sediment present near the estuary head is much finer than the theoretical competence of the flow; hydraulic sorting accounts for this discrepancy by preventing coarse sediment from reaching the estuary head.

Thus the difference in proportion of population C from the estuary mouth to the head is largely a function of hydraulic sorting; the hydraulic regime of each area also affects the proportions of each grain size population. Both the C - A and A - B boundaries occur at coarser grain sizes at the estuary head than at the mouth as a result of the stronger hydraulic regime at the estuary head. Thus the large B population at the estuary head (see Chapter 6) is a result of the higher concentration of suspended material produced by increased resuspension as a result of shallowing and increased flow strength, and the small B population at the estuary mouth is a result of the relatively weak hydraulic regime. The proportion of population A does not vary dramatically with location (see Chapter 6); its exact proportion and grain size range are governed by hydraulic regime throughout the study area.

Textural Parameters

GENERAL TRENDS: Textural parameter values can be interpreted in light of hydraulic sorting. Normally, mean grain size is expected to be coarser in regions with strong currents and finer in areas with relatively weak currents; the reverse is true in the Avon River estuary (see Figs. 3-9, 6-2 and 6-6). Separation of the original grain size population at the estuary mouth by hydraulic sorting causes the inverse relationship between mean grain size and current strength. The previously discussed deficiency of coarse sediment at the estuary head is expressed as finer mean grain sizes by textural analysis. Mean grain sizes at the estuary mouth are representative of the local current regime as there are no grain size deficiencies and on the sand bodies there is virtually no coarse "lag" that cannot be transported.

Grain size sorting also can be related to hydraulic sorting. As illustrated in Figures 6-3 and 6-7, sediment tends to be better sorted at the head of the estuary than at the mouth. Inman (1949) used hydraulic theory to explain the general tendency for fine sand to be better sorted than finer or coarser material. As sediment in the intermittent suspension population moves further from its source, in this case from the estuary mouth to the head, it should become more poorly sorted rather than better sorted (Inman, 1949). In addition, elimination of coarse sediment input into the estuary head by hydraulic sorting reduces the range of grain sizes present which, in turn, causes better sorting at the estuary head than at the mouth.

Thus, in the Avon River estuary, textural parameters are not always indicative of the strength of the hydraulic regime; textures at the estuary mouth do reflect current strength but textures at the estuary head do not. It is beyond the scope of this thesis to investigate the relationship between current strength and textural parameters in other sedimentary environments or to apply this relationship to ancient sediments; however, it appears that the statistical parameters commonly used to describe texture do not necessarily reflect hydraulic regime and that interpretation of paleo-hydraulics from textural parameters is not simple. In this study, cumulative curve characteristics are more useful than statistical parameters for interpreting hydraulic environment.

TRENDS IN MEAN GRAIN SIZE ON A SAND BODY SURFACE: As discussed in Chapter 6, three of the six major intertidal sand bodies, Middle Ground, Hantsport Bar, and Boot Island Bar, have distinct trends in mean grain size. These trends can be explained by local hydraulic environment and physiography.

Middle Ground: Mean grain size on Middle Ground grades from very fine sand near the sand body center to medium sand at either end (see Fig. 6-2); the trend reflects local physiography and its effect on hydraulic regime. Seismic investigations of Minas Basin conducted by Bedford Institute of Oceanography reveal block-faulted bedrock at the core of Middle Ground (C. Amos, 1976, pers. comm.); the sand body center is underlain by bedrock but the ends are not. Bedrock extends vertically to approximately 2 m below the sediment surface. (The effect of the bedrock on formation and stability of Middle Ground is discussed in Chapter 10.)

The bedrock core of Middle Ground is responsible for the region of fine sediment near the sand body center. Since the bedrock extends vertically almost to the half-tide mark, the bedrock surface is not subjected to peak velocities during either the flood or ebb tidal stage as peak velocities occur at lower water levels (see Fig. 3-7 and the discussion of hypsometry in Chapter 3). Relatively weak currents over the bedrock surface allow deposition of relatively fine sediment.

Hantsport Bar: The gradation from fine sand at the north to medium sand at the south end of Hantsport Bar (see Fig. 6-6) also is a function of local hydraulic conditions resulting from phhsiography. The tidal prism of the Kennetcook River and size and position of ebb and flood areas alter local hydraulics. Near the south end of Hantsport Bar the large ebb dominant tidal prism of the Kennetcook River causes swift ebb currents on the southwestern edge of Hantsport Bar (see Fig. 3-9). The flood channel to the east of Hantsport Bar decreases in width from north to south (see Fig. 7-7); decrease in area increases current velocities towards the south. Relatively strong currents over both ebb and flood zones at the southern end of the sand body cause deposition of comparatively coarse sediment.

Towards the north end of Hantsport Bar the flood channel to the east of the sand body is relatively wide, so that currents are slower, and finer sediment is deposited in the flood zone (see Figs. 6-6 and 7-7). On the ebb side of Hantsport Bar, the expanding jet of the Kennetcook River ebb tidal prism decreases in velocity as it proceeds north so that mean grain size decreases in the same direction. The large ebb area at the north end of Hantsport Bar results from a widening of the ebb dominant zone (see Fig. 7-7); the lowest maximum currents recorded near Hantsport Bar were measured over this region and mean grain size also is finest in this area (see Figs. 3-9 and 6-6).

Boot Island Bar: The gradation from fine sand at the northern end to coarse sand at the southern end of Boot Island Bar is a result of local hydraulics; again, the cause of the local current regime probably is physiography. It appears that maximum U_* increases from north to south on Boot Island Bar; Boot Island Bar stations 3 and 4 were sampled during the same tidal cycle and follow such a pattern (see Fig. 3-9). However, Boot Island Bar station 5, located near the southern end of the sand body, has a very low maximum U_*; the extremely low tidal coefficient (0.62) for [illegible] measured tidal cycle may account for this apparent anomaly. Since mean grain size at the estuary mouth is directly related to current strength, the southern end of Boot Island Bar probably conforms to the trend; thus the north - south increase in mean grain size probably is due to increasing maximum current velocity from north to south.

North to south increase in current velocity on Boot Island Bar probably results from constriction of flood currents by Boot Island. Southwest flowing flood currents are confined between the main ebb channel to the east and Boot Island to the south (see Fig. 7-6); the reduced cross-sectional area of the flood zone results in higher current velocities and, consequently, in coarser sediments from north to south.

Summary

Grain size distribution in the Avon River estuary can be explained by hydraulic processes; sediment size parameters tend to reflect maximum current velocities rather than average flow conditions. Each segment of a cumulative curve is the expression of a different sediment transport mechanism; the C population stems from traction, the A population from intermittent suspension, and the B population from suspension.

The A - B population boundary occurs at the grain size whose settling velocity is approximately equal to 1/5 of the magnitude of the maximum shear velocity at each location. The C - A boundary reflects the hydraulic condition that settling velocity nearly equals maximum shear velocity. At the estuary mouth, the coarsest grain size present corresponds to the competence of the maximum shear velocity as predicted by Shields' criterion; at the estuary head, the same criterion predicts the occurrence of much coarser grains than actually are present.

Hydraulic sorting causes the observed grain size difference between the estuary head and mouth, and creates a deficiency of coarse sediment at the estuary head. The intermittent suspension and suspension populations at the estuary mouth are transported into the head of the Avon River estuary while the traction population remains at the estuary mouth. The observed inverse relationship between hydraulics and textural parameters also is a function of hydraulic sorting. Textural parameters at the estuary mouth reflect hydraulic conditions while at the estuary head mean grain size is much finer than expected; hydraulic sorting limits the penetration of coarse sediment into the Avon River. Textural trends on individual sand bodies result from local flow conditions caused by physiography.

CHAPTER 9

BEDFORM STABILITY

Bedform distribution in the Avon River estuary (see Chapter 5) is a function of variation of hydraulic conditions and sediment distribution; bedforms are a response to local hydraulics and grain size. Approximate hydraulic and sedimentologic limits can be determined for each bedform type by relating observed combinations of hydraulics, grain size, and bedform type to established bedform classifications.

Bedform Classifications

In the following discussion, the terminology that describes bed geometry has been adopted from Southard (1975); a bedform is regarded as an individual element of the bed geometry and a bed configuration is the overall bed geometry.

Many authors have discussed the concept of flow regime in relation to bedform hierarchy; that is, the sequence of bed configurations expected as flow power increases; some bed configuration hierarchies are based on field observation (Harms and Fahnestock, 1965; Boothroyd, 1969; Coleman, 1969; Boothroyd and Hubbard, 1975), others have been derived experimentally (Simons and Richardson, 1961, 1971; Simons et al., 1965a; Bogardi, 1961; Harms, 1969; Mercer, 1971; Southard, 1971, 1975; Southard and Boguchwal, 1973). Generally, bed configuration hierarchies described from field data correspond to sequences generated in flume experiments although large bedforms found in nature cannot be produced experimentally. A typical bed configuration sequence is: plane bed → ripples → dunes → plane bed (movement) → antidunes (flow strength increases from left to right). The relationship of this sequence to bed configurations in the Avon River estuary will be discussed later in this chapter.

Bed configuration stability fields that have been derived experimentally define limits of each type of bed configuration plotting two or more hydraulic and/or sedimentologic parameters against each other. Application of experimental schemes to field conditions, particularly macrotidal conditions, is limited by several factors. Virtually all bed configuration stability fields have been derived for steady flow conditions; tidal environments have unsteady flow conditions and small changes in flow strength can cause large changes in bed configuration (Simons and Richardson, 1962). Allen (1973), Karcz (1972), and Southard (1971) question the accuracy with which experimentally derived bed configuration stability fields can duplicate natural systems.

Two major application problems arise because of unsteady flow in tidal environments. Unsteady flow conditions create the problem of bedform response to changing flow. In natural systems, bedforms lag behind changes in flow strength (Allen et al., 1969; Kachel and Sternberg, 1971; Allen, 1974; Allen and Friend, 1976a). Allen and Friend (1976b) derived an equation for minimum bedform response time to flow changes; not surprisingly, their results indicate that response time is less for smaller bedforms. The main questions are: do bed configurations observed at low tide exist for the complete tidal cycle, and under what flow conditions do the observed bed configurations form? These questions will be discussed later in this chapter.

One of the more commonly used bedform classification schemes was derived by Southard (1971); three-dimensional stability fields are constructed by plotting water depth versus mean current velocity versus median grain size. The data are displayed on two graphs: one is mean grain size versus current speed and the other is current speed versus water depth. Because of the large water depth and current speed fluctuations in a macrotidal environment, it is necessary to plot flow conditions that create the observed, stable bed configuration. Plotting current speed versus water depth through a tidal cycle indicates that observed bedform is a function of near-maximum current speeds, and that near-maximum conditions persist for much of the tidal cycle (Fig. 9-1).

Plots of current speed versus water depth and mean grain size versus current speed were constructed using maximum current speed and the water depth associated with that speed (Fig. 9-2). Ripples, megaripples, and sand waves each plot in a separate field; rippled sand waves can be distinguished from megarippled sand waves on Fig. 9-2B but there is no separation on Figure 9-2A. The significance of the apparently anomalous point, N1, will be discussed later in this chapter. The bedform stability fields of the present study correspond to experimentally derived fields of Southard (1975) and Costello (1974) and the fields established by Dalrymple (1977) for Cobequid Bay bedforms (Fig. 9-2).

Klein and Whaley (1972) separated sand waves from megaripples in Minas Basin using Southard's (1971) method by plotting current speed and water depth during times of bedform migration. Based on data of Klein (1970), they assumed that sand waves migrated only during flood flow and megaripples only during ebb. Migration was assumed to be occurring when boils were present on the water surface. Their results indicate that sand waves and megaripples are stable at similar flow strengths but sand waves migrate at shallower water depths (Klein and Whaley, 1972).

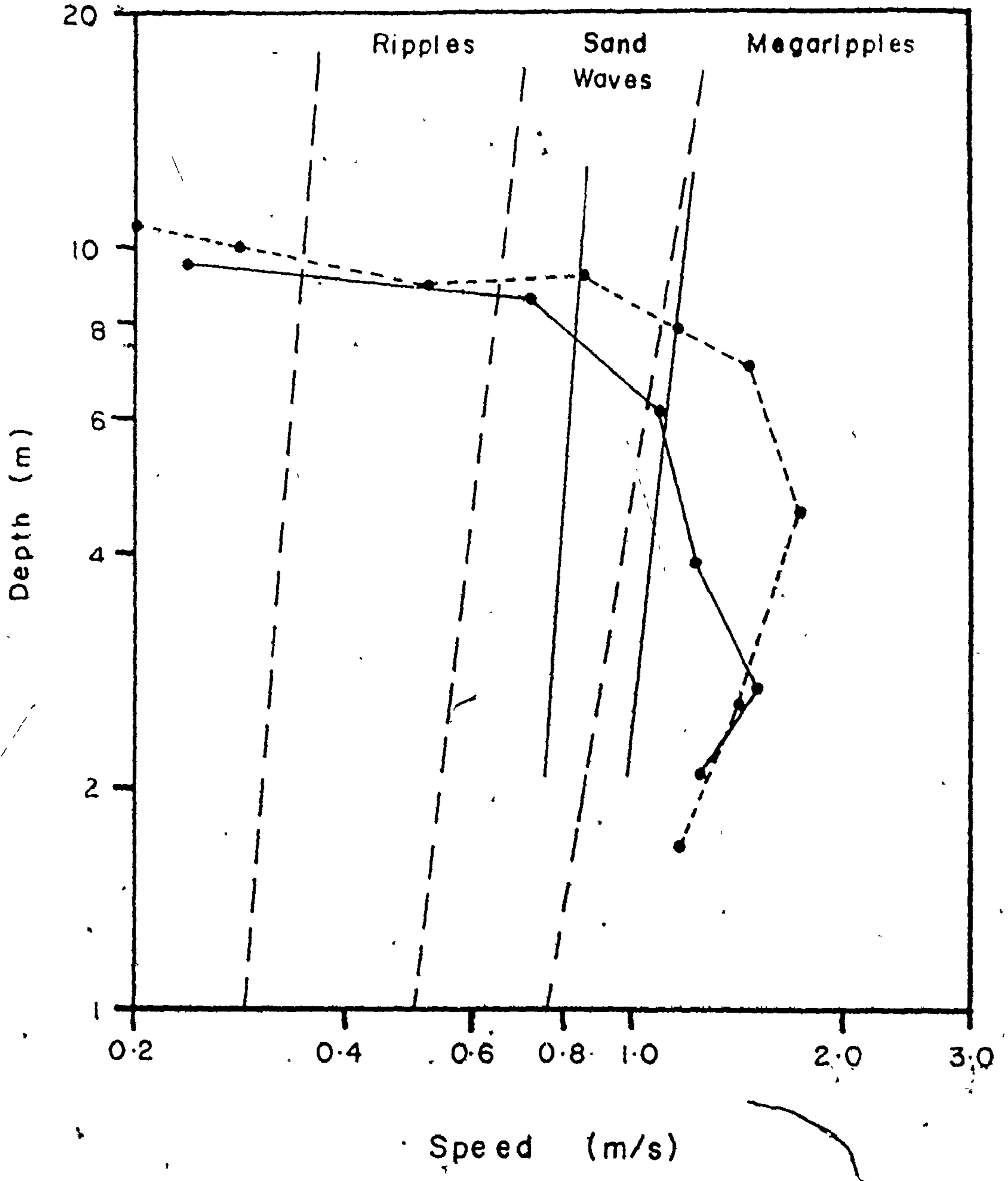

Fig. 9-1. Relation of observed bedform to water depth and current speed through a tidal cycle. The dashed field boundaries were extrapolated from Costello (1974); the solid field boundaries are from Dalrymple (1977). Each data point represents measured current speed and water depth at one time during a tidal cycle; data was collected at half hour intervals. A solid line connects ebb current points, and a dashed line connects flood current points. The observed bed configuration was flood dominant megaripples.

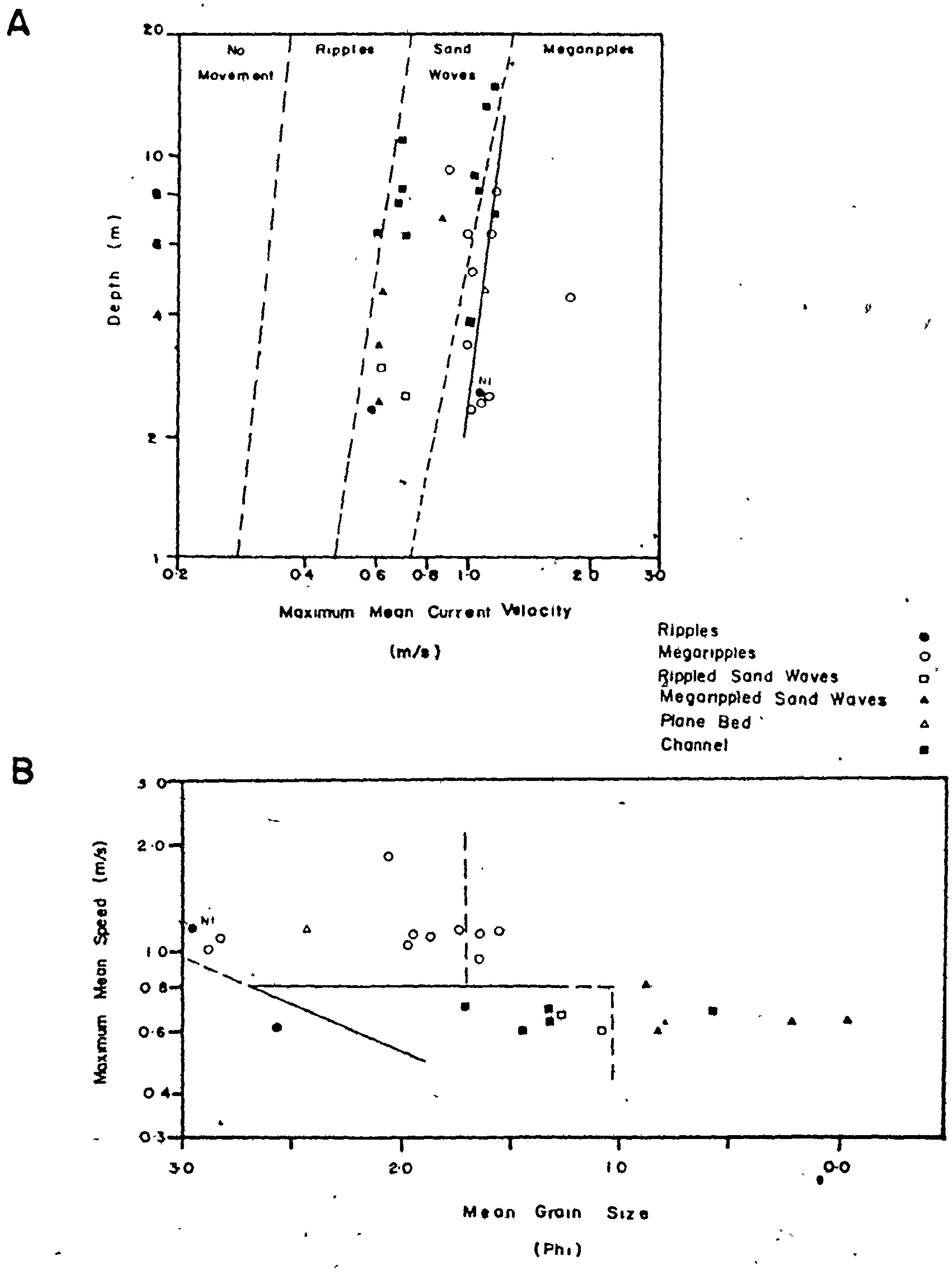

Fig. 9-2. Observed bedform as a function of A) maximum current velocity and water depth and B) current speed and mean grain size. In part A, dashed field boundaries were extrapolated from Costello (1974); solid field boundaries are from Dalrymple (1977). In part B, solid field boundaries are from Southard (1971); dashed field boundaries are from Dalrymple (1977). "Channel" indicates that the bed is subtidal so that bed configuration could not be observed.

The results of the present study disagree with those of Klein and Whaley (1972) (Fig. 9-2). Sand waves and megaripples occupy different regions on a plot of current speed versus water depth, but it is current speed rather than water depth that forms the boundary between the stability fields (Fig. 9-2A). Klein and Whaley's assumption that each bedform type migrates in one direction only is not valid for the Avon River estuary (see the discussion of bedform reversal in Chapter 7). Many sand waves in the Avon River estuary have megaripples superimposed on them, and it is the migration of these megaripples that causes migration of the sand waves (see Chapter 5); thus flow depths are identical for the two bedforms. Also, Klein and Whaley's (1972) results disagree with the experimentally derived stability fields of Costello (1974).

Observed bed configuration was plotted on a graph of average maximum shear velocity (see Chapter 3) versus mean grain size (Fig. 9-3). Again, ripples, rippled sand waves, megarippled sand waves, and megaripples each occupy a separate field; ripples and megaripples lie within the experimentally derived ripple and megaripple regions of Vanoni (1974).

Simons and Richardson's (1961, 1971) bedform classification based on plotting stream power versus median grain size is shown in Figure 9-4; observed bed configuration is plotted on the graph. Average

Fig. 9-3. Observed bedform as a function of maximum shear velocity and mean grain size. The solid and dashed field boundaries separating ripples, dunes, and plane bed are from Vanoni (1974). The line separating ripples from no movement is based on Shields' criterion and the line separating traction and suspension is a plot of shear velocity equal to settling velocity. The dashed line separating dunes and sand waves is based on data from the Avon River estuary and on data from Dalrymple (1977) for Cobequid Bay.

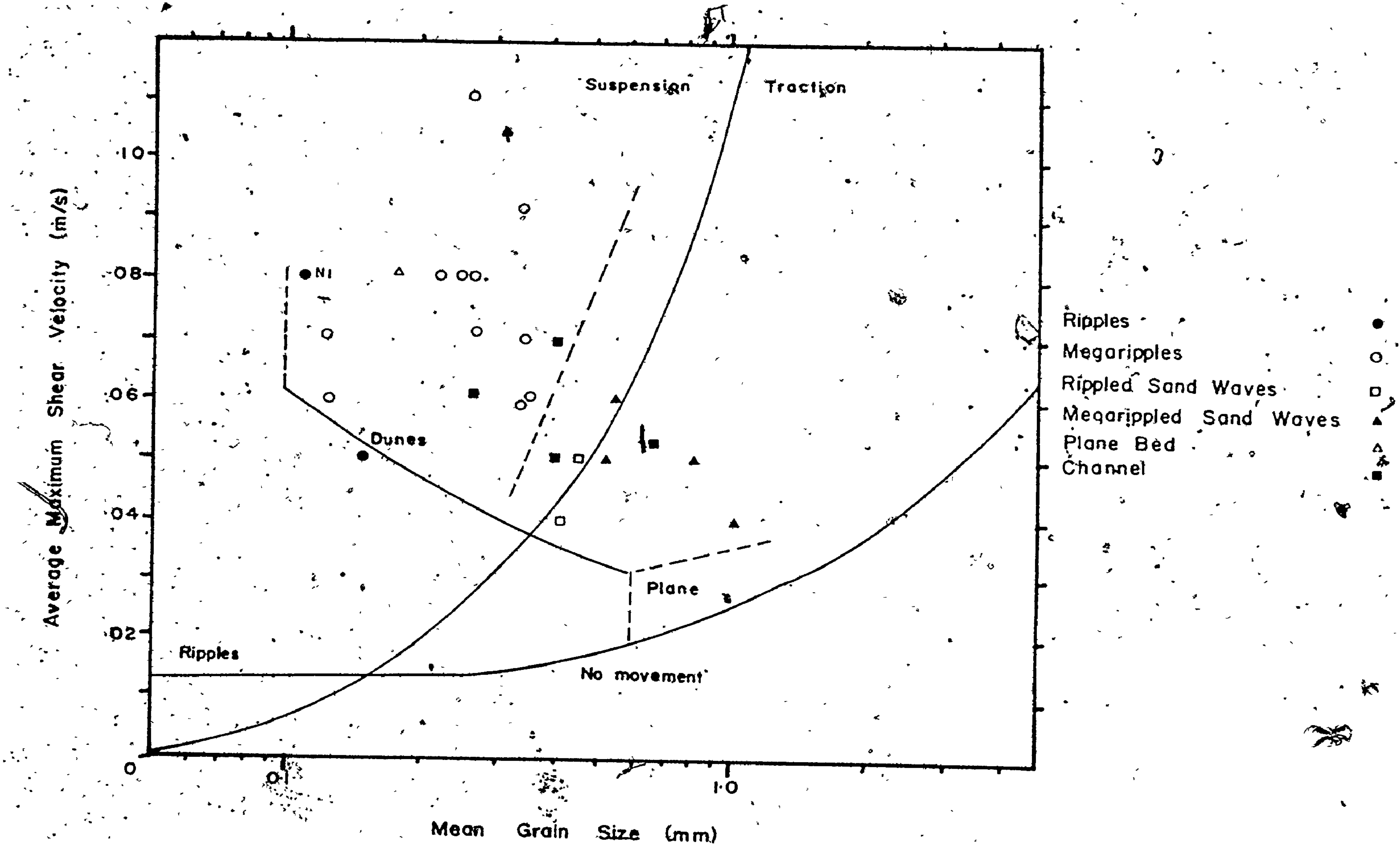
Average Maximum Shear Velocity (m/s)
·10
·08
·06
·04
·02
0
0·1
1·0
Mean Grain Size (mm)
Suspension
Traction
Dunes
Plane
Ripples
No movement
N1
Ripples ●
Megaripples ○
Rippled Sand Waves □
Megarippled Sand Waves ▲
Plane Bed △
Channel ■

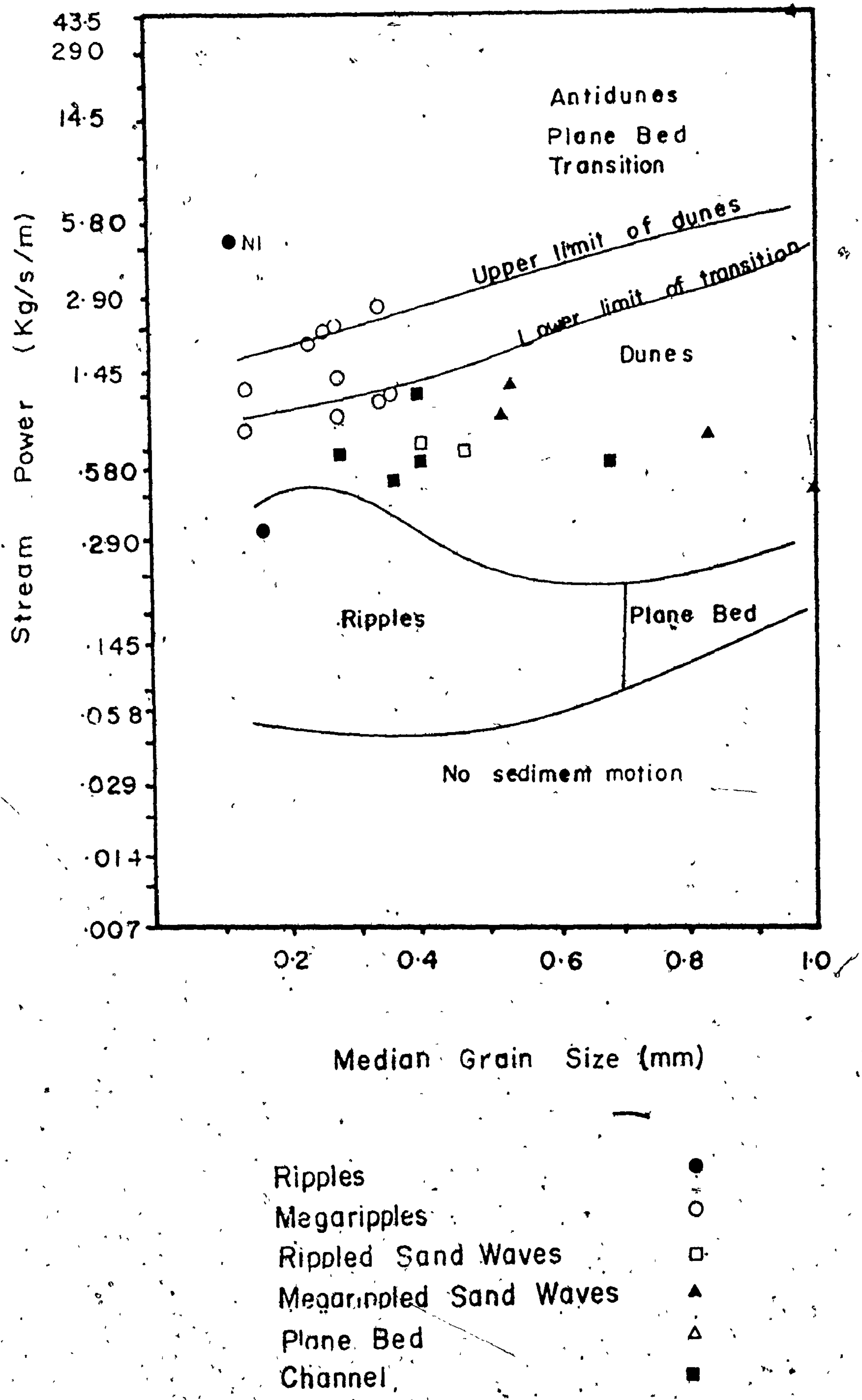

Fig. 9-4. Bedforms as a function of stream power and median grain size.

maximum stream power (see Chapter 3) was used as bedforms reflect near-maximum flow conditions (Fig. 9-1). Figure 9-4 was taken from Allen (1968); stream power and median grain size values on the axes and stability field boundaries are those that were derived experimentally by Simons and Richardson (1961) and modified by Allen (1968).

Most of the Avon River estuary data fit the bedform stability regions of Allen (1968) (Fig. 9-4). As expected, ripples and megaripples fit the categories of ripples and dunes respectively, and areas with plane bed fall into the dunes respectively, and areas with plane bed fall into the transition zone; the apparently anomalous rippled point, N1, reflects an observed bed configuration that is not in equilibrium with flow conditions. The significance of point N1 will be discussed later in this chapter.

Sand waves cannot be distinguished from megaripples in terms of stream power, but the tendency for sand waves to be coarser than megaripples (see Chapter 6) causes separation of the two bedform types within the dune stability field (Fig. 9-4); the stability field of sand waves as opposed to that of megaripples also will be discussed later in this chapter. Klein and Whaley (1972) tried to separate Minas Basin sand waves from megaripples with a plot of stream power versus median grain size but were unsuccessful probably as a result of their assumption about migration time of sand waves versus megaripples. They also found that stream power values of megaripples and sand waves overlapped and were within the ripple and dune fields of Figure 9-4. The dunes and megaripples that they studied had nearly identical mean grain sizes so that no grouping of each bedform type occurred.

Athaullah (1968) separated upper flow regime, transitional, and lower flow regime bedforms by plotting Froude number against the ratio of water depth to median grain size. Most data points from the Avon River estuary are beyond his experimental range (Fig. 9-5); extrapolation of his flow regime boundaries do not yield good separation of bed configurations (Fig. 9-5).

There is not a good separation of lower flow regime and transitional bed configurations; the only station with plane bed, plotted as point N1 (see the discussion later in this chapter), lies in the appropriate region, but so do several megarippled stations (Fig. 9-5). However, Athaullah's trend of flow regime transition occurring at progressively lower Froude numbers as D/d_{50} increases appears to be applicable to the Avon River estuary as a transitional bed configuration forms at a Froude number of 0.23 (Fig. 9-5).

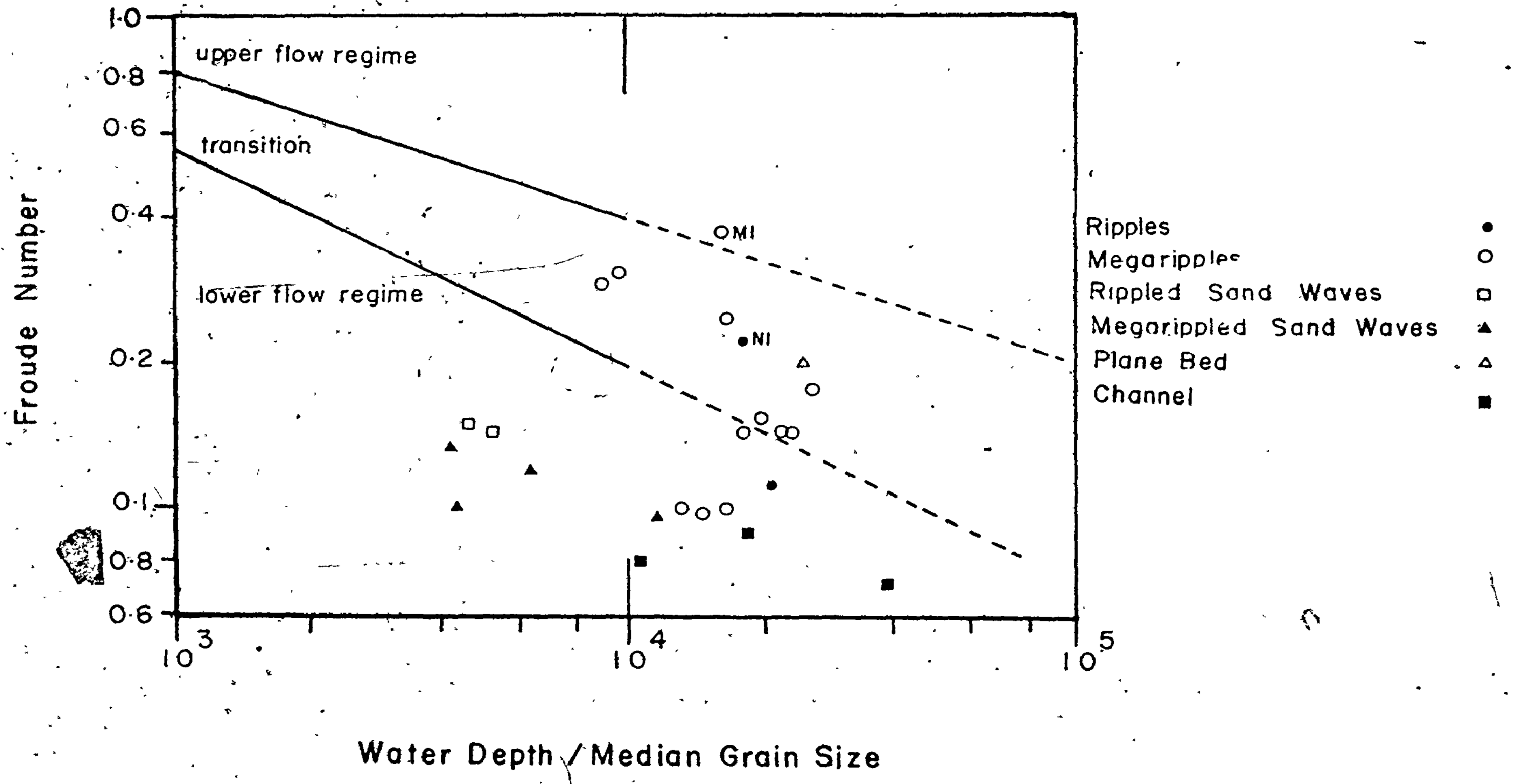

Fig. 9-5. Froude number versus water depth/median grain size as a criterion for bedform stability fields. Stability fields are from Athaullah (1968); Beyond 10^4 on the x axis they have been extrapolated.

Of the three approaches to bedform classification presented in Figures 9-2 to 9-4, the approach of Southard (1971, 1975) (Fig. 9-2) appears to work best. Observed bed configurations fall into distinct stability fields that agree with experimentally derived classifications (Costello, 1974; Southward, 1975) and with classifications based on field observations (Boothroyd and Hubbard, 1975; Dalrymple, 1977; Knight, 1977). Simons and Richardson's (1971) method (Fig. 9-4) separates ripples, transitional, and upper flow regime features from larger bedforms but does not differentiate megaripples and sand waves in terms of flow strength.

Stability Limits of each Bedform Type

Stability fields can be constructed based on the fields displayed on Figures 9-2 to 9-4 and on other hydraulic and sedimentologic data. Absolute boundary conditions cannot be determined for most bedforms; but relative limits and bedform sequences can be established; stability range for each bed configuration is discussed below.

RIPPLES: Ripples are the products of relatively low flow strengths and relatively fine grain sizes. Ripple distribution at the estuary mouth (see Fig. 5-4) reveals that maximum current velocities are low (see Fig. 3-9) and mean grain sizes are fine (see Fig. 6-2) in these areas. Figures 9-2 to 9-4 all indicate that ripples are stable under conditions of low flow strength and fine mean grain size.

Ripples at the estuary head do not fit the low flow strength criterion; both Newport Bar and Mitchener Bar are high current velocity areas (see Fig. 3-9) with fine mean grain sizes (see Fig. 6-6). This apparent discrepancy can be resolved by examination of ripple form and internal structures on Mitchener Bar and Newport Bar as well as consideration of point Nl on Figures 9-2 to 9-4.

As discussed in Chapter 5, ripples on Newport Bar and Mitchener Bar tend to be straight-crested or sinuous rather than linguoid like those at the estuary mouth. Allen (1969) relates degree of crest sinuosity to flow duration; straight-crested and sinuous ripples are produced by shorter duration flows than are linguoid forms. Thus, ripples on Newport Bar and Mitchener Bar form during shorter duration flows than ripples at the estuary mouth. Also, internal structures in rippled areas at the estuary head are different from those at the estuary mouth. Rippled areas at the estuary mouth are underlain by small-scale cross-bedding (see Chapter 5); at the estuary head there is some small-scale cross-bedding underlying ripples, but the main internal structure is parallel lamination (see Chapter 5). Parallel lamination generally is formed on an upper flow regime plane bed (Walker, 1965).

Surface configuration and internal structures of ripples at the estuary head indicate that those ripples are not in equilibrium with average maximum flow conditions. Because current velocities are high (see Fig. 3-9) and parallel lamination is found (see Chapter 5), it appears that upper flow regime plane bed is representative of average maximum flow conditions and that ripples form during late-stage, low velocity flow prior to sand body emergence. Straight-crested and sinuous ripples are present because late-stage flow duration is insufficient to develop linguoid bedforms. If these late-stage structures are discounted, point N1 on Figures 9-2 to 9-4 correctly identifies the bed configuration (plane bed) corresponding to average maximum flow conditions.

Thus, in the Avon River estuary ripples are a function of relatively low current velocities and relatively fine mean grain sizes; ripples at the estuary mouth are located in areas where low current velocities are the average maximum flow conditions. At the estuary head, the low velocity - fine mean grain size criterion for ripples is met only during late-stage flow; the equilibrium bedform for average maximum flow conditions, upper flow regime plane bed, is reflected in ripple morphology and internal structures. Criteria for ripple stability are listed in Table 9-1.

TABLE 9-1. Criteria for Bedform Stability

Observed Bedform	Mean Grain Size	Increasing Flow Strength	Flow Regime
Ripples	fine	↓	lower
Sand Waves	coarse		lower
Megaripples	medium		lower
Transverse Bars	fine		transitional
late-stage[1] Ripples	fine		upper

---

[1] reworked plane bed or antidunes

MEGARIPPLES: In the Avon River estuary, megaripples exist in areas of high flow strength and intermediate mean grain size. Figure 9-4 illustrates the limits of megaripple stability in Simons et al. (1965a) classification; stream power confines megaripples between ripples and upper flow regime plane bed while grain size constructs a boundary between megaripples and sand waves. Figure 9-4 also depicts the close correlation of megaripples with the dune field of Allen (1968).

Southard's (1971, 1975) classification scheme indicates that megaripples occupy the highest flow strength field in the lower flow regime (Fig. 9-2); plotting shear velocity against mean grain size also places megaripples in the highest flow strength region (Fig. 9-3). These classifications also place megaripples at finer mean grain sizes than sand waves (Figs. 9-2 and 9-3).

On Figures 9-2 to 9-4 there are a few points within megaripple fields where megaripples were not the observed bed configuration, and a few megaripples were observed at stations that fell outside of the established fields. This probably reflects a longer relaxation time for megaripples than for ripples; relaxation time is the time required for a bedform to be altered into another form. Because megaripples are much larger than ripples (see Chapter 5), they should have a longer relaxation time since relaxation time is related directly to bedform (Allen and Friend (1976b). Since megaripples are the products of average maximum flow conditions, flows that could initiate change towards a different bedform are too short in duration to eradicate megaripples. (See Table 9-1 for the stability criteria of megaripples.)

SAND WAVES: The stability field for sand waves consists of intermediate flow strength and coarse mean grain size. Figure 9-2 best illustrates the relationship between sand waves and other bedforms; sand waves occur in coarse sediment and at flow strengths that are intermediate between ripples and megaripples. As previously discussed, Simons and Richardson's (1971) classification does not distinguish sand waves from megaripples in terms of flow strength (Fig. 9-4); the possible significance of the grain size boundary between the two bed configurations will be discussed later in this chapter. Figure 9-3 also indicates that sand waves occur in coarse sediment and at intermediate flow strengths. Rippled sand waves have different stability fields from megarippled sand waves on Figures 9-2 to 9-4; megarippled sand waves tend to be associated with coarser sediment and greater flow strength than rippled sand waves although the distinction is not apparent on Figure 9-2A.

TRANSVERSE BARS: Transverse bars cannot be placed on Figure 9-1 since no current velocity measurements were recorded over them because they occupy such a small area (see Figs. 3-2 and 5-3). However, currents over other parts of Mitchener Bar are strong (see Fig. 3-9) and mean grain size on transverse bars is fine (see Fig.

Culbertson and Scott (1970) found transverse bars to be transitional between the lower and upper flow regimes.

The association of fine mean grain size and high current velocities is similar to the conditions for upper flow regime plane bed; an area of late-stage ripples underlain by parallel lamination adjoins the region of transverse bars on Mitchener Bar as does a zone of megaripples (see Fig. 5-3). It appears likely that transverse bars are representative of transition or upper regime flow conditions.

Although transverse bars and upper flow regime plane bed may be bed configurations with overlapping stream power - grain size characteristics, the occurrence of transverse bars may be controlled by other factors. Transverse bars usually are associated with fluvial systems (Smith, 1971). As transverse bars occur only on a small area of Mitchener Bar (see Figs. 5-3 and 5-4), and Mitchener Bar appears to be a point bar (see Chapters 4 and 10), transverse bar development may be caused by some flow characteristic of fluvial systems and may not be a function simply of flow strength and grain size.

TRANSITIONS BETWEEN BED CONFIGURATIONS: Since each bed configuration observed in the Avon River estuary occupies a distinct field on plots of flow strength versus mean grain size (Figs. 9-2 and 9-3), there must be a set of hydraulic and grain size conditions that cause a transition between stable bed configurations.

Boot Island Bar provided an opportunity to investigate the transition between ripples and sand waves as regions of these bedforms are adjacent on that sand body (see Fig. 5-4). Current velocity stations Boot Island Bar 3, 4, and 5 (see Fig. 3-2 for locations) were recorded over a rippled area, at the transition, and over a zone of flood dominant sand waves, respectively. Figure 9-6 compares water depth - current speed plots through a tidal cycle for each station; the station over sand waves (Fig. 9-6C) has a higher average maximum current speed than the station at the transition (Fig. 9-6B) which in turn has a greater average maximum current speed than the station with ripples (Fig. 9-6A). Average maximum current speed at the ripple - sand wave transition corresponds closely with the ripple - sand wave boundary established experimentally by Costello (1974) (Fig. 9-6B). There also is a grain size change from ripples to sand waves. Mean grain size at each of the three stations is listed on Figure 9-6; sand waves are coarser than the transition zone which is coarser than ripples. Transition from ripples to sand waves apparently is governed by increasing flow strength; for a mean grain size of 1.09 phi, the transition occurs at the flow conditions measured at Boot Island Bar station 4 as illustrated on Figure 9-6B.

The transition from megaripples to sand waves could not be documented from field observations as there is no place in the estuary with a transition between the two bed configurations. However,

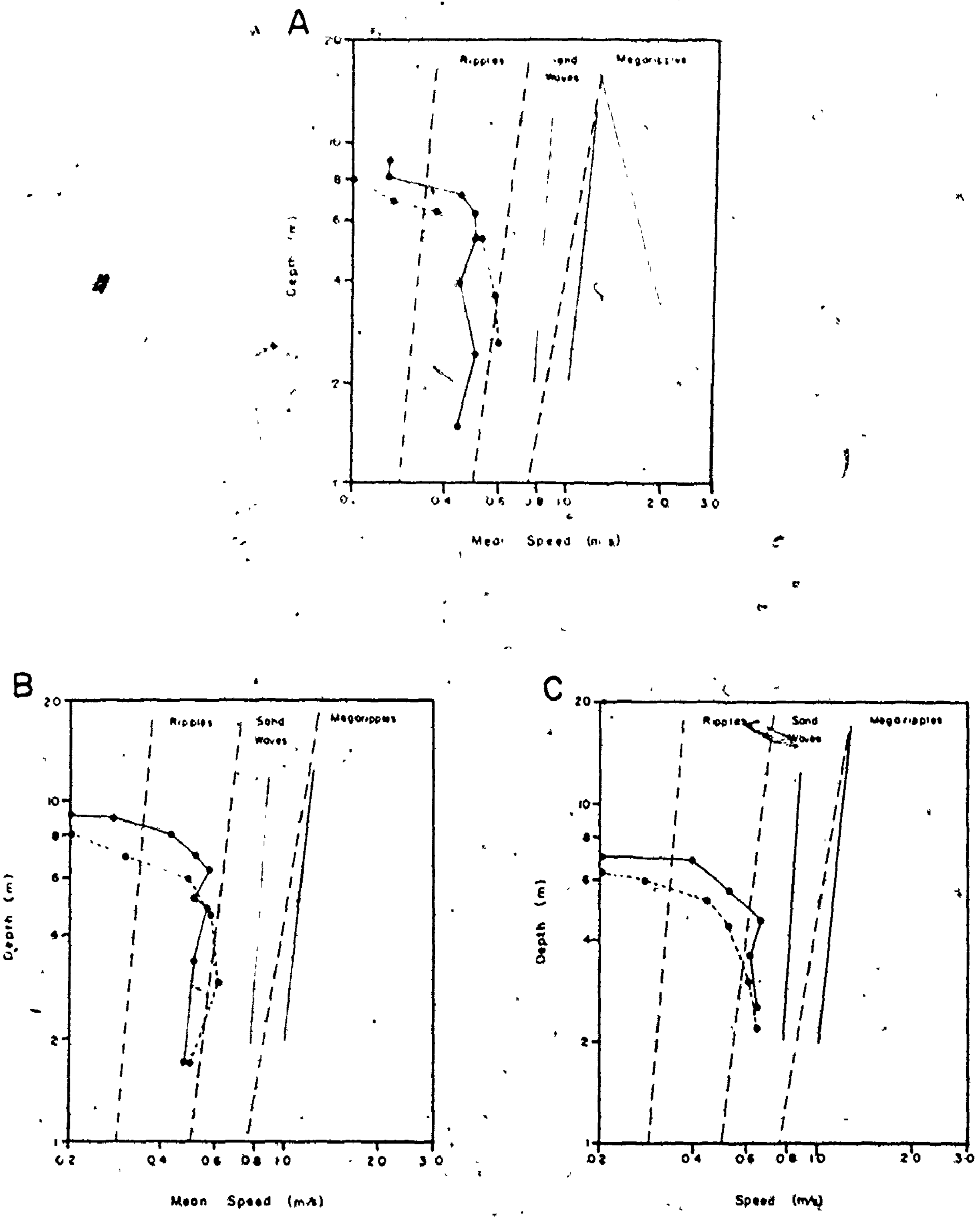

Fig. 9-6. Mean speed versus water depth through a tidal cycle for 3 stations. Dashed field boundaries were extrapolated from Costello (1974). Solid field boundaries are from Dalrymple (1977). Data points connected with a dashed line are flood currents; those connected with a solid line are ebb currents. The observed bed configurations are A) ripples, B) transitional between ripples and sand

C)

9-3 implies that the transition from sand waves to megaripples may be a function of transport mechanism. The curve for $w-U_*$ has been plotted on Figure 9-3; megaripples fall above the curve and sand waves lie either close to the curve or below it. As discussed in Chapter 8, $U - w$ is a criterion for suspension; points that plot above the curve should be from areas where transport is mostly by intermittent suspension while those that plot below the curve should be from areas where traction is the dominant transport mechanism. Thus, Figure 9-3 indicates that the transition from sand waves to megaripples occurs when the dominant transport mechanism changes from traction to intermittent suspension. Dalrymple (1977) also found a similar relationship between megaripples and sand waves; the field boundaries on Figure 9-3 were constructed using Dalrymple's (1977) data and data from the Avon River estuary. Of course, transport mechanism control of bed configuration is not a case of either traction or intermittent suspension transport; bed configuration is related to the relative importance, or proportion, of each mechanism.

Seven of the 59 sediment samples whose cumulative curves were dissected (see Chapter 6) were collected from sand waves; 9 others were collected from megaripples at the estuary mouth. Characteristics of the dissected cumulative curves also imply that the transition from sand waves to megaripples is a function of a change in transport mechanism. As discussed in Chapter 8, the C (coarse) population signifies transport by traction and the A (intermediate) population is a function of intermittent suspension. Sediment samples from sand waves average 52.0% C population and 46.7% A; those from megaripples at the estuary mouth average 24.5% C and 74.2% A. If sand waves are related to transport dominantly by traction, it would explain the association of sand waves with coarse mean grain sizes displayed on Figures 9-2 to 9-4; intermittent suspension is less likely to occur at coarse sizes.

OVERALL TRENDS AND BEDFORM SEQUENCES: Several trends in bedform distribution can be explained in terms of bedform stability criteria and bedform response to average maximum hydraulic conditions. Among these is the tendency for bedforms to increase in size in the direction of net sediment transport. Sand waves on Boot Island Bar demonstrate this trend; sand waves are very small at the ripple - sand wave transition which is at Boot Island Bar station 4 (see Fig. 3-2) and grow to 1 m in height at the southern end of the sand body. Sand waves on Western Bar and megaripples on Middle Ground and Hantsport Bar also exhibit this trend. Gee (1975) and Allen and Friend (1976b) have shown that dunes (megaripples) grow with time until a limiting size is attained; a megaripple migrating in the net sediment transport direction would increase in size in that direction, and the same process may apply to sand waves.

Increase in bedform height also could be due to a downstream increase in flow strength; on Boot Island Bar sand wave height increases in the same direction as flow strength.

The bedform distribution displayed on Figure 5-3 and 5-4 reveals an increase in flow regime in the onshore direction; such a trend conforms with the increase in flow strength from the mouth to the head of the estuary (see Fig. 3-9). At the estuary mouth, bedforms are entirely lower flow regime forms including ripples, sand waves, and megaripples.

The flat area of fine sediment on Middle Ground (see Figs. 5-4 and 6-2) results from shielding of this area from strong currents by underlying bedrock (see discussions in Chapters 8 and 10); the flat surface probably is caused by organic binding of the sediment by the polychaete Spiophanes wigleyi. Up to 300,000 worm tubes per m^2 have been counted in this area (V. Tunnicliffe, 1975, pers. comm.).

Lower flow regime bedforms are represented within the Avon River by sand waves on the central sand ridge near Summerville (see Fig. 4-1) and by megaripples on Hantsport Bar, Mitchener Bar, and Newport Bar (see Fig. 5-3). On Newport Bar and Mitchener Bar transitional forms (transverse bars) and upper flow regime plane bed are representative of average maximum flow conditions; at low tide, upper flow regime features are covered by late-stage ripples. Thus, progressively higher flow regime bed configurations are observed in the onshore direction from the estuary mouth. Observations indicate that this trend continues into the Kennetcook and St. Croix rivers. No sand waves were observed in these rivers; most bedforms were megaripples, transverse bars, and surfaces covered by sinuous, late-stage ripples. Observations were limited to 8 km upstream of where these rivers empty into the Avon River estuary (see Fig. 2-1).

The criteria for bedform development (Table 9-1), overall trends of bedform distribution, mean grain size, and flow strength allow the construction of a bedform sequence for the Avon River estuary; this sequence is illustrated on Figure 9-7A. A similar sequence derived by Boothroyd and Hubbard (1975) for mesotidal estuaries is displayed in Figure 9-7B. The two sequences differ in that, in the mesotidal sequence (Fig. 9-7B), megaripples and sand waves occur at the same flow strength, and sand waves evolve from low-order megaripples while in the Avon River estuary (Fig. 9-7A) sand waves share a common boundary with ripples and are stable at lower flow strengths than megaripples.

A. Avon River Estuary Bedform Sequence

lower flow regime plane bed → ripples → rippled sand waves → megarippled sand waves → megaripples → transverse bars → upper fl regime plane bed

FLOW STRENGTH

Low ——————————→ High

B. Mesotidal Estuary Bedform Sequence (Boothroyd and Hubbard, 1975)

linear ripples → cuspate ripples → linear megaripples → cuspate megaripples → planed-off megaripples → rhomboid megaripples → plane bed

linear megaripples ↓ sand waves

Fig. 9-7. Comparison of Bedform Sequences from the Avon River Estuary and Mesotidal Estuaries

Summary

Observed bedform distribution in the Avon River estuary is a function of average maximum flow conditions. Stability fields for each bedform type can be best distinguished by plotting current speed versus water depth and mean grain size versus current speed.

Ripples are found in areas of low flow strength and fine mean grain size. Megaripples are stable in regions with high flow strengths and fine to intermediate grain sizes; sand waves exist in areas of intermediate flow strength and require relatively coarse mean grain sizes. Transverse bars occur in a region of high flow strength and fine mean grain size; they appear to be transitional between lower and upper flow regime bedforms. Upper flow regime plane bed is formed in areas with high current velocities and fine mean grain sizes but is re-worked into ripples by late-stage flow.

A transition from ripples to megaripples results from an increase in flow strength; observed hydraulic conditions at the transition fit experimentally derived boundaries. The transition between sand waves and megaripples seems to be a function of a change in transport mechanism; sand waves appear to be associated with traction transport and megaripples with transport by intermittent suspension.

Bedform distribution indicates an increase in flow regime in the onshore direction. Only lower flow regime bedforms (ripples, megaripples, and sand waves) exist at the estuary mouth. Megaripples extend into the Avon River but sand waves are excluded because flow strength is too great and mean grain sizes are too fine. Transitional (transverse bars) and upper flow regime features (upper flow regime plane bed and antidunes) are found only on Mitchener Bar and Newport Bar. Increasing flow regime bed~~forms in~~ the onshore direction reflect increasing flow strength in the same direction; the bedform sequence that develops as flow strength increases is illustrated in Figure 9-7A.

CHAPTER 10

CONTROL OF SAND BODY SHAPE AND POSITION BY SEDIMENT TRANSPORT PATHS

Sediment transport processes are responsible for sand body shape and position in the Avon River estuary; each sand body reflects sediment transport paths produced by local hydraulics. As discussed in Chapter 7, sediment transport paths form cells that tend to be centered on sand body crests (see Fig. 7-5). However, for the purpose of discussing sand body shape and position as a function of sediment transport paths, sand body crests can be considered as boundaries between sediment transport zones. Generally, each sediment transport zone consists of a central channel that slopes up on either side to a sand body crest or shoreline; net sediment transport is in one direction within the transport zone. Thus, sand body crests represent channel boundaries as net sediment transport is in opposite directions on either side of a crest. Similar relationships among sediment transport zones have been described in other tide-dominated environments (Coastal Research Group, 1969; Ludwick, 1974; among others).

Houbolt (1968) attributes the development of asymmetric sand body and channel systems to longitudinal helical flow that causes sediment accumulation along the margins of a channel. However, measured current directions do not indicate that helical flow exists in the Avon River estuary; measured deflections are opposite to those predicted by helical flow. Sand body axes are oblique to flow directions so that bottom currents are deflected by the sand bodies.

Bottom currents are deflected upslope on the upstream side of the sand body; on the downstream side, bottom currents are deflected towards the sand body axis (Fig. 10-1). Knight (1977) believes that friction slows the portion of the flow nearest the sand body causing a curved flow path (Fig. 10-1); spiral flow on the downstream side of the sand body crest could cause the observed deflection.

Current directions near Hantsport Bar illustrate this principle; bottom currents are deflected by an average of 2° on the stoss side of the sand body and 6.5° on the lee side (Fig. 10-2). The stoss side is always the upstream side of the sand body crest, and the lee side is always the downstream side. The magnitude of the upstream and downstream deflections vary with position as sand bodies are asymmetric (see Chapter 4); the steep and gentle sides cause different amounts of deflection. Average deflections for other sand bodies are

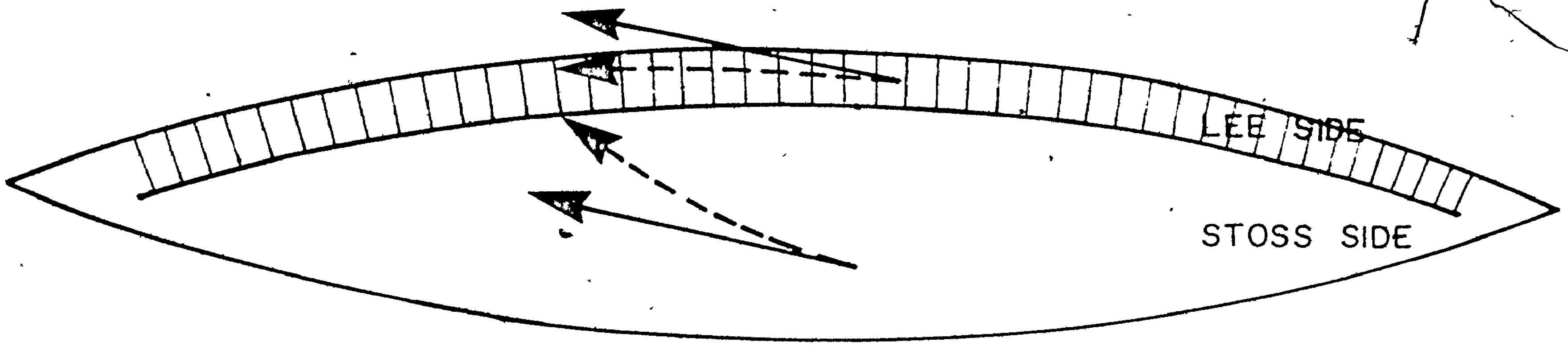

Fig. 10-1. Relation of bottom and surface current directions to sand bodies. The lee side of the sand body is steeper than the stoss side. Bottom currents are shown with dashed arrows and surface currents with solid arrows.

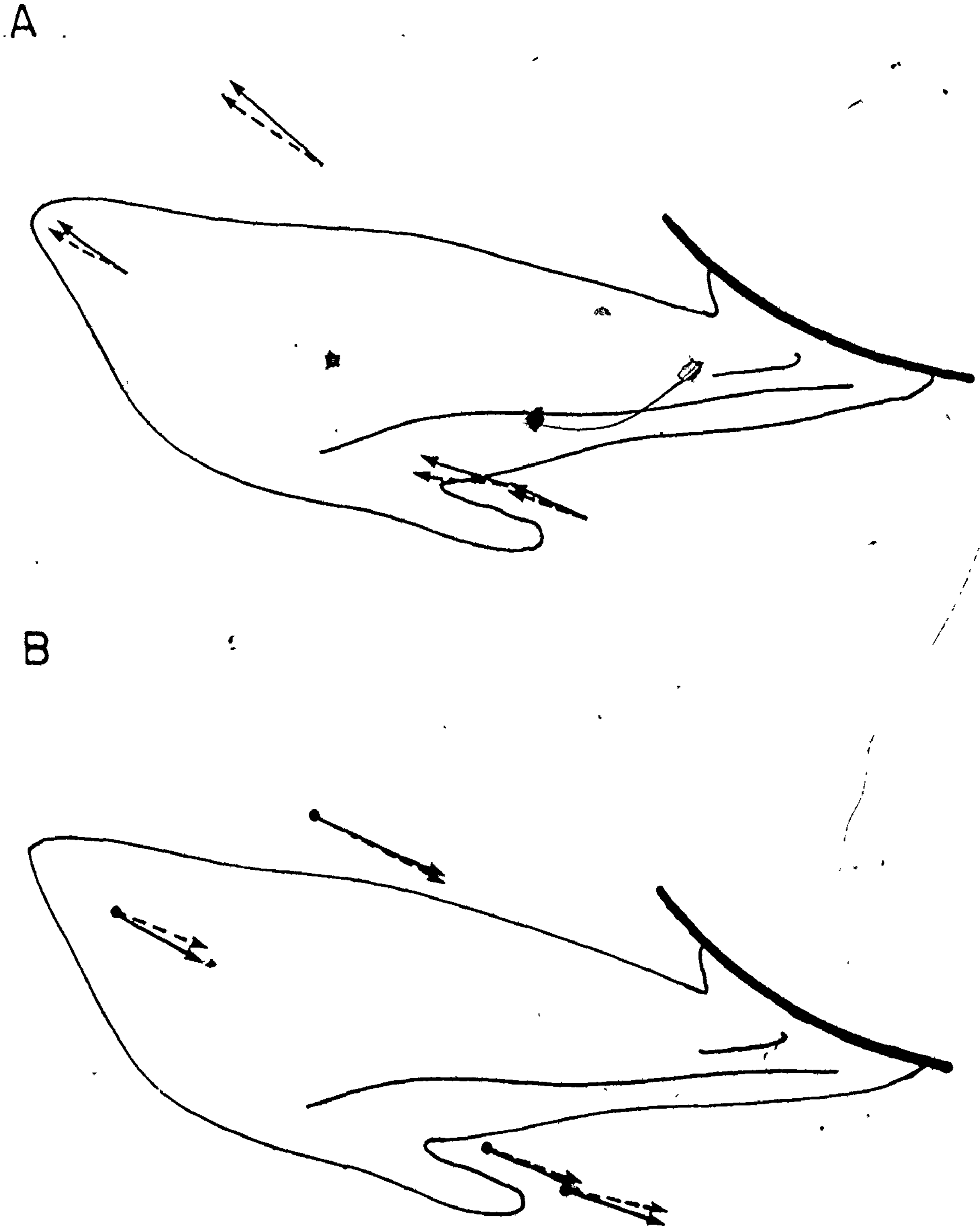

Fig. 10-2. Surface and bottom current directions near Hantsport Bar for A) ebb and B) flood. Surface currents are solid arrows and bottom currents are dashed arrows.

listed in Table 10-1; all raw current direction data is in Table B-1.

The relationship depicted in Figure 10-1 also explains the tendency for sediment transport to be oblique to sand body crests and for transport to have a slight upslope component (see Figs. 7-6 and 7-7); deflected bottom currents have a transverse directional component which causes upslope transport (Fig. 10-1). Bedform crest orientation reflects the transverse component of sediment transport; bedform strike is oblique to sand body crests (see Chapter 5). Sediment transport paths and bedform crests that are oblique to sand body crests have been described from other tidal environments (Houbolt, 1968; Terwindt, 1971) and from other parts of Minas Basin (Klein, 1970; Knight and Dalrymple, 1975; Dalrymple et al., 1975).

Individual Sand Bodies

Each intertidal sand body can be related to two or more sediment transport zones; the position of each transport zone can be explained in terms of local flow conditions produced by local physiography. The transport zones that are responsible for the shape and position of each sand body are discussed below.

BOOT ISLAND BAR: Boot Island Bar is the product of a junction of three sediment transport zones; two of these are flood transport

TABLE 10-1. Average Bottom Current Deflection on each Sand Body; numbers are degrees of difference between bottom and surface currents averaged for all stations on the sand body. Upstream values are deflection towards the sand body and downstream values are deflection towards the sand body axis; this relationship is depicted in Figure 10-1.

Sand Body	Upstream	Downstream
Boot Island Bar	3.3	10.3
Western Bar	3.5	5.5
Middle Ground	1.0	8.0
Hantsport Bar	2.0	6.5
Mitchener Bar	1.0	7.0
Newport Bar	4.0	11.5

zones and the third is an ebb transport zone (see Fig. 7-5). The position of each zone results from Boot Island Bar being part of an ebb tidal delta (see Chapter 4). Flood transport zones are created by flood dominant flow in the marginal flood channel (see Fig. 4-2) cutting across the channel margin linear bar (Boot Island Bar) and into the main ebb channel (see Fig. 7-5). Flood dominant flow is forced to cut across Boot Island Bar by a bedrock barrier to flow (Boot Island and the associated wave-cut platform) (see Fig. 2-5). The ebb transport zone on Boot Island Bar stems from the main ebb channel (see Fig. 7-5).

WESTERN BAR: Western Bar also is part of the Ebb tidal delta (see Fig. 4-2) and is composed of two ebb and two flood sediment transport zones (see Fig. 7-5). The southern flood transport zone is part of the northerly flood zone on Boot Island Bar (see Fig. 7-5). The northern flood transport zone on Western Bar also results from flood dominant flow in the marginal flood channel to the west of the ebb tidal delta cutting across the channel margin linear bar; small flood transport zones bisect channel margin linear bars in other ebb tidal deltas (Oertel, 1975).

The eastern ebb sediment transport zone on Western Bar is part of the main ebb channel (see Fig. 7-5); the western ebb zone probably results from local flow complexities possibly caused by the presence of the wave-cut platform near Boot Island (see Fig. 2-5) which extends under Western Bar (C. Amos, 1976, pers. comm.). The boundary between the western ebb transport zone and the flood transport zone to the east (see Fig. 7-5) is marked by a region of ice-rafted boulders; the boulders remain exposed because net sediment transport on either side of this area is away from the region of boulders (see Fig. 7-5) so that sediment tends to be eroded, rather than deposited in this zone.

MIDDLE GROUND: Middle Ground has the shape and position of a channel margin linear bar (see Fig. 4-2) but its existence is not related entirely to the ebb tidal delta. As discussed earlier (see Chapters 7 and 8), the center part of Middle Ground is cored by block-faulted bedrock (C. Amos, 1976, pers. comm.); sediment transport zone position reflects the presence of a bedrock core.

Presence of a bedrock core also is reflected in the surface features of Middle Ground. A vertical aerial photograph of the sand body reveals the fine-grained flat region near the sand body center (see Plate 4-2). North of this region, there is a well-developed drainage pattern that results from run-off prior to emergence; the bedrock core probably does not extend under the region of well-developed drainage as underlying bedrock would alter the drainage pattern. The southern extent of the bedrock probably coincides with the southern end of the flat-bedded area (see Plate 4-2); again, there is a change in drainage pattern as well as surface bedform. The bedrock core cannot extend as far south as the megarippled zone (see Fig. 5-4) as the flow strengths required for megaripple formation cannot occur over the bedrock surface (see the discussion in Chapter 8).

The shape of Middle Ground is controlled by its bedrock core. Sediment accumulation has the form of two overlapping half-bodies around the bedrock core; half-bodies result from flow that is deflected around a stationary object (Streeter, 1971, p. 409). Figure 10-3 illustrates the effect of bedrock on the growth of Middle Ground. The area north of the bedrock is protected from strong ebb currents, and swift flood currents cannot influence the region immediately south of the bedrock (Fig. 10-3); sediments are deposited in each of the shadow zones during the appropriate tidal stage.

Middle Ground is modified by the main ebb channel to the west and the marginal flood channel to the east (see Fig. 7-5). At the southeastern edge of the sand body the marginal flood channel crosses the sand body and joins the main ebb channel, possibly as a response to constriction by the eastern shoreline (see Fig. 7-5). The main ebb channel transports the sediment moved into it from the marginal flood channel to the north causing the formation of a large ebb spit (see Fig. 7-5).

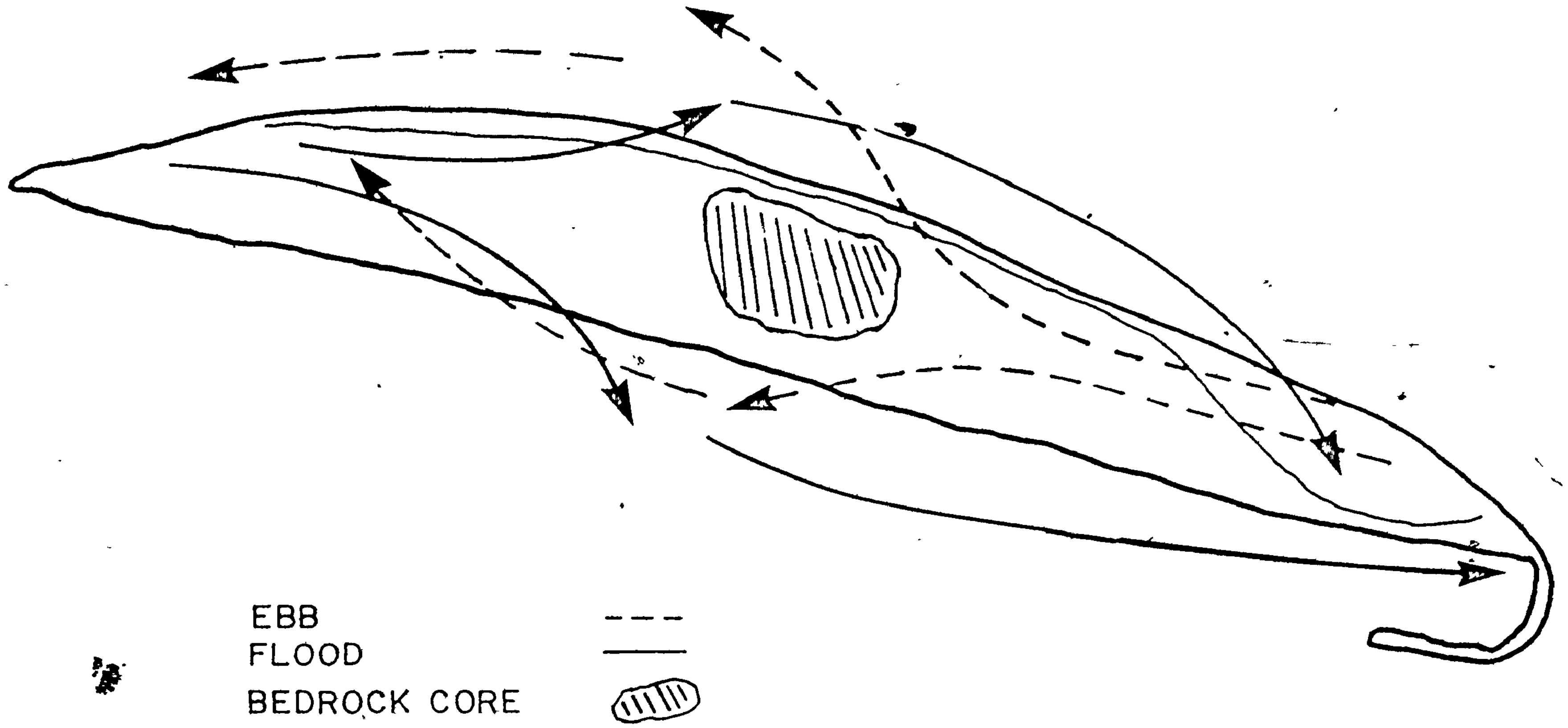
EBB
FLOOD
BEDROCK CORE

Fig. 10-3.Formation process of Middle Ground; the process is explained in the text.

The northern end of Middle Ground has net flood sediment transport (see Fig. 7-5) as it is exposed to strong flood currents but is protected from strong ebb flows. The southern end of the sand body is not influenced greatly by ebb flow since the strongest ebb currents develop after sand body emergence (see Chapter 3).

Thus the sediment transport zones on Middle Ground are a function of both ebb tidal delta development and Middle Ground's bedrock core. If the bedrock core did not exist, a sand body probably would occupy a site near that of Middle Ground as both edges of an ebb tidal delta should be bounded by channel margin linear bars (see Fig. 4-2), but it is unlikely that the sand body would rise so far above the sea bottom. Along the western edge of the sand body, the junction between the major flood and ebb transport zones on Middle Ground is marked by numerous ice-rafted boulders; as on Western Bar, this is probably a lag deposit that results from sediment being removed from this area. However, it may be that this is a preferred zone for deposition of ice-rafted material.

HANTSPORT BAR: Four sediment transport zones exist on Hantsport Bar; these include two large ebb zones, a large flood zone, and a small flood zone along the western edge of the sand body (see Fig. 7-5). The positions of all four transport zones can be related to topography and resulting flow paths. As discussed in Chapters 4 and 7, Hantsport Bar is a channel margin linear bar with respect to the Kennetcook

River and the channel to the east of the sand body is a marginal flood channel (see Fig. 7-5).

Position of the major ebb sediment transport zone at the southwest side of Hantsport Bar (see Fig. 7-5) is controlled by the interaction of the ebb tidal prisms of the Avon and Kennetcook rivers. As depicted in Figure 10-4, channel margin linear bars normally parallel a central ebb channel that extends straight out from a river mouth or tidal inlet. The ebb tidal prism of the Kennetcook River is deflected to the north by the Avon River ebb tidal prism; the ebb channel is forced to the north. Thus, the ebb transport zone at the southwest part of Hantsport Bar, the crest of Hantsport Bar, and the flood transport zone to the east of the sand body are all deflected to the northeast (Fig. 10-4).

The ebb transport zone at the north end of Hantsport Bar and the flood transport zone on the western edge of the sand body result from the abrupt widening of the Avon River south of Hantsport (see Fig. 7-5). Flood currents diverge as they enter the wider region and are deflected to the river margins by the central ebb zone (see Fig. 7-5). The orientation of the ebb transport zone at the north end of Hantsport Bar reflects a shift in the ebb channel to the north of the sand body; the shift is produced by the flow barrier created by the shoreline at Hantsport and the bedrock ledge north of Hantsport (see Fig. 4-1).

MITCHENER BAR: Parts of two sediment transport zones form Mitchener Bar; these include the ebb channel to the east of the sand body, and the flood channel that bisects the sand body (see Fig. 7-5). As described in Chapters 4 and 9, Mitchener Bar appears to be a tidal point bar at a bend in the Avon River (Fig. 10-5), it is similar in form to the scroll bars of Jackson (1976a,b) (Fig. 10-5). Sediment transport zones develop from flow that is moving straight ahead as it reaches the bend in the river; a different part of the sand body is sheltered from peak currents for each tidal stage so that net transport direction at each location reflects the tidal stage with stronger currents (Fig. 10-5).

NEWPORT BAR: The effect of sediment transport paths on the position and shape of Newport Bar probably is not as simple as indicated on Figure 7-5. Newport Bar probably is a flood tidal delta as described by Hayes (1975) (Fig. 10-6). There is a depression, or small channel, that cuts across the northern end of Newport Bar (see Fig. 4-3); this corresponds to the flood ramp in Hayes' model (Fig. 10-6). Several short term changes have been observed in the flood ramp; at times there is a well-developed small channel in this region, at others, a shallow depression. The duration of each configuration usually is just a few days and does not appear to be related to neap - spring tidal range changes.

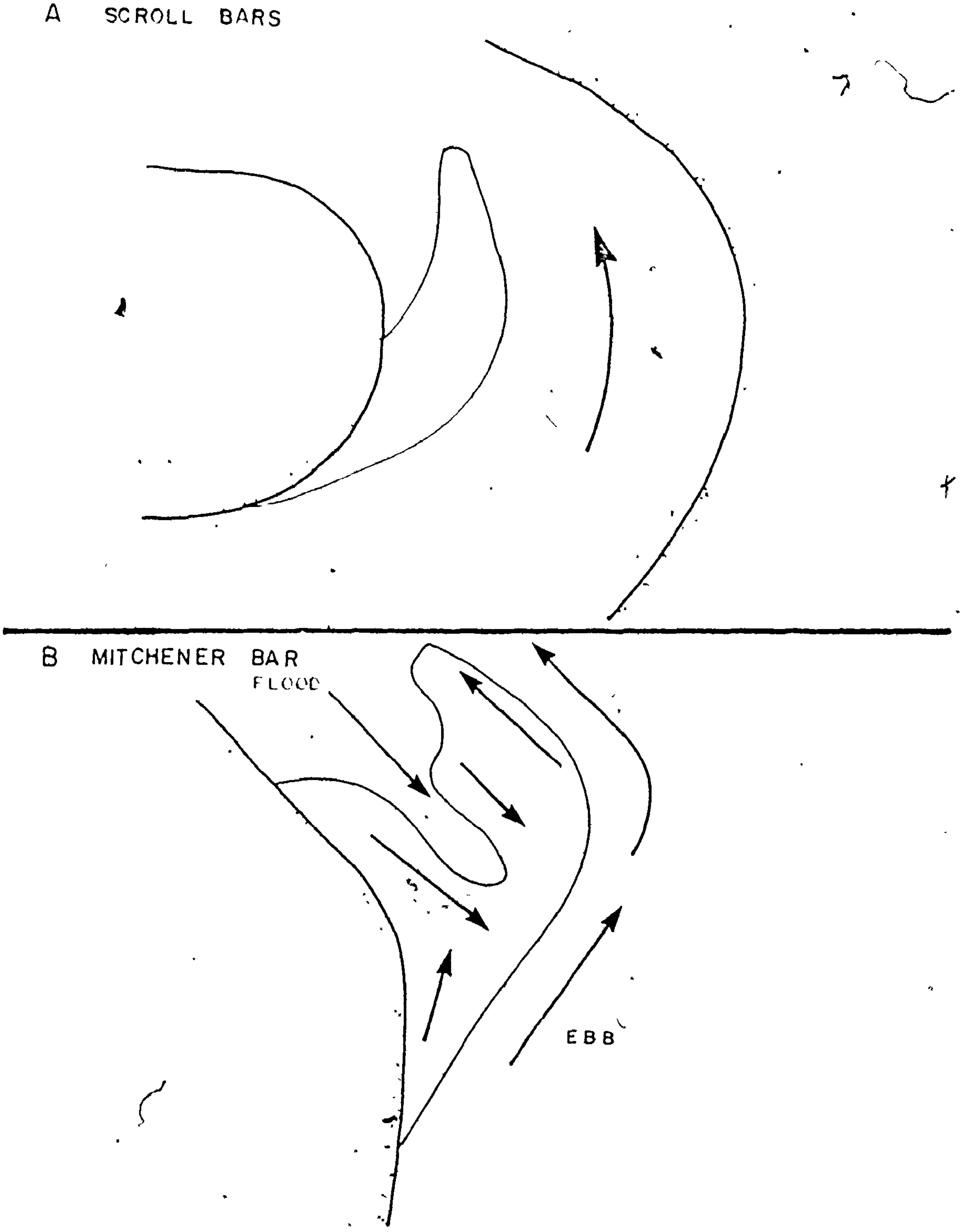
A SCROLL BARS
B MITCHENER BAR
FLOOD
EBB

Fig. 10-5. Mitchener Bar and scroll bars. Scroll bar shape (A) is from Jackson (1976a, b); arrows are net sediment transport directions.

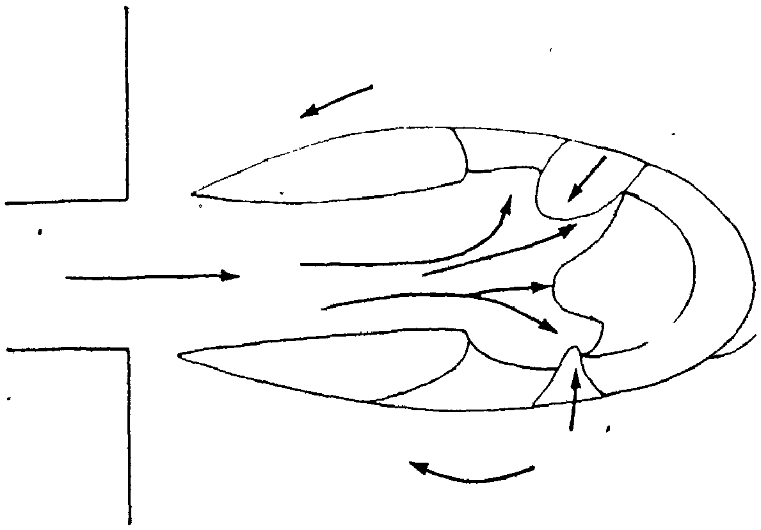

A FLOOD TIDAL DELTA MODEL

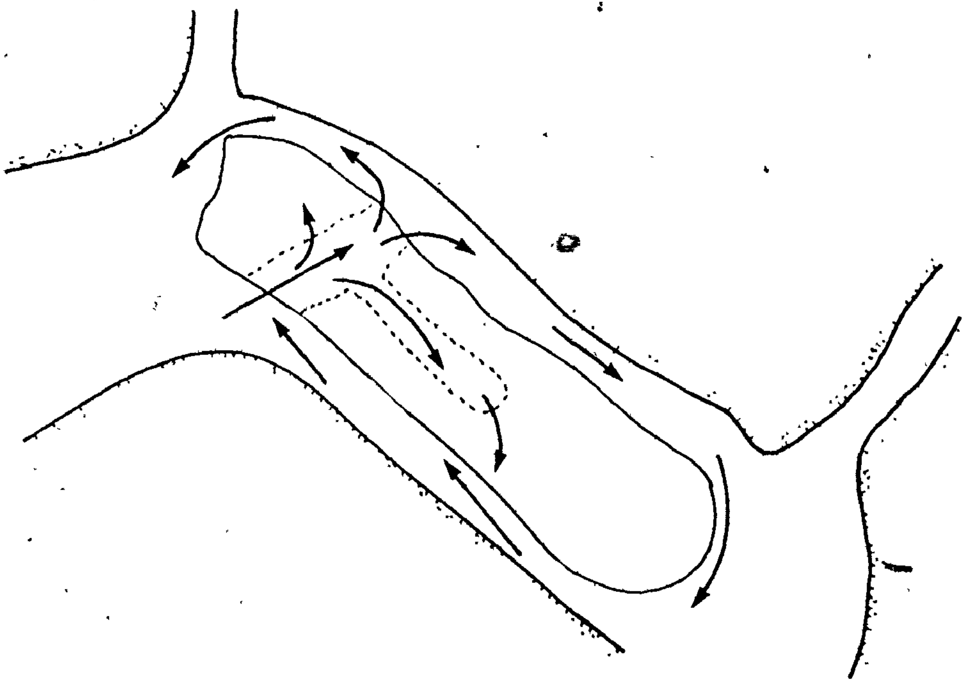

B NEWPORT BAR

Fig. 10-6. Comparison of Newport Bar to flood tidal deltas. Arrows indicate net sediment transport directions for A) mesotidal flood tidal delta model of Hayes (1975) and B) Newport Bar.

Sediment transport directions illustrated on Figure 7-7 fit the flood tidal delta model for Newport Bar. The northern end of the channel to the east of the sand body has net sediment transport in the ebb direction while net transport in the southern end of the same channel is in the flood direction (see Fig. 7-7). These transport directions agree with Hayes' (1975) definition of marginal "ebb" channels (Fig. 10-6); the position of the sand body crest also fits the flood tidal delta model.

The shape of Newport Bar is related to its flood tidal delta origin and the shoreline configuration of the Avon River. Flood currents reach the bend in the river near Mitchener Bar and proceed straight ahead over the flood ramp (Fig. 10-6); the sudden widening of the river relative to flow direction created by the bend causes formation of the flood tidal delta in a similar manner to those formed landward of a tidal inlet (Hayes, 1975). In a typical flood tidal delta, there are ebb dominant areas on either side of the flood ramp (Fig. 10-6). The bend in the Avon River aligns the south side of the tidal delta with the flood direction so that flow must complete a full circle before it can ebb (Fig. 10-6); the ebb transport zone to the west of Newport Bar is a result of this phenomenon.

CENTRAL SAND RIDGE: The central sand ridge near Summerville (see Fig. 4-1) is formed by an ebb transport zone to the east and a flood transport zone to the west (see Fig. 7-5). The bedrock ledge north of Hantsport influences the positions of the ebb and flood transport zones; ebb flow is deflected to the east of the ledge so that the western half of the river is protected from strong ebb currents (see Fig. 4-1).

Stability of the System

As noted in Chapter 4, aerial photograph, echo sounding, surveying, and chart data all suggest that sand bodies in the Avon River estuary are in dynamic equilibrium, sediment transport studies also suggest that the system is in dynamic equilibrium (see Chapter 7). As discussed in Chapter 4, comparison of soundings on British Admiralty charts from 1865, 1908, and 1916 shows that all three have identical depths recorded in each position (see Fig. 4-9); this could reflect either no change in the sand bodies with time, or that no new soundings were made when the chart was updated. Also, aerial photographs from 1963 and 1974 do not indicate any change in sand body position or shape between those years (see Plates 4-1 to 4-4).

Echo sounding and surveying data of the present study (measurements were carried out over a two-year period) do not reveal any large changes since the earlier charts (see Table 4-1 and the discussion in Chapter 4) and agree with a Canadian Hydrographic Survey chart surveyed in 1969 (Canadian Hydrographic Survey, 1972). Figures 10-7 and 10-8 compare the results of the present study and the 1969 survey. The figures are contour maps of each sand body constructed

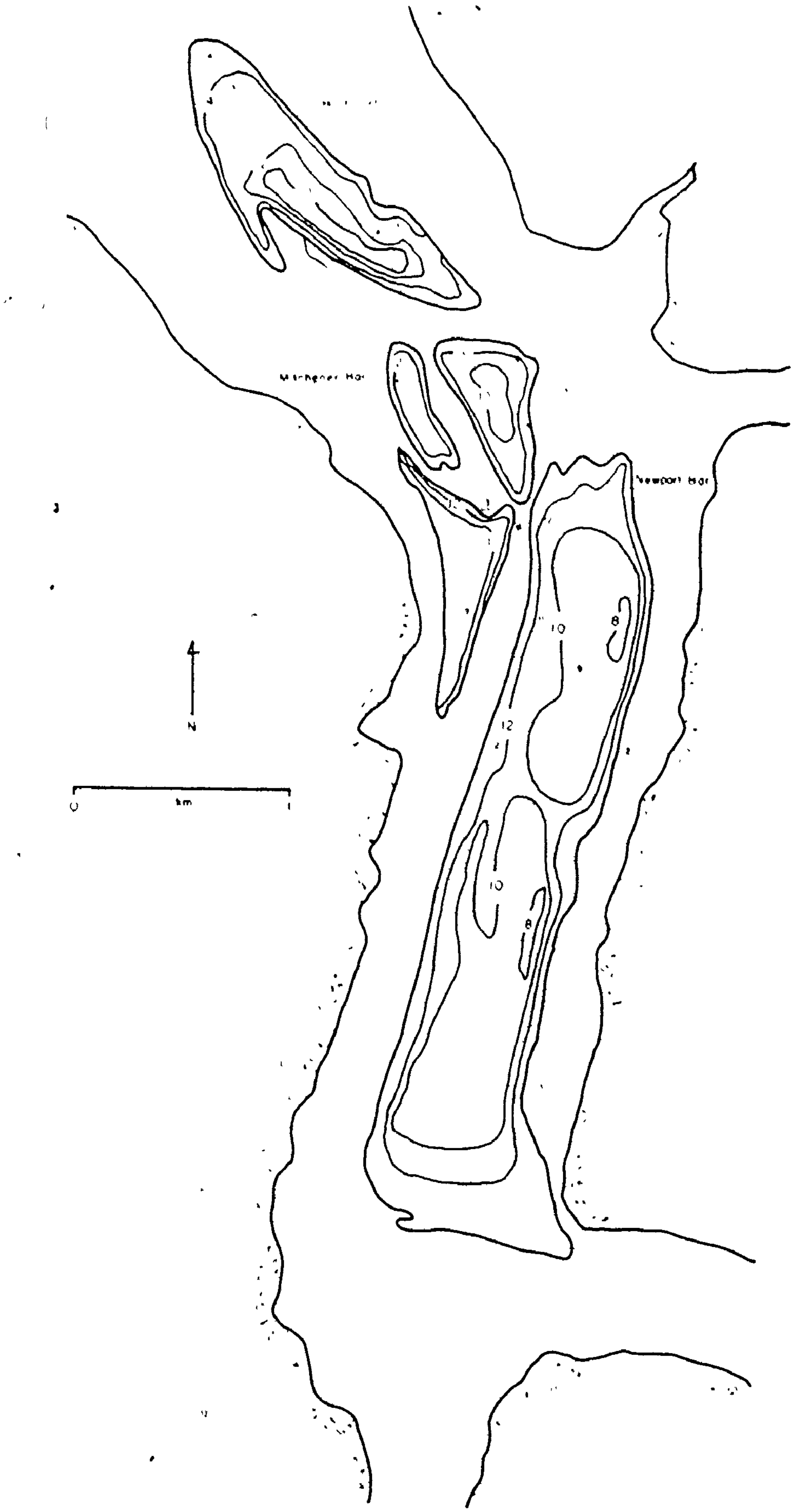
Mitchener Bar
Newport Bar
10
8
12
10
8
N
0
km
1

Fig. 10-7. Contour map and soundings of sand bodies at the estuary head. Contours are from data of the present study; the small case soundings [illegible] all [illegible]

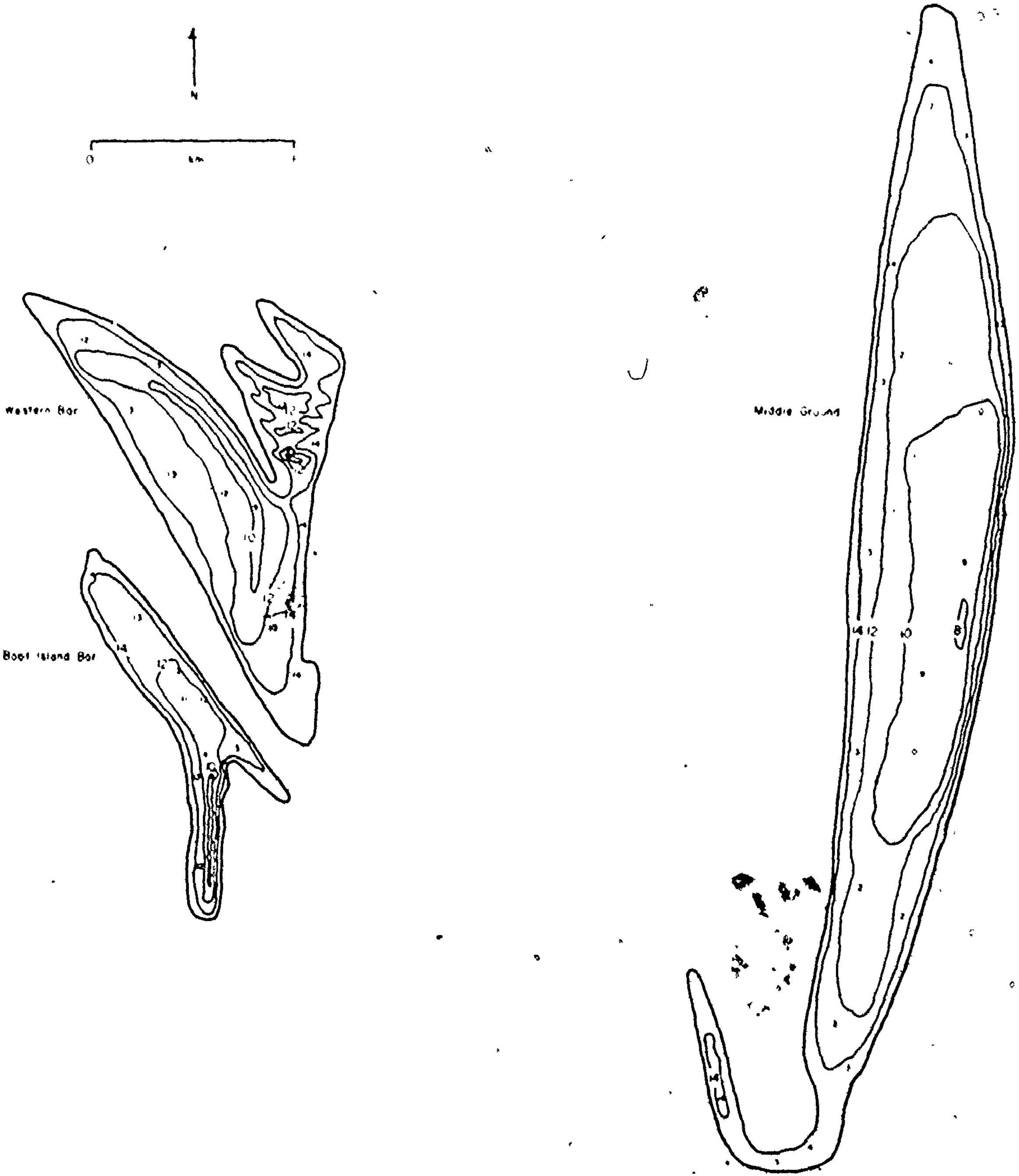
N
0
km
1
Western Bar
Boot Island Bar
Middle Ground
14
12
10
8

Fig. 10-8. Contour map and soundings of sand bodies at the estuary mouth. Contours are from data of the present study; the small case soundings are from 1969 Canadian Hydrographic Survey data; all depths are meters below higher high water.

from surveying data of the present study with soundings from the 1969 survey superimposed on them. Cross-sections drawn by Amos (1976) from a recent hydrographic survey conducted by Bedford Institute of Oceanography also correspond to the results of the present study and to those of the 1969 survey; Figure 10-9 compares cross-sections from the 3 studies.

However, Amos (1976) claims that nearly 2 m of vertical accretion has occurred since 1969 based on his interpretation of the 1969 hydrographic data (Fig. 10-9); deposition is attributed to environmental response to construction of the causeway at Windsor in 1970 (see Chapter 2). Amos (1976) calculates that this accretion represents approximately 8.0×10^7 m^3 of sediment in seven years. Sediment transport rates calculated in the present study discount the possibility of rapid accretion as, for 8.0×10^7 m^3 of sediment to be deposited in seven years, the net transport rate would have to be 7.66 m^3 per tidal cycle per meter width of the entire Avon River; this is almost an order of magnitude larger than any sediment transport rate computed in this study. Also, since the whole width of the Avon is not flood dominant, transport rates in the flood transport zones would have to be even larger.

Net sediment transport rates for four cross-sections across the estuary indicate that there is little, if any, net sediment transport into the Avon River estuary (see Chapter 7); the cross-section

Fig. 10-9. Comparison of cross-sections across the estuary for 3 surveys. Depths are meters below higher high water. 1969 is the Canadian Hydrographic Survey data (Canadian Hydrographic Survey, 1972), 1975 is from the present study, and 1976 is from Amos (1976).

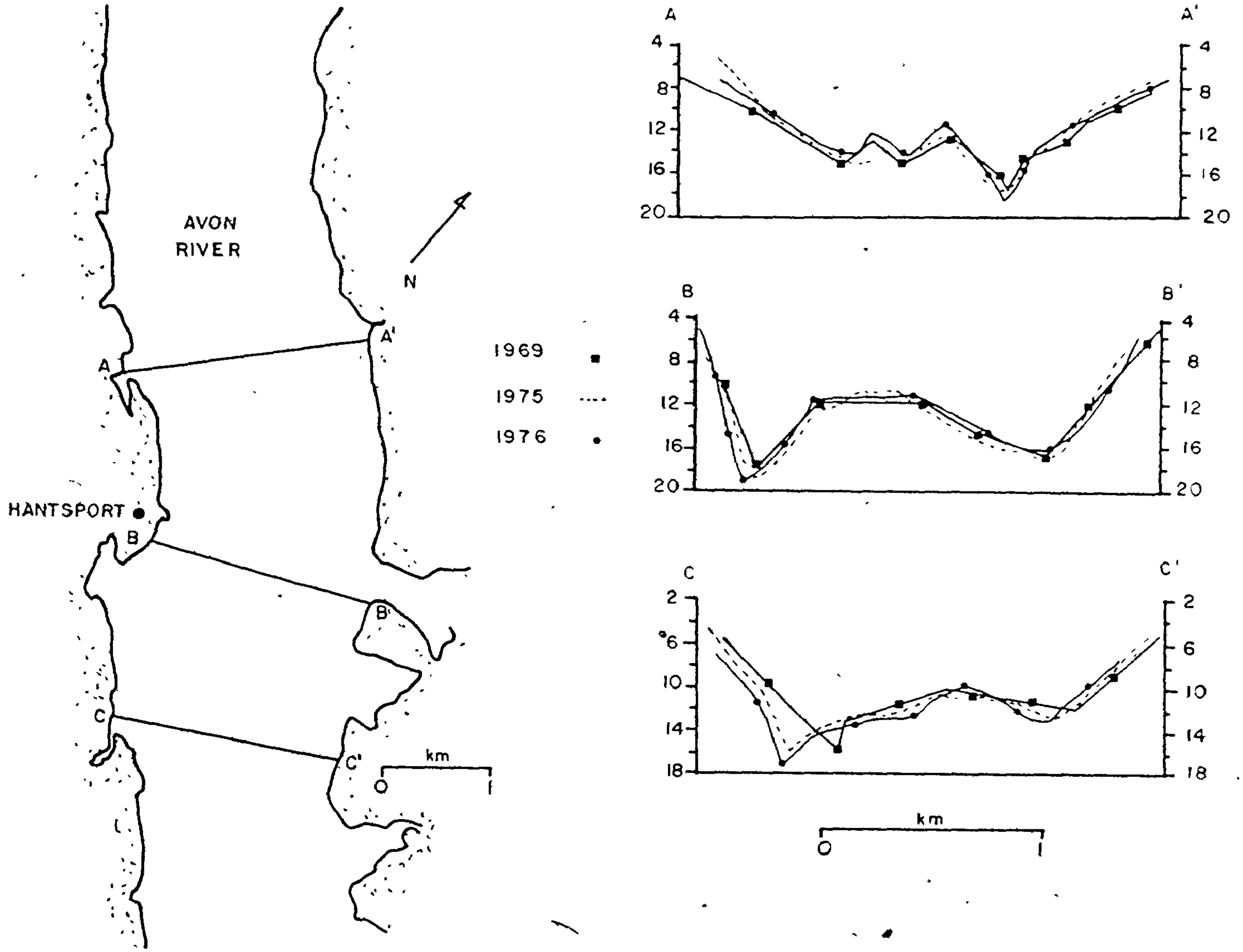
AVON
RIVER
N
A
A'
HANTSPORT
B
B'
C
C'
km
0
1
1969 ■
1975 ----
1976 •
A
A'
4
8
12
16
20
B
B'
C
C'
2
6
10
14
18
km
0
1

at Hantsport Bar (see Fig. 7-5) has a computed net transport rate of 0.03 m^3/tidal cycle in the ebb direction (see Table 7-2). This is 2 orders of magnitude lower than the rates required to produce the recent accretion in this area reported by Amos (1976).

Tidal range at Hantsport has decreased an average of approximately 0.5 m since construction of the causeway in 1970 (Amos, 1976); however, this change is small relative to normal neap to spring variations (see Chapter 3). It is probable that sediment distribution would be affected by the change in tidal range, but it is unlikely that a 0.5 m decrease in tidal range could cause 2 m of vertical accretion.

Amos (1976) can account for less than 1/3 of the required sediment volume by shoreline erosion and indicates that the only available source is the ebb tidal delta at the estuary mouth. A 45% decrease in the volume of the ebb tidal delta would be required to provide the necessary sediment; a decrease of this scale would be noticeable on aerial photographs and on hydrographic records but it has not been observed. It seems likely that large-scale deposition has not occurred since construction of the Windsor causeway; the apparent accretion reported by Amos (1976) appears to be the result of his interpretation of the 1969 survey data (Fig. 10-9). Thus, all hydrographic data, as well as aerial photographs and sediment transport rates, indicate that the Avon River estuary is in approximate dynamic equilibrium and has been since at least 1865.

Sediment Source

POSSIBLE SOURCES: There are four possible sources of sediment in the Avon River estuary including river input, remnant glacial till, shoreline erosion, and tidal current transport of sediment into the estuary from Minas Basin. The relative importance of each of these sources can be evaluated using data collected in the present study; each potential sediment source is discussed below.

River Input: The Avon, St. Croix, Kennetcook, and Cogmagun rivers (see Fig. 2-1) probably do not contribute much sediment to the Avon River estuary. None of these rivers discharge much sediment even at peak flow stage, and most of their sediment load is fine sediment (Amos, 1976). However, it is possible that extremely large floods with an occurrence intensity of 1,000 years, for example, may contribute some sediment to the estuary.

Remnant Glacial Till: Glacial till originally deposited within the Avon River estuary potentially is an important sediment source. Pleistocene glacial outwash also is a possible sediment source, but relatively little is found near the Avon River estuary (see Fig. 2-4). If till within the estuary were an important sediment source then there should be a high proportion of coarse sediment in the system. While there are significant amounts of coarse sediment at the estuary mouth, there is little coarse sediment at the estuary head (see Chapter 6). Also, glacial till probably would include a significant amount of sediment that would be too coarse for the hydraulic regime to transport; this sediment should be found as lag deposits. Little, if any, lag sediment has been found in the Avon River estuary (see Chapter 8) although it is possible that lag sediments are concentrated in subtidal channels or are buried beneath intertidal sand bodies.

Shoreline Erosion: Shoreline erosion apparently contributes a substantial amount of sediment to the Avon River estuary; shoreline retreat within Minas Basin, including the Avon River estuary, averages approximately 0.5 m per year (Amos, 1976). However, if shoreline erosion within the estuary itself were the major source of sediment, the coarse sediment deficiency at the estuary head would not be as pronounced as it is (see Chapter 6). Coarse sediment that presently is at the estuary head may be the product of shoreline erosion, but shoreline erosion within the estuary itself probably is not the major sediment source in the system.

Tidal Current Transport of Sediment from Minas Basin: Transport of sediment from Minas Basin into the Avon River estuary by tidal currents probably is a major source of sediment in the system. Tidal currents are capable of transporting all sediment presently in the system (see Chapter 8); also, the excess fine sediment at the estuary head as a result of hydraulic sorting (see Chapter 8) indicates transport of the finer sizes from the mouth into the estuary head. Thus, grain size distributions infer that tidal current transport of offshore sediment is an important source of sediment in the Avon River estuary.

RELATIVE IMPORTANCE OF CONTRIBUTING SOURCES: As discussed above, river input can be eliminated as a major sediment source in the Avon River estuary. Grain size distributions imply that tidal current transport of offshore sediment is the most important source of sediment, that shoreline erosion contributes a substantial amount of sediment, and that remnant glacial till may or may not be an important sediment source. In order to establish the relative importance of each sediment source, a mineralogical examination was conducted of sediment samples collected from each of the six major intertidal sand bodies. The examination used standard petrographic techniques; the method is described in detail in Appendix F; results of the investigation are listed in Table 10-2.

The only apparent trends in the mineralogical data are the greater abundance of rock fragments at the estuary mouth relative to the estuary head, and the higher proportions of non-quartz mineral grains at the estuary head than at the mouth (Table 10-2). These trends reflect the difference in mean grain size from the estuary mouth to the head (see Chapter 6) and are a function of hydraulic sorting (see Chapter 8). Two of the sediment samples from the estuary mouth that were examined petrographically were sieved and the finer than 2 phi

TABLE 10-2. Petrography (all values are percentages)

Sand Body	Sample Number	Qtz	Feld-spar	SS. Frags.	Shale Frags.	Basalt	Musco-vite	Bio-tite	Horn-blende	Meta-morphic Frags.	Opaque	Other
Boot Island Bar	B3E2C	58.9	10.0	12.6	13.8	3.0	-	-	-	0.6	1.0	-
	B3W2C	62.0	6.8	9.8	17.0	3.0	0.2	-	-	0.2	0.8	0.2
Western Bar	W3E2C	51.7	8.7	16.7	18.3	3.3	-	-	0.2	0.6	0.4	0.2
	W3W2C	58.1	10.7	10.9	16.7	2.5	0.2	-	-	0.4	0.6	-
Middle Ground	G6E2C	51.6	9.5	5.8	24.8	2.6	-	-	-	2.2	2.4	1.2
	G6W2C	58.9	9.3	4.6	21.9	4.6	0.4	-	-	0.2	0.4	-
Hantsport Bar	H4E2C	60.7	8.2	4.0	21.8	2.2	0.8	-	-	-	1.6	0.6
	H4W2C	59.5	8.3	7.4	21.0	0.6	0.2	0.4	0.4	0.2	1.8	0.2
Mitchener Bar	M2E2C	63.8	5.8	4.7	20.3	3.2	0.2	-	0.8	0.2	0.8	0.2
	M9B2C	52.7	6.0	9.6	24.4	1.8	0.6	0.6	2.4	0.6	0.8	0.6
Newport Bar	N4E2R	50.0	7.6	8.4	22.9	0.4	2.2	1.4	0.6	0.2	5.8	0.4
	N4W2R	67.1	3.2	2.6	20.7	0.2	2.0	0.2	-	-	4.0	-
Aver. Head		59.0	6.5	6.1	21.9	1.4	1.0	0.4	0.7	0.2	2.5	0.3
Aver. Mouth		56.9	9.2	10.1	18.8	3.2	0.1	0.0	0.0	0.7	0.9	0.3
G6W2C (finer than 2 phi)		64.2	9.3	6.6	13.9	1.3	0.7	0.7	0.9	0.3	1.4	0.7
W3W2C (finer than 2 phi)		60.7	10.7	5.3	14.7	0.7	1.3	1.2	1.1	1.4	2.0	0.9

fraction was re-examined petrographically, the results are listed in Table 10-2. Both samples are more similar in composition to samples from the estuary head than those from the mouth in that there are fewer sandstone fragments and accessory minerals are more abundant (Table 10-2). The variation in abundance of sandstone fragments does not signify different sediment sources for the head and mouth of the system. Because of hydraulic sorting, coarse sediment, with a relatively large proportion of sandstone fragments, does not penetrate to the estuary head (see Chapter 8) so that fewer sandstone fragments are found there. Also, many of the constituent grains in the sandstone fragments are as large as the finer grains at the estuary head; these cannot be transported to the head except as individual grains. Accessory minerals are concentrated in the finer grain sizes as a result of the hydraulic equivalence of their high densities (Blatt et al., 1972); the nearly uniform composition of the finer grain sizes throughout the estuary implies that most sediment was derived from the same source.

Grain size distributions and mineralogy indicate that transport by tidal currents or remnant glacial till is the most likely major source of sediment in the Avon River estuary. The presence of sandstone and shale fragments suggests that shoreline erosion contributes a substantial amount of sediment as the fragments appear to be derived from the Horton Bluff Formation and the Annapolis Formation which outcrop along the Avon River estuary (see Fig. 2-3). If remnant glacial till is the source of most of the sediment in the system, then lag sediment must be present in subtidal channels and the intertidal sand bodies represent glacial sediments that have been reworked by tidal currents; this possibility cannot be discounted as lag deposits are present in several areas in the estuary (Fig. 10-10). Amos (1976) reports a lack of sand-sized sediment in central Minas Basin and attributes it to transport of the sand fraction into Cobequid Bay and into the Avon River estuary (see Fig. 2-2); this supports an offshore source area for sediment in the Avon River estuary.

There is an area of rapid coastline erosion to the west of the Avon River estuary in Minas Basin (Amos, 1976, pers. comm.) that is a potential sediment source; longshore drift probably is west to east as dominant winds are from the west (see Chapter 2). However, tidal currents may offset the effect of longshore drift. Tee (1975, reported in Greenberg, 1976) predicts clockwise residual currents in Windsor Bay; this agrees with the observed tidal ellipse at the mouth of the Avon River estuary (see Chapter 3) (Fig. 10-10). Currents in the western end of Minas Basin have not been measured in enough detail to verify sediment transport direction or rate; 2 stations monitored by Amos (1976) agree with Tee's (1975) model (Fig. 10-10). Thus, specific offshore sediment sources for the Avon River estuary cannot be identified.

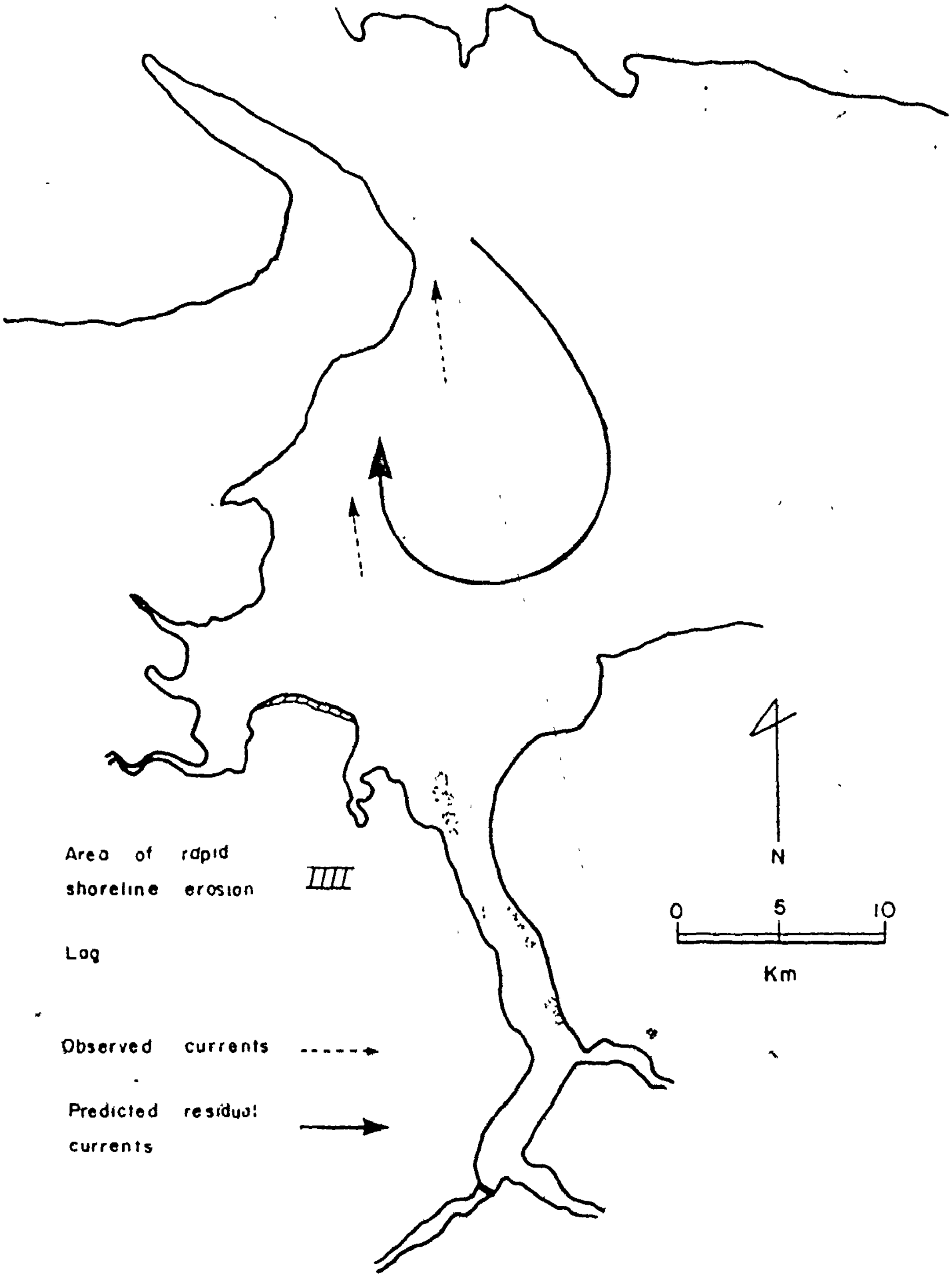
Area of rapid shoreline erosion
Lag
Observed currents
Predicted residual currents
N
0
5
10
Km

Fig. 10-10. Areas of lag, rapid shoreline erosion, and predicted and measured residual currents in Windsor Bay. Lag areas are known areas; other lag may exist. Predicted currents are from Tee (1975; reported in Greenberg, 1976); observed currents are from Amos (1976, pers. comm.).

It may be concluded that sediment in the Avon River estuary probably has been derived from three sources. The most important appears to be tidal current transport from an offshore sediment source. Any remnant glacial till in the system has been reworked so that coarse lag remains in subtidal channels and the remainder is deposited on intertidal sand bodies. Some sediment produced by shoreline erosion within the stuary also has been incorporated into intertidal sand bodies.

Summary

Intertidal sand bodies in the Avon River estuary lie between sediment transport zones of opposite net sediment transport direction; sand body crests represent transport zone boundaries. Position and size of sediment transport zones is a function of hydraulics and local physiography; transport is oblique to sand body crests as a result of flow that is oblique to sand body crests and bedform orientation reflects an upslope component of sediment transport. Surveying, echo sounding, and sediment transport rate data of the present study all indicate that the Avon River estuary is in dynamic equilibrium.

Sediment transport patterns indicate that the intertidal sand bodies form the following morphologic units. Boot Island Bar and Western Bar are part of an ebb tidal delta. The bedrock core of Middle

Ground causes deposition in areas protected from strong currents; the sand body surface is modified to fit the expected ebb tidal delta morphology. Hantsport Bar also is part of an ebb tidal delta while Mitchener Bar is a tidal point bar and Newport Bar is a flood tidal delta.

Grain size distributions suggest that tidal current transport of sediment from offshore into the estuary is the most probable major sediment source for the Avon River estuary. Mineralogical analysis implies a substantial component is derived from shoreline erosion at the mouth of the estuary; remnant glacial till may be an important source but no coarse lag sediments have been observed.

CHAPTER 11

CONCLUSIONS

The important conclusions of the present study have been grouped according to topic; they include observed, calculated and inferred results. Following each conclusion a chapter(s) is referenced that contains the discussion(s) which provide the basis for the conclusion.

Hydraulic Environment

Three conclusions about hydraulic environment are listed below; those with maximum influence on sediment transport and distribution have been included. Many other aspects of the hydraulic environment are described in Chapter 3.

1. Strong currents measured in the Avon River estuary are generated by tides; other hydraulic processes do not strongly affect sediment movement in the estuary (Chapter 3).
2. Either flood or ebb currents are dominant at any one location; a distinct pattern of ebb and flood dominant regions exists (Chapter 3).

3. Current velocities increase from the estuary mouth to the estuary head (Chapter 3).

Grain Size Distribution

1. Mean grain size tends to be much finer at the estuary head than at the mouth; this results in an inverse relationship between maximum current velocity and mean grain size (Chapters 3 and 6).

2. There is a large coarse sediment population at the estuary mouth that is not present at the head of the system (Chapter 6).

3. Grain size distribution reflects maximum, rather than average, flow conditions (Chapter 8).

4. At the estuary mouth, the shear stress required to transport the maximum grain size present according to Shields' criterion corresponds to the maximum measured shear stress during a tidal cycle; at the estuary head the coarsest grain size present is finer than the predicted competence of the flow (Chapter 8).

5. Each grain size population represents a transport mechanism; the coarse population is transported by traction, the intermediate by intermittent suspension, and the fine population is moved by suspension (Chapter 8).

6. The traction - intermittent suspension boundary occurs at a grain size where settling velocity approximately equals maximum shear velocity (Chapter 8).

7. The intermittent suspension - suspension boundary corresponds to the condition that maximum shear velocity is approximately 5 times settling velocity (Chapter 8).

8. The difference in mean grain size between the estuary head and mouth is a result of hydraulic sorting; different transport mechanisms have different transport rates which produces the hydraulic sorting (Chapter 8).

9. For sediment to enter the estuary head, it must cross an ebb dominated zone north of Hantsport Bar. This is only possible if the distance that the sediment can be transported during the flood stage is greater than the width of the ebb zone. Coarse sediment, moved by traction, cannot cross the ebb dominant zone in a few tidal cycles, but finer sediment, transported by intermittent suspension, can cross this zone before it is entrained into the ebb system. Thus, fine sediment can penetrate to the estuary head, but coarse sediment is returned to the estuary mouth (Chapter 8).

Bedforms and Internal Structures

1. There are four bedform types in the Avon River estuary; ripples, megaripples, sand waves, and transverse bars (Chapter 5).

2. Internal structures reflect surface bed configurations (Chapter 5).

3. Bedforms reflect maximum, not average, flow conditions (Chapter 9).

4. Bedform stability fields are best distinguished on plots of current speed versus mean grain size and current speed versus water depth; ripples occur at low current speeds and fine mean grain sizes, sand waves at coarse mean grain sizes and intermediate current speeds, and megaripples form at high current speeds in areas with intermediate mean grain sizes (Chapter 9).

5. Flow regime tends to increase towards the estuary head (Chapter 9).

6. Upper flow regime plane bed is the stable bedform in part of the estuary head; observed ripples form during late-stage flow (Chapter 9).

Sand Body Position, Sediment Source, and System Stability

SAND BODY POSITION

1. Sand bodies lie between sediment transport zones; sand body crests are transport zone boundaries. Transport is oblique to sand body crests with an upslope component; transport zone position is a function of local physiography and hydraulics (Chapters 7 and 10).

2. Shallow sand body surfaces tend to be flood dominant and deep channels tend to be ebb dominant (Chapter 7).

3. Western Bar and Boot Island Bar are part of a large ebb tidal delta at the estuary mouth (Chapters 4 and 10).

4. Middle Ground formed around a bedrock core and has been modified to fit the ebb tidal delta model (Chapters 4 and 10).

5. Hantsport Bar is part of an ebb tidal delta with respect to the Kennetcook River (Chapters 4, 7 and 10).

6. Mitchener Bar is a tidal point bar and Newport Bar is a flood tidal delta (Chapters 4 and 10).

7. The Avon River estuary fits a mesotidal estuary model rather than a macrotidal estuary model (Chapters 4 and 10).

SEDIMENT SOURCE

1. Three sources probably contribute sediment to the Avon River estuary; shoreline erosion, glacial till deposited in the estuary, and tidal current transport of offshore sediment (Chapter 10).

2. Shoreline erosion contributes significant sediment but is not the major sediment source (Chapter 10).

3. Transport into the system from an offshore source by tidal currents probably is the major sediment source (Chapter 10).

SYSTEM STABILITY

1. Aerial photograph, echo sounding, surveying, and chart data do not indicate any changes in sand body size, position, or shape since 1865 (Chapters 4 and 10).

2. Net sediment transport per tidal cycle through 4 cross-sections of the Avon River is essentially zero (Chapter 7).

3. All data suggest that the Avon River estuary is in approximate dynamic equilibrium (Chapter 10).

It is hoped that the preceding pages have revealed the "beauty" that Joseph Howe obviously missed as he arrived in Windsor in 1828.

> "... It being high tide, you see none of the mud and much of the beauty of the Avon ..."
>
> \- Joseph Howe, 1828

REFERENCES

Ackers, P. and White, W.R., 1973, Sediment transport: new approach and analysis: Proc. Amer. Soc. Civil Eng., Jour. Hyd. Div., v. 99, pp. 2041 - 2060.

Akima, H., 1972, Algorithm 433 - Interpolation and smooth curve fitting based on local procedures: Communications of the A.C.M., v. 15, pp. 914 - 918.

Allen, G.P., Deressequier, A. and Klingebiel, A., 1969, Evolution des structures sédimentaires sur un banc sableux d'estuaire en fraction de l'amplitude des marées: Compte Rendus Acad. Sci. Paris, V. 269, Series D., pp. 2167 - 2169.

Allen, J.R.L., 1968, Current ripples: North-Holland Pub. Co., Amsterdam, 433 p.

________, 1969, On the geometry of current ripples in relation to stability of fluid flow: Geogr. Annlr., v. 51A, pp. 61 - 96.

________, 1973, Features of cross-stratified units due to random and other changes in bed forms: Sedimentology, v. 20, pp. 189 - 202.

________, 1974, Reaction, relaxation, and lag in natural sedimentary systems: general principles, examples, and lessons: Earth Sci. Rev., v. 10, pp. 263 - 342.

Allen, J.R.L. and Friend, P.F., 1976a, Changes in intertidal dunes during two spring - neap cycles, Lifeboat Station bank, Wells-next-the-Sea, Norfolk (England): Sedimentology, v. 23, pp. 329 - 346.

________ and ________, 1976b, Relaxation time of dunes in decelerating aqueous flows: Jour. Geol. Soc. London, v. 132, pp. 17 - 26.

Amos, C.L., 1976, The effects of tidal power structures on the sediment transport and loading in the Bay of Fundy - Gulf of Maine system: Acadia Univ. Inst., Workshop on Environmental Implications of Fundy Tidal Power, 22 p.

Athaullah, M., 1968, Prediction of bedforms in erodible channels: Unpub. Ph.D. thesis, Colorado State Univ., 144 p.

Atlantic Tidal Power Engineering and Management Committee, 1969, Report to Atlantic Tidal Power Programming Board on feasibility of tidal power development in the Bay of Fundy: Halifax, Nova Scotia.

Bagnold, R.A., 1956, The flow of cohesionless grains in fluids: Phil. Trans. Roy. Soc. London, Series A, v. 249, pp. 235 - 297.

________, 1973, The nature of saltation and of "bedload" transport in water: Proc. Roy. Soc. London, Series A, v. 332, pp. 473 - 504.

Balazs, R.J. and Klein, G. de Vries, 1972, Roudness - mineralogical relations of some intertidal sands: Jour. Sed. Petrology, v. 42, pp. 425 - 433.

Barr, J.L., Dinkelman, M.G. and Sandusky, C.L., 1970, Large epoxy peels: Jour. Sed. Petrology, v. 40, pp. 445 - 449.

Bell, W.A., 1929, Horton - Windsor district, Nova Scotia: Geol. Survey Can., Mem. 155, 268 p.

________, 1960, Mississippian Horton Group of type Windsor - Horton district, Nova Scotia: Geol. Survey Can., Mem. 314, 112 p.

Blatt, H., Middleton, G.V. and Murray, R.C., 1972, Origin of sedimentary rocks: Prentice-Hall Co., Englewood Cliffs, New Jersey, 634 p.

Bogardi, J.L., 1961, Some aspects of the application of the theory of sediment transportation to engineering problems: Jour. Geophys. Res., v. 66, pp. 3337 - 3346.

Boothroyd, J.C., 1969, Hydraulic conditions controlling the formation of estuarine bedforms: in Hayes, M.O., (ed.), Coastal Environments: N.E. Massachusetts and New Hampshire, Coastal Research Group contribution No. 1, Dept. of Geology, Univ. of Massachusetts, pp. 417 - 427.

Boothroyd, J.C. and Hubbard, D.K.,1975, Genesis of bedforms in mesotidal estuaries: in Cronin, L.E., (ed.), Estuarine Research, v. 2, pp. 217 - 234.

Bourcart, J. and Boillot, G., 1960, La répartition des sédiments dans la baie du Mont Saint-Michel: Rev. Geog. Phys. Geol. Dyn., v. 3, pp. 189 - 199.

Bowden, K. F., 1962, Measurement of turbulence near a sea bed in a tidal current: Jour. Geophys. Res., v. 67, pp. 3181 - 3186.

Burger, J.A. and Klein, G. de Vries, 1969, A field technique for making epoxy relief - peels in sandy sediments saturated with salt-water: Jour. Sed. Petrology, v. 39, pp. 338 - 341.

Canada Department of the Environment, Water Resources Branch, 1974, Historical streamflow summary: Atlantic Provinces to 1973: 135 p.

Canada Department of Transport, Meteorological Branch, 1967, Temperature and precipitation tables for Atlantic Provinces: v. 6, 28 p.

Canada Department of Transport, Meteorological Branch, 1968 - 1972, Meteorological observations in Canada, monthly report.

Canadian Hydrographic Service, 1972, Avon River and approaches: Chart 4140.

Canadian Hydrographic Service, 1974 - 1976, Canadian tide and current tables: v. 1, Atlantic coast and Bay of Fundy.

Carver, R.E., 1971, Procedures in sedimentary petrology: John Wiley and Sons, New York, 653 p.

Cassie, R.M., 1954, Some uses of probability paper in the analysis of size frequency distributions: Austr. Jour. Marine and Freshwater Res., v. 5, pp. 513 - 522.

________, 1963, Tests of significance for probability paper analysis New Zealand Jour. Sci., v. 6, pp. 474 - 482.

Coastal Engineering Research Center, 1973, Shore Protection Manual: U.S. Army Corps of Engineers, v. 1.

Coastal Research Group, 1969, Coastal environments: N.E. Massachusetts and New Hampshire: (Hayes, M.O., ed.), Contribution No. 1, Coastal Research Group, Department of Geology, Univ. of Massachusetts, 462 p.

Coleman, J.M., 1969, Brahmaputra River: channel processes and sedimentation: Sed. Geol., v. 3, pp. 129 - 239.

Committee on Sedimentation, 1966, Sediment transport mechanics: initiation of motion: Proc. Amer. Soc. Civil Eng., Jour. Hyd. Div., v. 92, pp. 291 - 314.

Costello, W.R., 1974, Development of bed configurations in coarse sands: Unpub. Ph.D. thesis, Mass. Inst. Techn., report 74-1, 119 p.

Crosby, D.G., 1962, Wolfeville map-area, Nova Scotia (21 H 1): Geol. Survey Can., Mem. 325, 67 p.

Culbertson, J.K. and Scott, C.H., 1970, Sandbar development and movement in an alluvial channel, Rio Grande near Bernado, New Mexico: U.S. Geol. Survey Prof. Paper 700-B, pp. 237 - 241.

Dalrymple, R.W., 1973, Sediment texture and transport studies in an intertidal environment: a progress report: Maritime Sed., v. 9, pp. 45 - 58.

________, 1977, Sediment dynamics of macrotidal sand bars, Bay of Fundy: Unpub. Ph.D. thesis, McMaster Univ., 635 p.

________, Knight, R.J. and Middleton, G.V., 1975, Intertidal sand bars in Cobequid Bay (Bay of Fundy): in Cronin, L.E., (ed.), Estuarine Research, v. 2, pp. 293 - 307.

Davies, J.L., 1964, A morphogenetic approach to world shorelines: Zeits. für Geomorph., v. 8, pp. 127 - 142.

Defant, A., 1961, Physical Oceanography: v, 2, Pergamon Press, New York, 598 p.

Dickson, M., 1974, The sieve method of size analysis - an instructional manual: McMaster Univ., Dept. of Geology, Tech. Memo. 74-3, 17 p.

Dolet, M., Giresse, P. and Larsonneur, C., 1965, Sédiments et sédimentation dans la baie du Mont Saint-Michel: Bull. Soc. Linn. Norm., v. 6, pp. 51 - 65.

Duff, G.F.D., 1970, Tidal resonance and tidal barriers in the Bay of Fundy system: Jour. Fish. Res. Bd. Canada, v. 27, pp. 1701 - 1728.

Dyer, K.R., 1973, Estuaries: a physical introduction: John Wiley and Sons, London, 140 p.

Einstein, H.A., 1950, The bed-load function for sediment transportation in open channel flows: U.S. Dept. of Agriculture, Soil Conservation Ser., Tech. Bull. 1026, 71 p.

_________, Anderson, A.G. and Johnson, J.W., 1940, A distinction between bed load and suspended load: Amer. Geophys. Union Trans., 21st Annual Mtg., pp. 628 - 633.

Engelund, F., 1973, Steady transport of moderately graded sediment: Lyngby, Tech. Univ. Denmark, Inst. Hydrodynamics and Hydraulic Engineering, Prog. Rept. No. 29, pp. 3 - 12.

_________ and Hansen, E., 1967, A monograph on sediment transport in alluvial streams: Teknisk Vorlag, Copenhagen, 62 p.

Evans, G., 1965, Intertidal flat sediments and their environments of deposition in the Wash: Geol. Soc. London, Quart. Jour., v. 121, 209 - 245.

Finley, R.J., 1975, Hydrodynamics and tidal deltas of North Inlet, South Carolina: in Cronin, L.E., (ed.), Estuarine Research, v. 2, pp. 277 - 291.

Folk, R.L., 1974, Petrology of sedimentary rocks: Hemphill Pub. Co., Austin, Texas, 182 p.

________ and Ward, W.C., 1957, Brazos River bar: a study in the significance of grain size parameters: Jour. Sed. Petrology, v. 27, pp. 3 - 27.

Francis, J.R.D., 1973, Experiments on the motion of solitary grains along the bed of a water-stream: Proc. Roy. Soc. London, Series A, v. 332, pp. 443 - 471.

Freeman, J.C., Jr., Baer, L. and Jung, G.H., 1957, The bathystrophic storm tide: Jour. Mar. Res., v. 16, pp. 12 - 22.

Friedman, G.M., 1961, Distinction between dune, beach, and river sands from their textural characteristics: Jour. Sed. Petrology, v. 31, pp. 514 - 529.

Fuller, A.D., 1961, Size distribution characteristics of shallow marine sands from the Cape of Good Hope, South Africa: Jour. Sed. Petrology, v. 31, pp. 256 - 261.

Garrett, C., 1972, Tidal resonance in the Bay of Fundy, Gulf of Maine: Nature, v. 238, pp. 441 - 443.

Gee, D.M., 1975, Bedform response to unsteady flows: Proc. Amer. Soc. Civil Eng., Jour. Hyd. Div., v. 101, pp. 437 - 449.

Graf, W.H. and Acaroglu, E.R., 1966, Settling velocities of natural grains: International Assoc. Sci. Hydrology, v. 11, pp. 27 - 43.

Grant, D.R., 1970, Recent coastal submergence of the Maritime Provinces, Canada: Can. Jour. Earth Sci., v. 7, pp. 676 - 689.

Green, C.D., 1975, A study of hydraulics and bedforms at the mouth of the Tay estuary, Scotland: in Cronin, L.E., (Ed.), Estuarine Research, v. 2, pp. 323 - 344.

Greenberg, D., 1975, The effects of tidal power development on the physical oceanography of the Bay of Fundy and Gulf of Maine: Acadia Univ. Inst., Workshop on Environmental Implications of Fundy Tidal Power, 45 p.

Greenwood, B. and Davidson-Arnott, R.D.G., 1972, Quarternary coastline of the Maritime Provinces of Canada: history and sedimentation - a summary and selected bibliography: Maritime Sed., v. 8, pp. 98 - 100.

Griffiths, J.C., 1967, Scientific method in analysis of sediments: McGraw-Hill, New York, 508 p.

Harleman, D.R.L., 1966, Real estuaries: in Ippen, A.T., (ed.), Estuary and Coastline Hydrodynamics, McGraw-Hill, New York, pp. 522 - 545.

Harms, J.C., 1969, Hydraulic significance of some sand ripples: Geol. Soc. Amer. Bull., v. 80, pp. 363 - 396.

________ and Fahnestock, R.K., 1965, Stratification, bed forms, and flow phenomena (with an example from the Rio Grande): in Middleton, G.V., (ed.), Primary Sedimentary Structures and their Hydrodynamic Interpretation, Soc. Econ. Paleont. Mineralogists Spec. Pub. 12, pp. 84 - 115.

Hayes, M.O., 1975, Morphology of sand accumulation in estuaries: an introduction to the symposium: in Cronin, L.E., (ed.), Estuarine Research, v. 2, pp. 3 - 22.

________, Owens, E.H., Hubbard, D.K. and Abele, R.W., 1973, Investigation of form and processes in the coastal zone: in Coates, D.R., (ed.), Coastal Geomorphology, Proceedings of 3rd Annual Geomorphology Symposium Series, Binghamton, New York, pp. 11 - 41.

Hine, A.C., 1975, Bedform distribution and migration patterns on tidal deltas in the Chatham Harbor estuary, Cape Cod, Massachusetts: in Cronin, L.E., (ed.), Estuarine Research, v. 2, pp. 235 - 252.

Houbolt, J.J.H.C., 1968, Recent sediments in the southern bight of the North Sea: Geol. en Mijnbouw, v. 47, pp. 245 - 273.

Hubbard, D.K., 1975, Morphology and hydrodynamics of the Merrimack River ebb-tidal delta: in Cronin, L.E., (ed.), Estuarine Research, v. 2, pp. 253 - 266.

Inman, D.L., 1949, Sorting of sediments in the light of fluid mechanics: Jour. Sed. Petrology, v. 19, pp. 51 - 70.

________, 1952, Measures for describing the size distribution of sediments: Jour. Sed. Petrology, v. 22, pp. 125 - 145.

________, 1963, Sediments: physical properties and mechanics of sedimentation: in Shepard, F.P., Submarine Geology, Harper and Row, New York, pp. 101 - 151.

Jackson, R.G., 1976a, Depositional model of point bars in the lower Wabash River: Jour. Sed. Petrology, v. 46, pp. 579 - 594.

________, 1976b, Largescale ripples of the lower Wabash River: Sedimentology, v. 23, pp. 593 - 623.

Kachel, N.B. and Sternberg, R.W., 1971, Transport of bedload as ripples during an ebb current: Marine Geol., v. 10, pp. 229 - 244.

Kalinske, A.A., 1943, Turbulence and the transport of sand and silt by wind: N.Y. Acad. Sci. Annals, v. 44, pp. 41 - 54.

Karcz, I., 1972, Sedimentary structures formed by flash floods in southern Israel: Sed. Geol., v. 7, pp. 161 - 182.

Kerr, P.F., 1959, Optical mineralogy: McGraw-Hill, New York, 442 p.

Kindle, E.M., 1917, Recent and fossil ripple marks: Geol. Survey Can. Museum Bull., v. 25, pp. 1 - 56.

Klein, G. de Vries, 1963, Bay of Fundy intertidal zone sediments: Jour. Sed. Petrology, v. 33, pp. 844 - 854.

________, 1964, Sedimentary facies in Bay of Fundy intertidal zone, Nova Scotia, Canada: in van Straaten, L.M.J.U., (ed.), Deltaic and Shallow Marine Deposits, Developments in Sedimentology, v. 1, Amsterdam, Elsevier Publ., pp. 193 - 199.

________, 1968a, Intertidal zone sedimentation, Minas Basin north shore, Bay of Fundy, Nova Scotia: Ocean Sci. and Engineering of the Atlantic Shelf, Trans. of the National Symposium, Philadelphia, pp. 91 - 107.

________, 1968b, Report on advanced science seminar on intertidal zone sedimentation, Minas Basin, Bay of Fundy, Nova Scotia, Canada, July 6 to August 11, 1968: Maritime Sed., v. 4, pp. 52 - 56.

________, 1970, Depositional and dispersal dynamics of intertidal sand bars: Jour. Sed. Petrology, v. 40, pp. 1095 - 1127.

Klein, G. de Vries and Whaley, M.L., 1972, Hydraulic parameters controlling bedform migration on an intertidal sand body: Geol. Soc. Amer. Bull., v. 83, pp. 3465 - 3470.

Knight, R.J., 1971, Cobequid Bay sedimentology project - a progress report: Maritime Sed., v. 7, pp. 33 - 37.

_________, 1972, Cobequid Bay sedimentology project - a progress report: Maritime Sed., v. 8, pp. 45 - 60.

_________, 1977, Sediments, bedforms, and hydraulics in a macrotidal environment, Cobequid Bay (Bay of Fundy), Nova Scotia: Unpub. Ph.D. thesis, McMaster Univ., 693 p.

_________ and Dalrymple, R.W., 1975, Intertidal sediments from the south shore of Cobequid Bay, Bay of Fundy, Nova Scotia, Canada: in Ginsburg, R.N., (ed.), Tidal Deposits, Springer Verlag, New York, pp. 47 - 55.

_________ and _________, 1976, Winter conditions in a macrotidal environment, Cobequid Bay, Nova Scotia: Rev. Geog. Montr., v. 30, pp. 65 - 86.

Komar, P.D., 1976, Beach Processes and Sedimentation: Prentice-Hall, Englewood Cliffs, New Jersey, 429 p.

Kulm, L.D. and Byrne, J.V., 1967, Sediments of Yaquima Bay, Oregon: in Lauff, G.H., (ed.), Estuaries: Amer. Assoc. Adv. Sci. Pub. No. 83, pp. 226 - 238.

Land, L. S. and Hoyt, J.H., 1966, Sedimentation in a meandering estuary, Sedimentology, v. 6, pp. 191 - 207.

Larsonneur, G., 1975, Tidal deposits, Mont Saint-Michel Bay, France: in Ginsburg, R.N., (ed.), Tidal Deposits, Springer Verlag, New York, pp. 21 - 30.

Ludwick, J.C., 1974, Tidal currents and zig-zag sand shoals in a wide estuary entrance: Geol. Soc. Amer. Bull., v. 85, pp. 717 - 726.

MacMillan, D.H., 1966, Tides: American Elsevier, New York, 240 p.

McQuivey, R.S., 1973, Summary of turbulence data from rivers, conveyance channels, and laboratory flumes: U.S. Geol. Survey Prof. Paper 802-B, 66 p.

Meade, R.H., 1969, Landward transport of bottom sediments in estuaries of the Atlantic coastal plain: Jour. Sed. Petrology, v. 39, pp. 222 - 234.

Mercer, A.G., 1971, Analysis of alluvial bed forms: in Shen, H.W., (ed.), River Mechanics, v. 1, pp. 10-1 - 10-26.

Middleton, G.V., 1972, Brief field guide to intertidal sediments, Minas Basin, Nova Scotia: Maritime Sed., v. 8, pp. 114 - 122.

________, 1976, Hydraulic interpretation of sand size distributions: Jour. Geology, v. 84, pp. 405 - 426.

Middleton, G.V., Knight, R.J. and Dalrymple, R.W., 1976, Facies models for macrotidal environment, Cobequid Bay, Nova Scotia: Abstracts, Amer. Assoc. Petroleum Geologists Annual Meeting, New Orleans, pp. 90 - 91.

Milliman, J.D. and Emery, K.O., 1968, Sea levels during the past 35,000 years: Science, v. 162, pp. 1121 - 1123.

Moss, A.J., 1962, The physical nature of common sandy and pebbly deposits, part I: Amer. Jour. Sci., v. 260, pp. 337 - 373.

________, 1963, The physical nature of common sandy and pebbly deposits, part II: Amer. Jour. Sci., v. 261, pp. 297 - 343.

________, 1972, Initial fluviatile fragmentation of granitic quartz: Jour. Sed. Petrology, v. 42, pp. 905 - 916.

Oertel, G.F., 1972, Sediment transport on estuary entrance shoals and the formation of swash platforms: Jour. Sed. Petrology, v. 42, pp. 858 - 863.

________, 1973, Examination of textures and structures of mud in layered sediments at the entrance of a Georgia tidal inlet: Jour. Sed. Petrology, v. 43, pp. 33 - 41.

________, 1975, Ebb-tidal deltas of Georgia estuaries: in Cronin, L.E., (ed.), Estuarine Research, v. 2, pp. 267 - 276.

Oomkens, E. and Terwindt., J.H.J., 1960, Inshore estuarine sediments in the Haringvliet (Netherlands): Geol. en Mijnbouw, v. 39, pp. 701 - 710.

Passega, R., 1964, Grain size representation by CM patterns as a geological tool: Jour. Sed. Petrology, v. 34, pp. 830 - 847.

Pelletier, B.R. and McMullen, R.M., 1972, Sedimentary patterns in the Bay of Fundy and Minas Basin: in Gray, T.J. and Gashus, O.K., (eds.), Tidal Power, Plenum Press, New York, pp. 153 - 187.

Philopponneau, M., 1956, La baie du Mont Saint-Michel: Mem. Soc. Geol. Min. Bretagne, v. 11, pp. 7 - 65.

Postma, H., 1961, Transport and accumulation of suspended matter in the Dutch Wadden Sea: Netherlands Jour. Sea Res., v. 1, pp. 148 - 190.

Prest, V.K. and Grant, D.R., 1969, Retreat of the last ice sheet from the Maritime Provinces - Gulf of St. Lawrence region: Geol. Survey Can. Paper 69 - 33, 15 p.

Pritchard, D.W., 1967, What is an estuary: physical viewpoint: in Lauff, G.H., (ed.), Estuaries, Amer. Assoc. Adv. Sci. Pub. No. 83, pp. 3 - 5.

Pritchard, D.W. and Carter, H.H., 1971, Estuarine circulation patterns: in Schubel, J.R., (ed.), The Estuarine Environment - Estuaries and Estuarine Sedimentation, Amer. Geol. Inst. Short Course Notes, pp. IV-1 - IV-17.

Rao, D.B., 1968, Natural oscillations of the Bay of Fundy: Jour. Fish. Res. Bd. Canada, v. 25, pp. 1097 - 1114.

Raudkivi, A.J., 1967, Loose boundary hydraulics: Pergamon Press, New York, 331 p.

Reineck, H.-E., 1967, Layered sediments of tidal flats, beaches, and shelf bottoms of the North Sea: in Lauff, G.H., (ed.), Estuaries, Amer. Assoc. Adv. Sci. Pub. No. 83, pp. 191 - 206.

________ and Wunderlich, F., 1968, Classification and origin of flaser and lenticular bedding: Sedimentology, v. 11, pp. 99 - 105.

Robinson, A.H.W., 1960, Ebb-flood channel systems in sandy bays and estuaries: Geography, v. 45, pp. 183 - 199.

Schou, A., 1967, Estuarine research in the Danish moraine archipelago: in Lauff, G.H., (ed.), Estuaries, Amer. Assoc. Adv. Sci. Pub. No. 83, pp. 129 - 145.

Schubel, J.R., (ed.), 1971, The estuarine environment - estuaries and estuarine sedimentation: Amer. Geol. Inst. short course notes.

Seward-Thompson, B.L. and Hails, J.R., 1973, An appraisal of the computation of statistical parameters in grain size analysis: Sedimentology, v. 20, pp. 161 - 170.

Shea, J.H., 1974, Deficiencies of clastic particles of certain sizes: Jour. Sed. Petrology, v. 44, pp. 985 - 1003.

Shen, H.W., 1971, Wash load and bed load: in Shen, H.W. (ed.), River Mechanics, pp. 11-1 - 11-30.

Shields, A., 1936, Application of similarity principles and turbulence research to bed-load movement: Translated by Ott, W.P. and Van Uchelen, J.C., U.S. Dept. Agriculture, Soil Cons. Ser. Coop. Lab., Calif. Inst. Tech., 42 p.

Simons, D.B. and Richardson, E.V., 1961, Forms of bed roughness in alluvial channels: Proc. Amer. Soc. Civil Eng., Jour. Hyd. Div., v. 87, pp. 87 - 105.

________ and ________, 1962, The effect of bed roughness on depth - discharge relations in alluvial channels: U.S. Geol. Survey Water Supply Paper 1498-E, 26 p.

________ and ________, 1971, Flow in alluvial sand channels: in Shen, H.W., (ed.), River Mechanics, v. 1, pp. 9-1 - 9-89.

________, ________ and Nordin, C.F., Jr., 1965a, Sedimentary structures generated by flow in alluvial channels: in Middleton, G.V. (ed.), Primary Sedimentary Structures and their

Hydrodynamic Interpretation, Soc. Econ. Paleont. and Mineralogists Spec. Pub. 12, pp. 34 - 52.

Simons, D.B., Richardson, E.V. and Nordin, C.F., Jr., 1965b, Bedload equation for ripples and dunes: U.S. Geol. Survey Prof. Paper 462-H, 9 p.

Smith, J.D., 1969, Geomorphology of a sand ridge: Jour. Geol., v. 77, pp. 39 - 55.

Smith, N.D., 1971, Transverse bars and braiding in the lower Platte River, Nebraska: Geol. Soc. Amer. Bull., v. 82, pp. 3407 - 3420.

Southard, J.B., 1971, Representation of bed configurations in depth - velocity - size diagrams: Jour. Sed. Petrology, v. 41, pp. 903 - 915.

________, 1975, Bed Configurations: in Depositional Environments as interpreted from primary sedimentary structures and stratification sequences, chapter 2, Short Course No. 2, Soc. Econ. Paleont. and Mineral., Dallas, Texas.

________ and Boguchwal, L.A., 1973, Flume experiments on the transition from ripples to lower flat bed with increasing sand size: Jour. Sed. Petrology, v. 43, pp. 1114 - 1121.

Spencer, D.W., 1963, The interpretation of grain size distribution curves of clastic sediments: Jour. Sed. Petrology, v. 33, pp. 180 - 190.

Sternberg, R.W., 1966, Boundary layer observations in a tidal current: Jour. Geophys. Res., v. 71, 11. 2175 - 2178.

________, 1967, Measurements of sediment movement and ripple migration in a shallow marine environment: Marine Geol., v. 5, pp. 195 - 205.

________, 1968, Friction factors in tidal channels with differing roughness: Marine Geol., v. 6, pp. 243 - 260.

________, 1971, Measurements of insipient motion of sediment particles in the marine environment: Marine Geol., v. 10, pp. 113 - 119.

Streeter, V.L., 1971, Fluid mechanics: McGraw-Hill, New York, 755 p.

Swift, D.J.P. and McMullen, R.M., 1968, Preliminary studies of intertidal sand bodies in Minas Basin, Bay of Fundy, Nova Scotia: Can. Jour. Earth Sci., v. 5, pp. 175 - 183.

________, ________ and Lyall, A.K., 1967, A tidal delta with an ebb-flood channel system in the Minas Basin, Bay of Fundy: preliminary report: Maritime Sed., v. 3, pp. 12 - 16.

Tanner, W.F., 1959, Sample components obtained by the method of differences: Jour. Sed. Petrology, v. 29, pp. 408 - 411.

________, 1964, Modification of sediment size distributions: Jour. Sed. Petrology, v. 34, pp. 156 - 164.

Tee, K.T., 1975, Tide induced residual currents in Minas Channel and Minas Basin: Unpub. Ph.D. thesis, Dalhousie Univ.

Terwindt, J.H.J., 1971, Sand waves in the southern bight of the North Sea: Marine Geol., v. 10, pp. 51 - 67.

Todd, T.W., 1968, Dynamic diversion - influence of longshore current tidal flow interaction on chenier and barrier island plains: Jour. Sed. Petrology, v. 38, pp. 734 - 746.

Toffaleti, F.B., 1969, Definitive computations of sand discharge in rivers: Proc. Amer. Soc. Civil Eng., Jour. Hyd. Div., v. 95, pp. 225 - 248.

Trask, P.D., 1930, Mechanical analysis of sediments by centrifuge: Econ. Geol., v. 25, pp. 581 - 599.

Trescott, P.C., 1969, Groundwater resources and hydrogeology of the Windsor - Hantsport - Walton area, Nova Scotia: Nova Scotia Dept. of Mines, Groundwater Section, Report 69 - 2, 58 p.

Tricker, R.A.R., 1964, Bores, breakers, waves, and wakes: American Elsevier, New York, 250 p.

Vanoni, V.A., 1974, Factors determining bedforms of alluvial streams: Proc. Amer. Soc. Civil Eng., Jour. Hyd. Div., v. 100, pp. 363 - 377.

van Straaten, L.M.J.U. and Kuenen, Ph.H., 1957, Accumulation of fine grained sediment in the Dutch Wadden Sea: Geol. en Mijnbouw, v. 19, pp. 329 - 354.

van Veen, J., 1950, Eb-en Vloedschaar systemen in de Nederlandse getijwatern: Tijdechr. Koninkl. Ned. Aardryksk Gen. Amsterdam Waddensymposium, Groningen, Netherlands.

Visher, G.S., 1969, Grain size distributions and depositional processes: Jour. Sed. Petrology, v. 39, pp. 1074 - 1106.

_________ and Howard, J.D., 1974, Dynamic relationship between hydraulics and sedimentation in the Altamaha estuary: Jour. Sed. Petrology, v. 44, pp. 502 - 521.

Walker, R.G., 1965, The origin and significance of the internal sedimentary structures of turbidites: Proc. Yorkshire Geol. Soc., v. 33, pp. 1 - 29.

Weast, R.C., 1973, Handbook of Chemistry and Physics; 54th Edition: C.R.C. Press, Cleveland, Ohio, p. F - 68.

Wentworth, C.K., 1922, A scale of grade and class terms for clastic sediments: Jour. Geol., v. 30, pp. 377 - 392.

White, W.R., Milli, H. and Crabbe, A.D., 1975, Sediment transport theories: a review: Proc. Inst. Civ. Engr., v. 59, pp. 265 - 292.

White, W.R., Milli, H. and Crabbe, A.D., 1976, Sediment transport theories: a review - discussion: Proc. Inst. Civ. Engrs., v. 61, pp. 207 - 227.

Wright, L.D., Coleman, J.M. and Thom, B.G., 1973, Processes of channel development in a high-tide-range environment: Cambridge Gulf - Ord River Delta, Western Australia: Jour. Geol., v. 81, pp. 15 - 41.

________, ________ and ________, 1975, Sediment transport and deposition in a macrotidal river channel: Ord River, Western Australia: in Cronin, L.E., (ed.), Estuarine Research, v. 2, pp. 309 - 321.

________ and Sonu, C.J., 1975, Processes of sediment transport and tidal delta development in a stratified tidal inlet: in Cronin, L.E., (ed.), Estuarine Research, v. 2, pp. 63 - 76.

Yalin, M.S., 1972, Mechanics of sediment transport: Pergamon Press, New York, 290 p.

Yuen, K.B., 1969, Effect of tidal barriers upon the M_2 tide in the Bay of Fundy: Jour. Fish. Res. Bd. Canada, v. 26, pp. 2477 - 2492.

APPENDIX A: ECHO SOUNDING AND SURVEYING METHODS

Echo Sounding

Soundings were made using a Furuno 200A echo sounder; this model provides a continuous depth record. The transducer was mounted over the side of the 4.4 m Crosby Sled used for field work; it was placed as near amidships as possible to reduce interference caused by surface waves. Ship speed was kept as constant and as slow as possible to obtain maximum detail.

Traverses were run parallel and perpendicular to the river system; locations of all runs are shown in Figure A-1. Horizontal sextant sightings were used to locate the traverse positions. Sightings were made at the beginning and end of each traverse as well as at several intermediate points that were marked on the record.

Locations were plotted by assuming constant ship speed between sightings and linearly interpolating the record over the calculated distance. A correction was made for water level by relating the high tide level on each day to the Canadian Hydrographic Service bench mark on the government wharf at Hantsport (BM 1, 1969, 0.55 m above higher high water). Each traverse was corrected relative

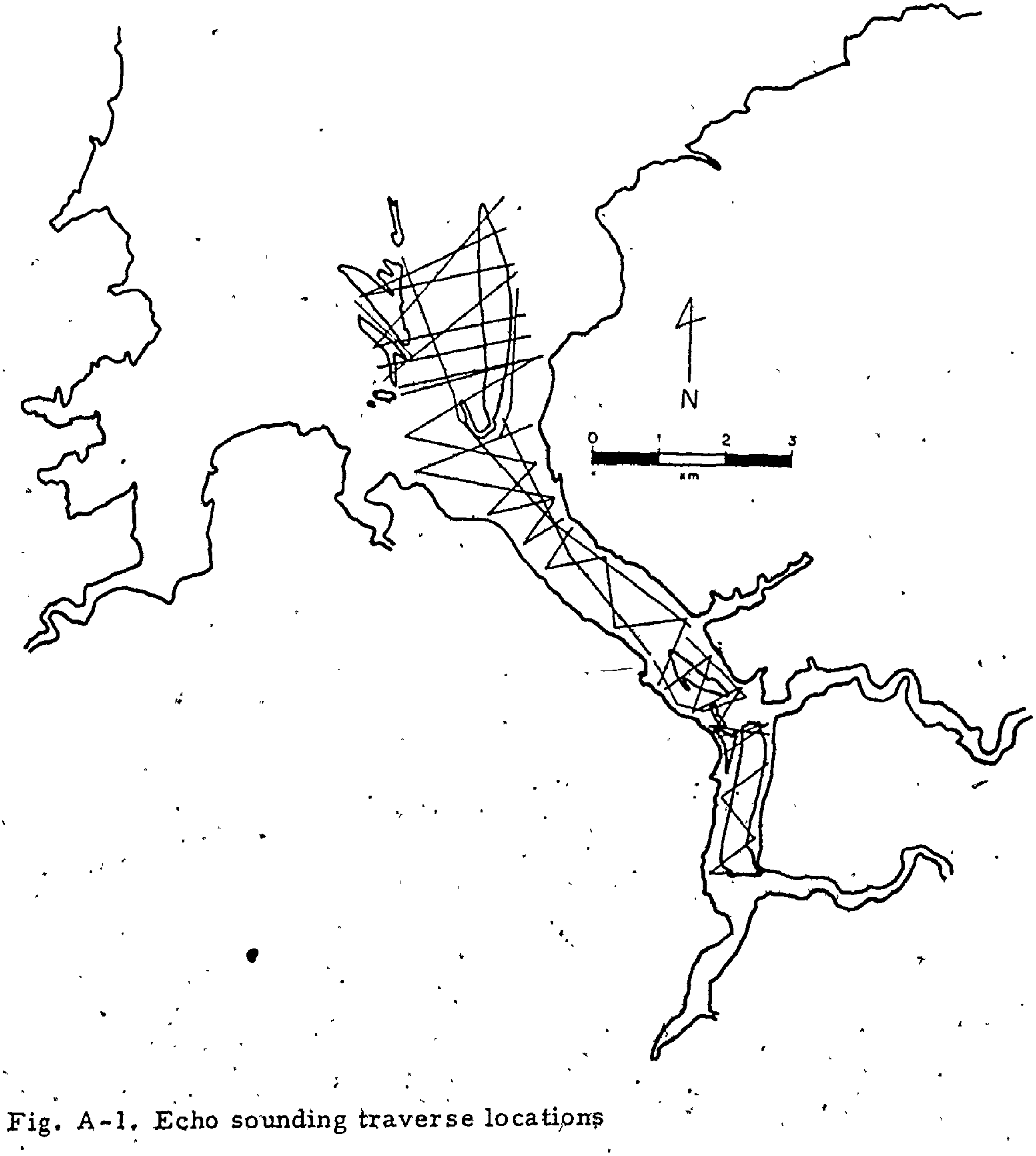

Fig. A-1. Echo sounding traverse locations to that day's high water level by estimating water level position at the beginning and end of the traverse and linearly interpolating the record. Water levels were estimated from tidal curves for days of similar tidal range at stations near the traverse locations. Thus, all the records were adjusted to a common base; the bathymetric map (see Fig. 2-7) was constructed from the adjusted echo sounding records.

Surveying

Sand bodies were surveyed using a Wilde NA2 level, a Wilde T2 theodolite, a metric stadia rod, and a compass. The procedure used in surveying a sand body was as follows:

The initial instrument position was located by horizontal sextant sightings; it was usually chosen to be near the sand body crest. Many points were surveyed in all directions; if no obvious slope change existed in a given direction the points were more greatly spaced than in other areas. For each point, the position of the upper and lower stadia marks, the center line, and the compass bearing from the instrument to the stadia rod were recorded. Points were surveyed to the maximum readable distance in several directions from each instrument position; the instrument was then moved and a backsight made to the last stadia rod position. This process was continued until the entire sand body was surveyed. If a sand body could not be completed in one day, a stake was left and surveying resumed at that point on the next day. 113 points were surveyed on Middle Ground, 34 on Boot Island Bar, and 78 on Western Bar; 36 sightings were taken on Mitchener Bar while Hantsport Bar had 61 and Newport Bar 147.

Newport Bar, Mitchener Bar, and Hantsport Bar were linked by sighting from one sand body to another. Two-way radios were used to aid in reading the stadia marks over such long distances. Hantsport Bar was tied in to the Canadian Hydrographic Service bench mark on the government wharf at Hantsport (BM 1, 1969, 0.55 m above higher high water) by sighting to the wharf and measuring the vertical distance to the bench mark. Boot Island Bar and Western Bar were linked in the same manner as the sand bodies at the head of the estuary, and Boot Island Bar was tied in to Canadian Hydrographic Service Post 5361 on Boot Island (2.79 m above higher high water) by surveying from the sand body to the post.

Middle Ground is too far from shore or any other sand body to be tied in by surveying. It was assumed that on an east-west line between Middle Ground and Western Bar the water surface was level. Using two-way radios, stakes were placed simultaneously at the water's edge on both sand bodies. These points were then tied in to other points on each sand body.

Contour maps were made from surveying data by plotting the initial point on a sand body and locating the other points relative to it. Distances were calculated by the formulae $(U_p - L).(4.07 \times 10^2)$ cm for the level and $(U_p - L).(1.014 \times 10^2)$ cm for the theodolite where U_p and L are the upper and lower stadia readings in cm respectively. Calculated distances were plotted on the appropriate bearings after the magnetic declination of 22° had been subtracted from the measured values. Linear interpolation of elevations was used to determine where a contour crossed a surveyed line.

APPENDIX B: MEASUREMENT OF CURRENT VELOCITY, WATER TEMPERATURE, AND SALINITY, AND ESTIMATION OF FRESH WATER INPUT

Measurement of Current Velocity, Water Temperature, and Salinity

Currents were measured using an Endeco Type 110 direct reading current meter; speeds are measured by electrical induction generated by an impellor and direction is measured with an internal compass. Speed is read in knots on a 0 to 5 scale with an accuracy of ±0.15 knots (±0.08 m/s) and direction is read in degrees with ±7.2° accuracy. Each current station was occupied for a complete tidal cycle; stations were located with horizontal sextant sightings. A reading was taken of current speed and direction with the meter at the water surface, the meter was lowered 0.91 m and speed and direction were recorded again. This was continued until the ballast weights on the meter struck bottom yielding an "instantaneous" vertical velocity profile; five to ten minutes were required to complete a profile at high tide. A vertical profile was measured each half hour for the thirteen hours that the station was occupied. All current measurements are presented in Table B-1.

Water temperature was measured with a direct reading thermometer within the Endeco Type 110 current meter. The scale was marked in degrees Celsius and was accurate to 0.2 °C. Temperature readings were taken concurrently with current speed, direction, and depth to the meter yielding vertical temperature profiles for every half hour of each measured tidal cycle. The thermometer was not always functioning properly; temperature was not measured during all tidal cycles.

Salinity was measured with a Beckman RS5 salinometer; this instrument measures salinity as a function of conductivity. Salinity is read in 0.01 parts per thousand. The salinometer probe was attached to the Endeco Type 110 current meter so that it would not interfere with operation of the meter. Vertical salinity profiles were recorded at the same time as current and temperature profiles. The salinometer was not available often; only 3 salinity stations could be recorded. All water temperature and salinity measurements are presented in Table B-2.

Estimation of Fresh Water Input

Fresh water input was estimated by stream gauging and from drainage basin measurements plus rainfall - runoff ratios of nearby rivers. Discharges were measured of the three major rivers flowing into the Avon River estuary, the Avon, the Kennetcook, and the St. Croix. The St. Croix and its major tributary, the Herbert, were each gauged with a Stevens A-71 stage recorder. The stage recorder is designed to record water surface level continuously; it was placed far enough upstream to eliminate tidal influence.

Problems were encountered in gauging both rivers. Vandals tampered with the stage recorder after ten months of operation on the St. Croix River; it was not re-installed. Also, few calibrations of current speed to water level were made on the St. Croix. The Herbert River was gauged successfully for only six months as ice buildup damaged the float causing termination of measurements. The operational period on the St. Croix River was August, 1974 to June, 1975 and August, 1975 to February, 1976 on the Herbert.

The Kennetcook River was gauged by Bedford Institute of Oceanography for the period August to December, 1975 and May to July, 1976. Water surface level was read from a permanently emplaced staff and calibrated with current velocity measurements. Discharge from the Avon River was estimated from Nova Scotia Department of Agriculture records for the period January, 1975 to December 31, 1975; their records are not of discharge but times when the sluice gate in the causeway at Windsor is open. The gate usually was opened long enough to allow a drop in water level of 1.3 m; 10% was added to the discharge estimates to account for leakage through the causeway (D.C. Milligan, 1976, personal communication). Discharge estimates from gauging on the St. Croix, Herbert, and Kennetcook Rivers plus estimates for the Avon River are presented in Table 3-1.

Drainage basin area of the Avon River, the St. Croix River, and the Kennetcook River was obtained from Montreal Engineering Co.; drainage area of the Cogmagun River was measured from topographic maps. Rainfall - runoff ratios were calculated for the Salmon River and the Annapolis River (see Fig. 2-1) (data from Canada Department of the Environment, Water Resources Branch, 1974); runoff per km^2 of drainage basin was computed. Assuming an equivalent rainfall - runoff ratio for the Avon River system, runoff per km^2 was calculated using rainfall data from Trescott (1969). Discharges estimated from drainage basin area and rainfall - runoff ratios are listed in Table 3-1.

TABLE B-1. Current Measurements

The following pages list all raw current velocity data. The name of the station, date of occupation, low and high tide heights (m), tidal coefficients, and the time of high tide (hours and minutes) are given for each day. Time relative to high tide (hours and hundredths; negative values are hours before high tide, positive values are hours after high tide), water depth (m), current speed (m/s), and direction (degrees from true north) are listed for each profile. All current stations are located on Figure 3-2.

```
BOOT ISLAND........1...  1  DATE - 22/ 7/75

      TIDAL HEIGHTS                        TIDAL COEFFICIENTS
       HIGH = 12.7     TIME - 1301.         EBB   = .7
       LOW  = [illegible]                   FLOOD = .7
       HIGH = 13.[illegible]

TIME                    TIME                    TIME                    TIME                    TIME
 DEPTH  SPEED  DIR       DEPTH  SPEED  DIR       DEPTH  SPEED  DIR       DEPTH  SPEED  DIR       DEPTH  SPEED  DIR
-6.17                   -5.67                   -5.17                   -4.67                   -4.17
  .25  [illegible]      .25   .077   171.        .2[illegible]          [illegible]             [illegible]
-3.67                   -3.17                   -2.67                   -2.17                   -1.67
  [illegible]           [illegible]             [illegible]             [illegible]             [illegible]
-1.17                   -.67                    -.17                    .33                     .83
  [illegible]           [illegible]             [illegible]             [illegible]             [illegible]


BOOT ISLAND........1...  1  DATE - 22/ 7/75

TIME                    TIME                    TIME                    TIME                    TIME
 DEPTH  SPEED  DIR       DEPTH  SPEED  DIR       DEPTH  SPEED  DIR       DEPTH  SPEED  DIR       DEPTH  SPEED  DIR
1.33                    1.83                    2.33                    2.83                    3.33
  [illegible]           [illegible]             [illegible]             [illegible]             [illegible]
3.83                    4.33                    4.83                    5.33                    5.83
  [illegible]           [illegible]             [illegible]             .25  [illegible]        .25  [illegible]
6.33
  .25   .203  192.


BOOT ISLAND........2...  1  DATE - 29/ 8/75

      TIDAL HEIGHTS                        TIDAL COEFFICIENTS
       HIGH = 13.[illegible]  TIME - 1916.  EBB   = .77
       LOW  = [illegible]                   FLOOD = .76
       HIGH = [illegible]

TIME                    TIME                    TIME                    TIME                    TIME
 DEPTH  SPEED  DIR       DEPTH  SPEED  DIR       DEPTH  SPEED  DIR       DEPTH  SPEED  DIR       DEPTH  SPEED  DIR
-5.25                   -4.75                   -4.25                   -3.75                   -3.25
  [illegible]           .2[illegible]           .2[illegible]           [illegible]             [illegible]
-2.75                   -2.25                   -1.75                   -1.25                   -.75
  [illegible]           [illegible]             [illegible]             [illegible]             [illegible]
-.25                    .25                     .75                     1.25                    1.75
  [illegible]           [illegible]             [illegible]             [illegible]             [illegible]
```

```
[illegible] . . . . [illegible]  DATE = [illegible]

TIME                   TIME                   TIME                   TIME                   TIME
 DEPTH  SPEED  DIR      DEPTH  SPEED  DIR      DEPTH  SPEED  DIR      DEPTH  SPEED  DIR      DEPTH  SPEED  DIR
[illegible]            [illegible]            [illegible]            [illegible]

 [illegible]           [illegible]            [illegible]            [illegible]


[illegible] . . . . . . . [illegible]  DATE = [illegible]

      TIDAL HEIGHTS                          TIDAL COEFFICIENTS
        HIGH = [illegible]   TIME = [illegible]
        LOW  = [illegible]                   [illegible]
        HIGH = 12.0                          [illegible]

TIME                   TIME                   TIME                   TIME                   TIME
 DEPTH  SPEED  DIR      DEPTH  SPEED  DIR      DEPTH  SPEED  DIR      DEPTH  SPEED  DIR      DEPTH  SPEED  DIR
-10.17                 -9.67                  -9.17                  -8.67                  -8.17

 [illegible]           [illegible]            [illegible]            [illegible]             .25  .412  290.

-7.67                  -6.67                  -6.17                  -3.67                  -3.17

  .25  .231  [illegible] [illegible]          [illegible]            [illegible]            [illegible]

-2.67                  -2.17                  -1.67                  -1.17                  -.67

 [illegible]           [illegible]            [illegible]            [illegible]            [illegible]


[illegible] . . . . . . . . . [illegible]  DATE = [illegible]

TIME                   TIME                   TIME                   TIME                   TIME
 DEPTH  SPEED  DIR      DEPTH  SPEED  DIR      DEPTH  SPEED  DIR      DEPTH  SPEED  DIR      DEPTH  SPEED  DIR
-.17                   .33                    .83                    1.33                   1.83

 [illegible]           [illegible]            [illegible]            [illegible]            [illegible]

2.33

 [illegible]


[illegible] . . . . . . .  DATE = [illegible]

      TIDAL HEIGHTS                          TIDAL COEFFICIENTS
        HIGH = [illegible]   TIME = [illegible]
        LOW  = [illegible]                   [illegible]
        HIGH = 12.0                          FLOOD = [illegible]

TIME                   TIME                   TIME                   TIME                   TIME
 DEPTH  SPEED  DIR      DEPTH  SPEED  DIR      DEPTH  SPEED  DIR      DEPTH  SPEED  DIR      DEPTH  SPEED  DIR
-9.92                  -9.42                  -8.92                  -8.42                  -7.92

 [illegible]           [illegible]            [illegible]             .25  .412  283.         .25  .389  283.

-6.42                  -5.42                  -4.92                  -2.92                  -2.42

  .25  .461  [illegible] [illegible]          [illegible]            [illegible]            [illegible]

-1.92                  -1.42                  -.92                   -.42                   .08

 [illegible]           [illegible]            [illegible]            [illegible]            [illegible]
```

[illegible]

[illegible]

TIME DEPTH	SPEED	DIR	TIME DEPTH	SPEED	DIR	TIME DEPTH	SPEED	DIR	TIME DEPTH	SPEED	DIR	TIME DEPTH	SPEED	DIR
[illegible]	[illegible]	[illegible]	[illegible]	[illegible]	[illegible]	[illegible]	[illegible]	[illegible]	[illegible]	[illegible]	[illegible]	[illegible]	[illegible]	[illegible]

[illegible]

TIDAL HEIGHTS — TIDAL COEFFICIENTS

[illegible]

TIME DEPTH	SPEED	DIR	TIME DEPTH	SPEED	DIR	TIME DEPTH	SPEED	DIR	TIME DEPTH	SPEED	DIR	TIME DEPTH	SPEED	DIR
[illegible]	[illegible]	[illegible]	[illegible]	[illegible]	[illegible]	[illegible]	[illegible]	[illegible]	[illegible]	[illegible]	[illegible]	[illegible]	[illegible]	[illegible]

[illegible]

TIME DEPTH	SPEED	DIR	TIME DEPTH	SPEED	DIR	TIME DEPTH	SPEED	DIR	TIME DEPTH	SPEED	DIR	TIME DEPTH	SPEED	DIR
[illegible]	[illegible]	[illegible]	[illegible]	[illegible]	[illegible]	[illegible]	[illegible]	[illegible]	[illegible]	[illegible]	[illegible]	[illegible]	[illegible]	[illegible]

```
[illegible]  DATE - [illegible]

     TIDAL HEIGHTS                  TIDAL COEFFICIENTS
     [illegible]    TIME - [illegible]     [illegible]

TIME                  TIME                  TIME                  TIME                  TIME
DEPTH  SPEED  DIR     DEPTH  SPEED  DIR     DEPTH  SPEED  DIR     DEPTH  SPEED  DIR     DEPTH  SPEED  DIR
[illegible]

[illegible]  DATE - [illegible]

TIME                  TIME                  TIME                  TIME                  TIME
DEPTH  SPEED  DIR     DEPTH  SPEED  DIR     DEPTH  SPEED  DIR     DEPTH  SPEED  DIR     DEPTH  SPEED  DIR
[illegible]

[illegible]  DATE - [illegible]

     TIDAL HEIGHTS                  TIDAL COEFFICIENTS
     [illegible]    TIME - [illegible]     [illegible]

TIME                  TIME                  TIME                  TIME                  TIME
DEPTH  SPEED  DIR     DEPTH  SPEED  DIR     DEPTH  SPEED  DIR     DEPTH  SPEED  DIR     DEPTH  SPEED  DIR
[illegible]
```

```
[illegible]

TIME                  TIME                  TIME                  TIME                  TIME
 DEPTH  SPEED  DIR     DEPTH  SPEED  DIR     DEPTH  SPEED  DIR     DEPTH  SPEED  DIR     DEPTH  SPEED  DIR

[illegible]

[illegible]

TIME                  TIME                  TIME                  TIME                  TIME
 DEPTH  SPEED  DIR     DEPTH  SPEED  DIR     DEPTH  SPEED  DIR     DEPTH  SPEED  DIR     DEPTH  SPEED  DIR

[illegible]

[illegible]

     TIDAL HEIGHTS                          TIDAL COEFFICIENTS
       HIGH = 13.[illegible]   TIME = [illegible]      EBB   = [illegible]
       LOW  = [illegible]                    FLOOD = [illegible]
       HIGH = 13.6

TIME                  TIME                  TIME                  TIME                  TIME
 DEPTH  SPEED  DIR     DEPTH  SPEED  DIR     DEPTH  SPEED  DIR     DEPTH  SPEED  DIR     DEPTH  SPEED  DIR
[illegible]           -7.25                 -6.75                 -6.25                 -5.75

[illegible]                                 .25    .324   283.    .25    .419   293.    .25    .194   263.

[illegible]           -6.75                 [illegible]           -3.75                 -3.25

[illegible]

[illegible]           -2.25                 -1.75                 -1.25                 -.75

[illegible]
```

```
[illegible]  DATE = [illegible]

TIME                  TIME                  TIME                  TIME                  TIME
 DEPTH  SPEED  DIR     DEPTH  SPEED  DIR     DEPTH  SPEED  DIR     DEPTH  SPEED  DIR     DEPTH  SPEED  DIR

-.25                  .25                   .75                   1.25                  1.75
 [illegible]           [illegible]           [illegible]           [illegible]           [illegible]

2.25                  2.75                  3.25                  3.75                  4.25
 [illegible]           [illegible]           [illegible]           [illegible]           [illegible]

4.75
 [illegible]


MIDDLE GROUND 1......  DATE = [illegible]

     FINAL HEIGHTS                      TIDAL COEFFICIENTS
       HIGH = 11.0    TIME = [illegible]     EBB = .69
       LOW  = [illegible]                   FLOOD = .67
       HIGH = 12.6

TIME                  TIME                  TIME                  TIME                  TIME
 DEPTH  SPEED  DIR     DEPTH  SPEED  DIR     DEPTH  SPEED  DIR     DEPTH  SPEED  DIR     DEPTH  SPEED  DIR

-.08                  .42                   .92                   1.42                  1.92
 [illegible]           [illegible]           [illegible]           [illegible]           [illegible]

2.42                  2.92                  3.42                  3.92                  4.42
 [illegible]           [illegible]           [illegible]           [illegible]           [illegible]


MIDDLE GROUND 1......  DATE = [illegible]

TIME                  TIME                  TIME                  TIME                  TIME
 DEPTH  SPEED  DIR     DEPTH  SPEED  DIR     DEPTH  SPEED  DIR     DEPTH  SPEED  DIR     DEPTH  SPEED  DIR

4.92                  5.42                  5.92                  6.42                  6.92
 [illegible]           [illegible]           [illegible]           [illegible]           [illegible]

7.42                  7.92                  8.42                  8.92                  9.42
 [illegible]           [illegible]           [illegible]           [illegible]           [illegible]

9.92                  10.42                 10.92                 11.42                 11.92
 [illegible]           [illegible]           [illegible]           [illegible]           [illegible]
```

```
MIDDLE GROUND 2......  I  DATE = 13/ 8/74

     TIDAL HEIGHTS                         TIDAL COEFFICIENTS
      HIGH = 11.3    TIME =  6130           EBB   =  .87
      LOW  = [illegible]                    FLOOD =  .67
      HIGH = 12.6

TIME                 TIME                 TIME                 TIME                 TIME
 DEPTH  SPEED  DIR    DEPTH  SPEED  DIR    DEPTH  SPEED  DIR    DEPTH  SPEED  DIR    DEPTH  SPEED  DIR

 .17                  .67                 1.17                 1.67                 2.17
 [illegible]          [illegible]          [illegible]          [illegible]          [illegible]

2.67                 3.17                 3.67                 4.17                 4.67
 [illegible]          [illegible]          [illegible]          [illegible]          [illegible]

5.17                 5.67                 6.17                 6.67                 7.17
 [illegible]           .25   .637   26.     .25   .777   16.     .25   .612  189.    [illegible]


MIDDLE GROUND 2......  I  DATE = 13/ 8/74

TIME                 TIME                 TIME                 TIME                 TIME
 DEPTH  SPEED  DIR    DEPTH  SPEED  DIR    DEPTH  SPEED  DIR    DEPTH  SPEED  DIR    DEPTH  SPEED  DIR

7.67                 8.17                 8.67                 9.17                 9.67
 [illegible]          [illegible]          [illegible]          [illegible]          [illegible]

10.17                10.67                11.17                11.67                12.17
 [illegible]          [illegible]          [illegible]          [illegible]          [illegible]


MIDDLE GROUND 2......  I  DATE = 21/ 8/74

     TIDAL HEIGHTS                         TIDAL COEFFICIENTS
      HIGH = 14.2    TIME = 16130           EBB   =  .92
      LOW  = [illegible]                    FLOOD =  .96
      HIGH = 13.8

TIME                 TIME                 TIME                 TIME                 TIME
 DEPTH  SPEED  DIR    DEPTH  SPEED  DIR    DEPTH  SPEED  DIR    DEPTH  SPEED  DIR    DEPTH  SPEED  DIR

-6.67                -6.17                -5.67                -5.17                -4.67
 [illegible]          [illegible]          [illegible]          [illegible]          [illegible]

-4.17                -3.67                -3.17                -2.67                -2.17
 [illegible]          [illegible]          [illegible]          [illegible]          [illegible]
```

```
MIDDLE GROUND 7..........   +  DATE - 21/ 8/76

TIME                    TIME                    TIME                    TIME                    TIME
 DEPTH   SPEED   DIR     DEPTH   SPEED   DIR     DEPTH   SPEED   DIR     DEPTH   SPEED   DIR     DEPTH   SPEED   DIR
-1.67                   -1.17                   -.67                    -.17                    .33
 [illegible]             [illegible]             [illegible]             [illegible]             [illegible]

.83                     1.33                    1.83                    2.33                    2.83
 [illegible]             [illegible]             [illegible]             [illegible]             [illegible]


MIDDLE GROUND 7..........   +  DATE = 21/ 8/76

TIME                    TIME                    TIME                    TIME                    TIME
 DEPTH   SPEED   DIR     DEPTH   SPEED   DIR     DEPTH   SPEED   DIR     DEPTH   SPEED   DIR     DEPTH   SPEED   DIR
3.33                    3.83
 [illegible]             [illegible]


MIDDLE GROUND 6..........   +  DATE - 26/ 6/75

       TIDAL HEIGHTS                          TIDAL COEFFICIENTS
        HIGH = 12.7     TIME - 1[illegible]      EBB   = .7[illegible]
        LOW  =  1.[illegible]                     FLOOD = .78
        HIGH = 13.1

TIME                    TIME                    TIME                    TIME                    TIME
 DEPTH   SPEED   DIR     DEPTH   SPEED   DIR     DEPTH   SPEED   DIR     DEPTH   SPEED   DIR     DEPTH   SPEED   DIR
-8.50                   -8.00                   -7.50                   -7.00                   -5.00
 [illegible]             [illegible]              .25     .[illegible]  [illegible]   .25   .103   [illegible]     .25   .231   130.

-4.50                   -4.00                   -3.50                   -3.00                   -2.50
  .25    .309   [illegible]   [illegible]        [illegible]             [illegible]             [illegible]

-2.00                   -1.50                   -1.00                   -.50                    -.00
 [illegible]             [illegible]             [illegible]             [illegible]             [illegible]


MIDDLE GROUND 6..........   +  DATE - 26/ 6/75

TIME                    TIME                    TIME                    TIME                    TIME
 DEPTH   SPEED   DIR     DEPTH   SPEED   DIR     DEPTH   SPEED   DIR     DEPTH   SPEED   DIR     DEPTH   SPEED   DIR
.42                     .92                     1.42                    1.92                    2.42
 [illegible]             [illegible]             [illegible]             [illegible]             [illegible]

2.92                    3.42                    3.92
 [illegible]             [illegible]             [illegible]
```

```
MIDDLE GROUND ...............   ! DATE = [illegible]

        TIDAL HEIGHTS                              TIDAL COEFFICIENTS
         HIGH = 13.[illegible]   TIME = [illegible]     EBB   = [illegible]
         LOW  = [illegible]                           FLOOD = [illegible]
         HIGH = 12.0

TIME                  TIME                  TIME                  TIME                  TIME
 DEPTH  SPEED  DIR     DEPTH  SPEED  DIR     DEPTH  SPEED  DIR     DEPTH  SPEED  DIR     DEPTH  SPEED  DIR

[illegible]           [illegible]           [illegible]           [illegible]           [illegible]

  .25   [illegible] [illegible]  [illegible] [illegible] [illegible]  [illegible]  [illegible]  [illegible]

[illegible]           [illegible]           [illegible]           [illegible]           [illegible]

  [illegible]

[illegible]           [illegible]           [illegible]           [illegible]           .[illegible]

  [illegible]


MIDDLE GROUND ...............   ! DATE = 23/ 7/75

TIME                  TIME                  TIME                  TIME                  TIME
 DEPTH  SPEED  DIR     DEPTH  SPEED  DIR     DEPTH  SPEED  DIR     DEPTH  SPEED  DIR     DEPTH  SPEED  DIR

 .50                  1.00                  1.50                  2.[illegible]          2.50

  .25   [illegible]     .25   [illegible]     .25   [illegible]     .25   [illegible]     .25   [illegible]

3.00                  3.50                  4.00                  4.50                  5.00

  .25   [illegible]     .25   [illegible]     .25   [illegible]    [illegible]            .25   .231   363.

5.50

  .25   .177   [illegible]


KITCHENER BAY ...............   ! DATE = 17/ [illegible]

        TIDAL HEIGHTS                              TIDAL COEFFICIENTS
         HIGH = 13.[illegible]   TIME = [illegible]     EBB   = [illegible]
         LOW  = [illegible]                           FLOOD = [illegible]
         HIGH = [illegible]

TIME                  TIME                  TIME                  TIME                  TIME
 DEPTH  SPEED  DIR     DEPTH  SPEED  DIR     DEPTH  SPEED  DIR     DEPTH  SPEED  DIR     DEPTH, SPEED  DIR

-2.[illegible]        -[illegible]          -1.[illegible]        -1.33                 -.[illegible]

  [illegible]

-.33                   .17                   .67                  1.17                  1.67

  [illegible]
```

```
[illegible]........ [illegible] DATE = [illegible]

TIME                  TIME                  TIME                  TIME                  TIME
 DEPTH  SPEED  DIR     DEPTH  SPEED  DIR     DEPTH  SPEED  DIR     DEPTH  SPEED  DIR     DEPTH  SPEED  DIR
[illegible]

NEWPORT [illegible]........ [illegible] DATE = [illegible]

    TIDAL HEIGHTS                    TIDAL COEFFICIENTS
     HIGH = [illegible]   TIME = [illegible]    EBB   = [illegible]
     LOW  = [illegible]                         FLOOD = [illegible]
     HIGH = [illegible]

TIME                  TIME                  TIME                  TIME                  TIME
 DEPTH  SPEED  DIR     DEPTH  SPEED  DIR     DEPTH  SPEED  DIR     DEPTH  SPEED  DIR     DEPTH  SPEED  DIR
[illegible]

NEWPORT [illegible]........ [illegible] DATE = [illegible]

    TIDAL HEIGHTS                    TIDAL COEFFICIENTS
     HIGH = 12.6   TIME = [illegible]    EBB   = [illegible]
     LOW  = [illegible]                  FLOOD = [illegible]
     HIGH = 12.7

TIME                  TIME                  TIME                  TIME                  TIME
 DEPTH  SPEED  DIR     DEPTH  SPEED  DIR     DEPTH  SPEED  DIR     DEPTH  SPEED  DIR     DEPTH  SPEED  DIR
[illegible]
```

NEWPORT BAY [illegible] DATE - [illegible]

TIDAL HEIGHTS

TIDAL COEFFICIENTS

EBB

FLOOD

TIME

DEPTH SPEED DIR

[illegible]

NEWPORT BAY [illegible] DATE - [illegible]

TIME

DEPTH SPEED DIR

[illegible]

NEWPORT BAY [illegible] DATE - [illegible]

TIDAL HEIGHTS

TIDAL COEFFICIENTS

EBB

FLOOD

TIME

DEPTH SPEED DIR

[illegible]

```
[illegible] DATE = 12/ 8/76

    TIDAL HEIGHTS                       TIDAL COEFFICIENTS
      HIGH = [illegible]   TIME = [illegible]
      LOW  = [illegible]
      HIGH = [illegible]

TIME                 TIME                 TIME                 TIME                 TIME
 DEPTH SPEED DIR      DEPTH SPEED DIR      DEPTH SPEED DIR      DEPTH SPEED DIR      DEPTH SPEED DIR
[illegible]

[illegible] DATE = 12/ 8/76

TIME                 TIME                 TIME                 TIME                 TIME
 DEPTH SPEED DIR      DEPTH SPEED DIR      DEPTH SPEED DIR      DEPTH SPEED DIR      DEPTH SPEED DIR
[illegible]

[illegible] DATE = 12/ 8/76

    TIDAL HEIGHTS                       TIDAL COEFFICIENTS
      HIGH = [illegible]   TIME = [illegible]   EBB   = [illegible]
      LOW  = [illegible]                        FLOOD = [illegible]
      HIGH = [illegible]

TIME                 TIME                 TIME                 TIME                 TIME
 DEPTH SPEED DIR      DEPTH SPEED DIR      DEPTH SPEED DIR      DEPTH SPEED DIR      DEPTH SPEED DIR
[illegible]

[illegible] DATE = 12/ 8/76

TIME                 TIME                 TIME                 TIME                 TIME
 DEPTH SPEED DIR      DEPTH SPEED DIR      DEPTH SPEED DIR      DEPTH SPEED DIR      DEPTH SPEED DIR
[illegible]
```

[illegible] : DATE - [illegible]

TIDAL HEIGHTS

HIGH = [illegible]
LOW = [illegible]
HIGH = [illegible]

TIME - [illegible]

TIDAL COEFFICIENTS

EBB = [illegible]
FLOOD = [illegible]

TIME
DEPTH SPEED DIR

[illegible]

[illegible] : DATE - [illegible]

TIME
DEPTH SPEED DIR

[illegible]

[illegible] : DATE - [illegible]

TIDAL HEIGHTS

HIGH = [illegible]
LOW = [illegible]
HIGH = [illegible]

TIME - [illegible]

TIDAL COEFFICIENTS

EBB = [illegible]
FLOOD = [illegible]

TIME
DEPTH SPEED DIR

[illegible]

```
WESTERN SEC A..............  1  DATE -  6/ 9/77

TIME               TIME               TIME               TIME               TIME
 DEPTH SPEED DIR    DEPTH SPEED DIR    DEPTH SPEED DIR    DEPTH SPEED DIR    DEPTH SPEED DIR

 .17                .67                1.17               1.67               2.17
 [illegible]        [illegible]        [illegible]        [illegible]        [illegible]

 2.67               3.17               3.67               4.17               4.67
 [illegible]        [illegible]        [illegible]        [illegible]        [illegible]

 5.17               5.67               6.17               6.67               7.17
 [illegible]        [illegible]        [illegible]        [illegible]        [illegible]


WESTERN SEC A..............  1  DATE -  6/ 9/77

TIME               TIME               TIME               TIME               TIME
 DEPTH SPEED DIR    DEPTH SPEED DIR    DEPTH SPEED DIR    DEPTH SPEED DIR    DEPTH SPEED DIR

 7.67
 [illegible]


MAIN CHANNEL...............  1  DATE -  5/ 7/76

      TIDAL HEIGHTS                           TIDAL COEFFICIENTS
        HIGH = 11.6      TIME -  7130          EBB   = .74
        LOW  =  1.1                            FLOOD = .79
        HIGH = 11.3

TIME               TIME               TIME               TIME               TIME
 DEPTH SPEED DIR    DEPTH SPEED DIR    DEPTH SPEED DIR    DEPTH SPEED DIR    DEPTH SPEED DIR

 -.92               .08                .54                1.08               1.58
 [illegible]        [illegible]        [illegible]        [illegible]        [illegible]


MAIN CHANNEL...............  1  DATE -  5/ 7/76

TIME               TIME               TIME               TIME               TIME
 DEPTH SPEED DIR    DEPTH SPEED DIR    DEPTH SPEED DIR    DEPTH SPEED DIR    DEPTH SPEED DIR

 2.08               2.58               3.04               3.58               4.08
 [illegible]        [illegible]        [illegible]        [illegible]        [illegible]

 4.58               5.08               5.58               6.08               6.58
 [illegible]        [illegible]        [illegible]        [illegible]        [illegible]
```

340

```
MAIN CHANNEL........  : DATE - [illegible]/ 7/76

TIME               TIME               TIME               TIME               TIME
 DEPTH  SPEED  DIR  DEPTH  SPEED  DIR  DEPTH  SPEED  DIR  DEPTH  SPEED  DIR  DEPTH  SPEED  DIR

7.00               7.50               8.0[illegible]      [illegible]        [illegible]

[illegible]

[illegible]        [illegible]        10.[illegible]      11.[illegible]     11.[illegible]

[illegible]


MAIN CHANNEL........  : DATE - [illegible]/ 7/76

TIME
 DEPTH  SPEED  DIR

12.[illegible]

[illegible]                                                    17.[illegible]


HORTON NORTH........  : DATE - 20/ 6/76

     TIDAL HEIGHTS                       TIDAL COEFFICIENTS
      HIGH = 13.[illegible]   TIME = [illegible]      EBB   = .[illegible]
      LOW  =   .7                         FLOOD = .[illegible]
      HIGH = 12.[illegible]

TIME               TIME               TIME               TIME               TIME
 DEPTH  SPEED  DIR  DEPTH  SPEED  DIR  DEPTH  SPEED  DIR  DEPTH  SPEED  DIR  DEPTH  SPEED  DIR

-7.17              -6.67              -6.17              -5.67              -5.17

[illegible]

-4.67              -4.17              -3.67              -3.17              -2.67

[illegible]
```

341

```
HORTON NORTH..................   1  DATE - 2[illegible]/ 6/76

TIME                      TIME                      TIME                      TIME                      TIME
 DEPTH   SPEED   DIR       DEPTH   SPEED   DIR       DEPTH   SPEED   DIR       DEPTH   SPEED   DIR       DEPTH   SPEED   DIR

-2.17                     -1.67                     -1.17                     -.67                      -.17

 [illegible]               [illegible]               [illegible]               [illegible]               [illegible]

.33                       .83                       1.33                      1.83                      2.33

 [illegible]               [illegible]               [illegible]               [illegible]               [illegible]


HORTON NORTH..................   1  DATE - 2[illegible]/ 6/76

TIME                      TIME                      TIME                      TIME                      TIME
 DEPTH   SPEED   DIR       DEPTH   SPEED   DIR       DEPTH   SPEED   DIR       DEPTH   SPEED   DIR       DEPTH   SPEED   DIR

2.83                      3.33                      3.83                      4.33                      4.83

 [illegible]               [illegible]               [illegible]               [illegible]               [illegible]

5.33

 [illegible]


HORTON SOUTH..................   1  DATE - 22/ 6/76

      TIDAL HEIGHTS                             TIDAL COEFFICIENTS
         HIGH = 11.3      TIME =  [illegible]      EBB   = [illegible]
         LOW  = [illegible]                        FLOOD = [illegible]
         HIGH = 11.8

TIME                      TIME                      TIME                      TIME                      TIME
 DEPTH   SPEED   DIR       DEPTH   SPEED   DIR       DEPTH   SPEED   DIR       DEPTH   SPEED   DIR       DEPTH   SPEED   DIR

-2.25                     -1.75                     -1.25                     -.75                      -.25

 [illegible]               [illegible]               [illegible]               [illegible]               [illegible]
```

```
NORTON SOUTH.............  !  DATE : 22/ 6/76

TIME                      TIME                      TIME                      TIME                      TIME
DEPTH   SPEED   DIR       DEPTH   SPEED   DIR       DEPTH   SPEED   DIR       DEPTH   SPEED   DIR       DEPTH   SPEED   DIR
.25                       .75                       1.25                      1.75                      2.25
[illegible]               [illegible]               [illegible]               [illegible]               [illegible]

2.75                      3.25                      3.75                      4.25                      4.75
[illegible]               [illegible]               [illegible]               [illegible]               [illegible]


NORTON SOUTH.............  !  DATE : 22/ 6/76

TIME                      TIME                      TIME                      TIME                      TIME
DEPTH   SPEED   DIR       DEPTH   SPEED   DIR       DEPTH   SPEED   DIR       DEPTH   SPEED   DIR       DEPTH   SPEED   DIR
5.25                      5.75                      6.25                      6.75                      7.25
[illegible]               [illegible]               [illegible]               [illegible]               [illegible]

7.75                      8.25                      8.75                      9.25                      9.75
[illegible]               [illegible]               [illegible]               [illegible]               [illegible]


NORTON SOUTH.............  !  DATE : 22/ 6/76

TIME                      TIME
DEPTH   SPEED   DIR       DEPTH   SPEED   DIR
10.25                     10.75
[illegible]               [illegible]
```

```
SUMMERVILLE..........  1  DATE - [illegible]

        TIDAL HEIGHTS                          TIDAL COEFFICIENTS
         HIGH = [illegible]   TIME = [illegible]     EBB   = [illegible]
         LOW  = [illegible]                          FLOOD = [illegible]
         HIGH = [illegible]

TIME                 TIME                 TIME                 TIME                 TIME
 DEPTH  SPEED  DIR    DEPTH  SPEED  DIR    DEPTH  SPEED  DIR    DEPTH  SPEED  DIR    DEPTH  SPEED  DIR

-4.67                -4.17                -3.67                -3.17                -2.67
 [illegible]          [illegible]          [illegible]          [illegible]          [illegible]

-2.17                -1.67                -1.17                -.67                 -.17
 [illegible]          [illegible]          [illegible]          [illegible]          [illegible]


SUMMERVILLE..........  1  DATE - [illegible]

TIME                 TIME                 TIME                 TIME                 TIME
 DEPTH  SPEED  DIR    DEPTH  SPEED  DIR    DEPTH  SPEED  DIR    DEPTH  SPEED  DIR    DEPTH  SPEED  DIR

.33                  .83                  1.33                 1.83                 2.33
 [illegible]          [illegible]          [illegible]          [illegible]          [illegible]

2.83                 3.33                 3.83                 4.33                 4.83
 [illegible]          [illegible]          [illegible]          [illegible]          [illegible]

5.33                 5.83                 6.33                 6.83                 7.33
  .25  [illegible]     .25  [illegible]     .25  [illegible]     .25  [illegible]     [illegible]

7.83
 [illegible]


[illegible] MOUTH....  1  DATE - [illegible]

        TIDAL HEIGHTS                          TIDAL COEFFICIENTS
         HIGH = 11.6      TIME = [illegible]        EBB   = [illegible]
         LOW  = [illegible]                          FLOOD = [illegible]
         HIGH = 11.9

TIME                 TIME                 TIME                 TIME                 TIME
 DEPTH  SPEED  DIR    DEPTH  SPEED  DIR    DEPTH  SPEED  DIR    DEPTH  SPEED  DIR    DEPTH  SPEED  DIR

-12.3[illegible]     -11.83               -11.33               -10.83               -10.33
 [illegible]          [illegible]          [illegible]          [illegible]          [illegible]

-9.83                -9.33                -8.83                -8.33                -7.83
 [illegible]          [illegible]          [illegible]          [illegible]          [illegible]

-7.33                -6.83                -6.33                -5.83                -5.33
 [illegible]          [illegible]          [illegible]          [illegible]          [illegible]
```

[illegible] MOUTH . DATE - [illegible]

TIME DEPTH SPEED DIR

[illegible]

[illegible] STATION [illegible] . DATE - 23/ 7/75

TIDAL HEIGHTS

HIGH = 12.6
LOW = [illegible]
HIGH = [illegible]

TIME = [illegible]

TIDAL COEFFICIENTS

EBB = .76
FLOOD = .79

TIME DEPTH SPEED DIR

[illegible]

[illegible] STATION [illegible] . DATE - 23/ 7/75

TIME DEPTH SPEED DIR

[illegible]

```
[illegible] STATION [illegible]   DATE - [illegible]

    TIDAL HEIGHTS                          TIDAL COEFFICIENTS
     HIGH = [illegible]   TIME - [illegible]    [illegible] = [illegible]
     LOW  = [illegible]                         [illegible] = [illegible]
     HIGH = [illegible]

TIME                  TIME                  TIME                  TIME                  TIME
 DEPTH  SPEED  DIR     DEPTH  SPEED  DIR     DEPTH  SPEED  DIR     DEPTH  SPEED  DIR     DEPTH  SPEED  DIR
-6.25                 -5.25                 -4.25                 -3.25                 -2.25

  [illegible]           [illegible]           [illegible]           [illegible]           [illegible]

-1.25                 -.25                  .75                   1.75                  2.75

  [illegible]           [illegible]           [illegible]           [illegible]           [illegible]

[illegible] STATION [illegible]   DATE - [illegible]

TIME                  TIME                  TIME                  TIME
 DEPTH  SPEED  DIR     DEPTH  SPEED  DIR     DEPTH  SPEED  DIR     DEPTH  SPEED  DIR
3.75                  4.75                  5.75                  6.58

  [illegible]           [illegible]           [illegible]           [illegible]
```

TABLE B-2. Temperature and Salinity Measurements

All temperature and salinity data are presented in the following pages. In addition to the station name, the time relative to high tide (hours and hundredths; negative values are hours before high tide, positive values hours after high tide), water depth (m), water temperature (°C), and salinity (‰) are listed for each profile. Missing temperature readings are listed as 0.0° C. All temperature and salinity stations are located on Figure 3-2.

```
BOOT ISLAND 1

TIME                 TIME                 TIME                 TIME                 TIME
  DEPTH  TEMP  SAL     DEPTH  TEMP  SAL     DEPTH  TEMP  SAL     DEPTH  TEMP  SAL     DEPTH  TEMP  SAL
-8.25                -7.75                -6.25                -3.75                -3.25
  [illegible]          .25  16.4  30.[illegible]  .25  17.8  [illegible]  [illegible]  [illegible]
-2.75                -2.25                -1.75                -1.25                -.75
  [illegible]          [illegible]          [illegible]          [illegible]          [illegible]
-.25                 .25                  [illegible]          1.25                 1.75
  [illegible]          [illegible]          [illegible]          [illegible]          [illegible]
2.25                 2.75                 3.25                 3.75
  [illegible]          [illegible]          [illegible]          [illegible]


BOOT ISLAND 2

TIME                 TIME                 TIME                 TIME                 TIME
  DEPTH  TEMP  SAL     DEPTH  TEMP  SAL     DEPTH  TEMP  SAL     DEPTH  TEMP  SAL     DEPTH  TEMP  SAL
-10.17               -9.67                -9.17                -8.67                -8.17
  [illegible]          [illegible]          [illegible]          [illegible]          .25  19.5
-7.67                -6.67                -6.17                -3.67                -3.17
  .25  17.8            .25  17.8            .25  16.6            [illegible]          [illegible]
-2.67                -2.17                -1.67                -1.17                -.67
  [illegible]          [illegible]          [illegible]          [illegible]          [illegible]


BOOT ISLAND 3

TIME                 TIME                 TIME                 TIME                 TIME
  DEPTH  TEMP  SAL     DEPTH  TEMP  SAL     DEPTH  TEMP  SAL     DEPTH  TEMP  SAL     DEPTH  TEMP  SAL
-.17                 .33                  .83                  1.33                 1.83
  [illegible]          [illegible]          [illegible]          [illegible]          [illegible]
2.33
  [illegible]
```

```
[illegible]

TIME                TIME                TIME                TIME                TIME
  DEPTH  TEMP  SAL    DEPTH  TEMP  SAL    DEPTH  TEMP  SAL    DEPTH  TEMP  SAL    DEPTH  TEMP  SAL
[illegible]

[illegible]

TIME                TIME                TIME                TIME                TIME
  DEPTH  TEMP  SAL    DEPTH  TEMP  SAL    DEPTH  TEMP  SAL    DEPTH  TEMP  SAL    DEPTH  TEMP  SAL
[illegible]

[illegible]

TIME                TIME                TIME                TIME                TIME
  DEPTH  TEMP  SAL    DEPTH  TEMP  SAL    DEPTH  TEMP  SAL    DEPTH  TEMP  SAL    DEPTH  TEMP  SAL
[illegible]
```

[illegible]

TIME DEPTH TEMP SAL

[illegible]

[illegible]

TIME DEPTH TEMP SAL

[illegible]

[illegible]

TIME DEPTH TEMP SAL

[illegible]

```
[illegible]

TIME              TIME              TIME              TIME              TIME
  DEPTH TEMP SAL    DEPTH TEMP SAL    DEPTH TEMP SAL    DEPTH TEMP SAL    DEPTH TEMP SAL
[illegible]       1.37              [illegible]       [illegible]       [illegible]

[illegible]

MIDDLE GROUND [illegible]

TIME              TIME              TIME              TIME              TIME
  DEPTH TEMP SAL    DEPTH TEMP SAL    DEPTH TEMP SAL    DEPTH TEMP SAL    DEPTH TEMP SAL
[illegible]       .42               .97               1.42              1.92

[illegible]

2.42              2.97              3.42              3.92              4.42

[illegible]

MIDDLE GROUND [illegible]

TIME              TIME              TIME              TIME              TIME
  DEPTH TEMP SAL    DEPTH TEMP SAL    DEPTH TEMP SAL    DEPTH TEMP SAL    DEPTH TEMP SAL
4.92              5.42              5.92              6.42              6.97

[illegible]

7.42              7.92              8.42              8.92              9.42

[illegible]

MIDDLE GROUND [illegible]

TIME              TIME              TIME              TIME              TIME
  DEPTH TEMP SAL    DEPTH TEMP SAL    DEPTH TEMP SAL    DEPTH TEMP SAL    DEPTH TEMP SAL
9.97              10.42             10.97             11.42             11.97

[illegible]
```

```
MIDDLE GROUND 2
TIME          TIME          TIME          TIME          TIME
 DEPTH TEMP SAL DEPTH TEMP SAL DEPTH TEMP SAL DEPTH TEMP SAL DEPTH TEMP SAL
.17           .67           1.17          1.67          2.17
[illegible]   [illegible]   [illegible]   [illegible]   [illegible]
2.67          3.17          3.67          4.17          4.67
[illegible]   [illegible]   [illegible]   [illegible]   [illegible]

MIDDLE GROUND 2
TIME          TIME          TIME          TIME          TIME
 DEPTH TEMP SAL DEPTH TEMP SAL DEPTH TEMP SAL DEPTH TEMP SAL DEPTH TEMP SAL
5.17          5.67          6.17          6.67          7.17
[illegible]    .25  20.6     .25  20.2     .25  20.2    [illegible]
7.67          8.17          8.67          9.17          9.67
[illegible]   [illegible]   [illegible]   [illegible]   [illegible]

MIDDLE GROUND 2
TIME          TIME          TIME          TIME          TIME
 DEPTH TEMP SAL DEPTH TEMP SAL DEPTH TEMP SAL DEPTH TEMP SAL DEPTH TEMP SAL
10.17         10.67         11.17         11.67         12.17
[illegible]   [illegible]   [illegible]   [illegible]   [illegible]

MIDDLE GROUND 2
TIME          TIME          TIME          TIME          TIME
 DEPTH TEMP SAL DEPTH TEMP SAL DEPTH TEMP SAL DEPTH TEMP SAL DEPTH TEMP SAL
-6.67         -6.17         -5.67         -5.17         -4.67
[illegible]   [illegible]   [illegible]   [illegible]   [illegible]
-4.17         -3.67         -3.17         -2.67         -2.17
[illegible]   [illegible]   [illegible]   [illegible]   [illegible]
```

3-2

```
[illegible]

TIME                TIME                TIME                TIME                TIME
  DEPTH  TEMP  SAL    DEPTH  TEMP  SAL    DEPTH  TEMP  SAL    DEPTH  TEMP  SAL    DEPTH  TEMP  SAL
[illegible]         [illegible]         [illegible]         [illegible]         [illegible]

[illegible]

[illegible]

TIME                TIME                TIME                TIME                TIME
  DEPTH  TEMP  SAL    DEPTH  TEMP  SAL    DEPTH  TEMP  SAL    DEPTH  TEMP  SAL    DEPTH  TEMP  SAL
[illegible]

[illegible]

TIME                TIME                TIME                TIME                TIME
  DEPTH  TEMP  SAL    DEPTH  TEMP  SAL    DEPTH  TEMP  SAL    DEPTH  TEMP  SAL    DEPTH  TEMP  SAL
2.17                [illegible]         3.17                3.67                4.17

[illegible]

[illegible]         5.17                5.67                [illegible]         [illegible]

   .25  20.2          .25  20.2          .2[illegible]  20.0     [illegible]         [illegible]
```

[illegible]

```
TIME                TIME                TIME                TIME                TIME
 DEPTH TEMP SAL      DEPTH TEMP SAL      DEPTH TEMP SAL      DEPTH TEMP SAL      DEPTH TEMP SAL
[illegible]
```

[illegible]

```
TIME                TIME                TIME                TIME                TIME
 DEPTH TEMP SAL      DEPTH TEMP SAL      DEPTH TEMP SAL      DEPTH TEMP SAL      DEPTH TEMP SAL
[illegible]
```

[illegible]

```
TIME                TIME                TIME                TIME                TIME
 DEPTH TEMP SAL      DEPTH TEMP SAL      DEPTH TEMP SAL      DEPTH TEMP SAL      DEPTH TEMP SAL
[illegible]
```

```
[illegible]

TIME                    TIME                    TIME                    TIME                    TIME
  DEPTH  TEMP  SAL        DEPTH  TEMP  SAL        DEPTH  TEMP  SAL        DEPTH  TEMP  SAL        DEPTH  TEMP  SAL
[illegible]

[illegible]

TIME                    TIME                    TIME                    TIME                    TIME
  DEPTH  TEMP  SAL        DEPTH  TEMP  SAL        DEPTH  TEMP  SAL        DEPTH  TEMP  SAL        DEPTH  TEMP  SAL
[illegible]

[illegible]

TIME                    TIME                    TIME                    TIME                    TIME
  DEPTH  TEMP  SAL        DEPTH  TEMP  SAL        DEPTH  TEMP  SAL        DEPTH  TEMP  SAL        DEPTH  TEMP  SAL
[illegible]
```

[illegible]

NORTON SOUTH

TIME DEPTH TEMP SAL

[illegible]

NORTON SOUTH

TIME DEPTH TEMP SAL

[illegible]

NORTON SOUTH

TIME DEPTH TEMP SAL

[illegible]

[illegible] SOUTH

TIME
DEPTH TEMP SAL

[illegible]

SUMMERVILLE

TIME
DEPTH TEMP SAL

[illegible]

359

```
SUMMERVILLE
....................

TIME                  TIME                  TIME                  TIME                  TIME
  DEPTH  TEMP  SAL      DEPTH  TEMP  SAL      DEPTH  TEMP  SAL      DEPTH  TEMP  SAL      DEPTH  TEMP  SAL
.33                   .83                   1.33                  1.83                  2.33
  [illegible]           [illegible]           [illegible]           [illegible]           [illegible]

2.83                  3.33                  3.83                  4.33                  4.83
  [illegible]           [illegible]           [illegible]           [illegible]           [illegible]

5.33                  5.83                  6.33                  6.83                  7.33
  .25  21.7  27.2       .25  21.6  27.0       .??  ?1.6  ??.?       .2?  21.3  27.6       [illegible]

7.83
  [illegible]


KENNETCOOK MOUTH
....................

TIME                  TIME                  TIME                  TIME                  TIME
  DEPTH  TEMP  SAL      DEPTH  TEMP  SAL      DEPTH  TEMP  SAL      DEPTH  TEMP  SAL      DEPTH  TEMP  SAL
-12.33                -11.83                -11.33                -10.83                -10.33
  [illegible]           [illegible]           [illegible]           [illegible]           [illegible]

-9.83                 -9.33                 -8.83                 -8.33                 -7.83
  [illegible]           [illegible]           [illegible]           [illegible]           [illegible]

-7.33                 -6.83                 -6.33                 -5.83                 -5.33
  [illegible]           [illegible]           [illegible]           [illegible]           [illegible]


KENNETCOOK MOUTH
....................

TIME                  TIME                  TIME                  TIME                  TIME
  DEPTH  TEMP  SAL      DEPTH  TEMP  SAL      DEPTH  TEMP  SAL      DEPTH  TEMP  SAL      DEPTH  TEMP  SAL
-4.83                 -4.33                 -3.83                 -3.33                 -2.83
  [illegible]           [illegible]           [illegible]           [illegible]           [illegible]

-2.33                 -1.83                 -1.33                 -.83                  [illegible]
  [illegible]           [illegible]           [illegible]           [illegible]           [illegible]
```

```
[illegible]

TIME                 TIME                 TIME                 TIME                 TIME
 DEPTH  TEMP  SAL     DEPTH  TEMP  SAL     DEPTH  TEMP  SAL     DEPTH  TEMP  SAL     DEPTH  TEMP  SAL

[illegible]

 [illegible]


[illegible]

TIME                 TIME                 TIME                 TIME                 TIME
 DEPTH  TEMP  SAL     DEPTH  TEMP  SAL     DEPTH  TEMP  SAL     DEPTH  TEMP  SAL     DEPTH  TEMP  SAL

[illegible]          [illegible]          [illegible]          [illegible]          [illegible]

 [illegible]          [illegible]          [illegible]          [illegible]          [illegible]

-3.00                -2.00                -1.00                1.00                 2.00

 [illegible]          [illegible]          [illegible]          [illegible]          [illegible]

3.00                 4.00                 5.00

 [illegible]          [illegible]          [illegible]


[illegible]

TIME                 TIME                 TIME                 TIME                 TIME
 DEPTH  TEMP  SAL     DEPTH  TEMP  SAL     DEPTH  TEMP  SAL     DEPTH  TEMP  SAL     DEPTH  TEMP  SAL

-6.25                -5.25                -4.25                -3.25                -2.25

 [illegible]          [illegible]          [illegible]          [illegible]          [illegible]

-1.25                -.25                 .75                  1.75                 2.75

 [illegible]          [illegible]          [illegible]          [illegible]          [illegible]

3.75                 4.75                 5.75                 6.50

 [illegible]          [illegible]          [illegible]          [illegible]
```

TABLE B-3. Hydraulic Parameters

This table presents all the hydraulic parameters calculated from the current velocity data in Table B-1. The station name, date occupied, tidal heights (m), time of high tide (hours and minutes), and tidal coefficients are listed as well as the time of each profile relative to high tide (hours and hundredths; negative values are hours before high tide, positive values hours after high tide). Each profile is designated as flood (F) or ebb (E). The calculated parameters and their units are:

Total Depth - water depth (m)

Bottom Direction - average direction of current flow (degrees)

Mean Speed - average current speed (m/s)

Discharge - volume flow rate of water (m^3/s)

Total Net Discharge - flood minus ebb discharge for the complete tidal cycle; positive values indicate net discharge in the flood direction, negative values in the ebb direction (m^3)

U100 - current speed 1 m above the bed (m/s)

Turb - turbulence intensity as a ratio of shear velocity (defined in Chapter 3) (dimensionless)

Ustar - shear velocity (m/s)

Tau - shear stress at the bed (Pa) or (kg/m.s)

Stream Power - power of the flow/unit area of bed (kg/s^3)

Energy Slope - slope of the energy grade line (dimensionless)

F - Darcy-Weisbach friction factor

Ks - bed roughness element height (m)

Zo - calculated height above the bed of zero velocity (m)

Froude Number - (dimensionless)

Reynolds Number - (dimensionless)

Correlation coefficients were calculated between the measured velocity profiles and the theoretical logarithmic velocity profile; all profiles not significant at the 80% level are marked with a large dot, profiles marked with a small dot are significant at the 80% level, and all others are significant at the 95% level.

```
BOOT ISLAND.........[illegible]   DATE - [illegible]

     TIDAL HEIGHTS                               TIDAL COEFFICIENTS
     HIGH = [illegible]   TIME - [illegible]      EBB   = [illegible]
     LOW  = [illegible]                           FLOOD = [illegible]
     HIGH = [illegible]

TIME   TOTAL  BOTTOM  MEAN   DISCHARGE  VISC  TURB   U    TAU  STREAM  ENERGY  F   KS   ZO   FROUDE  REYNOLDS
       DEPTH  ELEV.   SPEED                          STAR      POWER   SLOPE                 NUMBER  NUMBER
[illegible]

          TOTAL NET DISCHARGE [illegible]

BOOT ISLAND.........[illegible]   DATE - [illegible]

     TIDAL HEIGHTS                               TIDAL COEFFICIENTS
     HIGH = [illegible]   TIME - [illegible]      EBB   = [illegible]
     LOW  = [illegible]                           FLOOD = [illegible]
     HIGH = [illegible]

TIME   TOTAL  BOTTOM  MEAN   DISCHARGE  VISC  TURB   U    TAU  STREAM  ENERGY  F   KS   ZO   FROUDE  REYNOLDS
       DEPTH  ELEV.   SPEED                          STAR      POWER   SLOPE                 NUMBER  NUMBER
[illegible]

          TOTAL NET DISCHARGE [illegible]

BOOT ISLAND.........[illegible]   DATE - [illegible]

     TIDAL HEIGHTS                               TIDAL COEFFICIENTS
     HIGH = [illegible]   TIME - [illegible]      EBB   = [illegible]
     LOW  = [illegible]                           FLOOD = [illegible]
     HIGH = [illegible]

TIME   TOTAL  BOTTOM  MEAN   DISCHARGE  VISC  TURB   U    TAU  STREAM  ENERGY  F   KS   ZO   FROUDE  REYNOLDS
       DEPTH  ELEV.   SPEED                          STAR      POWER   SLOPE                 NUMBER  NUMBER
[illegible]

          TOTAL NET DISCHARGE [illegible]

BOOT ISLAND.........[illegible]   DATE - [illegible]

     TIDAL HEIGHTS                               TIDAL COEFFICIENTS
     HIGH = [illegible]   TIME - [illegible]      EBB   = [illegible]
     LOW  = [illegible]                           FLOOD = [illegible]
     HIGH = [illegible]

TIME   TOTAL  BOTTOM  MEAN   DISCHARGE  VISC  TURB   U    TAU  STREAM  ENERGY  F   KS   ZO   FROUDE  REYNOLDS
       DEPTH  ELEV.   SPEED                          STAR      POWER   SLOPE                 NUMBER  NUMBER
[illegible]

          TOTAL NET DISCHARGE [illegible]
```

304

```
[illegible]..........   I  DATE - [illegible]

      TIDAL HEIGHTS                        TIDAL COEFFICIENTS
        HIGH = 11.7    TIME - [illegible]     EBB   = [illegible]
        LOW  = [illegible]                    FLOOD = [illegible]
        HIGH = 11.6

  TIME       TOTAL  BOTTOM  MEAN   DISCHARGE  U100  TURB    U     TAU   STREAM  ENERGY   F    KS    ZO   FROUDE  REYNOLDS
             DEPTH  ELEV.   SPEED                          STAR          POWER   SLOPE                    NUMBER   NUMBER
  [illegible]

             TOTAL NET DISCHARGE -[illegible]

MANTSPORT BAR 1..........   I  DATE - [illegible]

      TIDAL HEIGHTS                        TIDAL COEFFICIENTS
        HIGH = 13.1    TIME - 1516[illegible]   EBB   = .7[illegible]
        LOW  = [illegible]                      FLOOD = .7[illegible]
        HIGH = 12.9

  TIME       TOTAL  BOTTOM  MEAN   DISCHARGE  U100  TURB    U     TAU   STREAM  ENERGY   F    KS    ZO   FROUDE  REYNOLDS
             DEPTH  ELEV.   SPEED                          STAR          POWER   SLOPE                    NUMBER   NUMBER
  [illegible]

             TOTAL NET DISCHARGE -.1007E+05

MANTSPORT BAR 2..........   I  DATE - 6/ 6/76

      TIDAL HEIGHTS                        TIDAL COEFFICIENTS
        HIGH = 13.1    TIME - 1516[illegible]   EBB   = .76
        LOW  = .9                               FLOOD = .77
        HIGH = 12.9

  TIME       TOTAL  BOTTOM  MEAN   DISCHARGE  U100  TURB    U     TAU   STREAM  ENERGY   F    KS    ZO   FROUDE  REYNOLDS
             DEPTH  ELEV.   SPEED                          STAR          POWER   SLOPE                    NUMBER   NUMBER
  [illegible]

             TOTAL NET DISCHARGE -.[illegible]E+0[illegible]

MANTSPORT BAR 3..........   I  DATE - 17/ 6/7[illegible]

      TIDAL HEIGHTS                        TIDAL COEFFICIENTS
        HIGH = 13.[illegible]    TIME - 7:25    EBB   = .77
        LOW  = .9                               FLOOD = .7[illegible]
        HIGH = 13.1

  TIME       TOTAL  BOTTOM  MEAN   DISCHARGE  U100  TURB    U     TAU   STREAM  ENERGY   F    KS    ZO   FROUDE  REYNOLDS
             DEPTH  ELEV.   SPEED                          STAR          POWER   SLOPE                    NUMBER   NUMBER
  [illegible]

             TOTAL NET DISCHARGE .[illegible]E+0[illegible]
```

```
MONTGOMERY BAY 1 ....................  *  DATE - 10/ 6/76

    TIDAL HEIGHTS                                  TIDAL COEFFICIENTS
       HIGH = 12.7      TIME - [illegible]            EBB   = [illegible]
       LOW  = [illegible]                             FLOOD = [illegible]
       HIGH = 13.1

 TIME        TOTAL   BOTTOM   MEAN   DISCHARGE  U100   TURB     U     TAU   STREAM   ENERGY    F     KS     ZO   FROUDE  REYNOLDS
             DEPTH   CIRC.   SPEED                            STAR          POWER    SLOPE                        NUMBER   NUMBER
 [illegible]

              TOTAL NET DISCHARGE [illegible]

MONTGOMERY BAY 2 ....................  *  DATE - 26/ 6/75

    TIDAL HEIGHTS                                  TIDAL COEFFICIENTS
       HIGH = 13.0      TIME - [illegible]            EBB   = .70
       LOW  = [illegible]                             FLOOD = .82
       HIGH = 13.6

 TIME        TOTAL   BOTTOM   MEAN   DISCHARGE  U100   TURB     U     TAU   STREAM   ENERGY    F     KS     ZO   FROUDE  REYNOLDS
             DEPTH   CIRC.   SPEED                            STAR          POWER    SLOPE                        NUMBER   NUMBER
 [illegible]

              TOTAL NET DISCHARGE -.1723E+05

MIDDLE GROUND 1 ....................  *  DATE - 13/ 8/76

    TIDAL HEIGHTS                                  TIDAL COEFFICIENTS
       HIGH = 11.8      TIME - 0950                   EBB   = .67
       LOW  = [illegible]                             FLOOD = .67
       HIGH = 12.6

 TIME        TOTAL   BOTTOM   MEAN   DISCHARGE  U100   TURB     U     TAU   STREAM   ENERGY    F     KS     ZO   FROUDE  REYNOLDS
             DEPTH   CIRC.   SPEED                            STAR          POWER    SLOPE                        NUMBER   NUMBER
 [illegible]

              TOTAL NET DISCHARGE  .2385E+05

MIDDLE GROUND 2 ....................  *  DATE - 13/ 8/76

    TIDAL HEIGHTS                                  TIDAL COEFFICIENTS
       HIGH = 11.8      TIME - 0950                   EBB   = .67
       LOW  = [illegible]                             FLOOD = .67
       HIGH = 12.6

 TIME        TOTAL   BOTTOM   MEAN   DISCHARGE  U100   TURB     U     TAU   STREAM   ENERGY    F     KS     ZO   FROUDE  REYNOLDS
             DEPTH   CIRC.   SPEED                            STAR          POWER    SLOPE                        NUMBER   NUMBER
 [illegible]

              TOTAL NET DISCHARGE  .4487E+05
```

[illegible]

TOTAL NET DISCHARGE [illegible]

[illegible] DATE = [illegible]

TIDAL HEIGHTS

TIME = [illegible]

TIDAL COEFFICIENTS

TIME TOTAL DEPTH BOTTOM [illegible] MEAN SPEED DISCHARGE [illegible] [illegible] [illegible] [illegible] [illegible] [illegible] [illegible] [illegible] [illegible] FROUDE NUMBER REYNOLDS NUMBER

[illegible]

TOTAL NET DISCHARGE [illegible]

[illegible] DATE = [illegible]

TIDAL HEIGHTS

TIME = [illegible]

TIDAL COEFFICIENTS

TIME TOTAL DEPTH BOTTOM [illegible] MEAN SPEED DISCHARGE [illegible] [illegible] [illegible] [illegible] [illegible] [illegible] [illegible] [illegible] [illegible] FROUDE NUMBER REYNOLDS NUMBER

[illegible]

TOTAL NET DISCHARGE [illegible]

```
[illegible]      DATE - [illegible]

   TIDAL HEIGHTS                          TIDAL COEFFICIENTS
   [illegible]     TIME    [illegible]    [illegible]

TIME   TOTAL  BOTTOM  MEAN   DISCHARGE  [illegible]  TURB  U     TAU  STREAM  ENERGY  F  KS  ZO  FROUDE  REYNOLDS
       DEPTH  CELL    SPEED                                STAR       POWER   SLOPE            NUMBER  NUMBER
[illegible]
          TOTAL NET DISCHARGE [illegible]

[illegible]      DATE - [illegible]

   TIDAL HEIGHTS                          TIDAL COEFFICIENTS
   [illegible]     TIME    [illegible]    [illegible]

TIME   TOTAL  BOTTOM  MEAN   DISCHARGE  [illegible]  TURB  U     TAU  STREAM  ENERGY  F  KS  ZO  FROUDE  REYNOLDS
       DEPTH  CELL    SPEED                                STAR       POWER   SLOPE            NUMBER  NUMBER
[illegible]
          TOTAL NET DISCHARGE [illegible]

[illegible]      DATE - [illegible]

   TIDAL HEIGHTS                          TIDAL COEFFICIENTS
   HIGH - [illegible]   TIME - [illegible]   EBB = [illegible]
   LOW  - [illegible]                        FLOOD = [illegible]
   HIGH - [illegible]

TIME   TOTAL  BOTTOM  MEAN   DISCHARGE  U10  TURB  U     TAU  STREAM  ENERGY  F  KS  ZO  FROUDE  REYNOLDS
       DEPTH  CELL    SPEED                        STAR       POWER   SLOPE            NUMBER  NUMBER
[illegible]
          TOTAL NET DISCHARGE [illegible]

[illegible]      DATE - [illegible]

   TIDAL HEIGHTS                          TIDAL COEFFICIENTS
   HIGH - [illegible]   TIME - [illegible]   EBB = [illegible]
   LOW  - [illegible]                        FLOOD = [illegible]
   HIGH - [illegible]

TIME   TOTAL  BOTTOM  MEAN   DISCHARGE  [illegible]  TURB  U     TAU  STREAM  ENERGY  F  KS  ZO  FROUDE  REYNOLDS
       DEPTH  CELL    SPEED                                STAR       POWER   SLOPE            NUMBER  NUMBER
[illegible]
          TOTAL NET DISCHARGE [illegible]
```

309

```
MAIN CHANNEL........   * DATE = [illegible]

     TIDAL HEIGHTS                        TIDAL COEFFICIENTS
      HIGH = [illegible]    TIME = [illegible]     EBB   = [illegible]
      LOW  = [illegible]                            FLOOD = [illegible]
      HIGH = [illegible]

 TIME    TOTAL  BOTTOM  MEAN   DISCHARGE  VISC  [illegible]  U     TAU  STREAM  ENERGY  F  KS  ZO  FROUDE  REYNOLDS
         DEPTH  [illegible]  SPEED                          STAR        POWER   SLOPE              NUMBER  NUMBER
 [illegible]

        TOTAL NET DISCHARGE = [illegible]

HORTON NORTH........   * DATE = [illegible]

     TIDAL HEIGHTS                        TIDAL COEFFICIENTS
      HIGH = [illegible]    TIME = [illegible]     EBB   = [illegible]
      LOW  = [illegible]                            FLOOD = [illegible]
      HIGH = [illegible]

 TIME    TOTAL  BOTTOM  MEAN   DISCHARGE  VISC  [illegible]  U     TAU  STREAM  ENERGY  F  KS  ZO  FROUDE  REYNOLDS
         DEPTH  [illegible]  SPEED                          STAR        POWER   SLOPE              NUMBER  NUMBER
 [illegible]

        TOTAL NET DISCHARGE = [illegible]

HORTON SOUTH........   * DATE = 227 6/78

     TIDAL HEIGHTS                        TIDAL COEFFICIENTS
      HIGH = [illegible]    TIME = [illegible]     EBB   = [illegible]
      LOW  = [illegible]                            FLOOD = [illegible]
      HIGH = [illegible]

 TIME    TOTAL  BOTTOM  MEAN   DISCHARGE  VISC  [illegible]  U     TAU  STREAM  ENERGY  F  KS  ZO  FROUDE  REYNOLDS
         DEPTH  [illegible]  SPEED                          STAR        POWER   SLOPE              NUMBER  NUMBER
 [illegible]

        TOTAL NET DISCHARGE = [illegible]

[illegible]........   * DATE = [illegible]

     TIDAL HEIGHTS                        TIDAL COEFFICIENTS
      HIGH = [illegible]    TIME = [illegible]     EBB   = [illegible]
      LOW  = [illegible]                            FLOOD = [illegible]
      HIGH = [illegible]

 TIME    TOTAL  BOTTOM  MEAN   DISCHARGE  VISC  [illegible]  U     TAU  STREAM  ENERGY  F  KS  ZO  FROUDE  REYNOLDS
         DEPTH  [illegible]  SPEED                          STAR        POWER   SLOPE              NUMBER  NUMBER
 [illegible]

        TOTAL NET DISCHARGE = [illegible]
```

```
[illegible] MOUTH........  I  DATE = [illegible]

     TIDAL HEIGHTS                          TIDAL COEFFICIENTS
       HIGH = [illegible]   TIME = [illegible]      EBB   = [illegible]
       LOW  = [illegible]                          FLOOD = [illegible]
       HIGH = [illegible]

 TIME     TOTAL  BOTTOM  MEAN   DISCHARGE  U100  TURB   U     TAU   STREAM  ENERGY  F   KS   ZO   FROUDE  REYNOLDS
          DEPTH  CIR.    SPEED                          STAR         POWER   SLOPE                   NUMBER  NUMBER
 [illegible]
              TOTAL NET DISCHARGE =[illegible]

[illegible] STATION [illegible]........  I  DATE = [illegible] 7/75

     TIDAL HEIGHTS                          TIDAL COEFFICIENTS
       HIGH = [illegible]   TIME = [illegible]      EBB   = [illegible]
       LOW  = [illegible]                          FLOOD = [illegible]
       HIGH = [illegible]

 TIME     TOTAL  BOTTOM  MEAN   DISCHARGE  U100  TURB   U     TAU   STREAM  ENERGY  F   KS   ZO   FROUDE  REYNOLDS
          DEPTH  CIR.    SPEED                          STAR         POWER   SLOPE                   NUMBER  NUMBER
 [illegible]
              TOTAL NET DISCHARGE =[illegible]

[illegible] STATION [illegible]........  I  DATE = [illegible]

     TIDAL HEIGHTS                          TIDAL COEFFICIENTS
       HIGH = [illegible]   TIME = [illegible]      EBB   = [illegible]
       LOW  = [illegible]                          FLOOD = [illegible]
       HIGH = [illegible]

 TIME     TOTAL  BOTTOM  MEAN   DISCHARGE  U100  TURB   U     TAU   STREAM  ENERGY  F   KS   ZO   FROUDE  REYNOLDS
          DEPTH  CIR.    SPEED                          STAR         POWER   SLOPE                   NUMBER  NUMBER
 [illegible]
              TOTAL NET DISCHARGE =[illegible]
```

APPENDIX C: INTERNAL STRUCTURE MEASUREMENT

Internal structures were examined using trenches and peels. Trenches were dug perpendicular to bedform crests; one wall was kept as vertical as possible and smoothed with a trowel. Trench length was governed by bedform wavelength; they were usually dug 0.5 to 0.75 m deep unless the water table was shallower than that depth. In areas of relatively coarse sediment, internal structures were visible after the vertical wall was allowed to dry and measurements could be made directly.

Using the method of Barr et al. (1970), epoxy peels were made in areas where structures could not be observed directly. A trench was dug as described above, and a Masonite board of the desired size and shape was positioned with its lower edge against the vertical trench face so that it made approximately a 45° angle with the face. End boards were emplaced to prevent the epoxy from squeezing out at the ends. The epoxy mixture was poured onto the board and then the Masonite was slowly raised until it lay against the trench face; the board was packed with sand to ensure that it remained in contact with the face and that the epoxy penetrated into the sediment. The peel was dug out after hardening.

In 1974, the epoxy mixture consisted of equal parts of Ciba-Geigy Araldite 6005 resin, Araldite 6010 resin, 850 hardener, and 830 hardener; this mixture had a hardening time of approximately 3 hours. Araldite 6005 was unavailable in 1975 so the mixture used was 2 parts of Araldite 6010 to one part of 850 hardener and one part of 830 hardener; the hardening time was similar to the 1974 mixture. The amount of epoxy mixture used was a function of the size of the peel to be made. Generally, 1 liter of mixture would make a 0.1 m^2 peel.

During the 1975 field season, it was discovered that the hardening time could be reduced significantly if a one-to-one mixture of Araldite 6010 and 850 hardener was prepared 45 minutes to one hour before pouring. The mixture was poured as it started to become warm and less viscous. The lowered viscosity allowed ample penetration and hardening time was reduced to approximately one hour after pouring. Several of the 1975 peels, and all of the 1976 peels, were made using this method.

Some areas did not allow trenching because of a very high water table. Internal structures were examined using modified Klovan box cores (Burger and Klein, 1969). The cores were oriented perpendicular to bedform crests and driven their full length into the sediment.

After removal, peels were made directly from the box cores using the method described above.

Measurements of internal structures were made in the field and on peels using a tape measure and a Brunton compass. Set thicknesses were defined by the average of at least 3 measurements from each set; dip angles also were averages of several measurements. Dip angles from peels were corrected for inclination of the peel. Ebb oriented structures at the surface of a peel or trench were not included in flood-to-ebb set ratios since they were formed by the last ebb tide and might be destroyed on the next flood tide. All measurements of internal structures are presented in Table C-2.

TABLE C-1. Bedform Measurements

Location	Length (m)	Height (m)	Strike (°)	Lee[1] Slope (°)	Stoss[2] Slope (°)	Migration Rate (cm/tidal cycle)
Boot Island	9.5	.15	39	26	18	- -
Bar	23.2S[3]	.50	35	34	4	- -
	2.4	.25	38	33	6	- -
	23.8S	.55	23	25	8	10 E[4]
	2.6	.20	38	31	7	5 E
	6.8	.30	53	25	15	8 E
	25.3S	.50	28	27	11	10 E
	2.6	.50	43	30	7	5 E
	6.8	.25	43	29	14	8 E
	39.8S	.65	33	32	10	20 F
	34.8	.60	38	27	9	20 F
	2.2	.30	45	34	6	5 F
	7.0	.30	48	32	24	15 F
	4.2	.20	63	35	7	5 F
	7.0	.30	43	25	19	10 F
	6.0	.23	48	32	4	3 F
	3.9	.29	51	34	8	4 F
	4.0	.35	45	32	9	3 E
	3.7	.24	46	33	11	3 F

[1] Lee Slope always denotes the ebb direction

[2] Stoss Slope always refers to the flood direction

[3] S indicates sand waves; T signifies transverse bars; all others are megaripples

[4] E refers to migration in the ebb direction; F in the flood direction

TABLE C-1 (continued)

Location	Length (m)	Height (m)	Strike (°)	Lee[1] Slope (°)	Stoss[2] Slope (°)	Migration Rate (cm/tidal cycle)	
Boot Island	3.8	.26	49	28	13	3	E
Bar (cont.)	3.8	.31	47	31	15	4	F
	45.6S	.60	36	33	10	-	-
	3.0	.20	67	25	4	-	-
	2.8	.25	60	26	4	-	-
	17.6S	.10	41	20	7	-	-
	41.2S	.95	38	28	8	15	E
	19.1S	.15	48	31	7	15	E
	3.3	.05	63	23	2	55	E
	5.1	.10	63	26	7	55	E
	41.2S	1.00	36	21	13	15	E
	14.6S	.20	38	32	12	15	E
	3.3	.15	43	28	8	38	F
	42.4S	.90	38	35	14	5	F
	18.4S	.20	33	20	7	38	F
	49.6S	1.20	38	28	8	5	F
	6.7	.25	53	20	7	5	F
	18.0S	.25	53	24	8	25	E
	3.0	.33	47	27	9	15	E
	12.3	.36	49	19	11	5	F
	4.7	.22	46	18	13	10	F
	3.6	.23	51	23	2	5	E
	2.9	.25	48	32	8	15	E

TABLE C-1 (continued)

Location	Length (m)	Height (m)	Strike (°)	Lee[1] Slope (°)	Stoss[2] Slope (°)	Migration Rate (cm/tidal cycle)	
Boot Island Bar (cont.)	3.7	.21	50	24	5	5	E
	12.0	.29	45	21	10	5	F
	9.5	.34	48	14	13	10	F
Hantsport Bar	5.0	.48	63	21	8	-	-
	4.4	.33	88	32	7	-	-
	2.1	.10	73	27	4	-	-
	4.3	.41	53	24	3	-	-
	5.2	.53	63	25	6	-	-
	2.7	.30	68	27	7	-	-
	4.9	.30	50	24	9	10	E
	5.2	.30	63	18	5	72	E
	5.4	.30	66	28	5	28	E
	6.0	.30	66	23	6	92	F
	5.6	.30	56	18	11	65	F
	9.0	.70	70	22	15	50	F
	4.5	.30	66	29	6	30	E
	3.8	.25	57	25	3	13	E
	2.1	.29	67	24	9	10	F
	3.2	.25	69	33	10	40	F
	2.4	.12	70	28	6	-	-
	2.2	.21	65	28	10	50	E
	8.7	.29	64	31	3	-	-

TABLE C-1 (continued)

Location	Length (m)	Height (m)	Strike (°)	Lee[1] Slope (°)	Stoss[2] Slope (°)	Migration Rate (cm/tidal cycle)	
Hantsport Bar	2.9	.31	67	24	9	80	E
(cont.)	3.3	.22	68	36	5	40	F
	3.0	.25	66	23	5	50	E
	3.6	.35	66	27	7	80	E
	3.3	.20	68	16	6	10	F
	2.8	.30	54	30	4	-	-
	2.9	.26	72	24	6	-	-
	4.6	.12	74	26	6	-	-
	2.3	.17	63	26	7	-	-
	2.9	.09	69	12	5	-	-
	2.6	.17	58	29	5	-	-
	2.2	.15	77	29	5	-	-
	4.8	.15	81	22	1	13	E
	5.2	.38	68	30	1	30	E
	10.4	.15	72	27	1	50	F
	5.6	.41	68	31	1	10	E
	5.3	.30	71	20	3	92	F
	5.3	.30	67	24	5	28	E
	5.6	.30	76	29	2	72	E
	5.6	.30	76	33	2	65	F
Middle Ground	4.7	.50	98	26	1	4	F

TABLE C-1 (continued)

Location	Length (m)	Height (m)	Strike (°)	Lee[1] Slope (°)	Stoss[2] Slope (°)	Migration Rate (cm/tidal cycle)	
Middle Ground	3.0	.50	93	26	4	8	F
(cont.)	16.3	1.00	78	38	6	22	F
	13.3	.40	113	30	6	42	F
	6.6	.20	53	31	12	3	F
	14.5	.20	98	23	8	16	F
	5.4	.50	83	16	1	4	F
	2.9	.40	103	16	2	8	F
	16.5	.90	58	33	8	22	F
	13.4	.40	103	27	6	42	F
	6.2	.20	63	31	6	3	F
	12.1	.10	73	14	3	16	F
	14.2	.20	77	9	6	25	F
	6.2	.20	66	24	5	10	F
	14.3	.40	103	27	7	5	F
	16.1	1.00	73	31	7	5	F
	14.5	.20	78	11	3	25	F
	6.4	.20	63	29	3	10	F
	14.2	.50	108	31	4	5	E
	17.5	.90	70	34	8	5	F
	4.2	.15	82	23	4	55	F
	2.5	.18	94	10	6	35	F
	12.8	.23	70	25	5	5	E
	3.9	.14	77	28	9	8	F

TABLE C-1 (continued)

Location	Length (m)	Height (m)	Strike (°)	Lee[1] Slope (°)	Stoss[2] Slope (°)	Migration Rate (cm/tidal cycle)	
Middle Ground	16.2	.32	87	28	6	3	F
(cont.)	4.9	.20	91	29	6	5	F
	2.0	.11	73	26	6	55	F
	2.5	.30	68	16	12	35	F
	13.8	.40	96	25	4	3	F
	3.7	.22	82	28	13	8	F
	19.4	.48	84	25	4	5	E
	5.7	.25	80	28	5	5	E
Mitchener Bar	- T	.45	12	25	1	19	F
	- T	.45	130	27	1	22	F
	12.0	.90	58	31	11	--	-
	9.0	.80	61	27	7	48	F
	- T	.45	14	26	1	19	F
	- T	.44	126	27	1	22	F
	7.2	.76	63	26	6	48	F
	- T	.50	128	21	1	300	F
	3.1	.48	67	30	6	110	F
	20.4	.51	59	28	7	-	-
	12.4	.52	63	26	5	-	-
	- T	.34	131	15	1	300	F
	4.7	.58	64	35	3	110	F

TABLE C-1 (continued)

Location	Length (m)	Height (m)	Strike (°)	Lee[1] Slope (°)	Stoss[2] Slope (°)	Migration Rate (cm/tidal cycle)	
Newport Bar	10.7	.60	96	15	27	115	F
	23.0	.50	64	6	17	100	F
	35.0	.70	33	3	18	150	F
	23.2	.90	116	30	21	25	F
	11.3	.50	96	8	12	115	F
	23.5	.60	60	11	21	100	F
	23.5	.80	98	28	11	25	F
	35.0	.60	93	4	15	150	F
	13.9	.80	92	30	18	130	F
	11.1	.65	98	29	21	105	F
	15.5	.20	86	25	6	180	F
	35.2	.30	88	29	7	305	F
	45.4	.32	96	28	3	305	F
	11.7	.77	91	25	19	130	F
	10.1	.60	93	21	21	105	F
	13.8	.20	92	24	6	180	F
Western Bar	3.9	.22	75	34	10	3	E
	2.6	.18	70	35	3	40	E
	3.7	.36	85	20	10	10	F
	4.3	.11	91	21	12	15	F
	2.7	.23	79	19	5	40	F

TABLE C-1 (continued)

Location	Length (m)	Height (m)	Strike (°)	Lee[1] Slope (°	Stoss[2] Slope (°)	Migration Rate (cm/tidal cycle)	
Western Bar	8.3	.24	78	30	10	15	E
(cont.)	1.7	.10	68	32	6	20	E
	4.6	.23	81	28	7	20	E
	5.9	.51	73	23	11	-	-
	3.7	.56	68	30	9	-	-
	2.7	.20	83	21	14	-	-
	2.4	.20	78	27	18	-	-
	2.4	.18	53	22	6	-	-
	2.4	.18	28	32	9	-	-
	4.9	.10	68	29	13	-	-
	3.2	.28	73	20	15	-	-
	3.0	.15	108	13	3	25	E
	3.1	.25	48	34	9	20	E
	2.8	.30	78	24	36	30	F
	4.5	.15	93	23	4	4	E
	2.7	.15	48	31	11	5	E
	3.6	.20	80	29	12	6	E
	60.0S	1.30	60	30	8	20	E
	89.2S	1.30	60	30	8	30	F
	4.8	.40	83	30	15	100	F
	7.5	.20	103	30	5	75	E
	2.5	.25	73	32	8	18	E

TABLE C-1 (continued)

Location	Length (m)	Height (m)	Strike (°)	Lee Slope[1] (°)	Stoss Slope[2] (°)	Migration Rate (cm/tidal cycle)	
Western Bar	4.0	.40	78	34	13	10	E
(cont.)	1.4	.30	23	28	14	42	E
	4.3	.25	83	30	12	33	E
	4.2	.10	98	23	7	25	E
	2.9	.25	48	28	7	20	E
	3.9	.20	73	33	8	6	E
	2.6	.20	98	34	7	5	E
	4.7	.15	98	32	11	4	E
	5.6	.35	86	31	12	31	F
	3.1	.20	74	29	7	40	E
	2.8	.26	82	11	13	10	F
	1.9	.27	88	11	10	15	F
	3.0	.23	70	33	7	3	E
	2.1	.13	85	7	4	40	F
	8.2	.29	78	33	7	15	E
	1.3	.09	81	29	10	20	E
	3.9	.14	77	28	6	20	E
	63.6S	1.35	40	26	8	20	E
	76.6S	1.30	48	29	15	30	F
	3.9	.20	88	29	9	33	E
	1.4	.15	33	25	5	42	E
	3.9	.45	76	35	10	10	E
	4.8	.50	93	29	18	100	F
	5.2	.10	93	39	4	75	E
	2.4	.35	83	34	11	18	E

TABLE C-2. Internal Structure Measurements

Peel Number	Structure	Average Dip Angle (°)	Average Set Thickness (cm)	Ebb-Flood Thickness Ratio
Boot Island Bar A	large-scale flood cross-bedding	22	12	1.6
	large-scale ebb cross-bedding	15	13	
Boot Island Bar B	large-scale flood cross-bedding	31	8	1.2
	large-scale ebb cross-bedding	25	9	
Boot Island Bar C	large-scale flood cross-bedding	24	12	1.2
	large-scale ebb cross-bedding	22	14	
Hantsport Bar A	large-scale ebb cross-bedding	29	30+	-
Hantsport Bar B	large-scale ebb cross-bedding	26	8	-
Hantsport Bar C	large-scale flood cross-bedding	30	11	1.0
	large-scale ebb cross-bedding	30	11	
	large-scale trough cross-bedding	-	12	
	ebb	27	6	

TABLE C-2 (continued)

Peel Number	Structure	Average Dip Angle (°)	Average Set Thickness (cm)	Ebb-Flood Thickness Ratio
Middle Ground A	small-scale flood cross-bedding	20	2	2.2
	small-scale ebb cross-bedding	19	4	
Middle Ground B	large-scale flood cross-bedding	27	9	-
Middle Ground C	large-scale ebb cross-bedding	15	30+	-
Middle Ground D	large-scale flood cross-bedding	26	13	0.2
	large-scale ebb cross-bedding	10	6	
Middle Ground E	large-scale flood cross-bedding	28	13	-
Middle Ground F	small-scale flood cross-bedding	18	6	0.8
	small-scale ebb cross-bedding	20	5	
Mitchener Bar A	large-scale flood cross-bedding	17	16+	1.1
	large-scale ebb cross-bedding	26	9	
	reactivation surface	12	-	

TABLE C-2 (continued)

Peel Number	Structure	Average Dip Angle (°)	Average Set Thickness (cm)	Ebb-Flood Thickness Ratio
Mitchener Bar B	low-angle ebb cross-bedding	8	20+	
	parallel lamination	-	10	
Mitchener Bar C	small-scale flood cross-bedding	20	3	3.0
	small-scale ebb cross-bedding	13	3	
	parallel lamination	-	8	
Mitchener Bar D	parallel lamination	-	30+	-
Newport Bar A	parallel lamination	-	30+	
Newport Bar B	large-scale flood cross-bedding	15	15	0.3
	large-scale ebb cross-bedding	12	9	
	parallel lamination	-	6	
Newport Bar C	small-scale trough cross-bedding	-	13	-
	small-scale flood cross-bedding	30	4	

TABLE C-2 (continued)

Peel Number	Structure	Average Dip Angle (°)	Average Set Thickness (cm)	Ebb-Flood Thickness Ratio
Newport Bar D	small-scale trough cross-bedding	-	20	0.4
	small-scale flood cross-bedding	22	4	
	small-scale ebb cross-bedding	26	2	
	flaser bedding	-	-	
Western Bar A	large-scale ebb cross-bedding	15	30+	-
Western Bar B	large-scale flood cross-bedding	20	11	1.1
	large-scale ebb cross-bedding	22	12	
	reactivation surface	7	-	
Western Bar C	large-scale ebb cross-bedding	20	60+	-
Western Bar D	large-scale ebb cross-bedding	16	30	-

TABLE C-2 (continued)

Peel Number	Structure	Average Dip Angle (°)	Average Set Thickness (cm)	Ebb-Flood Thickness Ratio
Western Bar E	large-scale flood cross-bedding	27	20	0.5
	large-scale ebb cross-bedding	32	9	
	reactivation surface	8		
Western Bar F	large-scale flood cross-bedding	19	22	0.4
	large-scale ebb cross-bedding	26	8	

APPENDIX D: SEDIMENT SAMPLE ANALYSIS

Mechanical Analysis

The procedure used for mechanical analysis was identical to that of Dickson (1974); also see Folk (1974) and Carver (1971). Samples were washed, dried, and split. The -3.50 to -1.00 phi fraction was hand sieved at 1/4 phi intervals and the -1.00 to 4.00 phi fraction was sieved at 1/4 phi intervals using a Rotap; each nest of sieves was shaken for ten minutes. The weight of each 1/4 phi fraction was then recorded. Since only a few samples had appreciable amounts of fine sediment, analysis was not extended beyond 4.00 phi.

Calculation of Textural Parameters

Textural parameters were calculated using a computer program written by R.W. Dalrymple; the program was designed specifically to accept sieve data obtained by the method of Dickson (1974). For each sample, the frequency curve was generated by differentiation of the cumulative curve; locations of modes were estimated from the percentage data. Percentiles were interpolated from the cumulative curve by the method of Akima (1972) for data that was not too open-ended.

Median, mean, standard deviation, skewness, and kurtosis were calculated by the methods of Folk and Ward (1957), Inman (1952), and Trask (1930) unless the data was too open-ended. Moment statistics were computed by the method of Seward-Thompson and Hails (1973) using a linear interpolation between data points of the cumulative curve. Open-endedness of more than 5% in either the fine or coarse tail was not accepted. Computed textural parameters for all sediment samples are presented in Table D-1.

TABLE D-1. Grain Size Distributions

Grain size distributions of all 471 sediment samples are listed on the following pages. The sample name appears above cumulative weight percentages at the 1/4 phi intervals; the corresponding phi classes are listed in the left-hand column of the page. In addition, values of the moment measure mean, standard deviation, skewness, and kurtosis are printed below the cumulative weight percentages. A blank space below the cumulative weight percentages indicates that the sample is too open-ended for calculation of moment measure textural parameters.

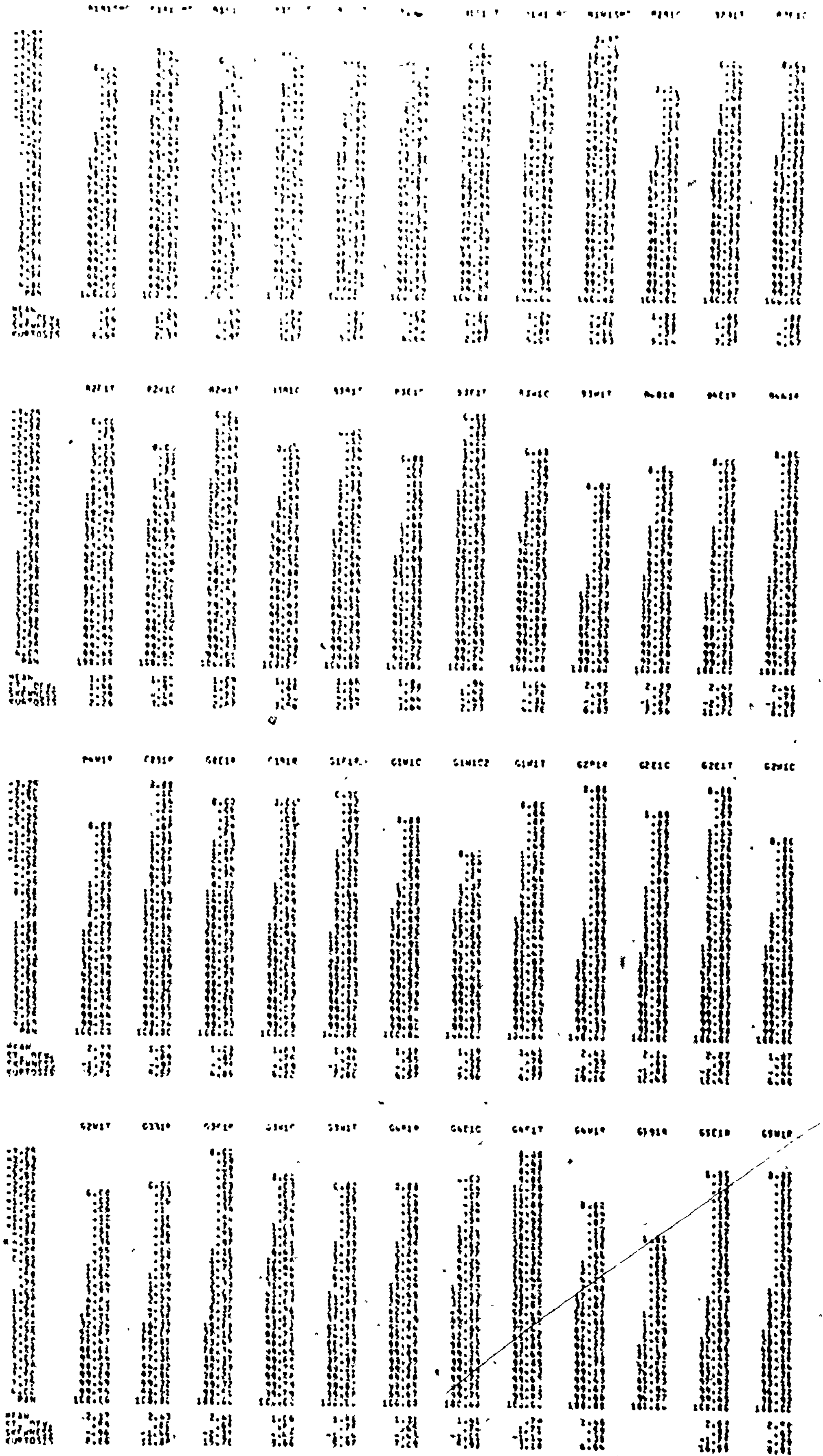
MEAN
STD.DEV.
SKEWNESS
KURTOSIS

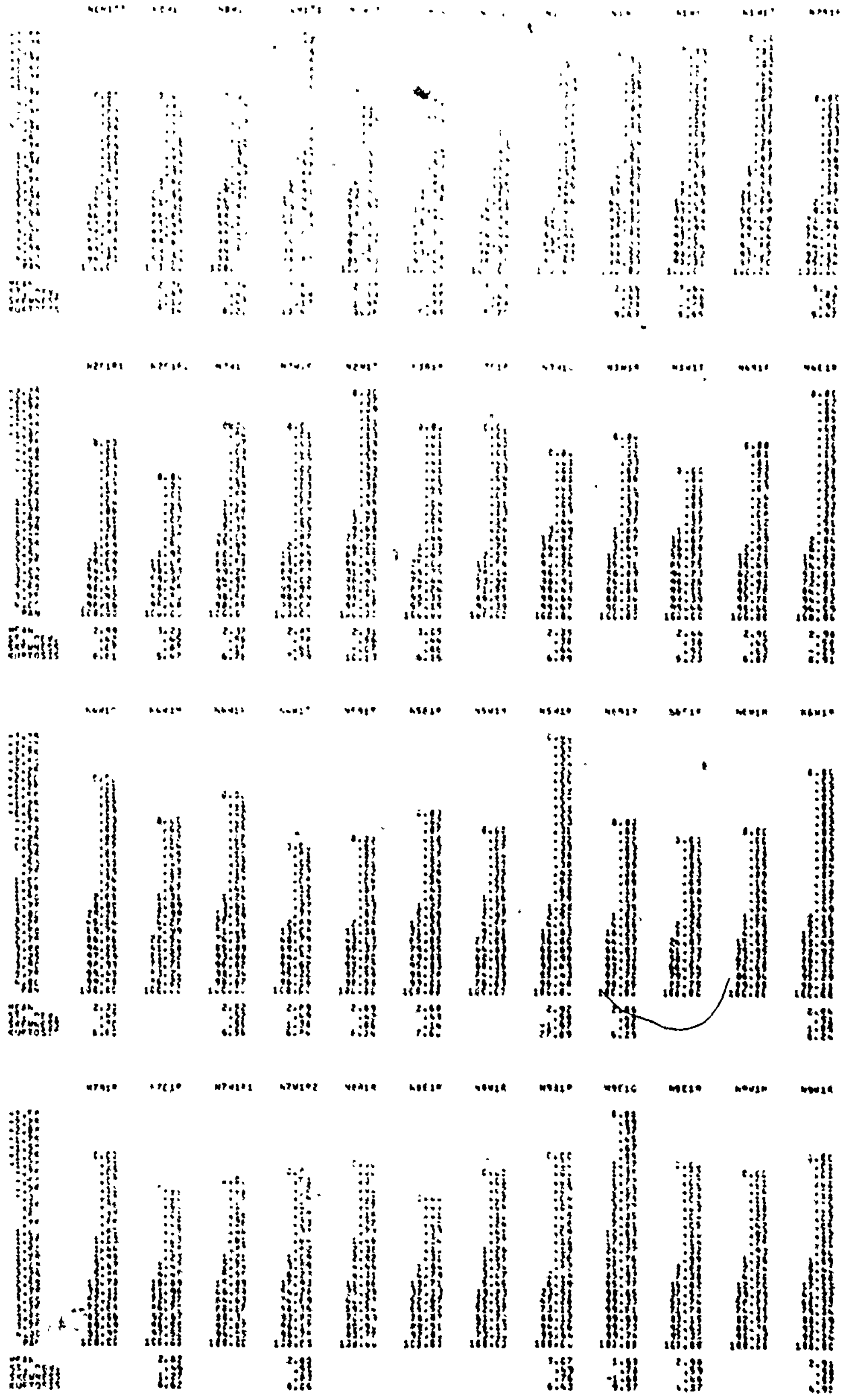

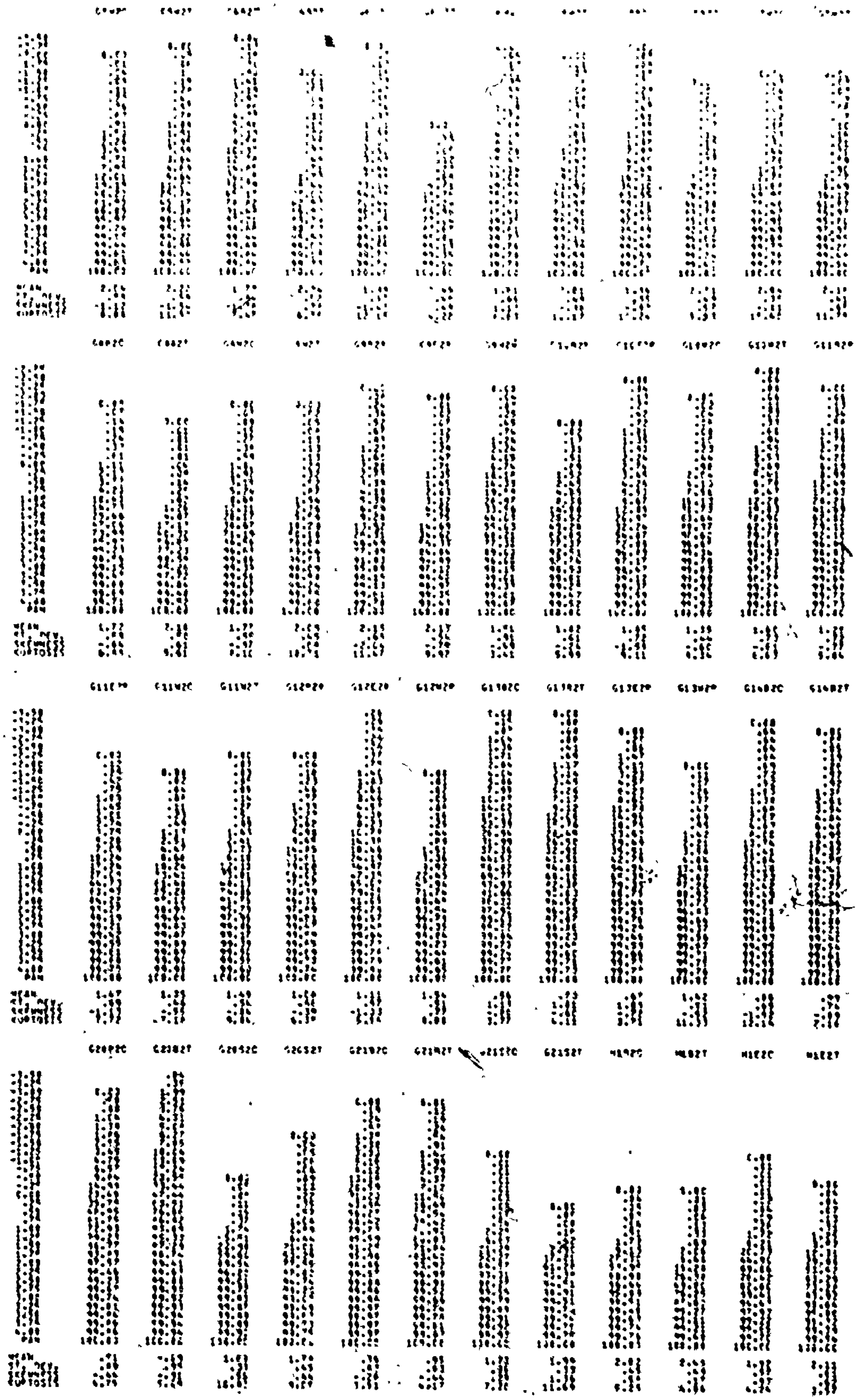

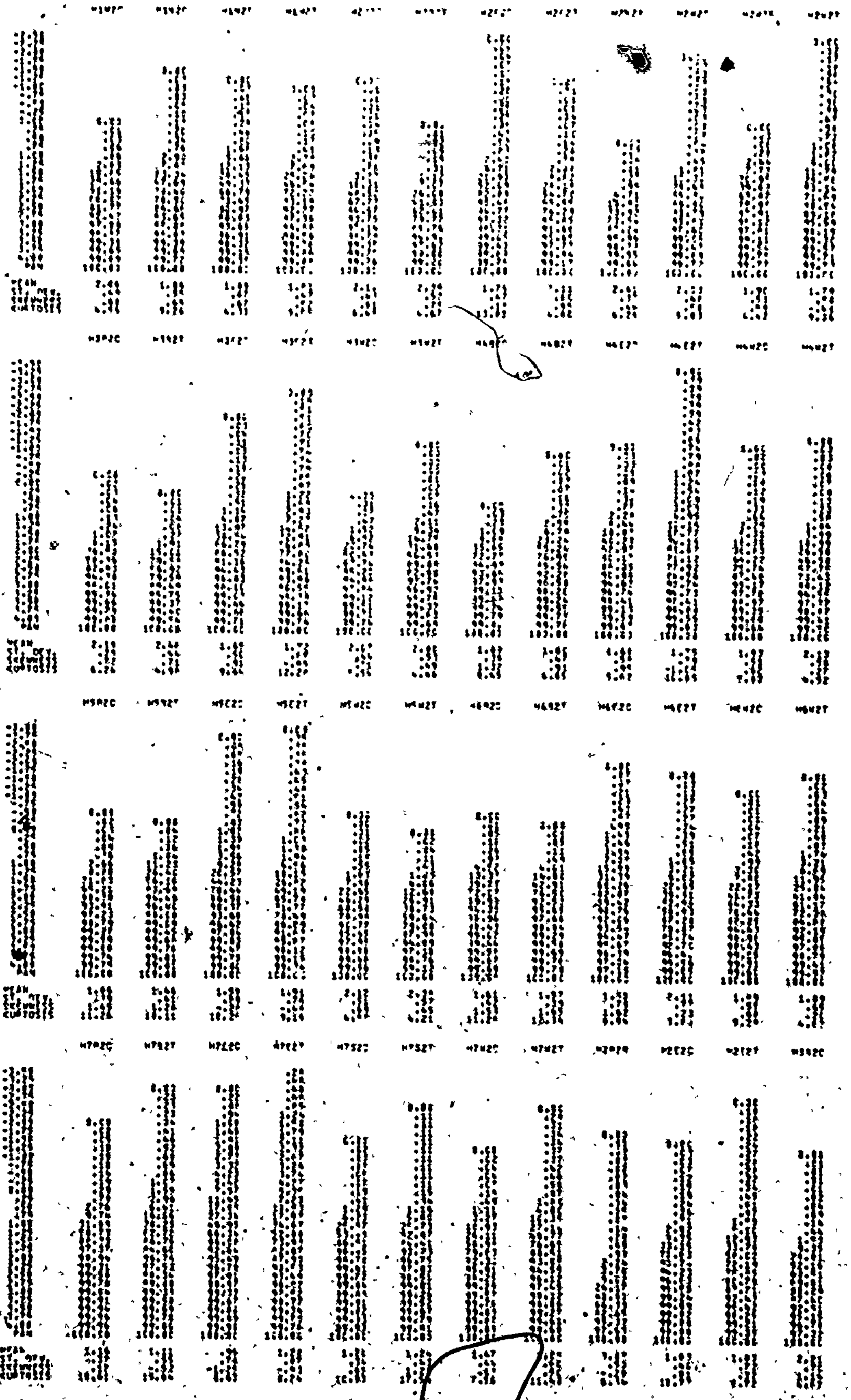

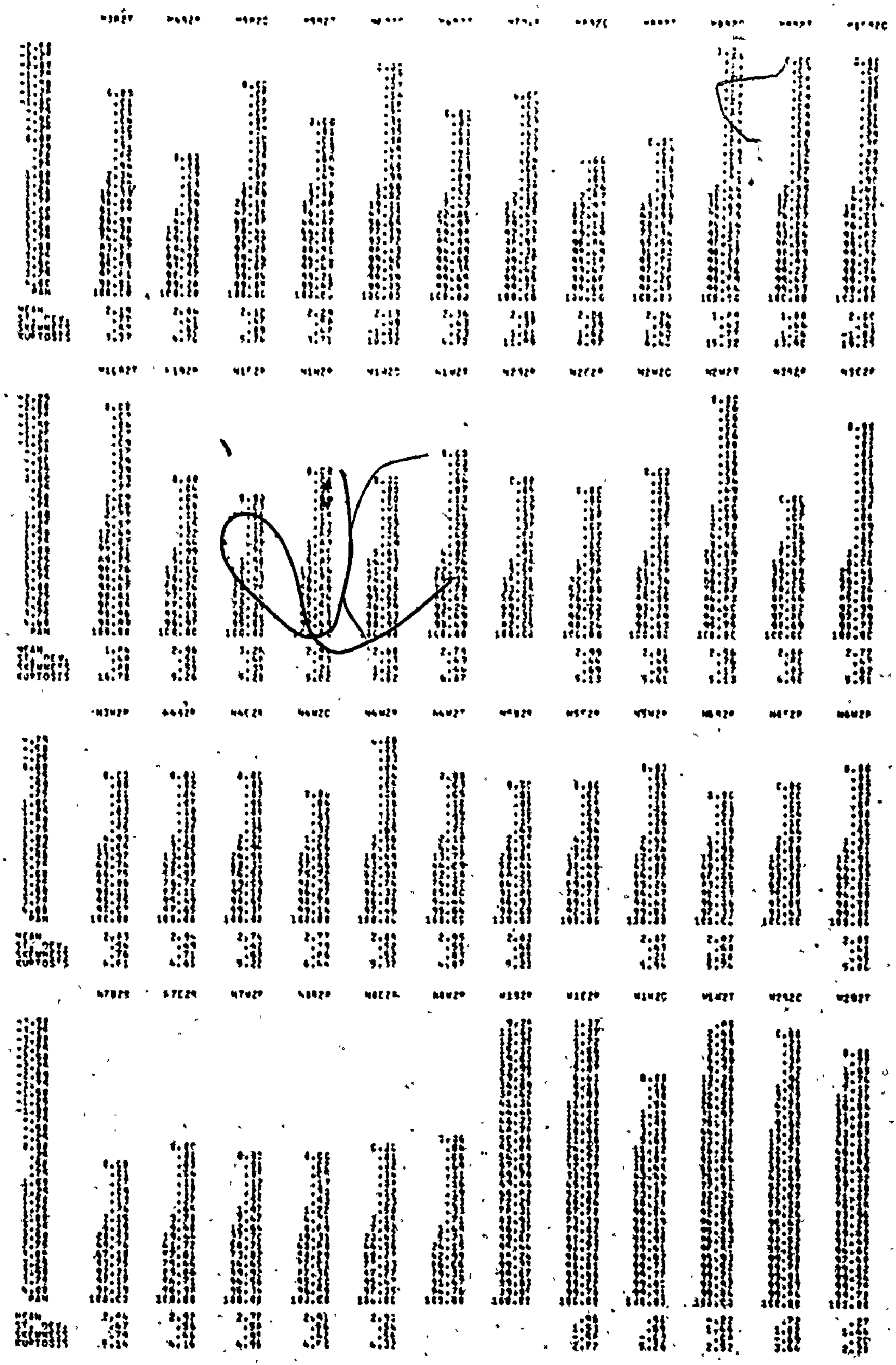

APPENDIX E: CALCULATION OF SEDIMENT TRANSPORT RATES

Bedform Migration

Bedform migration rate was measured by emplacing a stake at the bedform crest. A mark was made on the stake at the sediment surface and a washer was placed over the stake; the diameter of the washer was large enough to permit free movement on the stake.

Distances from the stake to adjacent bedforms were measured after one, or at most two, tidal cycles. Distance from the sediment surface to the mark on the stake and the washer were measured also; height and wavelength of the bedform was measured at both low tides. Bedform migration rates were then calculated from the measured distances; the washer was used to determine if more than one bedform crest had passed the stake.

Sediment transport rates could then be calculated for a unit width of the bedform by assuming a triangular cross-section perpendicular to the crest of the bedform and calculating the area of that cross-section using bedform height. The volume of sediment transported per unit width equals the bedform height times the migration distance times the concentration of grains; a grain concentration of 0.60 was used as it is similar to values reported by Inman (1963), Raudkivi (1967), and Kachel and Sternberg (1971). The formula used for transport rate is essentially identical to that of Simons et al. (1965b).

Calculation of sediment transport rates from bedform migration rates is limited by the degree to which the cross-sectional area of a bedform can be approximated as bedform shape is extremely variable. Also, the estimated concentration of grains may not be entirely accurate. In addition, all sediment transported as bedload may not move as part of a bedform; some sediment may bypass each bedform so that bedform migration rate would underestimate transport rate. The accuracy of sediment transport rates calculated from bedform migration rates depends directly on the accuracy with which the magnitude of all these factors can be estimated.

Transport Formulae

APPLICATION: The five sediment transport formulae were applied to the Avon River estuary by calculating an instantaneous sediment transport rate for each current velocity profile at each current velocity station. Input variables included hydraulic parameters computed from current velocity measurements (see Appendix B) and the grain size distribution at each station. Since profiles were recorded at equal time intervals (1/2 hour), a vector summation of the instantaneous rates could be calculated; this yielded the net sediment transport rate and direction for a tidal cycle at that station. The computed instantaneous transport rates for each profile, and the net transport for each station, are listed in Table E-1.

LIMITATIONS: There are several inherent limitations in the application of transport formulae to a system like the Avon River estuary. All the formulae were derived for unidirectional flow and for more uniform flow conditions than are found in a macrotidal estuary. Einstein's and Toffaleti's equations account for transport rates at different size fractions but the other equations do not; since there probably are three active mechanisms of sediment transport, using D_{50} or D_{35} to compute a representative rate for the entire sample may not be justified. Also, White et al. (1975, 1976) found no equation that was better than within a factor of 2 of the actual sediment transport rate more than 68% of the time.

Probably the largest source for error in computed sediment transport rate concerns the accuracy of the calculated hydraulic data used as input. As described in Appendix B, for each velocity profile a best-fit line was calculated relating current speed to the logarithm of the water depth; hydraulic parameters were computed based on the slope of this line. However, a number of regression lines at each station are not statistically significant at the 95% level probably as a result of large-scale turbulence fluctuations. Sediment transport rates have been calculated from these profiles and are included in the net transport rate for each station; if turbulence effects could be eliminated from the hydraulic data, re-calculated sediment transport rates could alter the net transport rate and/or direction at several stations that have numerous insignificant profiles and low net sediment transport rates.

Current velocity profiles that have negative slopes to their depth - current speed regression lines due to turbulence fluctuations were eliminated from sediment transport computations since resulting transport rates would be meaningless. Also, at low flow stages when only one current velocity reading could be made because of insufficient water depth, hydraulic parameters, and thus sediment transport rates, could not be calculated. This probably results in a decrease in computed flood transport relative to ebb because, at low flow stages, ebb currents tend to be slower than low stage flood currents.

Thus, several factors are capable of significantly altering net sediment transport rate. This is particularly true at stations with low net transport rates and large numbers of statistically insignificant and/or one point current velocity profiles; there are several such stations (see Table E-1). However, at most stations net sediment transport rates and directions are consistent with rates and directions computed from bedform migration rates; transport equations are useful in this study but the numerous sources of error must be remembered.

TABLE E-1: Sediment Transport Rates Computed with Engelund and Hansen's Transport Formula

Times are in hours from high tide, transport rates for each profile are in m^3 per hour per unit width, net transport rates are m^3 per tidal cycle per unit width, and the net direction is the vector resultant of the sum of the profiles in degrees from true north. Transport rates followed by an asterisk were computed from hydraulic profiles whose water depth - current velocity regression line were statistically insignificant at the 95% level. Profiles for which no rate could be calculated are not included in the table. Transport rates have been rounded to the nearest 0.01 m^3; net transport rates were calculated before rounding. The tidal coefficient for the measured tidal cycle is in brackets below the station name.

NEWPORT BAR 1			NEWPORT BAR 2			NEWPORT BAR 3			NEWPORT BAR 4		
(0.75)			(0.70)			(0.56)			(0.68)		
Time	Dir.	Rate	Time	Dir.	Rate	Time	Dir.	Rate	Time	Dir.	Rate
-8.25	E	0.86	-10.08	E	0.01*	-1.92	F	0.03	-3.33	F	0.14*
-7.75	E	12.54	-9.58	E	0.03	-1.42	F	0.00*	-2.83	F	0.35
-3.50	F	0.45	-9.08	E	0.06	-0.42	F	0.00*	-2.33	F	0.26
-2.50	F	0.77	-2.83	F	7.36	0.08	E	0.00	-1.83	F	0.11
-2.00	F	0.00*	-2.33	F	0.24	0.58	E	0.00	-1.33	F	0.01
-1.00	F	0.00	-1.83	F	0.00	1.08	E	0.01	-0.83	F	0.00*
-0.50	F	0.00*	-1.33	F	0.01	1.58	E	0.08	-0.33	F	0.00*
1.00	E	0.00*	-0.83	F	0.00	2.08	E	0.26	0.17	F	0.00*
1.50	E	0.00	-0.33	F	0.00*	2.58	E	0.62	0.67	E	0.00
2.00	E	0.03	1.17	E	0.00	3.08	E	0.56	1.17	E	0.00
2.50	E	0.03	1.67	E	0.00*	3.58	E	0.79	1.67	E	0.02
3.00	E	0.13	2.17	E	0.03	4.08	E	0.51*	2.17	E	0.07
3.50	E	0.03				4.58	E	0.97	2.67	E	0.06
			NET	200	3.75	8.08	F	0.41	3.17	E	0.04*
NET	8	6.20				8.58	F	0.07*	3.67	E	0.05
						9.08	F	0.24			
						9.58	F	0.14	NET	180	0.32
						10.08	F	0.10			
						10.58	F	0.01			
						NET	11	1.39			

MITCHENER BAR 1			HANTSPORT BAR 1			HANTSPORT BAR 2			HANTSPORT BAR 3		
(0.85)			(0.76)			(0.76)			(0.76)		
Time	Dir.	Rate	Time	Dir.	Rate	Time	Dir.	Rate	Time	Dir.	Rate
-2.83	F	2.49	-8.42	E	1.36	-8.67	E	0.01*	0.58	E	0.00
-2.33	F	3.25	-7.92	E	1.15	-8.17	E	0.00	1.08	E	0.00
-1.83	F	0.22	-3.92	F	0.00	-7.67	E	0.00	1.58	E	0.13
-1.33	F	0.26	-3.42	F	0.00*	-4.17	F	0.00	2.08	E	0.11
-0.83	F	0.02	-2.92	F	0.00*	-3.67	F	0.03*	2.58	E	0.29
-0.33	F	0.00	-2.42	F	0.02	-3.17	F	0.63	3.08	E	0.02
0.17	F	0.00	-1.92	F	0.01	-2.67	F	0.93	3.58	E	0.09
0.67	E	0.00	-1.42	F	0.01	-2.17	F	0.17	4.08	E	0.10
1.17	E	0.03	-0.92	F	0.00	-1.67	F	0.01	8.58	F	0.15
1.67	E	0.04*	0.08	E	0.00*	-1.17	F	0.02	9.08	F	0.15
2.17	E	0.00	1.08	E	0.00*	-0.42	F	0.00	9.58	F	0.27
2.67	E	0.27	1.58	E	0.02	1.33	E	0.02*	10.08	F	0.48
3.17	E	0.97*	2.08	E	0.01	1.83	E	0.07	10.58	F	0.17
3.67	E	0.41	2.58	E	0.01	2.33	E	0.90	11.08	F	0.01
4.17	E	9.07	3.08	E	0.03	2.83	E	0.62	11.58	F	0.00
8.67	F	0.06*	3.58	E	0.06	3.33	E	0.01*	12.08	F	0.00*
9.17	F	0.09				3.83	E	0.04	12.58	F	0.00
			NET 306		1.29						
NET 357		2.45				NET 200		0.10	NET 142		0.24

HANTSPORT BAR 4			HANTSPORT BAR 5			MIDDLE GROUND 1			MIDDLE GROUND 2		
	(0.73)			(0.78)			(0.63)			(0.63)	
Time	Dir.	Rate	Time	Dir.	Rate	Time	Dir.	Rate	Time	Dir.	Rate
-1.67	F	0.02	-7.75	E	0.67*	-0.08	E	0.00	0.17	E	0.00
-1.17	F	0.00	-7.25	E	0.14*	0.42	E	0.00	0.67	E	0.00
-0.67	F	0.00	-4.25	[illegible]	0.59	0.92	E	0.00	1.17	E	0.05
-0.17	F	0.00	-3.75	F	0.21	1.42	E	0.01	1.67	E	0.09
0.83	E	0.00*	-3.25	F	0.00*	1.92	E	0.16	2.17	E	0.09
1.33	E	0.04	-2.75	F	0.02	2.42	E	0.06	2.67	E	0.16
1.83	E	0.06	-2.25	F	0.04	2.92	E	0.01	3.17	E	0.05
2.33	E	0.09	-1.75	F	0.01	3.42	E	0.00*	3.67	E	0.20
2.83	E	0.08	-1.25	F	0.00	3.92	E	0.04	4.17	E	0.01
3.33	E	0.20	-0.75	F	0.00*	4.42	E	0.00*	4.67	E	0.03
3.83	E	0.31	-0.25	F	0.00*	4.92	E	0.01	5.17	E	0.16
4.33	E	0.27	0.25	E	0.00*	5.42	E	0.00*	7.17	F	0.04
4.83	E	0.39	0.75	E	0.00	5.92	E	0.00	7.67	F	0.04
5.33	E	0.00*	1.25	E	0.01	6.92	F	0.00*	8.17	F	0.05
5.83	E	0.00*	1.75	E	0.14	7.42	F	0.01	8.67	F	0.13
6.33	E	0.00	2.25	E	0.08	7.92	F	0.00	9.17	F	0.01
6.83	F	0.00*	2.75	E	0.03	8.42	F	0.00	9.67	F	0.00
7.33	F	0.66	3.25	E	0.39	8.92	F	0.01	10.17	F	0.00
7.83	F	0.61	3.75	E	0.41	9.92	F	0.00	11.17	F	0.00
8.33	F	0.01	4.25	E	1.36	10.42	F	0.00	11.67	F	0.00
8.83	F	0.22	4.75	E	1.97*				12.17	F	0.00
9.33	F	0.24				NET 351		0.13			
9.83	F	0.22	NET 297		2.17				NET 357		0.27
10.33	F	0.04									
10.83	F	0.00									
NET 139		0.29									

MIDDLE GROUND 3			MIDDLE GROUND 4			MIDDLE GROUND 5			BOOT ISLAND BAR 1		
(0.88)			(0.74)			(0.78)			(0.74)		
Time	Dir.	Rate	Time	Dir.	Rate	Time	Dir.	Rate	Time	Dir.	Rate
-8.67	E	0.09	-8.58	E	0.00*	-4.92	F	0.00	-4.67	F	0.00
-8.17	E	0.00	-8.08	E	0.00	-4.42	F	0.01*	-4.17	F	0.00
-7.67	E	0.01	-4.08	F	0.00	-3.92	F	0.00*	-3.67	F	0.01
-7.17	E	0.00*	-3.58	F	0.00*	-3.42	F	0.01	-3.17	F	0.01
-4.67	F	0.05	-3.08	F	0.00*	-2.92	F	0.01	-2.67	F	0.00
-4.17	F	0.02	-2.58	F	0.00	-2.42	F	0.02	-2.17	F	0.00*
-3.67	F	0.14	-2.08	F	0.01	-1.92	F	0.01	-1.67	F	0.00
-3.17	F	0.00*	-1.58	F	0.00	-1.42	F	0.01	-1.17	F	0.00
-2.67	F	0.00*	-1.08	F	0.00	-0.92	F	0.00*	-0.67	F	0.00*
-2.17	F	0.01*	-0.58	F	0.00	-0.42	F	0.00	-0.17	E	0.00
-1.67	F	0.00	-0.08	F	0.00	0.08	E	0.00	0.33	E	0.00
-1.17	F	0.03	0.42	E	0.00	0.58	E	0.00	0.83	E	0.00
-0.67	F	0.00	0.92	E	0.00	1.08	E	0.00	1.33	E	0.04
-0.17	F	0.00	1.42	E	0.01	1.58	E	0.00	1.83	E	0.04
0.33	E	0.00*	1.92	E	0.06	2.08	E	0.03	2.33	E	0.14
0.83	E	0.00	2.42	E	0.08	2.58	E	0.02	2.83	E	0.08
1.83	E	0.08	2.92	E	0.00	3.08	E	0.00	3.33	E	0.01
2.33	E	0.19	3.42	E	0.00*	3.58	E	0.02	3.83	E	0.01
2.83	E	0.09	3.92	E	0.00*	4.08	E	0.02*	4.33	E	0.01*
3.33	E	0.07				4.58	E	0.00	4.83	E	0.00
3.83	E	0.07	NET 333		0.07	NET 301		0.01	NET 331		0.15
NET 8		0.17									

BOOT ISLAND
BAR 2 (0.74)

Time	Dir.	Rate
-3.75	F	0.00
-3.25	F	0.00*
-2.75	F	0.00*
-2.25	F	0.00*
-0.75	F	0.00
0.25	E	0.00*
0.75	E	0.00
1.25	E	0.00*
1.75	E	0.02*
2.25	E	0.01
2.75	E	0.02*
3.25	E	0.00*
3.75	E	0.02
NET 315		0.03

BOOT ISLAND
BAR 3 (0.79)

Time	Dir.	Rate
-10.17	E	0.01*
-9.67	E	0.00*
-3.67	F	0.01*
-3.17	F	0.01*
-2.67	F	0.00*
-2.17	F	0.00
-1.17	F	0.00
-0.67	F	0.00*
-0.17	F	0.00
0.33	E	0.00
0.83	E	0.00
1.33	E	0.05
1.83	E	0.09
2.33	E	0.00
NET 299		0.06

BOOT ISLAND
BAR 4 (0.79)

Time	Dir.	Rate
-9.92	E	0.00
-9.42	E	0.00
-3.92	F	0.05
-3.42	F	0.00*
-2.92	F	0.01
-2.42	F	0.00*
-1.92	F	0.00
-1.42	F	0.00
-0.92	F	0.00
-0.42	F	0.00*
0.08	E	0.00
0.58	E	0.00
1.08	E	0.00
1.58	E	0.03
2.08	E	0.00*
2.58	E	0.00
NET 113		0.01

BOOT ISLAND
BAR 5 (0.62)

Time	Dir.	Rate
-0.08	F	0.00
0.42	E	0.00
0.92	E	0.00
1.42	E	0.00
1.92	E	0.00
2.92	E	0.00
8.92	F	0.01
9.42	F	0.01
9.92	F	0.00
10.42	F	0.00
10.92	F	0.00*
11.42	F	0.00
11.92	F	0.00
NET 119		0.01

WESTERN BAR 1

(0.62)

Time	Dir.	Rate
-0.25	F	0.00
0.75	E	0.00
1.25	E	0.00
1.75	E	0.02
2.25	E	0.01
2.75	E	0.01
3.25	E	0.02
7.75	F	0.02
8.25	F	0.04*
9.25	F	0.00*
9.75	F	0.00*
10.75	F	0.00
11.25	F	0.00*
11.75	F	0.00
12.25	E	0.00
NET 50		0.01

WESTERN BAR 2

(0.62)

Time	Dir.	Rate
1.00	E	0.00
1.50	E	0.01
2.00	E	0.01
2.50	E	0.03
3.00	E	0.00*
9.00	F	0.00*
9.50	F	0.00
10.00	F	0.00
11.00	F	0.00
11.50	F	0.00
12.50	E	0.00*
NET 337		0.02

WESTERN BAR 3

(0.85)

Time	Dir.	Rate
-7.50	E	0.10
-6.50	E	0.10
-5.00	F	0.00*
-4.50	F	0.00*
-4.00	F	0.07
-3.50	F	0.06
-3.00	F	0.00
-2.50	F	0.00*
-2.00	F	0.00
-1.50	F	0.00
-1.00	F	0.00*
-0.50	F	0.00
0.00	E	0.00
0.50	E	0.00
1.00	E	0.00
1.50	E	0.05
2.00	E	0.03
2.50	E	0.03
3.00	E	0.01
3.50	E	0.10
4.00	E	0.00*
4.50	E	0.00*
5.00	E	0.01*
NET 316		0.10

WESTERN BAR 4

(0.78)

Time	Dir.	Rate
-4.83	F	0.01*
-4.33	F	0.00
-3.83	F	0.01
-3.33	F	0.00
-2.83	F	0.00*
-1.83	F	0.00
-1.33	F	0.00
-0.83	F	0.00
-0.33	F	0.00*
0.17	E	0.00*
0.67	E	0.00
1.17	E	0.00
1.67	E	0.01
2.17	E	0.00
2.67	E	0.02
3.17	E	0.01
3.67	E	0.00
4.17	E	0.01
4.67	E	0.01
5.17	E	0.00*
5.67	E	0.00
6.17	E	0.00
6.67	F	0.00*
7.67	F	0.01
NET 323		0.01

BEDFORD
INSTITUTE
STATION 2 (0.76)

Time	Dir.	Rate
-6.42	E	0.01*
-5.00	F	0.01
-4.00	F	0.01
-2.00	F	0.01
-1.00	F	0.00
1.00	E	0.00
2.00	E	0.18
3.00	E	0.32
4.00	E	0.44
5.00	E	0.05*
NET 349		0.51

BEDFORD
INSTITUTE
STATION 3(0.89)

Time	Dir.	Rate
-6.25	E	0.00
-4.25	F	0.06
-2.25	F	0.03
-1.25	F	0.02
-0.25	F	0.00
0.75	E	0.00
1.75	E	0.04
2.75	E	0.27
3.75	E	0.01
4.75	E	0.01
5.75	E	0.00*
6.50	E	0.00
NET 321		0.12

MAIN
CHANNEL (0.77)

Time	Dir.	Rate
0.00	E	0.00*
0.50	E	0.00
1.00	E	0.00
1.50	E	0.00
2.00	E	0.03
2.50	E	0.03
3.00	E	0.05
3.50	E	0.02
4.00	E	0.02
4.50	E	0.01
5.00	E	0.01
5.50	E	0.00
6.00	E	0.00
6.50	F	0.00*
7.00	F	0.00*
7.50	F	0.00
8.00	F	0.00
9.00	F	0.01
9.50	F	0.00
10.00	F	0.00*
11.00	F	0.00
11.50	F	0.00*
12.00	F	0.00
NET 350		0.07

HORTON
NORTH (0.80)

Time	Dir.	Rate
-7.17	E	0.11
-6.67	E	0.04
-6.17	E	0.01
-5.67	F	0.00*
-4.67	F	0.00
-4.17	F	0.12
-3.67	F	0.00*
-3.17	F	0.00
-2.67	F	0.05
-2.17	F	0.00*
-1.67	F	0.00*
-1.17	F	0.00*
-0.67	F	0.00
0.33	E	0.00
0.83	E	0.00
1.33	E	0.00
1.83	E	0.02*
2.33	E	0.16
2.83	E	0.00
3.33	E	0.01
3.83	E	0.00
4.33	E	0.00
4.83	E	0.01
5.33	E	0.00*
NET 280		0.09

HORTON SOUTH (0.58)			SUMMERVILLE (0.70)			KENNETCOOK MOUTH (0.59)		
Time	Dir.	Rate	Time	Dir.	Rate	Time	Dir.	Rate
-2.25	F	0.03	-4.67	F	0.03*	-10.83	E	0.01
-1.75	F	0.02	-4.17	F	0.00*	-10.33	E	0.60
-1.25	F	0.01	-3.67	F	0.11	-9.83	E	0.01*
-0.25	F	0.00	-3.17	F	0.03	-9.33	E	0.29
0.25	E	0.00	-2.67	F	0.06	-8.83	E	0.44
0.75	E	0.00*	-2.17	F	0.02	-8.33	E	0.22
1.75	E	0.01	-1.67	F	0.00	-7.83	E	0.46
2.25	E	0.07	-1.17	F	0.00	-7.33	E	0.07*
2.75	E	0.07	-0.17	E	0.00*	-6.83	E	0.00*
3.25	E	0.03	0.33	E	0.00	-6.33	E	0.00
3.75	E	0.08	0.83	E	0.00	-5.33	F	0.00*
4.25	E	0.15	1.33	E	0.02	-4.83	F	0.00*
4.75	E	0.20	1.83	E	0.05	-4.33	F	0.01
5.25	E	0.03	2.33	E	0.21	-3.83	F	0.00*
5.75	E	0.01	2.83	E	0.04	-3.33	F	0.00*
6.25	E	0.00*	3.33	E	0.16	-2.83	F	0.00*
7.25	F	0.00*	3.83	E	0.20	-2.33	F	0.04
7.75	F	0.03	4.83	E	0.01	-1.83	F	0.01
8.25	F	0.13	7.83	F	0.00*	-1.33	F	0.00*
9.25	F	0.47				-0.83	F	0.00*
9.75	F	0.02	NET 299		0.22			
10.25	F	0.02				NET 244		1.01
10.75	F	0.01						
NET 125		0.14						

APPENDIX F: PETROGRAPHY

Twelve sediment samples were examined petrographically. A sample was chosen from a bedform crest on either side of the crest on each sand body. Each sample was impregnated with CIBA-GEIGY RP-103 casting resin and then thin sectioned.

Grains were identified and point-counted under a petrographic microscope using standard petrographic techniques (see Kerr, 1959). Approximately 500 counts were made on each sample; a grain was counted only if it fell directly beneath the cross hairs. The first two samples processed were recounted after the twelfth to check for consistency. Results of the investigation are presented in Table 10-2.